

**AN ANALYSIS FOR DIGITAL  
PROTECTION OF TRANSFORMERS**

**CENTRE FOR NEWFOUNDLAND STUDIES**

**TOTAL OF 10 PAGES ONLY  
MAY BE XEROXED**

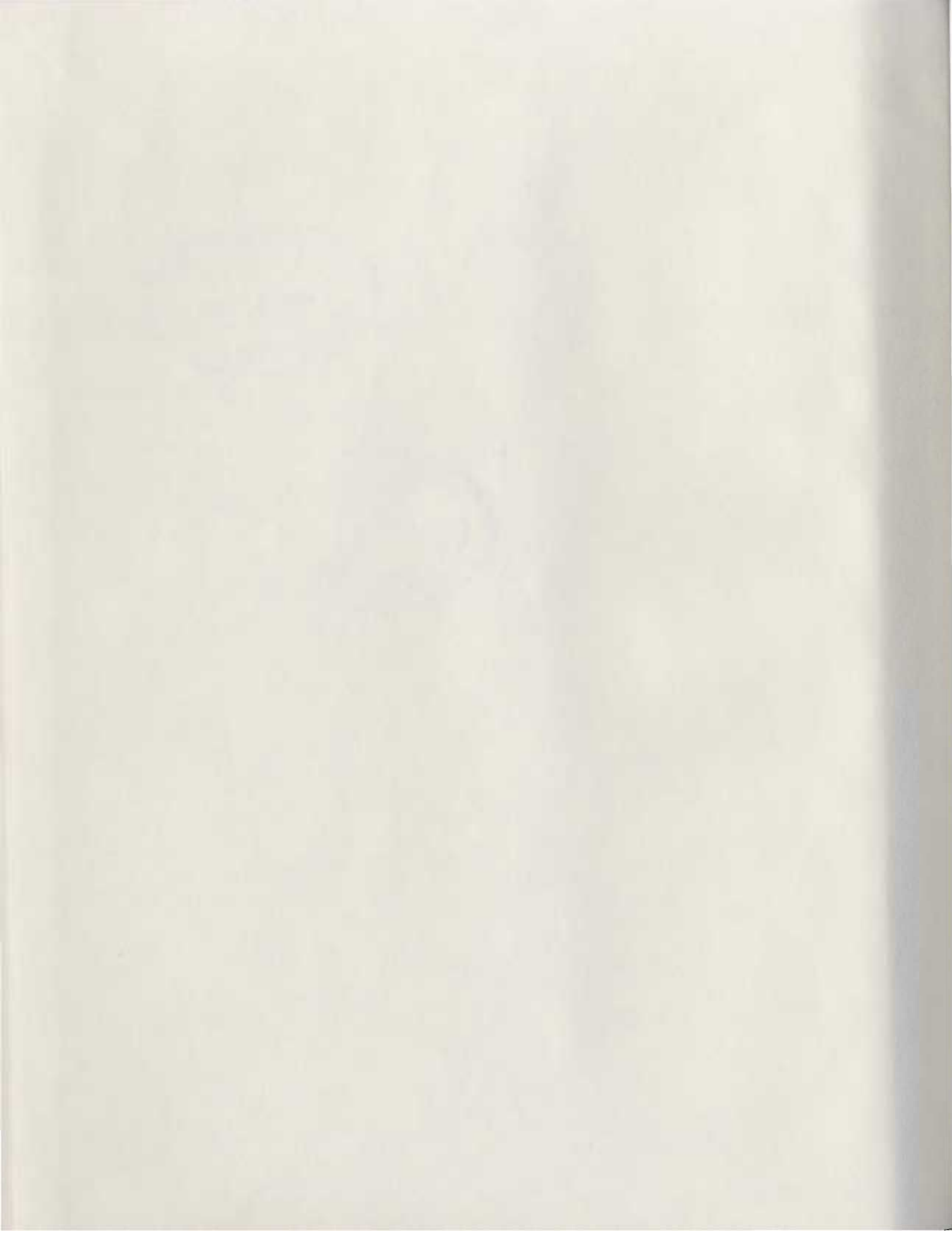
**(Without Author's Permission)**

**AMITABHA GANGOPADHYAY**



C07573







## CANADIAN THESES ON MICROFICHE

I.S.B.N.

## THESES CANADIENNES SUR MICROFICHE



National Library of Canada  
Collections Development Branch

Canadian Theses on  
Microfiche Service

Ottawa, Canada  
K1A 0N4

Bibliothèque nationale du Canada  
Direction du développement des collections

Service des thèses canadiennes  
sur microfiche

### NOTICE

The quality of this microfiche is heavily dependent upon the quality of the original thesis submitted for microfilming. Every effort has been made to ensure the highest quality of reproduction possible.

If pages are missing, contact the university which granted the degree.

Some pages may have indistinct print especially if the original pages were typed with a poor typewriter ribbon or if the university sent us a poor photocopy.

Previously copyrighted materials (journal articles, published tests, etc.) are not filmed.

Reproduction in full or in part of this film is governed by the Canadian Copyright Act, R.S.C. 1970, c. C-30. Please read the authorization forms which accompany this thesis.

THIS DISSERTATION  
HAS BEEN MICROFILMED  
EXACTLY AS RECEIVED

### AVIS

La qualité de cette microfiche dépend grandement de la qualité de la thèse soumise au microfilmage. Nous avons tout fait pour assurer une qualité supérieure de reproduction.

S'il manque des pages, veuillez communiquer avec l'université qui a conféré le grade.

La qualité d'impression de certaines pages peut laisser à désirer, surtout si les pages originales ont été dactylographiées à l'aide d'un ruban usé ou si l'université nous a fait parvenir une photocopie de mauvaise qualité.

Les documents qui font déjà l'objet d'un droit d'auteur (articles de revue, examens publiés, etc.) ne sont pas microfilmés.

La reproduction, même partielle, de ce microfilm est soumise à la Loi canadienne sur le droit d'auteur, SRC 1970, c. C-30. Veuillez prendre connaissance des formules d'autorisation qui accompagnent cette thèse.

LA THÈSE A ÉTÉ  
MICROFILMÉE TELLE QUE  
NOUS L'AVONS REÇUE

AN ANALYSIS FOR DIGITAL PROTECTION  
OF TRANSFORMERS

BY

• Amitabha Gangopadhyay

A thesis submitted in partial fulfilment  
of the requirements for the degree of  
Master of Engineering

Faculty of Engineering and Applied Sciences  
Memorial University of Newfoundland

July 1984

St. John's

Newfoundland

Canada A1B 3X5

ABSTRACT

This thesis presents an analysis for digital differential protection of transformers. For digital differential protection of transformers, it is of utmost importance to test the algorithms on simulated data of both fault and magnetizing inrush currents. For this purpose, a detailed analysis of inrush current for both single and three-phased transformers are carried out. Computer software package programs are developed to simulate the inrush and fault currents. Measured waveforms of the inrushes are compared with the simulated waveforms and the harmonic contents of both the measured and simulated waveforms are analysed up to 4 cycles. There exists a reasonably good agreement between simulated and measured waves.

Three algorithms are analysed for the digital differential protection purpose. Discrete Fourier technique has been used as the reference algorithm. Rectangular transform and Walsh function are analysed in detail for their suitability in microprocessor applications for both 16 and 8 samples/cycle basis. Their performances are compared with Discrete Fourier on 16 samples/cycle basis. Rectangular transform and Walsh function are tested on simulated inrush and fault current data under various switching conditions. It is found that the Rectangular transform converges more rapidly than the other transforms during a fault in the

transformer. Finally, on-line implementation of this new digital relay is suggested in near future.



ACKNOWLEDGEMENTS

The author would like to express his deep gratitude to his supervisor, Professor M. A. Rahman for his necessary guidance and valuable suggestions during the entire period of this work.

The author is grateful to Dr. P. K. Dash, the visiting professor for his close guidance and encouragement at the initial stage of this work.

The author is also thankful to Mr. Dwight House for his assistance in Fourier Analysis.

The author would like to thank Levinia Vatcher for typing this thesis.

The financial support received from the Memorial University, is gratefully acknowledged.

TABLE OF CONTENTS

	Page
ABSTRACT	ii
ACKNOWLEDGEMENTS	iv
TABLE OF CONTENTS	v
LIST OF TABLES	viii
LIST OF FIGURES	ix
NOMENCLATURE	xix

## CHAPTER 1

INTRODUCTION	1
1.1 The Role of Protective Relaying and Digital Computers for Power System Protection	1
1.2 Microprocessor Based Protection	4
1.3 Expected Benefits of a Digital Protection System	6
1.4 Transformer Protection by Digital Relay	9
1.5 Objective of this Thesis	16
1.6 Outline of this Thesis	17

## CHAPTER 2

PRINCIPLES OF DIFFERENTIAL RELAYING	19
2.1 Conventional Current Balance Relays	19
2.2 Differential Protection of Transformers	21
2.3 Differential Scheme for Three Phase Transformers	26
2.4 Differential Relays with Harmonic Restraint	28
2.5 Concepts of Digital Relaying	31
2.6 Sampling Rate	36
2.7 Digital Differential Protection of Transformers	38

	<u>Page</u>
CHAPTER 3	
MAGNETIZING INRUSH PHENOMENA FOR SINGLE AND THREE-PHASE TRANSFORMERS	44
3.1 Magnetizing Inrush Current in Single-phase Transformers	44
3.1.1 Inrush Phenomena	44
3.1.2 Analysis of Magnetizing Inrush for Single-phase Transformers	56
3.2 Magnetizing Inrush Current in 3-phase Transformer Banks	67
3.2.1 Inrush Phenomena	67
3.2.2 Analysis of 3-phase Inrushes	75
3.2.3 Analysis Taking Into Account the Mutual Inductive Couplings	81
3.3 Experimental Results and Computer Simulations	91
3.3.1 Single-phase Case	91
3.3.2 Three-phase Cases	134
3.4 Discussion on Application of Simulated Results	161
CHAPTER 4	
ALGORITHMS FOR TRANSFORMER PROTECTION	176
4.1 Classification of Algorithms	176
4.2 Discrete Fourier Transform Technique	177
4.3 Rectangular Transform Technique	193
4.4 Walsh Function Technique	218
4.5 Comparative Analysis of Algorithms	230
CHAPTER 5	
SUMMARY AND CONCLUSIONS	251
5.1 Conclusions	251
5.2 Scope of Future Works	257

## APPENDIX A

INTERNAL CONNECTION DIAGRAMS FOR STANDARD PERCENTAGE BIASED DIFFERENTIAL RELAY	260
---	-----

## APPENDIX B

DEVELOPMENT OF MAGNETIZING INRUSH EQUATIONS FOR SINGLE AND THREE-PHASE TRANSFORMERS	262
--	-----

B.1 Development of Magnetizing Inrush Equations For a Single-phase Transformer	262
---	-----

B.2 Development of Magnetizing Inrush Equations for a Y-Δ Transformer	272
--	-----

B.3 Development of Magnetizing Inrush Equations for 3-phase Transformers Considering Mutual Inductive Couplings	277
---	-----

## APPENDIX C

VARIATION OF FLUX IN THREE-PHASE TRANSFORMERS	283
---	-----

C.1 Variation of Flux Phenomena	283
---------------------------------	-----

C.2 Derivation	285
----------------	-----

## APPENDIX D

WALSH FUNCTION WITH SAMPLING RATES OF 16 & 8 SAMPLES/CYCLE	291
---	-----

D.1 16 Samples/cycle	291
----------------------	-----

D.2 8 Samples/cycle	297
---------------------	-----

REFERENCES	300
------------	-----



LIST OF TABLES

No.	DESCRIPTION	Page
3.1	Comparison of measured and simulated positive inrush current peaks in a single-phase transformer	168
3.2	Comparison of positive current peaks and conduction angles of measured and simulated inrush currents in a single-phase transformer.	169
3.3	Comparison of current peaks and conduction angles of measured and simulated inrush currents in a single-phase transformer.	170
3.4	Comparison of harmonics in measured and simulated inrush waveforms in a single-phase transformer	171
3.5	A three-phase transformer parameters under different mode of connections	172
3.6	Comparison of measured and simulated inrush current peaks in all three-phases of a Y- $\Delta$ transformer energized from Y-side	173
3.7	Comparison of harmonics in measured and simulated inrush waveforms in all three phases of a Y- $\Delta$ transformer energized from Y-side	174
3.8	Comparison of measured and simulated inrush current peaks in all three phases of a $\Delta$ -Y transformer energized from $\Delta$ -side	175
4.1	Comparison of convergence times of algorithms in case of a symmetrical fault	249
4.2	Comparison of convergence times of algorithms in case of an asymmetrical fault (fault initiation angle = 0°)	250

LIST OF FIGURES

No.	DESCRIPTION	Page
2.1(a)	A balanced-beam type of current-balance relay	20
(b)	Operating characteristic of a current-balance relay	20
2.2	A two-element current-balance relay	22
2.3	Current differential relaying	23
(a)	Internal Fault condition	23
(b)	Through Fault condition	23
2.4(a)	Basic circuit connection for biased differential protection	25
(b)	Biased relay characteristic illustrating performance under internal and external faults	25
2.5	Percentage biased differential protection	29
2.6	Functional block diagram of a digital relay	33
2.7	Illustration of converting an analog signal to digital form	37
2.8	Illustration of Frequency Folding	39
2.9	Illustration of Aliasing Effect	39
2.10	Schematic diagram of digital differential protection of single-phase transformer	40
2.11	Schematic diagram of digital differential protection of three-phase transformers	42
3.1	Effect of switching angle & residual flux	45
(a)	Switched on at $90^\circ$ of voltage wave	45
(b)	Switched on at $0^\circ$ of voltage wave	45
(c)	Effect of residual flux	47
3.2	(a) Effect of Positive Residual Flux	48
	(b) Successive Switching by Point-on-wave Switch	48

No.	DESCRIPTION	Page
3.3	Voltage, flux and current during a magnetizing inrush	50
3.4(a)	Derivation of magnetizing inrush current from excitation characteristic	52
(b)	Effect of residual flux on inrush current shape with former equal to saturation density	53
(c)	Effect of residual flux on inrush current shape with former less than the saturation density	53
(d)	Inrush phenomena with different residual flux levels and switching angles	55
3.5(a)	Phasor diagram of magnetizing current (assuming it to be a vector quantity)	57
(b)	Equivalent diagram of single phase transformer under no load condition	57
(c)	Magnetizing current circuit under core saturated condition.	57
3.6(a)	Switching at $\lambda=0^\circ$	60
(b)	Switching at $\lambda=180^\circ$	63
(c)	Switching at an arbitrary angle $\lambda$	66
3.7	Transient fluxes and inrush currents in a 3-phase transformer energized at $90^\circ$ of V	70
	(a) a-phase conditions	70
	(b) b-phase conditions	70
	(c) c-phase conditions	70
3.8	Instantaneous current directions for transformer <u>a</u> experiencing an inrush	72
3.9	Typical inrush currents of a Y- $\Delta$ transformer energized from Y-side	74
3.10	Typical inrush currents of a $\Delta$ -Y transformer energized from $\Delta$ -side	76

No.	DESCRIPTION	Page
3.11(a)	Equivalent diagram for phase a transformer	78
(b)	A Y-Δ connected bank with source impedance on Y-side	78
3.12	Diagram of a 3-phase, 3-limb transformer showing assumed flux paths and reference directions	82
3.13	Circuit diagram of single-phase point-on-wave switch	93
3.14(a)	Switching at $\lambda=0^\circ$ (applied voltage inverted)	94
(b)	Positive Inrush	94
3.15	Positive inrush at same $\lambda=0^\circ$	95
3.16(a)	Switching at $\lambda=180^\circ$ (applied voltage inverted)	96
(b)	Negative Inrush	96
3.17	Flow chart of program for calculating various parameters of transformer under switching transient	99
3.18	Flow chart of program for digital simulation of single-phase inrush	100
3.19(a)	Recorded waveform of a positive inrush current in a single-phase transformer	103
(b)	Digital simulation of positive inrush current shown in (a)	104
3.20(a)	Recorded waveform of a positive inrush at ( $\lambda=0^\circ$ )	105
(b)	Simulation of inrush current shown in (a) for the first four cycles	106
3.21(a)	Recorded waveform of a negative inrush ( $\lambda=180^\circ$ )	107
(b)	Simulation of inrush current shown in (b) for the first four cycles	108



No.	DESCRIPTION	Page
3.21(c)	Amplified 1st cycle of inrush current shown in (a)	109
(d)	Amplified 2nd cycle of inrush current shown in (a)	110
(e)	Amplified 3rd cycle of inrush current shown in (a)	111
(f)	Amplified 4th cycle of inrush current shown in (a)	112
3.22(a)	Simulation of negative inrush reproduced from Fourier Analyzer	113
(b)	Amplified 1st cycle of inrush current shown in (a)	114
(c)	Amplified 2nd cycle of inrush current shown in (a)	115
(d)	Amplified 3rd cycle of inrush current shown in (a)	116
(e)	Amplified 4th cycle of inrush current shown in (a)	117
3.23(a)	Continuous frequency spectrum of 1st cycle of inrush shown in Fig. 3.21(c)	118
(b)	Discrete frequency spectrum of 1st cycle of inrush shown in Fig. 3.21(c)	119
(c)	Continuous frequency spectrum of 2nd cycle of inrush shown in Fig. 3.21(d)	120
(d)	Discrete frequency spectrum of 2nd cycle of inrush shown in Fig. 3.21(d)	121
(e)	Continuous frequency spectrum of 3rd cycle of inrush shown in Fig. 3.21(e)	122
(f)	Discrete frequency spectrum of 3rd cycle of inrush shown in Fig. 3.21(e)	123
(g)	Continuous frequency spectrum of 4th cycle of inrush shown in Fig. 3.21(f)	124

No.	DESCRIPTION	Page
3.23(h)	Discrete frequency spectrum of 4th cycle of inrush shown in Fig. 3.21(f)	125
3.24(a)	Continuous Frequency Spectrum of 1st Cycle of inrush shown in Fig. 3.22(b)	126
(b)	Discrete frequency spectrum of 1st cycle of inrush shown in Fig. 3.22(b)	126a
(c)	Continuous frequency spectrum of 2nd cycle of inrush shown in Fig. 3.22(c)	127
(d)	Discrete frequency spectrum of 2nd cycle of inrush shown in Fig. 3.22(c)	128
(e)	Continuous frequency spectrum of 3rd cycle of inrush shown in Fig. 3.22(d)	129
(f)	Discrete frequency spectrum of 3rd cycle of inrush shown in Fig. 3.22(d)	130
(g)	Continuous frequency spectrum of 4th cycle of inrush shown in Fig. 3.22(e)	131
(h)	Discrete frequency spectrum of 4th cycle of inrush shown in Fig. 3.22(e)	132
3.25	Flow chart of the program for simulation of oscillatory inrush in Y-Δ transformer.	137
3.26(a)	Recorded waveform of phase-a inrush of a Y-Δ transformer energized from Y-side ( $\lambda=0^\circ$ )	138
(b)	Recorded waveform of phase-b inrush of a Y-Δ transformer energized from Y-side	139
(c)	Recorded waveform of phase-c inrush of a Y-Δ transformer energized from Y-side	140
3.27(a)	Simulation of phase-a inrush shown in Fig. 3.26(a)	141
(b)	Simulation of phase-b inrush shown in Fig. 3.26(b)	142
(c)	Simulation of phase-c inrush shown in Fig. 3.26(c)	143

No.	DESCRIPTION	Page
3.28(a)	Simulation of Fig. 3.27(a) reproduced from Fourier Analyzer	144
(b)	Simulation of Fig. 3.27(b) reproduced from Fourier Analyzer	145
(c)	Simulation of Fig. 3.27(c) reproduced from Fourier Analyzer	146
3.29(a)	Discrete frequency spectrum of 1st cycle of inrush shown in Fig. 3.26(a)	147
(b)	Discrete frequency spectrum of 1st cycle of inrush shown in Fig. 3.26(b)	148
(c)	Discrete frequency spectrum of 1st cycle of inrush shown in Fig. 3.26(c)	149
3.30(a)	Discrete frequency spectrum of 1st cycle of inrush shown in Fig. 3.27(a)	150
(b)	Discrete frequency spectrum of 1st cycle of inrush shown in Fig. 3.28(b)	151
(c)	Discrete frequency spectrum of 1st-cycle of inrush shown in Fig. 3.28(c)	152
3.31(a)	Amplified 1st cycle of inrush current in phase-a shown in Fig. 3.26(a)	153
(b)	Amplified 1st-cycle of inrush current in phase-b shown in Fig. 3.26(b)	154
(c)	Amplified 1st cycle of inrush current in phase-c shown in Fig. 3.26(c)	155
3.32(a)	Amplified 1st cycle of inrush current in phase-a shown in Fig. 3.28(a)	156
(b)	Amplified 1st cycle of inrush current in phase-b shown in Fig. 3.28(b)	157
(c)	Amplified 1st cycle of inrush current in phase-c shown in Fig. 3.28(c)	158
3.33	Flow chart of programming three-phase inrush currents by mutual inductive coupling method	160

No.	DESCRIPTION	Page
3.34(a)	Recorded waveforms of phase-a inrush of a $\Delta$ -Y transformer energized from $\Delta$ -side ( $\lambda=0^\circ$ )	162
(b)	Recorded waveform of phase-b inrush of a $\Delta$ -Y transformer energized from $\Delta$ -side	163
(c)	Recorded waveform of phase-c inrush of a $\Delta$ -Y transformer energized from $\Delta$ -side	164
3.35(a)	Simulation of phase-a inrush shown in Fig. 3.34(a)	165
(b)	Simulation of phase-b inrush shown in Fig. 3.34(b)	166
(c)	Simulation of phase-c inrush shown in Fig. 3.34(c)	167
4.1	Flow chart of programming logic of digital differential relay by Discrete Fourier algorithm	183
4.2(a)	Performance of Discrete Fourier algorithm with 16 samples/cycle during inrush in phase-a of a Y- $\Delta$ transformer	185
(b)	Performance of Discrete Fourier algorithm with 16 samples/cycle inrush in phase-b of a Y- $\Delta$ transformer	186
(c)	Performance of Discrete Fourier algorithm with 16 samples/cycle during inrush in phase-c of a Y- $\Delta$ transformer	187
4.3(a)	Performance of Discrete Fourier algorithm with 16 samples/cycle during an internal fault (fault initiation angle - $0^\circ$ )	188
(b)	Performance of Discrete Fourier algorithm with 16 samples/cycle during an internal fault (fault initiation angle - $90^\circ$ )	189
(c)	Performance of Discrete Fourier algorithm with 16 samples/cycle during an internal fault (fault initiation angle - $180^\circ$ )	190
4.4	Performance of Discrete Fourier algorithm with 16 samples/ cycle during an assymetrical internal fault (fault initiation angle - $0^\circ$ )	192



No.	DESCRIPTION	Page
4.5	Flow chart of programming logic of digital differential relay by Rectangular Transform	201
4.6(a)	Performance of Rectangular Transform algorithm with 16 samples/cycle during inrush in phase-a of a Y- $\Delta$ transformer	204
(b)	Performance of Rectangular Transform algorithm with 16 samples/cycle in phase-b of a Y- $\Delta$ transformer	205
(c)	Performance of Rectangular Transform algorithm with 16 Samples/cycle inrush in phase-c of a Y- $\Delta$ transformer	206
4.7(a)	Performance of Rectangular Transform algorithm with 16 samples/cycle during an internal fault (fault initiation angle $-0^\circ$ )	207
(b)	Performance of Rectangular Transform algorithm with 16 samples/cycle during an internal fault (fault initiation angle $-90^\circ$ )	208
(c)	Performance of Rectangular Transform algorithm with 16 samples/cycle during an internal fault (fault initiation angle $-180^\circ$ )	209
4.8	Performance of Rectangular Transform algorithm with 16 samples/cycle during an assymetrical internal fault (fault initiation angle $-0^\circ$ )	210
4.9(a)	Performance of Rectangular Transform algorithm with 8 samples/cycle during inrush in phase-a of a Y- $\Delta$ transformer	211
(b)	Performance of Rectangular Transform algorithm with 8 samples/cycle during inrush in phase-b of a Y- $\Delta$ transformer	212
(c)	Performance of Rectangular Transform algorithm with 8 samples/cycle during inrush in phase-c of a Y- $\Delta$ transformer	213
4.10(a)	Performance of Rectangular Transform algorithm with 8 samples/cycle during an internal fault (fault initiation angle $-0^\circ$ )	214

No.	DESCRIPTION	Page
4.10(b)	Performance of Rectangular algorithm with 8 samples/cycle during an internal fault (fault initiation angle - $90^\circ$ )	215
(c)	Performance of Rectangular Transform algorithm with 8 samples/cycle during an internal fault (fault initiation angle - $180^\circ$ )	216
4.11	Performance of Rectangular Transform algorithm with 8 samples/cycle during an assymetrical internal fault (fault initiation angle $0^\circ$ )	217
4.12	The first eight Walsh functions of integral index k for $0 \leq t \leq 1$	220
4.13	The first sixteen Walsh Functions of integral index k	221
4.14	Flowchart of programming logic of digital differential relay by Walsh function algorithm	228
4.15(a)	Performance of Walsh function algorithm with 16 samples/cycle during inrush in phase-a of a Y- $\Delta$ transformer	231
(b)	Performance of Walsh function algorithm with 16 samples/cycle during inrush in phase-b of a Y- $\Delta$ transformer	232
(c)	Performance of Walsh function algorithm with 16 samples/cycle during inrush in phase-c of a Y- $\Delta$ transformer.	233
4.16(a)	Performance of Walsh function algorithm with 16 samples/cycle during an internal fault (fault inititaion angle - $0^\circ$ )	234
(b)	Performance of Walsh function algorithm with 16 samples/cycle during an internal fault (fault initiation angle - $90^\circ$ )	235
(c)	Performance of Walsh function algorithm with 16 samples/cycle during an internal fault (fault initiation angle - $180^\circ$ )	236
4.17	Performance of Walsh function algorithm with 16 samples/cycle during an assymetrical internal fault (fault initiation angle - $0^\circ$ )	237

No.	DESCRIPTION	Page
4.18(a)	Performance of Walsh function algorithm with 8 samples/cycle during inrush in phase-a of a Y-Δ transformer	238
4.18(b)	Performance of Walsh function algorithm with 8 samples/cycle during inrush in phase-b of a Y-Δ transformer	239
4.18(c)	Performance of Walsh function algorithm with 8 samples/cycle during inrush in phase-c of a Y-Δ transformer	240
4.19(a)	Performance of Walsh function algorithm with 8-samples/cycle during an internal fault (fault initiation angle - 0°)	241
4.19(b)	Performance of Walsh function algorithm with 8 samples/cycle during an internal fault (fault initiation angle - 90°)	242
4.19(c)	Performance of Walsh function algorithm with 8 samples/cycle during an internal fault (fault initiation angle - 180°)	243
4.20	Performance of Walsh function algorithm with 8 samples/cycle during an assymetrical fault (fault initiation angle - 0°)	244
A.1	Internal connections for GE make harmonic restraint percentage biased differential relay type BDD15B	260
A.2	Schematic connections of the Westinghouse make harmonic restraint percentage biased differential relays type HU-1	261

NOMENCLATURE

A	area of the core
B	flux density in the core
$C_k$	rectangular cosine coefficient
$\bar{C}_k$	Fourier cosine coefficient
E	r.m.s. applied voltage
$E_1$	induced primary voltage
e	instantaneous applied voltage
$f_s$	sampling frequency
$f_c$	signal frequency
H	magnetizing field intensity
$I_1$	operating current
$I_2$	restraining current
$I_0$	steady state magnetizing current
$I_{h+e}$	in-phase component of magnetizing current
$I_m$	quadrature component of magnetizing current
$I_{m1}, I_{m2}, I_{m3}$	peak inrush currents
$I_{ma}$	phase-a individual inrush
$I_{mb}$	phase-b individual inrush
$I_{mc}$	phase-c individual inrush
$I_a$	phase-a total inrush
$I_b$	phase-b total inrush
$I_c$	phase-c total inrush
$I_d$	reflected inrush current in $\Delta$ -winding of Y- $\Delta$ transformer
l	length of conductor

xx

$L_s$	source inductance
$L_t$	leakage inductance of coil
$L$	total series inductance
$M_1 \dots M_g$	mutual inductive coupling between transformer limb sections
$N$	number of coil turns
$N_0$	operating coil turns
$N_r$	restraining coil turns
$p$	differential operator $\frac{d}{dt}$
$r_m$	transformer core resistance
$R_s$	circuit resistance
$R_t$	transformer coil resistance
$R$	total series resistance
$S_k^*$	Fourier sine coefficient
$S_k$	rectangular sine coefficient
$V_1$	applied primary voltage
$W_k$	Walsh coefficient
$X(j)$	current samples
$X_m$	transformer core reactance
$Z_p$	primary leakage impedance
$Z_{ss}$	secondary leakage impedance
$Z_{os}$	zero sequence impedance of system
$Z_s$	positive and negative sequence impedance of system
$\alpha$	extinction angle
$\beta$	angle of maximum inrush
$\gamma$	conduction angle

$\theta_s$	saturation angle
$\delta(i, j)$	Kronecker delta
$\phi_m$	peak flux
$\phi_R$	residual flux
$\phi_1 \dots \phi_8$	fluxes associated in core-limb
$\lambda$	switching angle
$\mu$	permeability of transformer material
$\mu(\tau)$	Moebius function
$\omega$	angular frequency

## CHAPTER 1

### INTRODUCTION

#### 1.1 The Role of Protective Relaying and Digital Computers for Power System Protection

The history of electrical power technology throughout the world is one of steady and, in recent years, rapid progress, which has made it possible to design and construct economic and reliable power systems, capable of satisfying the continuing growth in the demand for electrical energy. In this, power system protection and control play a significant part, and progress in design and development in these fields has necessarily had to keep pace with advances in the design of primary plant, such as generators, transformers, switchgears, overhead lines and underground cables. Indeed, progress in the field of protection and control is a vital prerequisite for the efficient operation and continuing development of power supply systems as a whole.

Thus, with the expansion of power system networks and with the increasing urge to go for larger power grids to increase the flexibility of power transmission, the complexity of the system increased more and more. The stability of the system becomes more sensitive as the power flow in the system becomes more complicated and the severity

of power swings increase in cases of abnormal conditions of a system. The role of on-line and off-line digital computers became more prominent to handle normal operation of vast networks. The first successful implementation of digital computer for on-line power system operation and control is the Supervisory Control and Data Acquisition (SCADA) system. Since then, there has been a continuing trend to extend the development of application programs for real-time control systems to encompass all phases of operations including forecasting, scheduling, monitoring, control, security assessment, economic dispatch and stability analysis of a system. Apart from installing a master computer for a central control station, digital computers also started being installed in remote substations with data exchange facilities with computers of other selected substations and the master computer. The concept of protecting the substation equipments by computers instead of conventional relays came with such wide application of digital computers in power systems. It became a field of interest to see that apart from the on-line supervisory and related functions of a sub-station computer, whether it is possible to employ it for protection purpose. And naturally, the early researches were carried out on the protection of incoming and outgoing feeders of a substation, rather than the protection of individual elements of the power system, like generators,



transformers and transmission and distribution lines etc. It is worthwhile to comment briefly on the scope of early researches.

The detailed scheme of fault protection by using a stored-program digital computer was first introduced by Rockefeller in a very well-written paper [29]. Though not much attention was given to hardware or programming aspects, the feasibility of protecting all the equipments in a EHV substation and the transmission lines coming out of it has been dealt with in detail. The paper goes into substantial detail of the relaying program organizations and clearly recognizes the problems associated with such a protective scheme using process control computers available at that time. In two papers [20,21], Mann and Morrison presented algorithms for the protection of transmission lines with a digital computer. They proposed complete computer programs and the need of the specific hardware for the implementation of those program. A feasibility study for both primary and back up protection using digital computer was presented by Cheetham [6,7].

The first digital computer relay that was in practice was again for distance protection of transmission lines and was developed as a joint project of Pacific Gas and Electric Corporation [14,30]. The system, called Prodar-70, was used to monitor a 230 KV line. A Westinghouse P-2000

digital computer was the heart of this system which performed phase and ground distance protections. Considerable field experience was gained in that project.

Since then, the topic of computer relaying, in general, has been the subject of extensive research and a number of digital computer relaying systems were proposed [8]. The heart of computer relaying for any type of protection is the algorithm that is being used. The algorithm's output forms a basis for the relaying decisions. In the case of a distance relay, the algorithm determines the apparent impedance of the transmission line from the relay location. In case of transformer protection, which is the subject of this thesis, the algorithm distinguishes the magnetizing inrush from the actual fault current of a transformer. An overview on the digital protection of transformers will be discussed in section 1.4. The essence of the computer relaying is that, its approach being highly mathematical, new ideas and approaches are evolving to solve the relaying problems. The algorithms for the transformer protection are reviewed in detail later on.

## 1.2 Microprocessor Based Protection

Computer relaying started in the era of minicomputers. Some early works mentioned above considered the use of a central substation computer that would handle

all the station relaying. Based on the hardware available at that time, it was logical to consider this as one possible approach. Now, however, with increasingly developing microprocessor and Large Scale Integration (LSI) technology, special attention is directed towards development trends in the protection field, where decentralized microprocessor applications seem to be the viable solution to cope with the increasingly stringent requirements for electric power supply reliability. With this approach, the central substation computer would be relegated mostly to non-relaying functions and an intermediate link between microprocessors and the central system operation computer complex. With steady decrease in costs of various chips and more developing technology, the microprocessors are becoming more popular now-a-days. The distinction between mini and micro computers seems to become less obvious as time goes on. The protection concept has also changed rapidly to utilize the microprocessors of present day. Apart from the advantage of cost, the relaying operations can be carried out more independently by several processors. The basic disadvantage of the microprocessor based protection scheme is the inability to take high computational burden. Sometimes, to simplify computation by arithmetic shift operation, the microprocessor takes more time to calculate the fault and gives delayed signal to circuit-breaker to trip. If it is

so, then the main objective to computer relaying is lost. To reduce the computational burden, new algorithms are formulated for faster computations. Also, hierarchical methods are proposed so that major calculations are being carried out by on-line or off-line digital computers and microprocessors utilize those off-line data with a minimum calculations. Also, developments in micro computer technology permit one to use co-processors and multi-processors to reduce the computational burden.

### 1.3 Expected Benefits of a Digital Protection System

Considering the amount of research going on in the field of digital relaying, it is worth considering the benefits that one can expect by switching to digital relaying techniques from conventional relaying. The most important advantages of a digital relaying system can be summarized as follows:

(1) Economics: In the long run, economy will be one of the important considerations. The cost of digital hardware has been steadily decreasing. The cost of conventional relaying has increased steadily during the same period. A relaying task that required a \$100,000 minicomputer in 1970, can now be handled by a microcomputer, the cost of which is 10 times lesser than the earlier one. In contrast with this, the cost of most of the conventional

protection system has increased, the amount of increase being dependent on the sophistication involved in any particular relaying system. Furthermore, the digital computer, being a programmable device, can be used to perform multiple functions.

(2) Performance: The complexity of electric power systems requires improved performance in protective relaying schemes. It is naturally expected, that in all cases, the performance of a digital relay will be at least equal to that of its conventional counterpart. The highly accuracy of a computer relay is definitely in comparison to the conventional relays. As far as the speed of the relay is concerned, software and hardware technology in computer research, offers even better speed response than the earlier versions. On the other hand, certain features such as memory action, come more naturally to a digital relay which keeps a digital relay a couple of steps ahead of the corresponding conventional relay.

(3) Reliability: One of the most significant advantages of a digital relay is the fact that the digital computer is continuously active. Consequently, large numbers of self-diagnosis are going on continuously within a digital relay. Additional diagnostic features, such as monitoring of many of its other peripherals, can be easily done. It is, therefore, possible to detect any accidental failure within a

digital relaying system immediately and necessary corrective measures can be taken.

(4) Flexibility: Digital relay is a programmable device. Hence, necessary modification required for a certain change in operating conditions can be made rather easily through a change in the original program. It is also possible to develop a common hardware system that will serve for several relays through different pre-programmed memory modules. This will to some extent reduce the repair and maintenance tasks. Like a reserve busbar of any substation, different channels for the input signals can be reserved for the digital relay, which shall remain unused under normal operating conditions and can be activated only under program control when trouble develops in the normal input paths. This flexibility in the routing of input data can be achieved in a digital relay only.

(5) By products: In a computer based relaying system, several features can be achieved as a natural byproduct of a digital relay which is not possible otherwise. A thorough sequence of event analysis can be furnished by exchanging the post transient data by several relaying computers. In case of transmission line protection, a digital relay can furnish the computed distance to a fault from the source.

#### 1.4 Transformer Protection by Digital Relay

Most of the research carried out so far has been in the field of digital protection of transmission lines and not much attention has been paid for digital protection of transformers.

Rockefeller [29] suggested a procedure for providing transformer differential protection as an integral part of an overall approach to substation protection with a digital computer. He did not approach the problem from the viewpoint of individual microprocessor based protection.

Sykes and Morrison [37] used recursive digital filters in the design of a harmonic restraint transformer differential relay. They tested the proposed scheme on digitized simulated data from magnetizing inrush and fault currents.

Here, the fault detection time was more than 3 cycles on a 60 Hz waveform. Malik, Dash and Hope [19] also proposed a harmonic restraint transformer differential relay but they used a cross-correlation technique to determine the fundamental and second harmonic quantities from the current waveforms which they used as "operating" and "restraining" components respectively. Their approach was tested on simulated data. This algorithm requires the multiplication of incoming current samples by sine and cosine weighting factors. Thus it requires hardware multiplying capabilities in the processor for fast computation. Another recent

algorithm for transformer protection has been presented by Schweitzer, Larson and Flechsig [32] where they used finite impulse response [FIR] filters for differentiating between transformer faults and magnetizing inrush. The approach was basically similar to the method of odd and even square wave correlation suggested by Malik et. al. [19] except that the criterion for discriminating magnetizing inrush conditions from internal faults is different. The FIR algorithm was implemented by Larson et. al. [17] on a Motorola MC 6800 microprocessor for protection of a 500VA transformer. This algorithm has yielded fault detection times varying from 1.25 to 1.5 cycles based on a 60 Hz waveform. Rahman, Dash and Downtown [24] suggested a least square estimation to establish the model coefficients from post fault differential current samples. It yielded fault-time detection in about one cycle based on 12 samples per cycle on a 60 Hz waveform. All the algorithms stated above, use the current differential technique and a software program in a digital computing device. By comparing the algorithms it was found that correlation with a pair of sine and cosine waveforms yields a faster fault detection time.

The major problem in testing any particular algorithm for transformer protection is simulation of data. Unlike distance protection, transformer protection has to deal with single input constraint, i.e. current. It is well



known that it has to differentiate between magnetizing inrush current during energizing of a transformer and fault current. Rockefeller [29] suggested that the magnetizing inrush current can be identified by monitoring the time deviations between successive peaks of the differential current. In a 60 Hz system, successive current peaks are 8 ms apart for an external fault and this is true before CT saturation. On the other hand, two types of waveforms are experienced due to magnetizing inrush; the successive peaks are either 4 ms or 16 ms apart. If the waveforms are 16 ms apart, again the successive peaks are unidirectional. It was, therefore, proposed that appropriate fault currents may be recognized by two successive peaks being 7.5 to 10 ms apart. Also, a requirement was imposed that a peak be 75 to 125 percent of previous peak and of opposite sign. This means that if two successive current peaks are monitored in a 7.5 ms to 10 ms interval with opposite sign, it will be interpreted as a fault current. Sykes and Morrison [37] used a 100 Hz bandpass filter to obtain the second harmonic component of the current waveform and utilized it as "restraining" signal. A 20 ms delay was included in the "operate" path to prevent false tripping on transient filter outputs associated with magnetizing inrush. In this sense, the relay is less efficient and allows more than a cycle time in case of an actual fault. Malik et al. [18] also used the second

harmonic restraint principle by cross-correlating the input currents with sine-cosine functions as well as with odd and even square waveforms. Internal faults and magnetizing currents were simulated numerically assuming that the ratios of saturation to magnetizing flux densities ( $B_s/B_m$ ), residual to magnetizing flux densities ( $B_r/B_m$ ) are 2.0 and 0.5 p.u. respectively. The saturated reactance is assumed of the order of 0.25 p.u. The decay rate is chosen with both time constants of 48 ms and 320 ms. Schweitzer et. al. [32] distinguished between the magnetizing current inrush and fault current by taking the ratio of maximum values of each pair of four filter outputs. They found that ratio lies between 0 and 0.146 during internal faults and between 0.334 and 0.586 during magnetizing inrush. They have also tested their proposed algorithm on simulated data of both magnetizing as well as fault currents. Hence, it is important to simulate both types of data correctly before implementing the entire scheme in any microprocessor system. Fault current is basically a sinusoid. Its offset and decaying time are dependent on the nature of the fault. Hence, the simulation of a fault waveform is relatively straightforward. However, the magnetizing inrushes have typical characteristics which depend on several factors. The shape of the magnetizing waveform will vary depending on the point of switching on the voltage waveform. In

case of single phase transformers, these waveforms are unidirectional, the successive peaks occur usually 10 ms apart. Again, for three phase transformers, magnetizing waveforms occur under different conditions. Successive peaks are 4 ms apart in staggered form. Thus, it is important to simulate accurately the magnetizing inrush waveforms. If any algorithm works on a simulated data-train, it is sure enough to say that the algorithm should work in real-life also, obviously considering all the ideal conditions such as no CT saturation, proper interfacing between the microprocessor and the transformer etc.

Though numerous researches [1,5,11,18,33,34,35] have been carried out on the magnetizing inrush phenomena of transformers, not much work has been done to simulate magnetizing inrush currents for digital protection purpose. Blume et. al. [5] explained magnetizing inrush phenomena for mainly single-phase transformers in 1944. His explanation was mainly physical and he provided an analysis to determine the average magnetizing inrush current depending on physical dimension and flux densities in the associated parts of a transformer body. Not much of the analytical treatment was present in the paper. Finzi et. al. [11] presented in 1951 a short analysis for predicting the inrush current where the time integral was solved by expansion of an exponential series. An AIEE committee report [1] was presented in the

same year which is mainly a survey on inrush currents and subsequent behaviour of the system experiencing the inrush. Malfunction of the relays and fuses which protect the transformers, was reported. Means of remedies were suggested in the report. No analytical treatment was covered. Specht [34] presented an analysis of inrush phenomena for single phase transformers and gave an analytical approach to find out the magnetizing inrush current of transformer. He also calculated the inrush of certain transformers and compared those results with actual waveforms. The paper presented an approximate method for solving the problem and later on, in 1969, Specht [35] presented an improved analytical method for predicting the inrush current. Although, his work suffered from the fact that he always considered energizing the transformer at voltage zero initial condition. He did not find out a generalized expression for magnetizing inrush, considering switching at any point of the voltage waveform. Also, to derive the expression of magnetizing current, he has chosen the axes offset by  $180^\circ$  from the voltage zero which was not necessary. Rockefeller et al. [33] also explained the inrush phenomena in 1958 and presented a somewhat different analysis for predicting magnetizing inrush currents in three phase transformer banks. In a recent paper [18], Macfadyen presented a method of calculating the inrush currents of a three phase transformer by solving nine basic

differential and five algebraic equations. No substantial research has been carried out so far to simulate numerically magnetizing inrush utilizing any of the methods stated above. Rahman et al. [24] used a relation to generate magnetizing inrush data which was derived from an expression given by Specht [35] with certain practical assumptions. They generated inrush current data which might be suitable for test purposes of an algorithm, but it is an approximate method and did not generate a true waveform of the inrush current. The harmonic contents of these waveforms were not analysed to show their actual resemblance with any particular waveform from a test transformer. Hence, to summarize this section, the two following basic points may be highlighted which are important for digital protection of transformers.

- 1) The accurate simulation of the magnetizing inrush current data for the off-line testing of any proposed algorithm.

- 2) The development of an algorithm which is fast enough to detect any fault condition of a transformer as well as restrain the relay from maloperation, during a magnetizing surge due to energization. The algorithm must also be simple enough so that, it can be implemented on modern microprocessors without sacrificing much of the computation time.

### 1.5 Objective of This Thesis

The proposed work of this thesis is the analysis, development and comparison of algorithms for transformer protection. The work can be divided in two major parts,

- 1) The magnetizing current phenomena is analyzed.

This has been done both for single phase and three phase transformers. Numerical methods for simulating these waveforms are presented.

- 2) To search for an algorithm which is fast enough but simple enough to implement in the microprocessor system.

Three different algorithms have been analyzed and compared to find their relative suitability. Walsh functions have been tried for the first time for transformer protection. Rectangular transform and Discrete Fourier Transform have been compared with Walsh Function. All these algorithms have been tried considering that the fault has occurred in one of the three-phases.

In all the algorithms, Fourier coefficients were derived for the waveforms. Finally, the fundamental and second harmonic quantities were extracted out of these coefficients. All the proposed algorithms have been tested on a PDP-11/60 minicomputer on off-line basis. To test the algorithms on magnetizing inrush, this phenomena has been thoroughly investigated for an accurate simulation. The

harmonic contents of both the actual and simulated waveforms have been analyzed on a Hewlett-Packard Fourier Analyzer System. An analysis to find out an expression for inrush current for switching at any point of a voltage waveform has been carried out. As was stated in Section 1.4, most of the earlier work on magnetizing inrush suffered from lack of analysis, particularly for switching at any arbitrary point on the voltage waveform. Finally, all these three algorithms have been implemented on an off-line basis, on an IBM Personal micro-computer with Intel-8088 microprocessor and Intel-8087 co-processor to find out the suitability of algorithms in fault-detection time. The last section of work was carried out in group-work.

#### 1.6 Outline of this Thesis

Chapter 2 describes the background of conventional differential relays and principles of their operation. It illustrates the basic operations of digital relays. It also gives a brief sketch of the function of various accessories needed with the operation of digital relays. Chapter 3 describes the magnetizing current phenomena for both single phase and three phase transformers. A detailed analysis and the methods of numerical simulation of magnetizing inrushes are presented.

The algorithms for digital differential relays are

described in Chapter 4. Three different algorithms are considered and are tested on simulated inrush and fault currents. Various conditions of inrush and faults are considered.

Chapter 5 contains the conclusion and suggestions for future research.



## CHAPTER 2

PRINCIPLES OF DIFFERENTIAL RELAYING2.1 Conventional Current Balance Relays

When it is desired to distinguish between two currents  $I_1$  and  $I_2$  in a circuit, the normal practice is to use one current as operating and the other one as a restraining quantity. Depending on the variation on the magnitude of one over the other, the operating or the restraining elements are actuated. An early developed "balanced-beam" electromagnetic attraction type relay structure is schematically shown in Fig. 2.1(a). It has one overcurrent element arranged to produce torque in opposition to another overcurrent element, both elements acting on the same moving structure.

If the negative-torque effect of the control spring is neglected, the torque equation of the relay is given by,

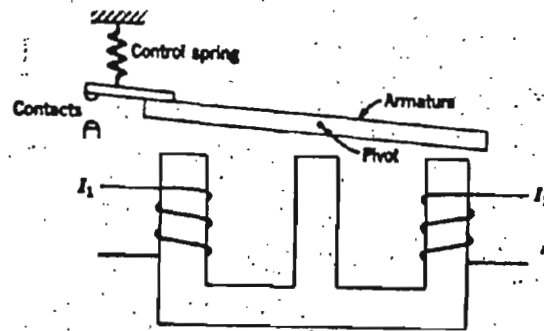
$$T = K_1 I_1^2 - K_2 I_2^2 \quad (2.1)$$

When the relay is on the verge of operation, the net torque is zero, and

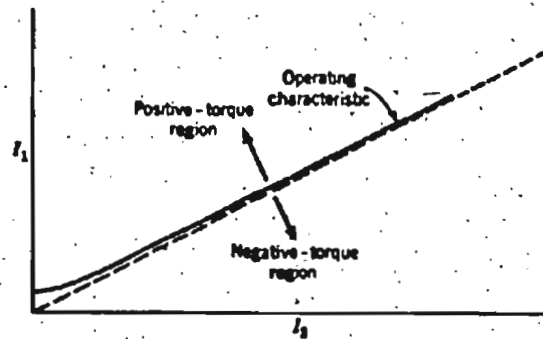
$$K_1 I_1^2 = K_2 I_2^2 \quad (2.2)$$

Therefore, the operating characteristic is,

$$\frac{I_1}{I_2} = \sqrt{\left(\frac{K_2}{K_1}\right)} = \text{constant} \quad (2.3)$$



(a)



(b)

Fig. 2.1 (a) A balanced-beam type of current-balance relay

(b) Operating characteristic of a current-balance relay (22)

The operating characteristic of the relay, including the effect of the control spring is shown in Fig. 2.1(b). Here,  $I_1$  is called the "operating" current, since it produces positive or pick up torque;  $I_2$  is called the "restraining" current.

Should it be desired to close a contact circuit when either of the two currents exceeds the other by a given percentage, two elements are used, as illustrated schematically in Fig. 2.2. For some applications, the contacts of the two elements may be arranged to trip different circuit breakers, depending on which element operates.

## 2.2 Differential Protection of Transformers

A transformer can be protected by a differential arrangement which also operates on a current balance principle. The principle of current comparator for a differential scheme is similar to that of an electromagnetic relay type as described in section 2.1. It also operates on the basis of "operating" and "restraining" quantities.

The restraining and operating principles of the differential relay are illustrated in Fig. 2.3(a) and (b) for internal and external or through faults respectively. For external faults, the difference of the C.T. secondary currents  $I_1 - I_2$  is ideally zero. Hence ideally, no current

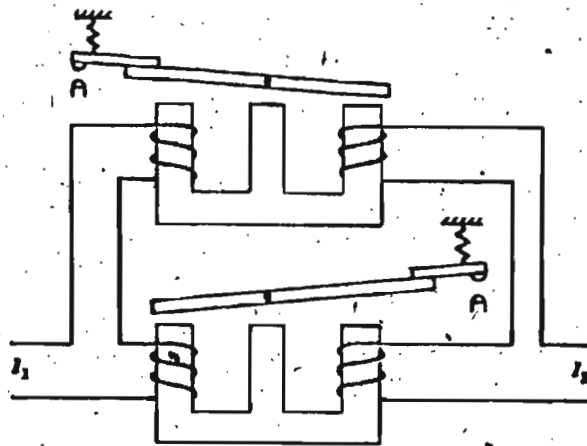
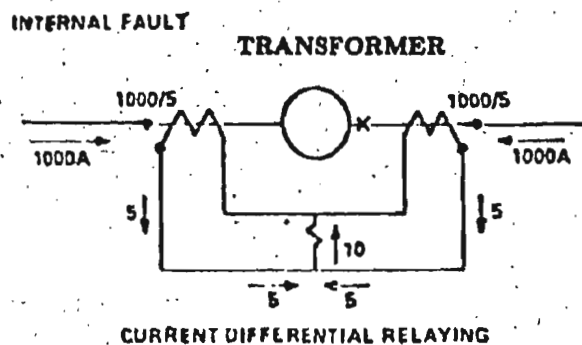
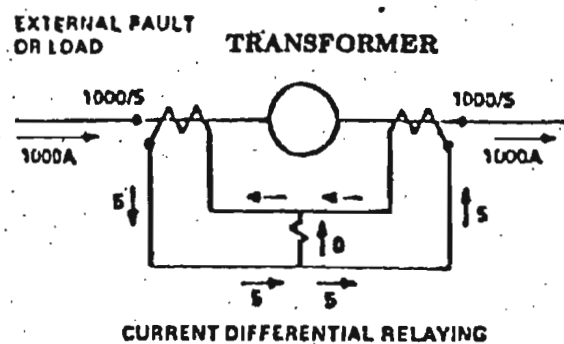


Fig. 2.2 A two-element current-balance relay(22)



(a)



(b)

Fig. 2.3 Current differential relaying  
 (a) Internal Fault condition  
 (b) Through Fault condition

flows through the operating coil of the relay, as shown in Fig. 2.3(b). For an internal fault, the difference  $I_1 - I_2 = 10A$  and the relay operates.

One of the most extensively used form of differential relay is the "percentage differential" type. The advantage of this type of relay is that it is less likely to operate incorrectly due to a C.T. mismatch or C.T. saturation during a through-fault. A bias feature is obtained by circulating the fault or external fault current in an additional winding which exerts a restraining force on the relay armature. The basic circuit connections are shown in Fig. 2.4(a). Usually, no current flows in the operating coil during through-fault conditions, but due to imperfect matching of the current transformers, some spill current may be present. This spill current will flow in the relay operating circuit but will not cause operation unless the relay operating bias setting ratio is exceeded. Thus from Fig. 2.4(a), neglecting control spring effect,

$$\text{Relay operating force} = K(I_1 - I_2)N_o$$

$$\text{Relay restraining force} = K\left(\frac{I_1 + I_2}{2}\right)N_r \quad 2.3(a)$$

where

$K$  = a constant

$N_o$  = operating coil turns

$N_r$  = restraining coil turns.

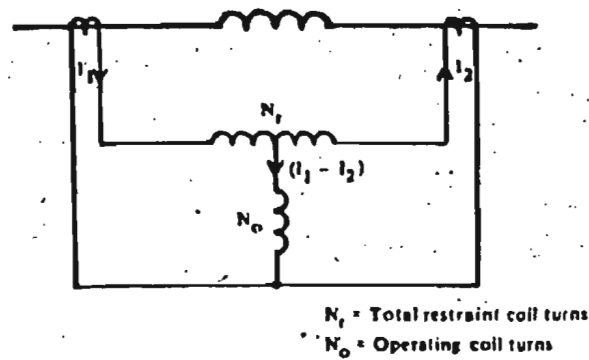


Fig. 2.4 (a) Basic circuit connection for biased differential protection

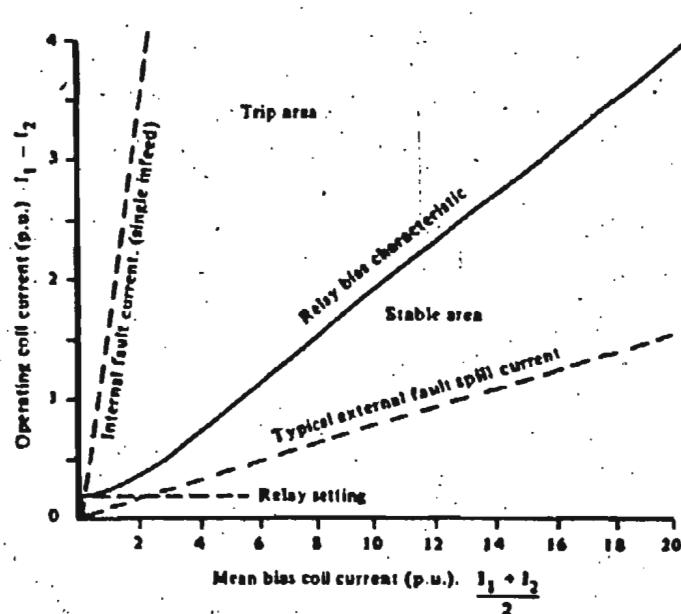


Fig. 2.4 (b) Biased relay characteristic illustrating performance under internal and external faults (39)

When, the relay is on the verge of operation

$$K(I_1 - I_2) N_O = K \left( \frac{I_1 + I_2}{2} \right) N_r \quad (2.4)$$

or

$$\frac{I_1 - I_2}{\frac{I_1 + I_2}{2}} = \frac{N_r}{N_O} \quad (2.5)$$

The Equation (2.5) shows that the characteristic has a slope determined by the ratio  $N_r/N_O$ , and the relay bias is defined as the difference current  $(I_1 - I_2)$  divided by the mean circulating current, which is fundamentally a constant ratio for all current magnitudes. This characteristic is shown in Fig. 2.4(b).

### 2.3 Differential Scheme for Three Phase Transformers

In order to apply this principle to a typical three-phase transformer, a number of conditions have to be satisfied.

(1) Transformer Ratio: The rated currents of the transformer on the primary and secondary sides usually differ in inverse ratio of the corresponding voltages. The current transformers should, therefore, have primary ratings to match the rated currents of the transformer windings to which they are applied.

(2) Transformer Connections: If the transformer is connected in star/delta, balanced three phase



through-current suffers a phase-change of  $30^\circ$ , which must be corrected in the C.T. secondary by appropriate connection of the C.T. secondary windings.

Furthermore, zero sequence current flowing on the star side of the power transformer will not produce current outside the delta on the other side. The zero sequence current must, therefore, be eliminated from the star side, by connecting the current transformers in delta, from which it follows that the current transformers on the delta side of the transformer must be connected in star, in order to give the  $30^\circ$  phase shift. This is a general rule, if the transformer are connected star/star, the current transformers on both sides would need to be connected in delta. When current transformers are connected in delta, their secondary ratings must be reduced to  $1/\sqrt{3}$  times the secondary rating of star connected current transformers. This is done so that the currents outside the delta may balance with the secondary currents of the star connected current transformers.

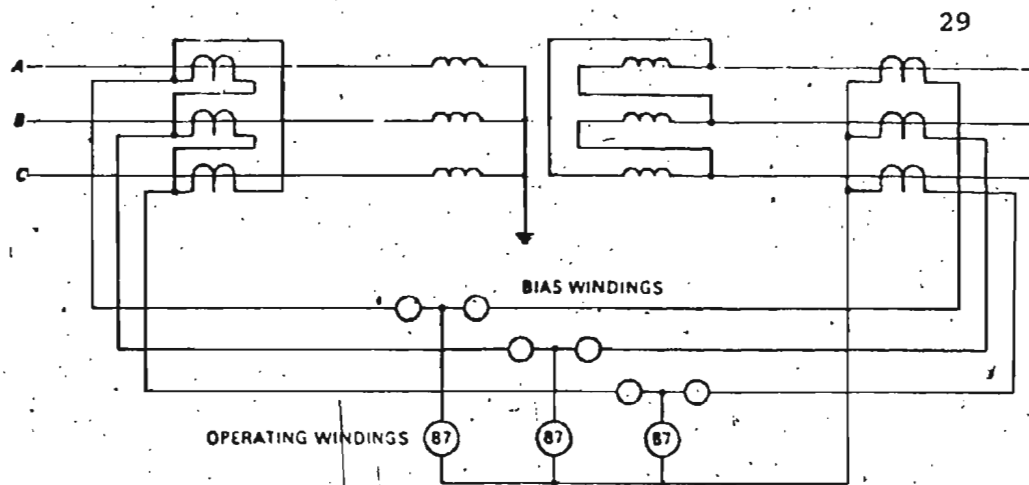
(3) Tap Changing Facility: If the transformer has a tapping range enabling its ratio to be varied, this must be taken care in the differential relay system. This is because, if the current transformers are chosen to balance for the mean ratio of the power transformer, a variation in ratio from the mean will create an unbalance proportional to the ratio change. Differential protection should be provided

with a proportional bias of an amount which exceeds in effect the maximum ratio deviation. This stabilizes the protection under through-fault conditions while still permitting the system to have good basic sensitivity.

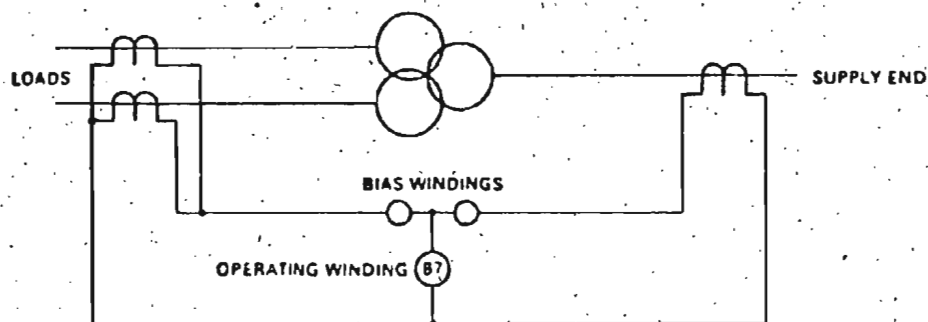
Fig. 2.5(a) shows percentage bias differential protection for a two winding transformer. When the power transformer has only one of its three windings connected to a source of supply, with the other two windings feeding loads at different voltages, a relay of the same design as that used for a two-winding transformer can be connected as shown in Fig. 2.5(b). The separate load currents are summed in the C.T. secondary circuits, and will balance with the infeed current on the supply side.

#### 2.4 Differential Relays With Harmonic Restraint

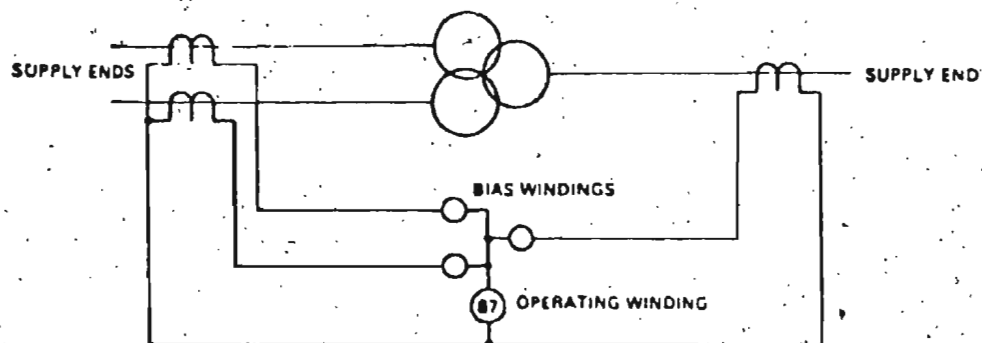
The magnetizing inrush phenomenon produces current input to the primary winding which has no equivalent on the secondary side. The whole of the inrush current appears, therefore, as unbalance and superficially is not distinguishable from internal fault current. The normal bias is not, therefore, effective and increase of the protection setting to a value which would avoid operation would make the protection of little value. The magnetizing inrush current has a high harmonic content, particularly the second harmonic. This second harmonic can be used for restraint.



(a) TWO WINDING TRANSFORMER



(b) THREE WINDING TRANSFORMER (one power source)



(c) THREE WINDING TRANSFORMER (three power sources)

Fig. 2.5 Percentage biased differential protection(13)

It thus desensitizes a relay during energization.

Various static circuits are available with different L-C filtering arrangements for the restraining purpose. Filters are designed either to pass or to block certain harmonics during faults or inrushes. Most of the designs can be classified under two categories. In one type, filters are tuned to the fundamental and other harmonics apart from 2nd harmonic. Thus it blocks the 2nd harmonic during inrush and setting is so done that the restraint is available by arithmetic sum of other harmonics. During fault, mainly the fundamental passes through the operating coil. This type is being used by the General Electric Company. The other type, used by Westinghouse Electric Corp., uses are L-C filters which are designed to pass fundamental and 2nd harmonic quantities separately. During inrush, 2nd harmonic quantity is fed to the restraining coil and during the fault, fundamental quantities are fed to the operating coil. There are some more harmonic restraint principles such as double harmonic restraint principle used by ASEA and three winding harmonic restraint feature used by GE, but those are mainly for special purposes. For general applications, the above two principles are being used all over the world. Two standard circuit designs are incorporated in Appendix-A to illustrate the above two principles of harmonic restraint differential relay.

## 2.5 Concepts of Digital Relaying

Until recently,° conventional<sup>d</sup> relays were serving the need of power system protection. The use of digital computers for protection of power system elements is an idea of quite recent origin. In most of the cases the digital relays are faster in operation than their conventional counterpart relays. They are more reliable in operation and have quite a number of specific advantages described in Section 1.3.

The concept of digital protection is different from that of conventional relaying in many ways. The conventional relaying is primarily dependent on the level of analog signal input to the relay and its effect on the operating or restraining coil of the relay. The behaviour of the relay depends on the circuit parameters of the relay and the electro-mechanical response according to the analog electrical output. However, digital relay is more concerned with the input signal processing and the interaction of these processed signals with the software program of the relay to determine a trip or no-trip decision of the relay. Unlike conventional relay, software part plays a significant role in digital relay. Development of algorithms for faster action is important in this case. Also an interface is required with the analog system to correctly match and feed the input data to the digital system of the computer relay. This

additional requirement of interfacing is absent in conventional relaying. A functional block diagram of a digital relay is shown in Fig. 2.6.

The inputs to the computer relay which are both the analog and digital signals, consist of system currents and voltages - primarily 60 Hz quantities in steady state. The primary analog signals are measured in KA and KV. The conventional current and voltage transducers, like CT and PT, reduce these signals to 5A and 120V levels. These signals from the secondary side of the transducers must be further attenuated to the acceptable computer input levels - usually  $\pm 10$  volts maximum. This level reduction must be accomplished by circuits which shield the computer from the transient voltages that exist on the secondary sides. The attenuated signals are then converted to digital form by Analog to Digital (A/D) converters. All of these functions are performed by the analog input subsystem shown in Fig. 2.6. The digital input subsystem handles the contact or voltage sense information needed by the relays. As in the case of analog wiring, there are transient voltages on the digital input sides also. Shielding of the computer input ports from these voltages is the function of the digital input subsystem.

The output of a digital relay is processed through its digital input subsystem. Digital outputs are usually

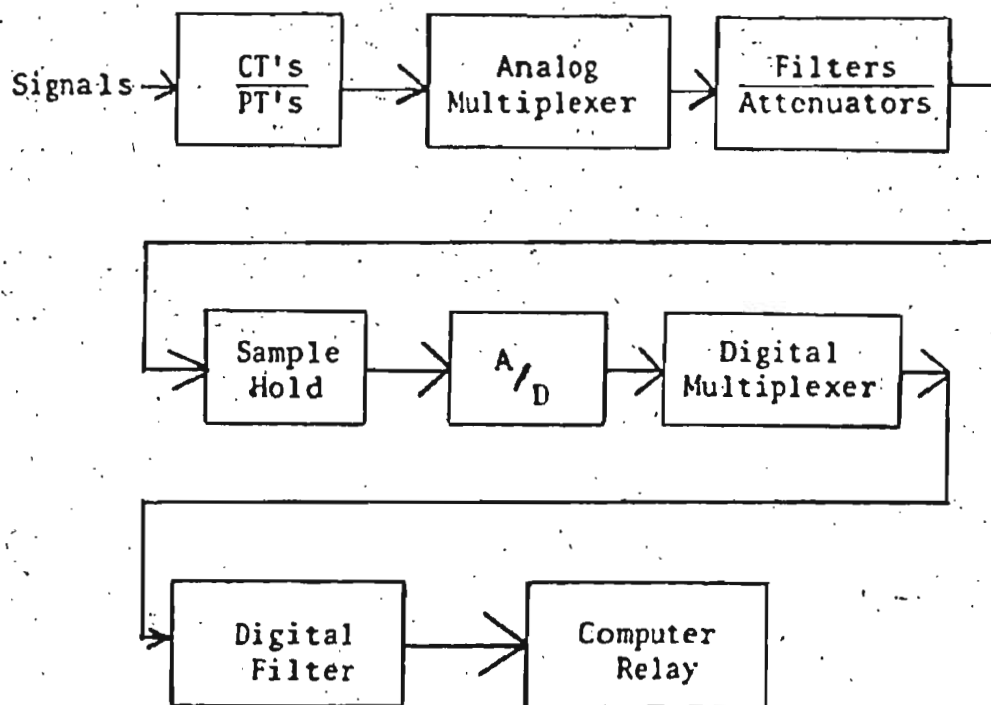


Fig. 2.6 Functional block diagram of a digital relay.

from its parallel output port, and in most cases these are Transistor Transistor Logic (TTL) level signals. Suitable voltage level is derived from these signals to fire thyristor gatings to finally operate the circuit-breakers.

The analog data is sampled continuously. The sampling rate depends on the Nyquist Sampling Theorem, the principles of which have been described briefly in Section 2.6. The other factors on which the sampling rate depends are the capability of A/D, the speed of the processor itself and the suitability of the algorithm used for the relaying program. The continuously generated sample set is entered into the computer memory. The data is maintained in a scratch pad Random Access Memory (RAM).

In most digital relay applications, the raw data samples are also stored in a secondary data file for historical recording of significant transient events on the power system. The organization and length of this historical data file depend upon the specific needs of the user and the available RAM.

It is understood that this data is moved as soon as possible to a secondary storage, thereby making room for the next occurrence of a transient. A suitable span of prefault data as well as appropriate time periods are also saved in this historical data file. The final disposition of these files depends upon the details of individual system design.



The digital filter program is essential to all the relaying applications. The analog data samples are corrupted by noise from many sources. In order to obtain accurate results, the digital filter must separate the desired components of the analog signals from the noise components. This function is handled by the digital filtering program. In most applications, the filter equations are recursive. Researches are going on to produce fast digital filter algorithms.

The relay logic program determines the functional behaviour of the relay. For example, the harmonic restraint differential relay requires the computation of weighted sum of certain harmonics. In most of the cases, the relay logic program is combined with the filtering program which requires the computation of weighted sum of certain harmonics. The relay logic program is combined with the filtering program so that the processor computation time is evaluated on the basis of the whole program from sample to sample.

The derived quantities from algorithm are compared with preset relay characteristics. The size and shape of these characteristics are fed into the computer by the relay setting program. The relay compares continuously the value of the derived quantities from data on sample-to-sample basis and makes the trip or no-trip decision.

## 2.6 Sampling Rate

Fig. 2.7 will serve as an illustration of how an analog signal is converted to a digital signal. Fig. 2.7(a) shows the analog signal which is to be converted. The train of pulses in Fig. 2.7(b) represents a fast-acting switch which connects the data acquisition system to the analog signal for a very short time and remains open for the rest of the period. The result of this operation is identical to multiplying the very short on-time of the sampling switch and the signal. The resultant modulated pulse train is shown in Fig. 2.7(c). Here, the amplitude of the analog signal is preserved within the signal envelope at discrete times. Replacing the sampling switch with a switch-capacitor combination enables the signal to be stored or held until the next sample pulse arrives. This type of signal acquisition, as illustrated in Fig. 2.7(d), is known as a sample and hold technique.

To determine, how often the sampling pulses should occur; that is, to determine the "sampling rate" for a given system, one must examine the analog signal characteristics. Obviously, the sample rate must be faster than any significant changes in the analog signal in order to retain all the useful information. The Nyquist Sampling Theorem defines a minimum allowable sample rate to be used. It states: If a continuous band width limited signal contains

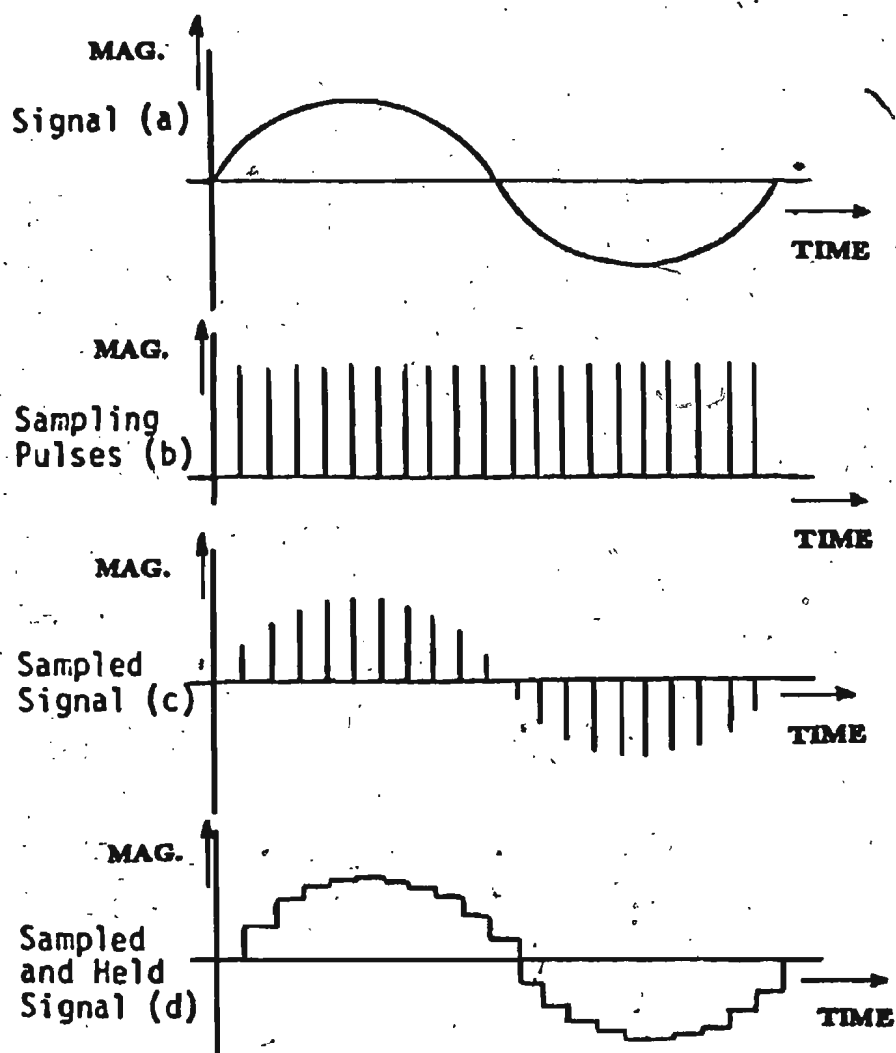


Fig. 2.7 Illustration of converting an analog signal to digital form

no frequency components higher than ' $f_c$ ', then the original signal can be completely recovered without distortion if it is sampled at the rate of at least ' $2f_c$ ' samples per second. Fig. 2.8 illustrates the sampling theorem. Fig. 2.8(a) shows the frequency spectrum of the desired signal. If the sample rate is chosen as ' $f_s$ ', then the sampled signal will be modulated by the frequencies in the analog signal, as is shown in Fig. 2.8(b). Should ' $f_s$ ' be less than ' $2f_c$ ', the high frequencies of the signals cannot be distinguished from the low frequencies of the sampled signal; thus distortion error exists which is termed as "frequency folding".

Another error related to a low sample rate is "aliasing". Aliasing error occurs due to the fact that the sampled signal may contain low frequencies that actually do not exist in the original signal. This is shown in Fig. 2.9.

## 2.7 Digital Differential Protection of Transformers

A schematic diagram of digital differential protection of a single-phase transformer is shown in Fig. 2.10. As seen from the figure, C.T.'s are connected in both the primary and secondary sides of the transformer. Each C.T. secondary is connected in series with a shunt. The values of the shunts are small to avoid unnecessary C.T. secondary burden. This is unlike to the normal current balance connection of conventional differential relays.

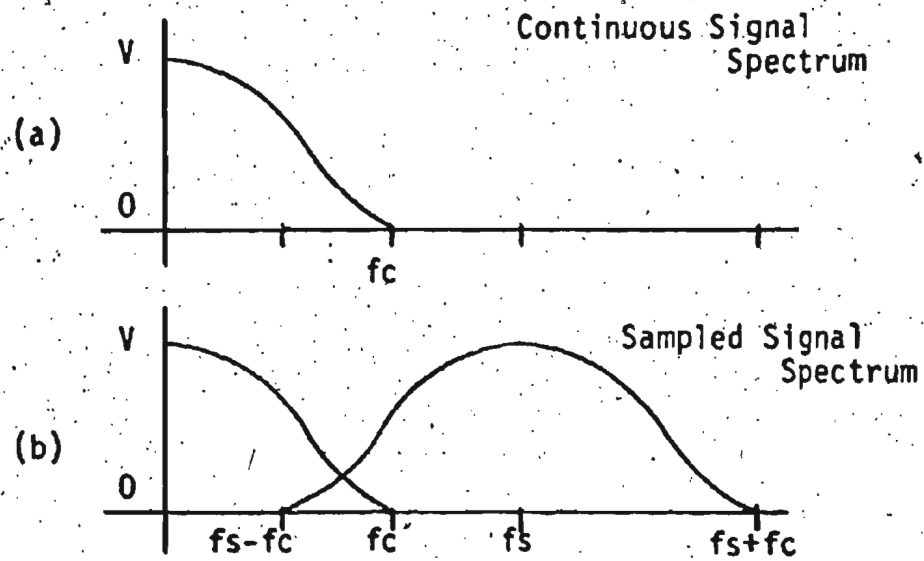


Fig. 2.8 Illustration of Frequency Folding

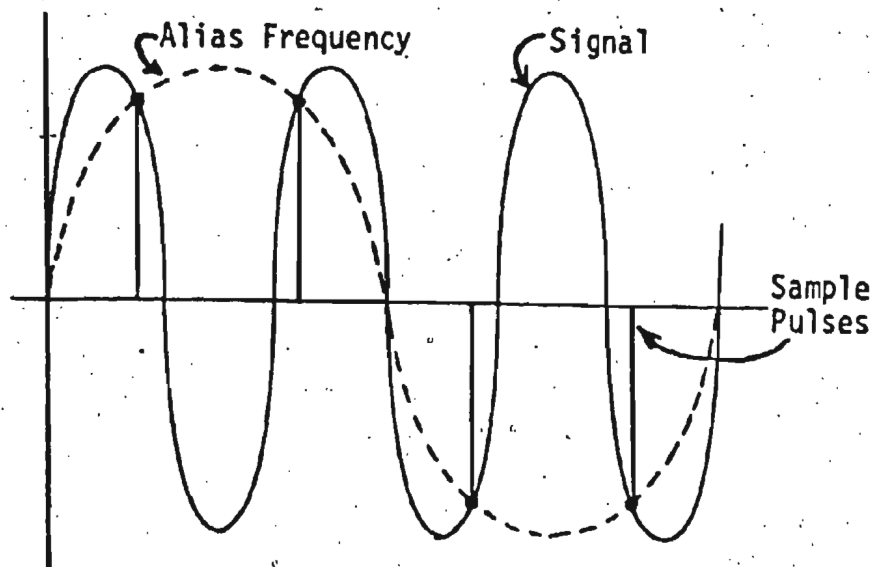


Fig. 2.9 Illustration of Aliasing Effect

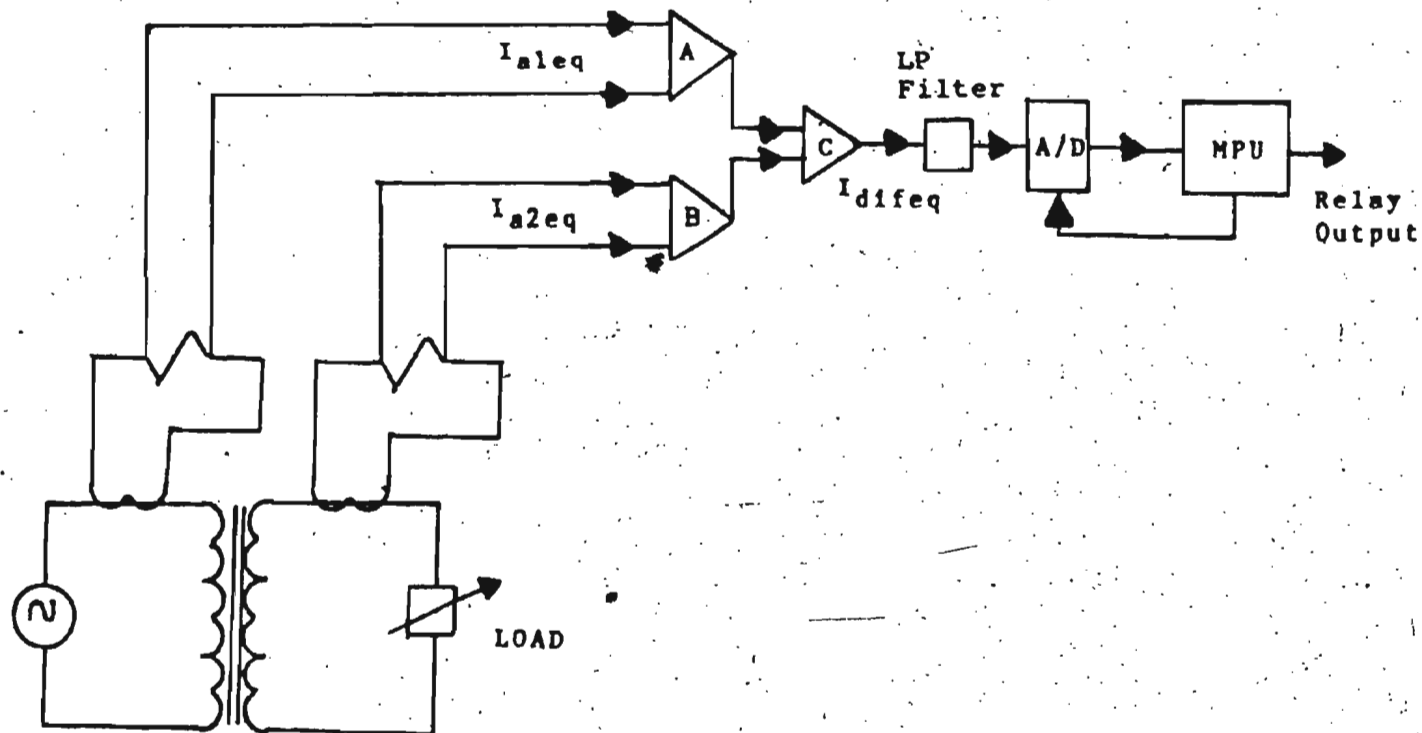


Fig. 2.10 Schematic diagram of digital differential protection of single-phase transformer

Drops across each shunt which are proportional to each C.T. output are fed into amplifier A and B. The output of the amplifier C represents the differential current. The low pass filters prevent aliasing and frequency folding effect described in previous section. Separate Sample & Hold is not necessary for a single-phase transformer protection as in-built S/H of the recent A/D serves that purpose. After processing of each sample by MPU, it gives signal to A/D for a start-conversion of signal.

For steady state operation and also for through-fault, theoretically ' $I_{diff}$ ' will be zero. In practice, C.T. mismatch and saturation effect do not make ' $I_{diff}$ ' exactly equal to zero. A threshold value is incorporated in the relay logic program to avoid undue tripping in such a case. For a fault in the protected zone of the transformer, substantial amount of ' $I_{diff}$ ' is produced. When it exceeds the threshold value of the present relay logic, a trip decision by the relay is initiated.

The magnetizing inrush also causes a substantial flow of ' $I_{diff}$ ', but tripping is prevented by comparison of the second harmonic quantity with the fundamental component provided in the relay program.

A scheme for three-phase protection of transformer is shown in Fig. 2.11. The C.T. connections are the same as conventional 3-phase transformer protection, i.e., C-T's on





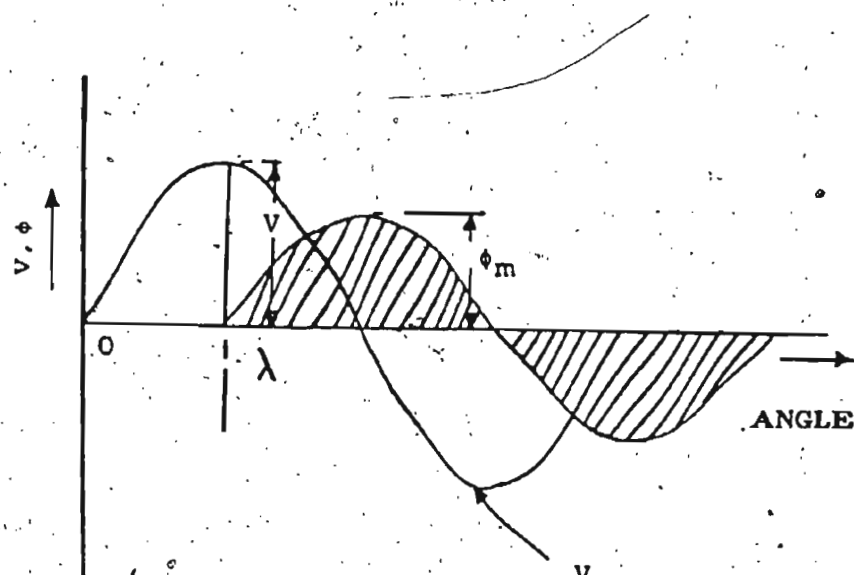
the star-side of the transformer are connected in delta and delta side C.T.'s are connected in star. Bias and operating windings of a conventional protection scheme is absent here.

Instead of, drops across each shunt which are proportional to the differential currents in each phase, are fed to the individual amplifiers A, B, C. Each of the outputs of A, B, C are fed to individual S/H. A signal from MPU through a common bus system enables all the analog samples of three phases to be held by each S/H at the same instant. The multiplexer, upon getting signal from MPU next, selects one of the signals from its three input channels. Thus one signal from one of the phases is selected at a time by multiplexer and passed to the A/D. Upon receiving a signal from MPU, A/D converts the signal and sends it to MPU for processing. When processing is completed, MPU sends its next signal to select sample from the next phase by multiplexer and the process is repeated. Trip or no-trip decision by the relay as well as prevention of tripping due to inrush is followed by a preset relay logic in the same way as described for single-phase case.

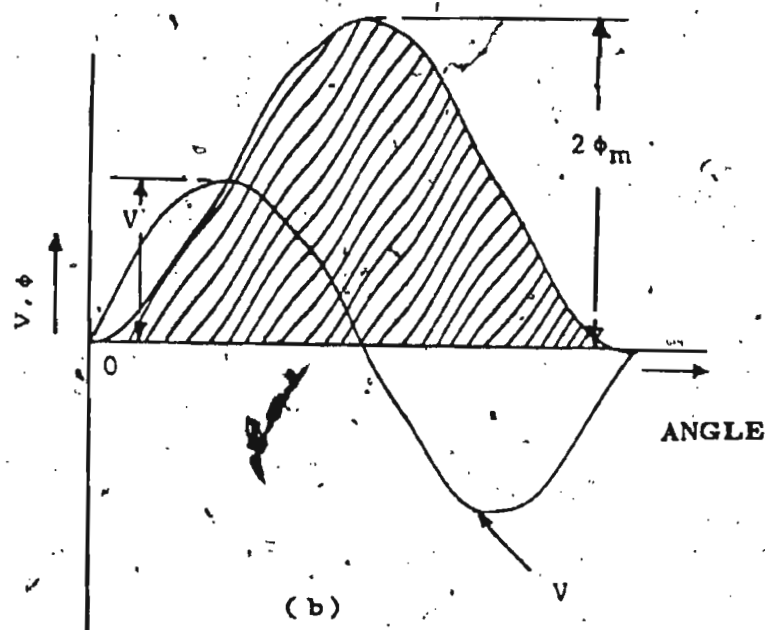
## CHAPTER 3

MAGNETIZING INRUSH PHENOMENA FOR SINGLE AND  
THREE PHASE TRANSFORMERS3.1 Magnetizing Inrush Current in Single Phase Transformers3.1.1 Inrush Phenomena

When a single phase transformer is energized from the line, at every instant, the applied voltage is ideally balanced by induced voltage due to the magnetizing current. The magnetizing current is produced by the flux associated in the core. The nature of the flux produced depends on the magnitude, polarity and rate of change of the applied voltage at the instant of switching. Assume first, that the core is initially unmagnetized and that the switch is closed at voltage peak. The condition is shown in Fig. 3.1(a) where ' $\lambda$ ' is the switching instant. The balancing e.m.f. demands a flux having maximum rate of change, so that the flux starts from zero in the required direction, as also does the magnetizing current. As observed from Fig. 3.1(a), if the switch is closed at  $90^\circ$  of the voltage waveform, flux will start growing from zero at that point. The flux will grow up as long as the voltage is positive and starts decreasing when the voltage is negative. Thus the positive half-cycle of the flux will correspond to the positive half-cycle of the voltage waveform but with a  $90^\circ$  phase shift. Hence, the flux is ideally  $90^\circ$  lagging the



(a)



(b)

Fig. 3.1 Effect of switching angle &amp; residual flux

(a) Switched on at  $90^\circ$  of voltage wave(b) Switched on at  $0^\circ$  of voltage wave

voltage waveform, if the transformer is switched on at  $90^\circ$ . If, however, the switch is closed at a voltage zero as in Fig. 3.1(b), the voltage is positive during the first half-period, throughout which the flux must, therefore, increase, with a total change corresponding to that of a 'normal' half-period. It, therefore, reaches a maximum of twice the normal peak, i.e.  $2\phi_m$ , a phenomenon called the 'doubling effect'.

In subsequent half-periods, the effect of losses rapidly reduces the flux waveform to symmetry about the time axis. The residual flux in the core can aggravate the condition. The residual flux is the flux in the core prior to energization of the transformer. If the primary voltage is applied at a zero instant and in such a direction that the rising field augments the existing residual flux ' $\phi_R$ ', as in Fig. 3.1(c), the sinusoid of flux variation has still the amplitude ' $2\phi_m$ ', but is entirely offset from zero and rises to a peak value ' $2\phi_m + \phi_R$ '.

Fig. 3.2(a) illustrates the effect of positive residual fluxes on inrush currents due to the switching of a transformer on two successive cycles of applied voltage waveform through thyristors. In Fig. 3.2(b) the applied voltage waveform is shown as inverted. The switching is done at  $90^\circ$  of the positive voltage waveform.

So, the inrush will be maximum if the transformer

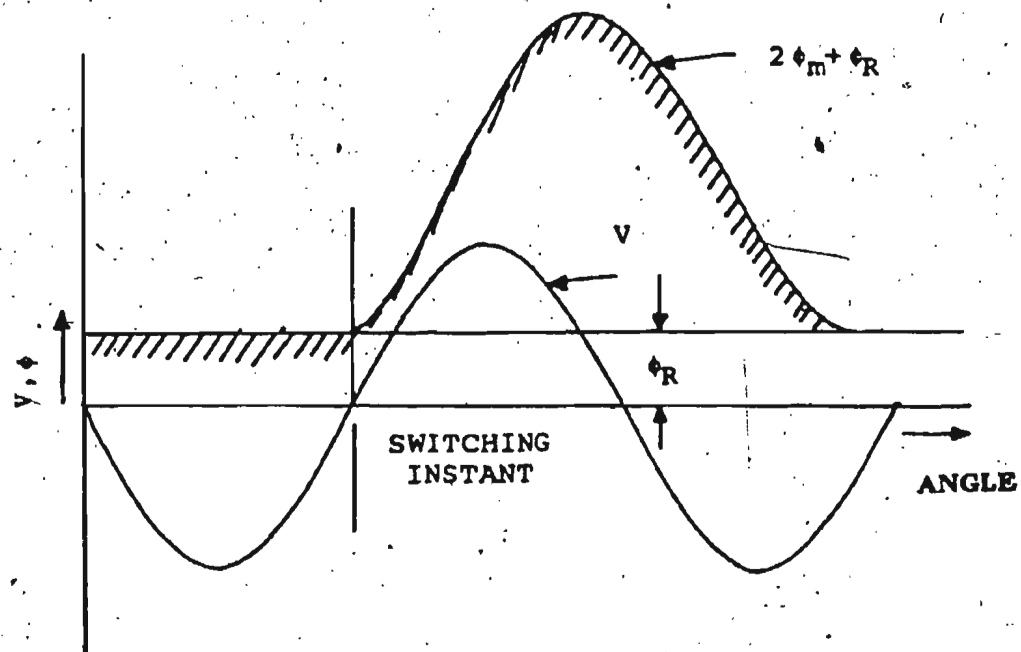
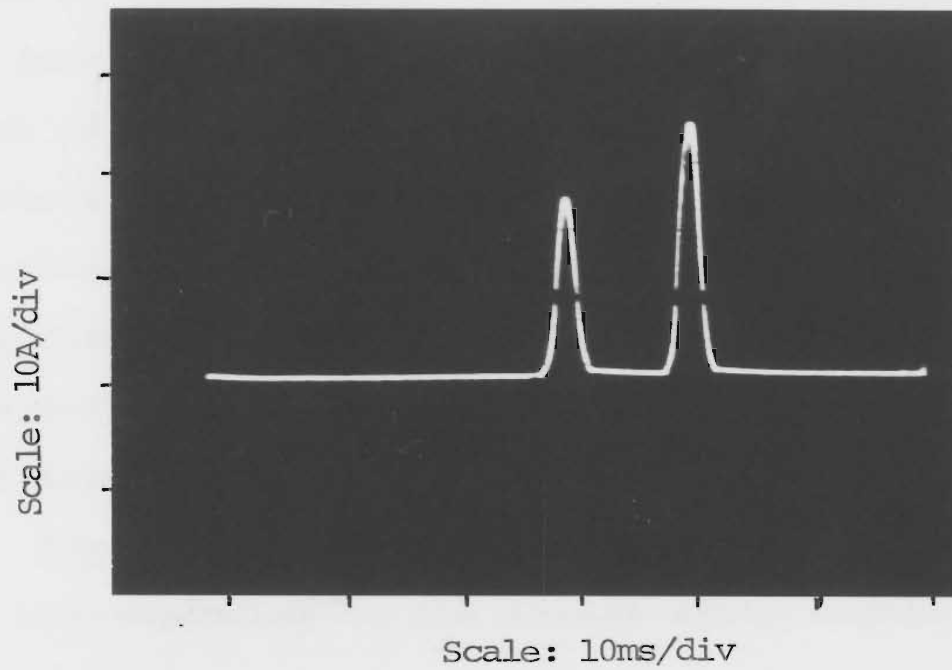
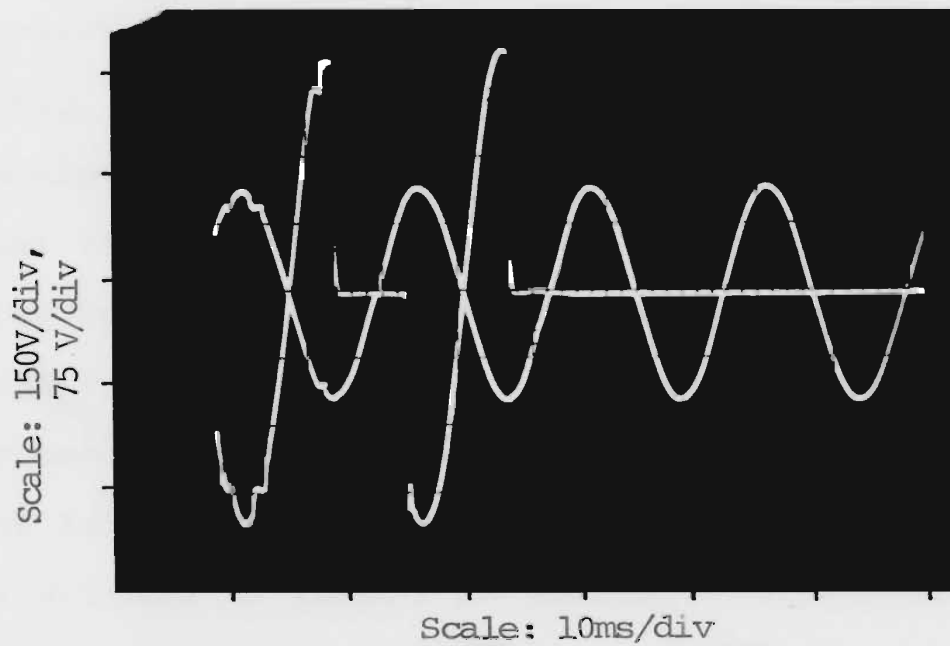


Fig. 3.1 (c) Effect of residual flux



(a)



(b)

Fig. 3.2 (a) Effect of Positive Residual Flux

(b) Successive switching by point-on-wave switch

is switched on at voltage zero. It will be minimum if switching is done at  $90^\circ$  of any half of the voltage waveform. The phenomenon of the inrush is physically explainable more easily with the help of 'transient flux'. Fig. 3.3 shows the fluxes for maximum inrush condition, wherein, the total flux is the actual flux for the first cycle.

The total flux of Fig. 3.3, may be viewed as consisting of two components,

A) Steady State Flux: the normal flux requirements corresponding to the steady-state magnitude of the existing voltage.

B) Transient Flux: the flux required to be added to the steady-state flux to make the total flux equal to the residual flux at the instant of circuit closure.

In Fig. 3.3, the residual flux is shown in the positive direction and is presumed to be maximum on the assumption that the existing current has been extinguished by circuit-breaker operation at a normal current zero following a positive half-cycle.

The maximum transient flux is produced by energizing the transformer at the zero point on the voltage wave when the voltage is rising in positive direction to go with the assumed positive residual flux. With negative residual, closing the circuit  $180^\circ$  later, would produce maximum transient flux of opposite polarity. If the breaker

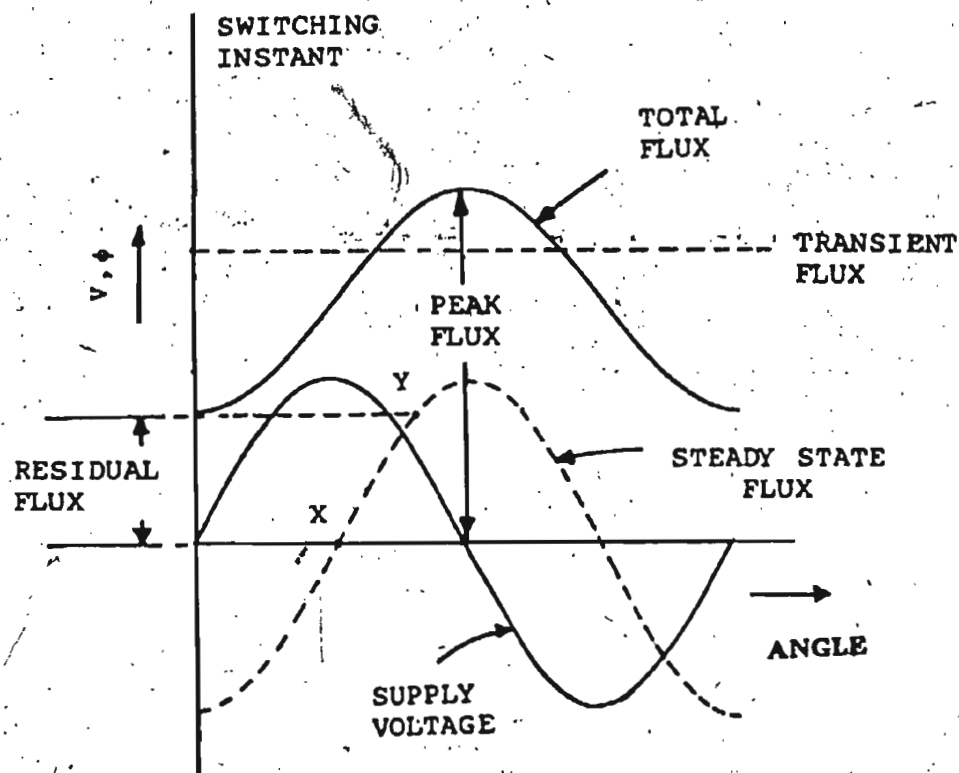


Fig. 3.3 Voltage, flux and current during a magnetizing inrush



closes  $90^\circ$  later at point 'X' of Fig. 3.3, the instantaneous value of the steady state flux is zero, and the transient flux, therefore, is equal to the residual flux. If the transformer is energized at point 'Y' of Fig. 3.3, where the steady state flux value equals the residual flux value, no transient flux is present. Under this condition, there would be no magnetizing inrush current.

In Fig. 3.4(a), the formation of inrush current is illustrated with the help of excitation curve. A simplified excitation curve has been assumed as two straight lines, from O to S, and from S to P. The inrush current 'I' for the condition of maximum transient flux was determined graphically by entering the excitation curve OSP with the instantaneous flux values. For example, a value of flux ' $\phi_x$ ', has been determined at  $90^\circ$  of the flux waveform ' $\phi$ '. By projecting this value on the left-hand side of excitation curve, the instantaneous value ' $I_x$ ' is obtained on the figure. Similarly, other points of inrush current waveform can be determined. However, as explained later on, the digital simulation of these waveforms are simpler and less difficult.

If the actual excitation curve is used, as shown by the hysteresis loop, legs will be produced near zero on the current wave, as shown by the dashed portion of the wave. These legs result from the bend in the excitation curve near

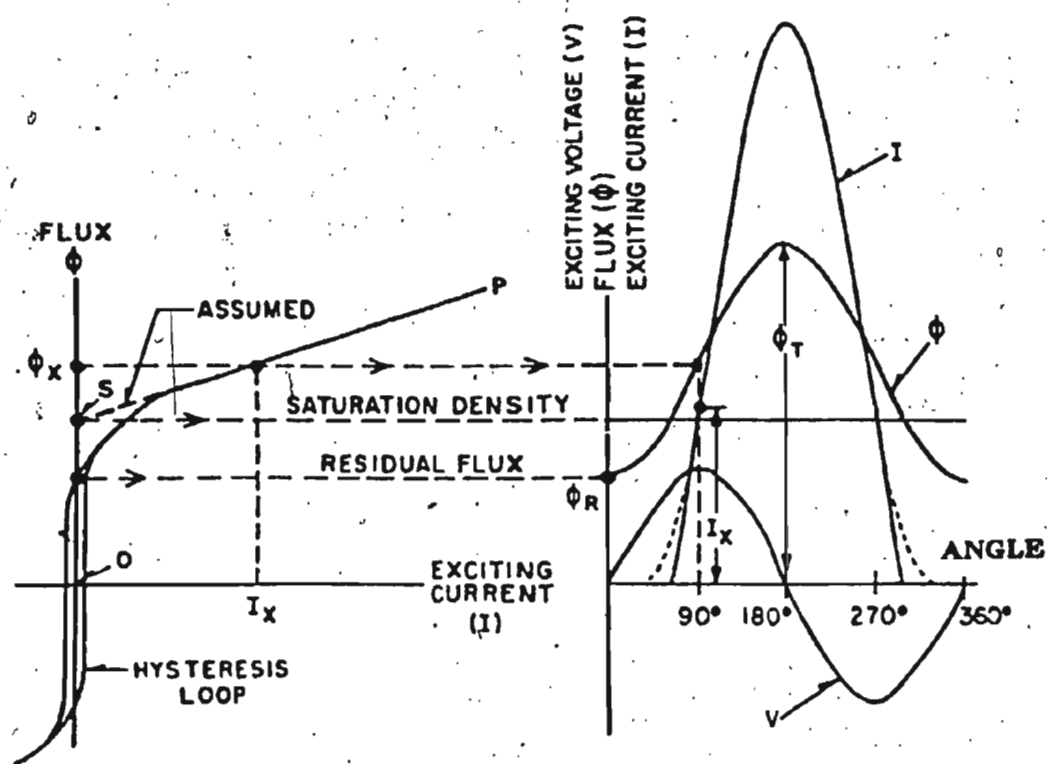


Fig. 3.4 (a) Derivation of magnetizing inrush current from excitation characteristic

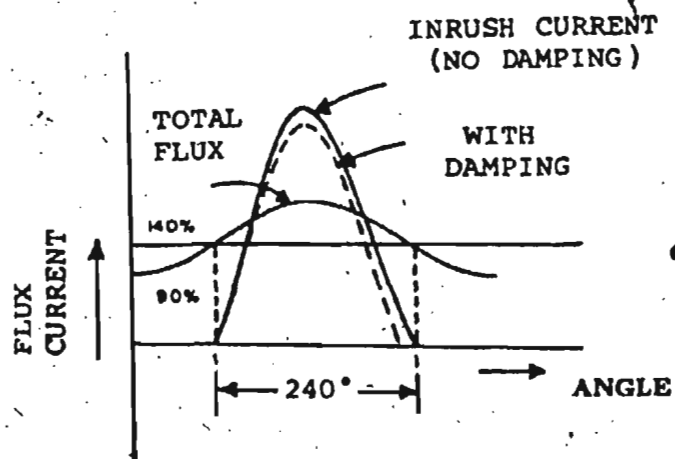
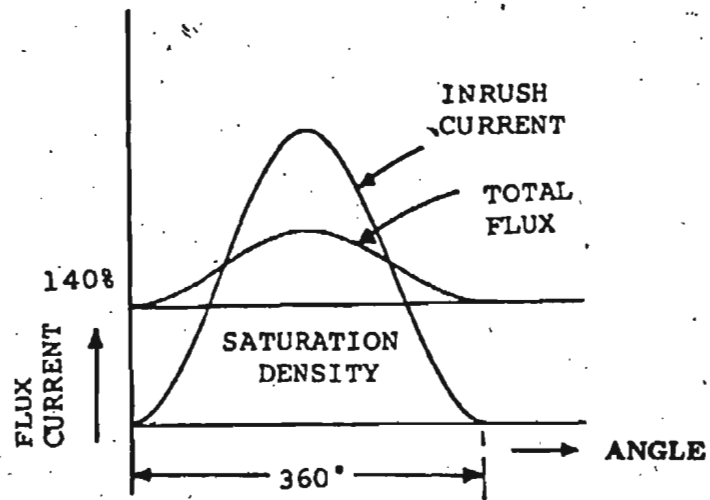


Fig. 3.4 (b) Effect of residual flux on inrush current shape with former equal to saturation density

(c) Effect of residual flux on inrush current shape with former less than the saturation density

the saturation point. By assuming, that the excitation curve consists of two straight lines, intersecting on the flux axis at a point S, called "saturation density", the inrush current legs are eliminated and the inrush current becomes an off-set sine wave with the negative portion of the current cut off.

If residual flux could ever be equal to saturation density, the inrush current would become a pure sine wave, fully offset as shown in Fig. 3.4(b). In fact, the residual is always less than the saturation density. Hence, it is no longer an exact sine wave but close to it as shown in Fig. 3.4(c). The inrush damps out in subsequent cycles and hence, the similarity of its with sine wave gets more and more distorted as its base becomes narrower.

The whole process has been illustrated in Fig. 3.4(d), where,  $\phi_{R1}$ ,  $\phi_{R2}$  are the residual fluxes,  $\theta_{s1}$ ,  $\theta_{s2}$  are the saturation angles, i.e. where the inrush currents start rising from zero and are measured from  $t=0$ ;  $\gamma_1$ ,  $\gamma_2$  and  $\gamma_3$  are the conduction angles, i.e. the time-period in terms of angles, during which the inrush current occurs. It is found from the Fig. 3.4(d) that the magnitude of the inrush current is more if the residual flux due to previous turn off is more. If the transformer is switched on at an angle of  $90^\circ$  of the voltage wave, the inrush current  $I_{m3}$  is smaller than  $I_{m1}$  and  $I_{m2}$ . Here, ' $\theta_{s3}$ ' is measured from  $90^\circ$  of the voltage waveform. Here  $\gamma_3$ , is also smaller compared to  $\gamma_1$  and  $\gamma_2$ .

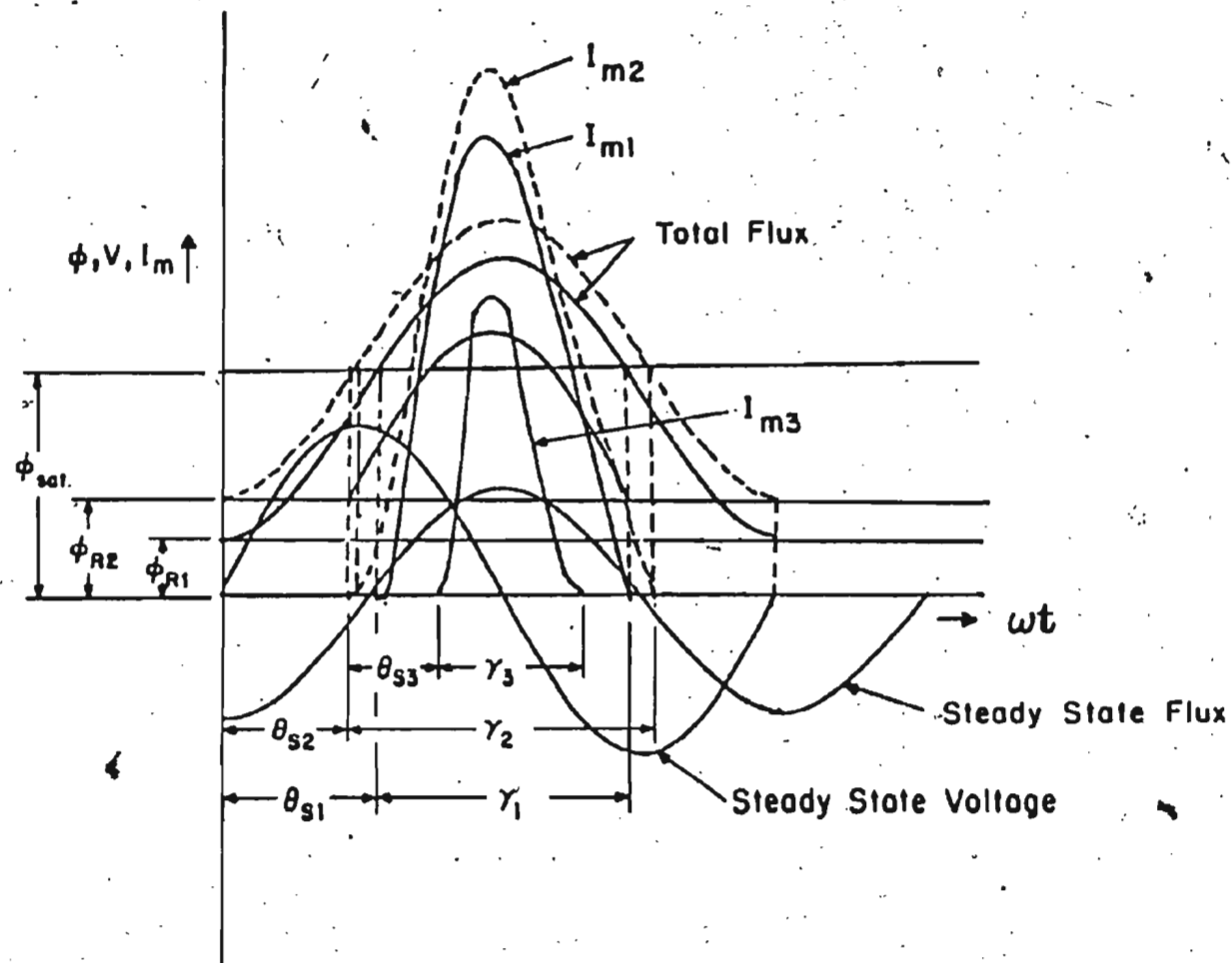


Fig. 3.4 (d) Inrush phenomena with different residual flux levels and switching angles

If switching is done later than  $180^\circ$  of the voltage waveform, the inrush will occur in the negative direction.

### 3.1.2 Analysis of Magnetizing Inrush For Single-Phase Transformers

It is well known that when a single phase transformer is energized at no-load, the steady state no load current ' $I_0$ ', has two components,

(1) ' $I_m$ ', which is responsible for producing the main flux ' $\phi$ ' and is in phase with ' $\phi$ '.

(2) ' $I_{h+e}$ ', which supplies the hysteresis and eddy current losses and in phase with  $V_1$ .

Thus,

$$I_0 = jI_m + I_{h+e} \quad (3.1)$$

The phasor diagram representation of Eqn. 3.1 is shown in Fig. 3.5(a) and the equivalent circuit at no-load is shown in Fig. 3.5(b). The component  $I_{h+e}$  is very small in comparison to  $I_m$  and steady state value of  $I_m$  is small in comparison to the normal full load current of the transformer. From a simplified equivalent circuit, the value of  $I_m$  is given as,

$$I_m = E_1 (g_m - jb_m) \quad (3.2)$$

where,  $g_m$  is the conductance,  $b_m$  is the susceptance.

Hence, it can be written as

$$E_1 = I_m Z_m = I_m (r_m + j x_m) \quad (3.3)$$

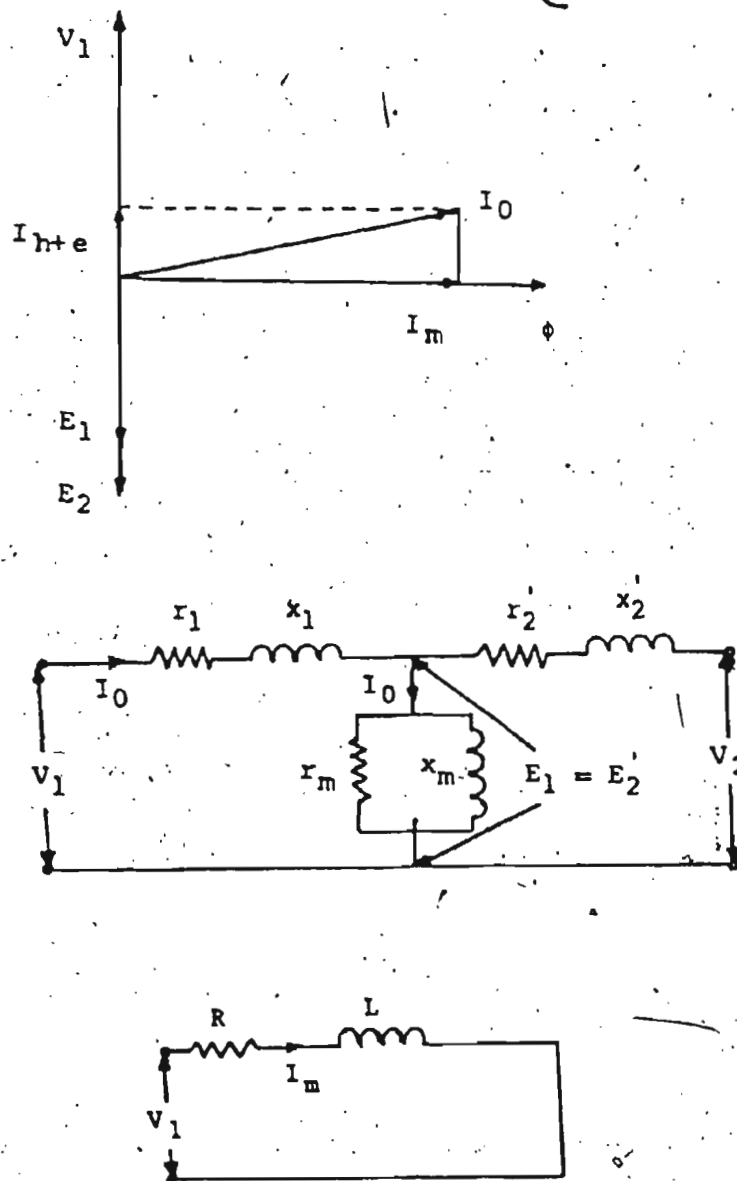


Fig. 3.5 (a) Phasor diagram of magnetizing current (assuming it to be a vector quantity)

(b) Equivalent diagram of single phase transformer under no load condition

(c) Magnetizing current circuit under core saturated condition.

In Eqn. 3.3,  $Z_m$  is the core impedance,  $r_m$  is the core resistance and  $X_m$  is the magnetizing reactance, so that

$$r_m = \frac{g_m}{g_m^2 + b_m^2}, \quad X_m = \frac{b_m}{g_m^2 + b_m^2} \quad (3.4)$$

The above equations are valid under steady state condition, i.e. when the flux is below the saturation level of the transformer. But during switching on of a transformer, the flux is driven well above the knee on magnetizing inrush. So, the watt component of the current can be disregarded on the basis that it is small compared to the magnetizing inrush current. When the flux is above saturation, the inrush current is no longer confined in the core, but flows through the series impedance between the transformer and the source as shown in Fig. 3.5(c). Then the effective inductance of the coil is the leakage inductance and not the inductance of the core. It is designated as ' $L_t$ ' and the source inductance can be added to it so that effective inductance of the flux path is

$$L = L_s + L_t \quad (3.5)$$

Also, the circuit resistance and transformer resistance can be combined to give a total resistance of

$$R = R_s + R_t \quad (3.6)$$

The inductance of Eqn. (3.5) is also not a constant parameter and depends on the behaviour of the circuit on a particular



switching position on the voltage waveform. Its value also varies from cycle to cycle as the inrush current damps out subsequently.

To obtain suitable expressions of inrush current in case of a single phase transformer, following three cases are considered.

- (A) Switching is done at switching angle  $\lambda=0^\circ$
- (B) Switching is done at switching angle  $\lambda=180^\circ$
- (c) Switching is done at arbitrary angle  $\lambda=\omega t$ .

Case A: Switching at  $\lambda=0^\circ$

Let the applied voltage be given by

$$e = \sqrt{2} E \sin \omega t \quad (3.7)$$

From Fig. 3.5(c), the voltage equation of the circuit can be written as,

$$e = \sqrt{2} E \sin \omega t = Ri + L \frac{di}{dt} \quad (3.8)$$

Where,  $E$  is the R.M.S. value of the applied voltage. The solution of Eqn. (3.8) is obtained as,

$$i = \frac{\sqrt{2}E}{Z} [\sin(\omega t - \phi) - e^{\frac{R}{X}(\theta_{s1} - \omega t)} \sin(\theta_{s1} - \phi)] \quad (3.9)$$

where,

$$X = \omega L, \quad Z = \sqrt{R^2 + X^2}, \quad \phi = \tan^{-1}\left(\frac{X}{R}\right), \text{ and}$$

$\theta_{s1}$  = saturation angle in the first cycle.

Eqn. (3.9) can be expanded and finally represented in the following form,

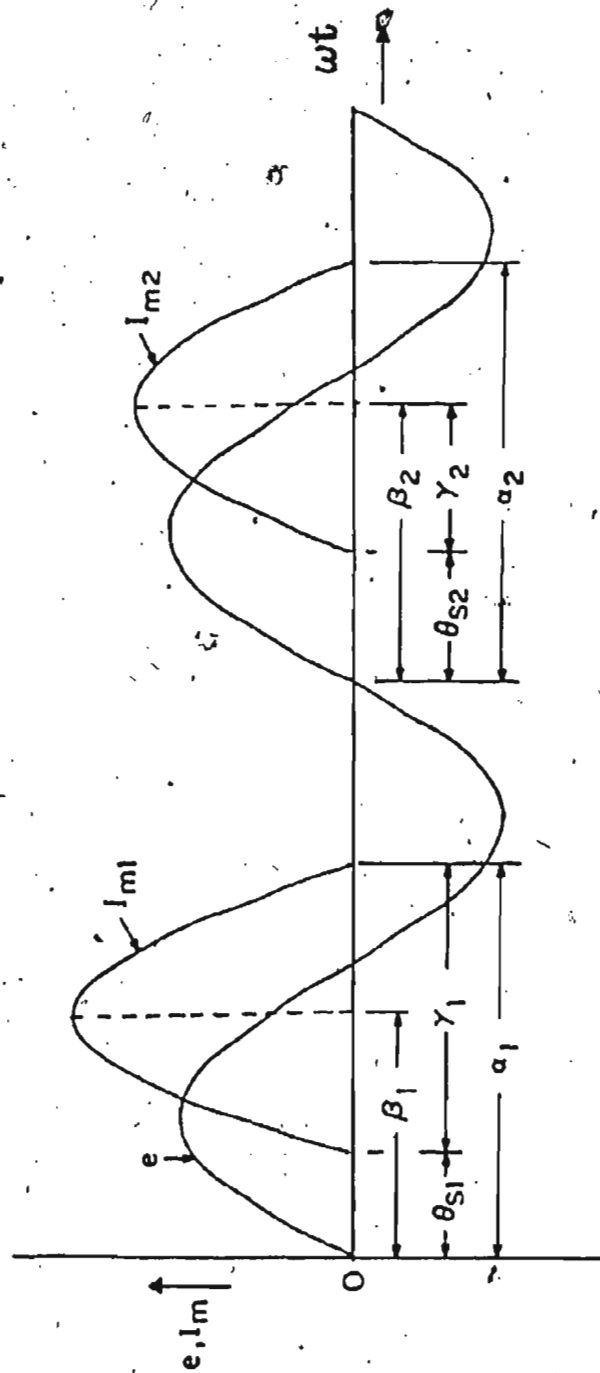


Fig. 3.6 (a) Switching at  $\lambda=0^\circ$

$$i = \frac{\sqrt{2}EX}{Z^2} \left[ \frac{R}{X} \sin \omega t - \cos \omega t - e^{\frac{R}{X}(\theta_{sl} - \omega t)} \left( \frac{R}{X} \sin \theta_{sl} - \cos \theta_{sl} \right) \right] \quad (3.10)$$

The detail derivation of Eqn. (3.9) and (3.10) are shown in Appendix B.

Eqns. (3.9) and (3.10) represent the first cycle of inrush current which changes from cycle to cycle depending on the variation of the values of  $Z$ ,  $X$  and  $\theta_{sl}$ . The equations are valid as long as the flux is above the saturation region.

This is shown in Fig. 3.6(a) where the instantaneous values of 'i' are designated as  $I_{m1}$  and  $I_{m2}$ .

From Fig. 3.6(a), the current becomes zero at  $\omega t = \alpha$ .

Substituting in Eqn. (3.10), yields,

$$\frac{R}{X} \sin \alpha - \cos \alpha - e^{\frac{R}{X}(\theta_{sl} - \alpha)} \left( \frac{R}{X} \sin \theta_{sl} - \cos \theta_{sl} \right) = 0 \quad (3.11)$$

Let

$$\theta_{sl} = \alpha - \gamma,$$

where

$\gamma$  = conduction angle of the inrush current

Substituting in, Eqn. 3.11 gives,

$$\tan \alpha = \frac{e^{\frac{(R/X)\gamma}{X}} - \frac{R}{X} \sin \gamma - \cos \gamma}{\frac{R}{X} \cdot e^{\frac{(R/X)\gamma}{X}} - \frac{R}{X} \cos \gamma + \sin \gamma} \quad (3.12)$$

If the value of ' $\gamma$ ' is known, corresponding ' $\alpha$ ' and  $\theta_{sl}$

values can be computed from Eqn. 3.12 and 3.11 respectively. The peak value of the current does not occur at the same angle as that of the flux waveform but occurs at an angle ' $\beta$ '. These are shown for two successive cycles in Fig. 3.6(a). This is found by differentiating Eqn. 3.10 with respect to time, and equating it to zero. Thus,

$$\frac{di}{dt} = \frac{\sqrt{2} EX}{Z^2} \left[ \omega \cdot \frac{R}{X} \cos \omega t + \omega \sin \omega t + \frac{R}{X} \cdot e^{\frac{R}{X}(\theta_{sl} - \omega t)} \cdot \left( \frac{R}{X} \sin \theta_{sl} - \cos \theta_{sl} \right) \right] \quad (3.13)$$

For maximum current,  $\frac{di}{dt} = 0$ , and the current is maximum at an angle  $\omega t = \beta$ . Using Eqn. (3.10), the expression for maximum current can be found in a convenient form as,

$$I_{p \max} = \frac{\sqrt{2} E}{X} \cdot \left( \frac{X}{R} \right) \cdot \sin \beta \quad (3.14)$$

Detail derivations are included in Appendix B.

#### Case B: Switching at $\lambda = 180^\circ$

If the switch is closed at  $\lambda = 180^\circ$ , the instantaneous value of the applied voltage in the interval  $\pi < \omega t < 2\pi$  is given by,

$$\begin{aligned} e &= \sqrt{2} E \sin (\pi + \omega t) \\ &= -\sqrt{2} E \sin \omega t \end{aligned} \quad (3.15)$$

So, it is the same thing as saying that the switching is done at  $\lambda = 0^\circ$ , of the negative half of the voltage wave. This is shown in Fig. 2.6(b) where the axis has been shifted and all the angles are measured from  $t=0$  as shown. Thus, the voltage

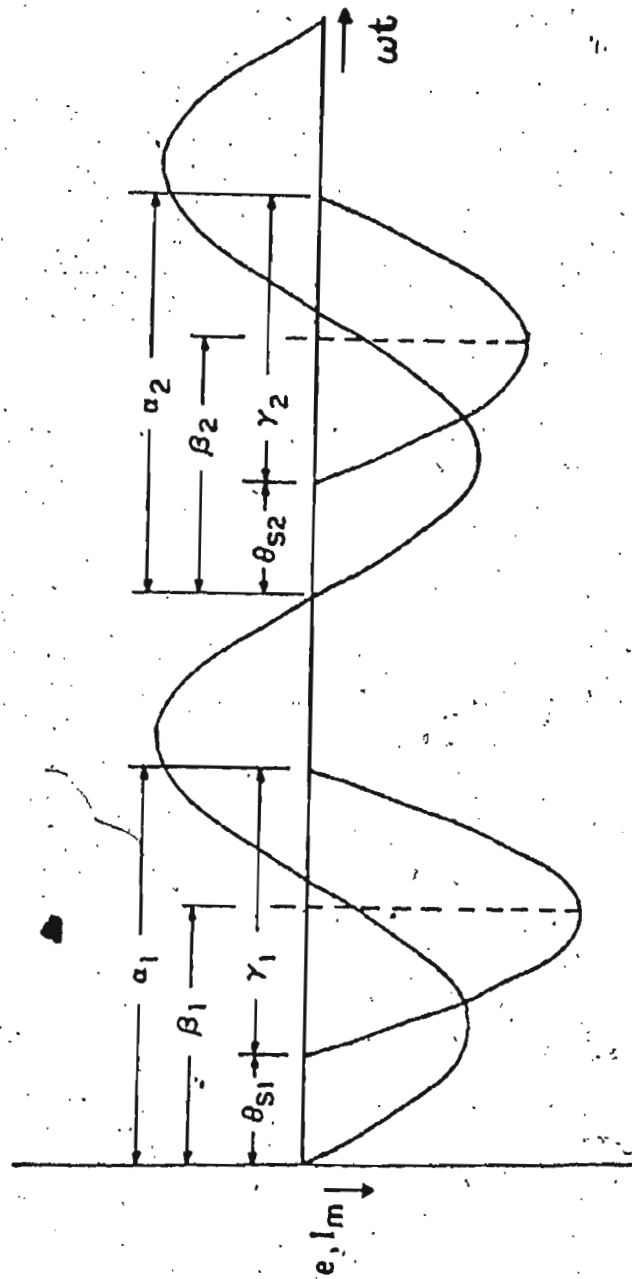


Fig. 3.6 (b) Switching at  $\lambda = 180^\circ$

equation can be written as

$$e = -\sqrt{2} E \sin \omega t = R_i + L \frac{di}{dt} \quad (3.16)$$

Following the same procedure, as in Case A, the solution of Eqn. (3.16) is obtained as,

$$i = -\frac{\sqrt{2} E}{Z} [\sin(\omega t - \phi) - e^{\frac{R}{X}(\theta_{sl} - \omega t)} \cdot \sin(\theta_{sl} - \phi)] \quad (3.17)$$

The Eqn. (3.17) can be rewritten in the form,

$$i = \frac{-\sqrt{2} EX}{Z^2} \left[ \frac{R}{X} \sin \omega t - \cos \omega t - e^{\frac{R}{X}(\theta_{sl} - \omega t)} \cdot \left( \frac{R}{X} \sin \theta_{sl} - \cos \theta_{sl} \right) \right] \quad (3.18)$$

As the current  $i=0$  at  $\omega t=\alpha$ , from Eqn. (3.18), it is found

$$\frac{R}{X} \sin \alpha - \cos \alpha - e^{\frac{R}{X}(\theta_{sl} - \alpha)} \left[ \frac{R}{X} \sin \theta_{sl} - \cos \theta_{sl} \right] = 0 \quad (3.19)$$

If ' $\gamma$ ' is the conduction angle, the value of ' $\alpha$ ' can be found in terms of ' $\gamma$ ' as before

$$\tan \alpha = \frac{e^{\frac{R}{X} \gamma} - \frac{R}{X} \sin \gamma - \cos \gamma}{\frac{R}{X} e^{\frac{R}{X} \gamma} - \frac{R}{X} \cos \gamma + \sin \gamma} \quad (3.20)$$

The expression for ' $\alpha$ ' in Eqn. (3.20) is the same as that in Eqn. (3.12), but all the angles in Eqn. (3.20) are measured from the new reference as shown in Fig. 3.6(b).

Similarly, the expression of maximum current can be

obtained by differentiating Eqn. (3.18) and setting it to zero as in Case A. Thus, if the current is maximum at an angle ' $\beta$ ', the expression for maximum current is obtained as,

$$I_{p \max} = - \left( \frac{\sqrt{2} E}{X} \right) \cdot \left( \frac{X}{R} \right) \cdot \sin \beta \quad (3.21)$$

Case C: Switching at an Arbitrary angle  $\lambda = \omega t$

This is shown in Fig. 3-6(c), where switching is done at an arbitrary angle ' $\lambda$ ' of the positive half cycle of the voltage waveform. If the time of inception on the voltage waveform is taken as  $\lambda = \omega t$  and set the new time axis as  $t' = 0$ , so that

$$t' = t - \lambda / \omega, \quad (3.21a)$$

then the transformed voltage equation is,

$$e = \sqrt{2} E \sin (\omega t' + \lambda) \quad (3.22)$$

where,

$$\omega t' = \omega t - \lambda \quad (3.22a)$$

Hence, the voltage equation can be written as before in terms of new reference frame,

$$e = \sqrt{2} E \sin (\omega t' + \lambda) = R i + L \frac{di}{dt} \quad (3.23)$$

The solution of Eqn. (3.23) in terms of ' $t$ ' can be found as

$$i = \frac{\sqrt{2} E}{Z} \left[ \sin(\omega t - \phi) - e^{-R/X(\omega t - \theta_{sl} - \lambda)} \cdot \sin(\theta_{sl} + \lambda - \phi) \right] \quad (3.24)$$

Expanding Eqn. (3.24), it can be written as

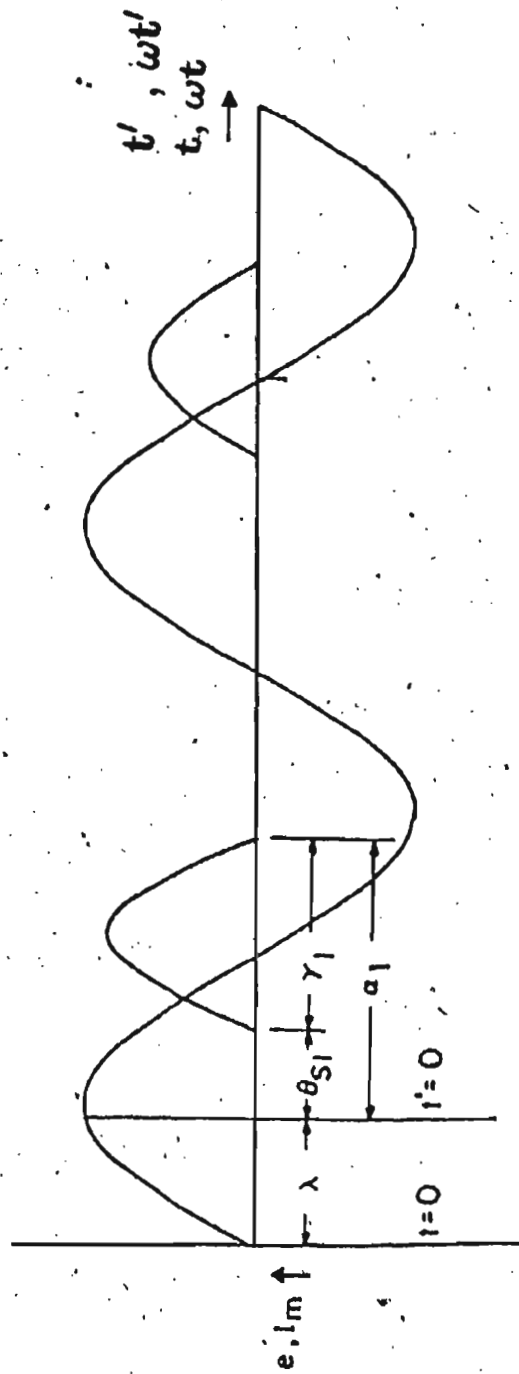


Fig. 3.6 (c) Switching at an arbitrary angle  $\lambda$



$$i = \frac{\sqrt{2} E X}{Z} \left[ \frac{R}{X} \sin \omega t - \cos \omega t - e^{-R/X(\omega t - \theta_{sl} - \lambda)} \left( \frac{R}{X} \sin(\theta_{sl} + \lambda) - \cos(\theta_{sl} + \lambda) \right) \right] \quad (3.25)$$

The detailed derivation of Eqn. 3.25 is included in Appendix

B. When the current is zero at  $\omega t' = \alpha$ ,

$$\frac{R}{X} \sin(\alpha + \lambda) - \cos(\alpha + \lambda) - e^{R/X(\theta_{sl} - \alpha)} \left( \frac{R}{X} \sin(\theta_{sl} + \lambda) - \cos(\theta_{sl} + \lambda) \right) = 0 \quad (3.26)$$

If  $\gamma = \alpha - \theta_{sl}$ , where  $\gamma$  is the conduction angle, it can be shown from Eqn. 3.26 that the value of  $\alpha$  as

$$\tan(\alpha + \lambda) = \frac{e^{R/X \gamma} - \frac{R}{X} \sin \gamma - \cos \gamma}{\frac{R}{X} \cdot e^{R/X \gamma} + \sin \gamma - \frac{R}{X} \cos \gamma} \quad (3.27)$$

The right hand side expression of Eqn. (3.27) is similar to that of Case A when switching is done at  $\lambda = 0^\circ$ . The only difference is that, in Eqn. (3.27), ' $\gamma$ ' and ' $\alpha$ ' are measured from  $t' = 0$  and not from  $t = 0$ . The peak current expression can be found using the same procedure as in case A and the expression for peak current is obtained as

$$I_{p \max} = \frac{\sqrt{2} E}{X} \cdot \left( \frac{X}{R} \right) \cdot \sin(\beta + \lambda) \quad (3.28)$$

Again, the detailed derivations are included in Appendix B.

### 3.2 Magnetizing Inrush Current in 3-Phase Transformer Banks

#### 3.2.1 Inrush Phenomena

Inrush current phenomena are more complicated in

the case of a 3-phase transformer bank. It is difficult to switch on all three phases at one time due to the inherent phase angle differences between the phases, thus without producing inrush currents in two phases at least. Again, the instantaneous values of the inrush currents in different phases will be different depending on the electrical connections of the energized windings and by magnetic coupling with any other closed windings which are present. Residual fluxes in the core also is not as simple as in a single phase case. As mentioned previously, the amount of residual flux left in the core of a transformer depends upon the point in the cycle at which the exciting current was interrupted at the time of bank de-energization. It is most likely, that one phase will be interrupted before the other two because of the phase difference between the total currents. Again, with a star-delta connected bank, interrupting the first-phase on the star side does not extinguish the excitation for the first phase core because of an electrical connection on the delta side. When these contingencies are taken into account, it follows that the amount of the residual to be expected in the three phase cores is rather unpredictable.

As the inrush current phenomena and subsequent analysis are different depending on whether the transformer is switched on from Y-side or from  $\Delta$ -side of the transformer,

both the cases are explained here as follows. First, a transformer with no closed winding is considered.

(A) Core-type transformer with primary winding grounded in star having no closed winding present: Let the switching of the transformer be done at such an instant when the phase 'a' voltage is maximum. For simplicity of analysis, it is also assumed that there is no residual flux in the core. In such a case, the transient asymmetry of the fluxes in each core, will be the same as separate single phases. Fig. 3.7(a) shows the flux condition in phase 'a'. As switching of phase 'a' is at  $90^\circ$  of the voltage waveform, practically the inrush will be negligible. The transient flux swing in phase 'b' will start from zero and the inrush will occur when the flux crosses the saturation level. As shown in Fig. 3.7(b), the inrush will take place in positive direction of voltage wave. For phase 'c', the relevant diagram is shown in Fig. 3.7(c) where the inrush takes place in the negative direction of voltage wave. It is also to be noted that the inrush in phase 'b' and 'c' occur in two different times in cycle. These currents have a return path to supply through the grounded neutral.

(B) Core-type Y- $\Delta$  transformer with neutral grounded: If the switching condition is same as in 'A', the exciting ampere turns required by the core will remain the same, since it is of no importance whether the core of the

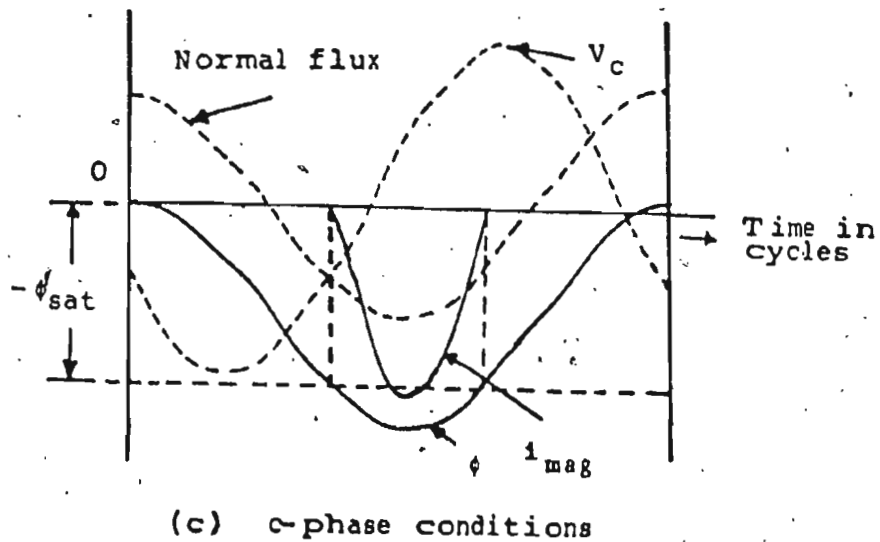
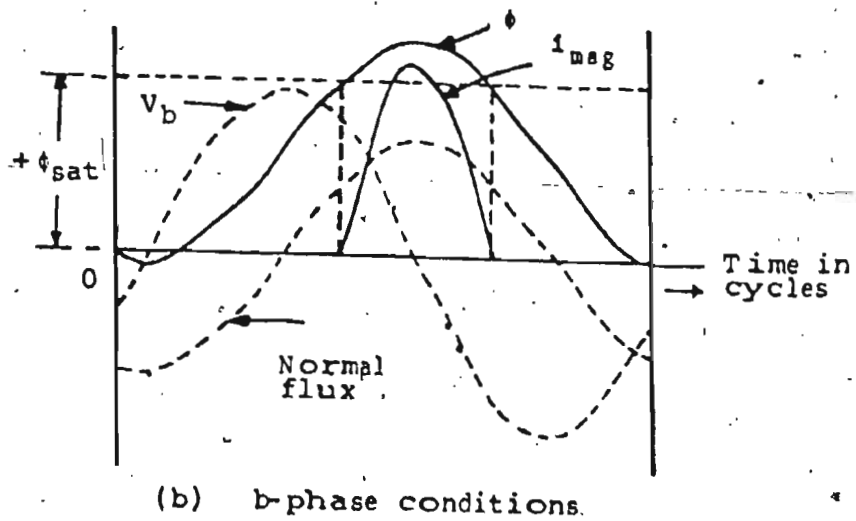
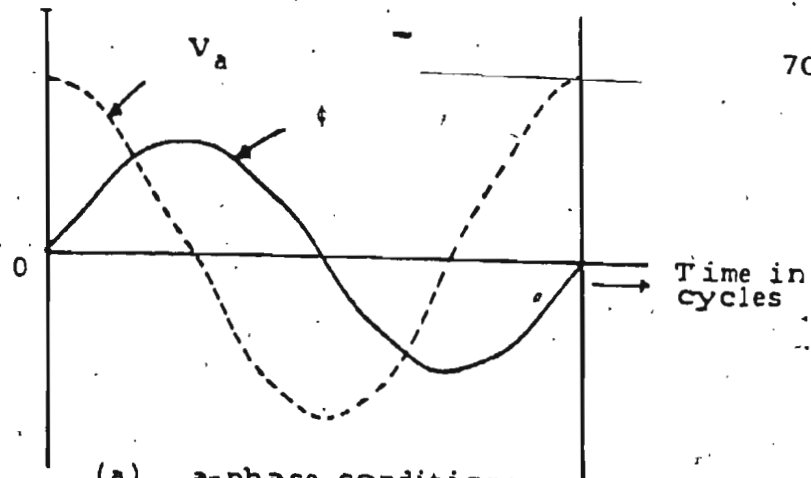


Fig. 3.7 Transient fluxes and inrush currents in a 3-phase transformer energized at 90° of  $V_a$

transformer obtains its existing ampere-turns from the primary winding capable of supplying ampere-turns or from any other linked winding capable of supplying ampere-turns. So currents may show up in all three phases while only one phase is experiencing the inrush. In this case, any core-limb demanding inrush ampere-turns during a certain part of a cycle is provided by the other two phases with an auxiliary source by virtue of the magnetic coupling of the closed delta winding. This is explained in Fig. 3.8, where it is presumed that phase 'a' is experiencing an inrush. In this case, phase 'a', needs an excess amount of exciting current for the duration of the inrush and an auxiliary source of supply is available through its secondary winding energized from the delta connected windings of phases 'b' and 'c'. The direction arrows for the currents flowing in the windings of phases 'b' and 'c' are in opposite direction. This is because phases 'b' and 'c' are helping the inrush in phase 'a'. Hence the incoming current in phase 'a' is being neutralized by outgoing current in the other two phases. If the connection to the ground were open, the magnitudes of phase 'b' and phase 'c' currents would each be equal to one-half the magnitude of phase 'a' current. With the ground connection complete as shown, the magnitudes of phase 'b' and phase 'c' currents will be something less than half the magnitude of phase 'a' current, depending upon the amount of

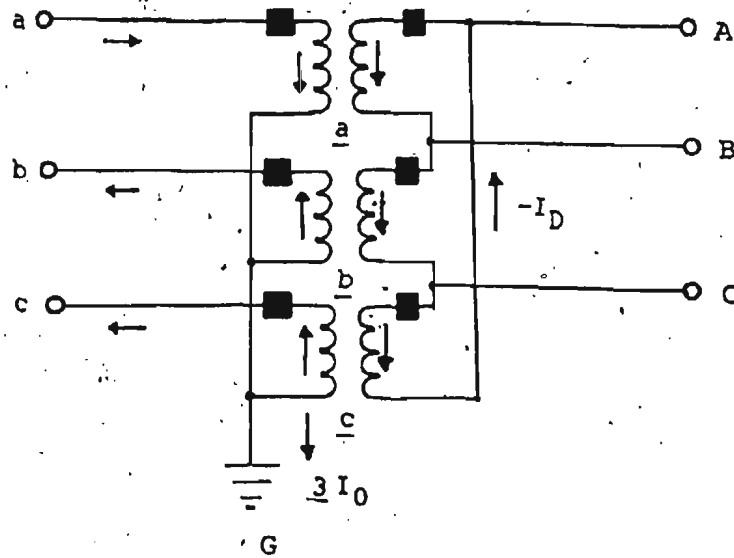


Fig. 3.8 Instantaneous current directions for transformer a experiencing an inrush

current  $3I_0$  flowing in the ground.

Typical star currents with ungrounded neutral are shown in Fig. 3:9. The helping effect of two phases to the third phase is evident in the traces for the three star currents  $I_a$ ,  $I_b$  and  $I_c$ . Inspection of these traces indicates that the inrush current starts in phase 'a' first. For the first portion of the cycle, phases 'b' and 'c' are helping phase 'a' as indicated by the wave-trace from the starting time up to the point 'x' on the wave trace for  $I_c$ . At point 'x' on  $I_c$ , phase 'c' begins to experience its own inrush, as the current begins to increase rapidly in magnitude. This presents a new problem in phase 'b', in that it is now called on to help supply the demands of both phase 'a' and phase 'b'. Since the two demands are in opposite directions, the current from phase 'b' flows in the direction of maximum instantaneous demand. From point 'p' to point 'q', phase 'a' requirements are greater than phase 'c'; therefore, the instantaneous value of  $I_b$  remains with a negative polarity but rising towards zero. From point 'q' to point 'R', the requirements of phase 'c' exceed that of phase 'a'. Phase 'b' current therefore increases with a positive polarity to help supply the demand. At the peak of phase 'b', current 'R', coincidental with point 'Y' on the trace for  $I_a$ , the inrush for phase 'a' has temporarily subsided, and phase 'a' and phase 'b' help phase 'c' until the peak of current

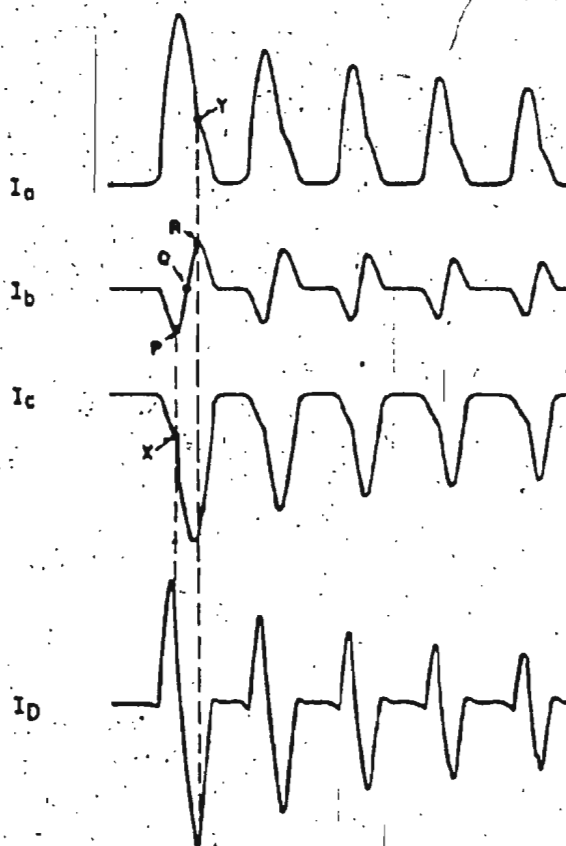


Fig. 3.9 Typical inrush currents of a Y- $\Delta$  transformer energized from Y-side



in phase 'c' subsides to zero. The whole process is repeated in the next half cycle.

(C) Core-type  $\Delta$ -Y transformer When a  $\Delta$ -connected primary is energized, no helping effect is found as the secondary is Y-connected. The current in each phase is independent of the other phases, and the inrush phenomena of each phase take place individually on a single-phase basis. As far as the line currents are concerned, they will be the instantaneous differences of the respective phases. A typical delta connected primary inrush is shown in Fig. 3-10.

### 3.2.2 Analysis of 3-Phase Inrushes

As explained in Section 3.2.1, the analysis of inrush current for Y-connected primary is more complicated than that of a  $\Delta$ -connected primary transformer. Also, the inrush waveform contains a number of harmonics. Hence, the sequence impedance values will change in actual cases whereas the analysis is restricted only to fundamental quantities. Due to these limitations, a quantitative analysis is done which can be applied later on for simulation purposes.

(a) Y-Connected Primary It is first presumed that the total amount of magnetizing current required for the core of each of the phases will be a known quantity which can be analysed as described in Section 3.1.2. These inrush currents are designated as  $I_{ma}$ ,  $I_{mb}$  and  $I_{mc}$  for phases 'a',

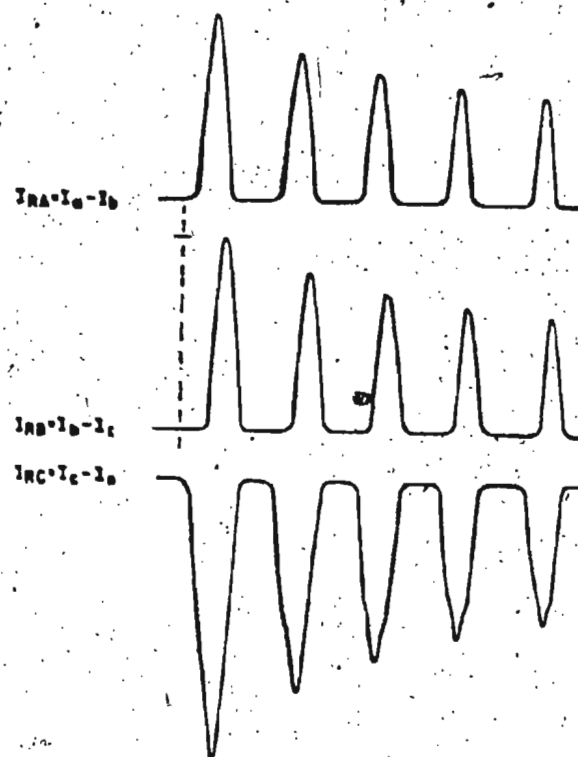


Fig. 3.10 Typical inrush currents of a Δ-Y transformer energized from Δ-side

'b' and 'c', respectively. Fig. 3-11 (a) shows the equivalent circuit for the phase 'a' transformer, where  $I_{ma}$  is the current flowing through the magnetizing branch of the transformer. The total leakage impedance of the transformer is split into two parts,  $Z_p$  and  $Z_{ss}$ .  $Z_p$  represents the primary leakage impedance and  $Z_{ss}$  represents the secondary leakage impedance referred to the primary side. ' $X_m$ ' is the magnetizing branch reactance and ' $E_m$ ' represents the excitation voltage. Similarly, for each of the phases, equivalent circuits can be drawn.

Fig. 3.11 (b) shows the circuit used for the analysis. The generated voltages at the ultimate source are shown as  $E_a$ ,  $E_b$  and  $E_c$ . The total system impedance up to the transformer input terminals are shown as  $Z_s$  and  $Z_{0s}$ .  $Z_s$  represents both the positive and negative sequence impedance of the system, while  $Z_{0s}$  represents the zero-sequence impedance of the system. The  $\Delta$ -terminals A, B and C on the secondary side is disconnected from the rest of the system. The only reflected current that can flow in the delta winding is  $I_d$ . In Fig. 3.11(a), the sign of  $I_d$  is negative because it flows in opposite direction to that of the primary as shown in Fig. 3.11 (b). All the input currents in Fig. 3.11(b) are unidirectional. This is done so as to facilitate having general form of equations which will allow for the possibility of any two phases helping the third, regardless

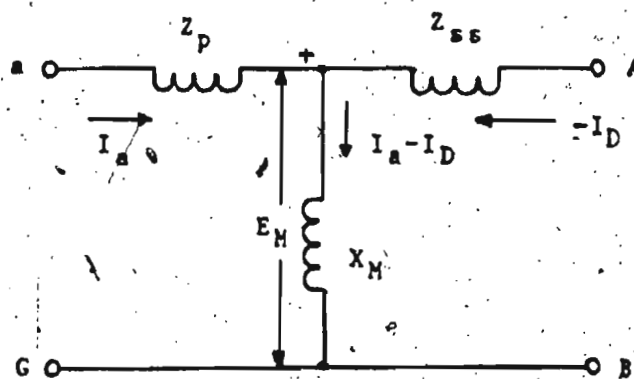


Fig. 3.11 (a) Equivalent diagram for phase a transformer

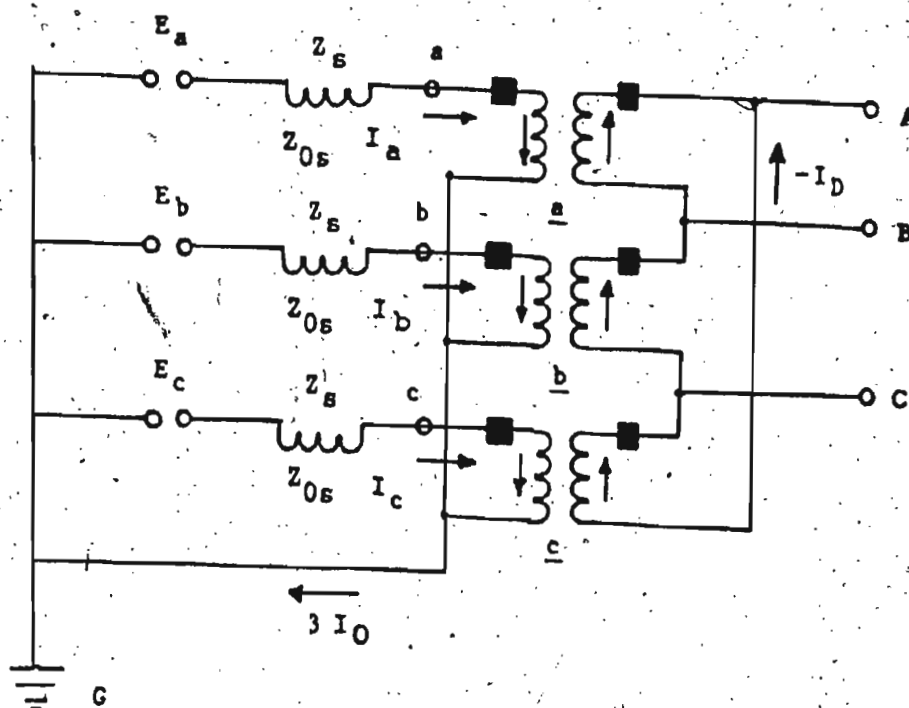


Fig. 3.11 (b) A Y-Δ connected bank with source impedance on Y-side

of which one is involved. Now, from

Fig. 3.11(a), one obtains:

$$I_a - I_{ma} = I_D \quad (3.29)$$

$$I_b - I_{mb} = I_D \quad (3.30)$$

$$I_c - I_{mc} = I_D \quad (3.31)$$

From Fig. 3.11(b),

$$I_a + I_b + I_c = 3I_0 \quad (3.22)$$

$$E_a + E_b + E_c = 0 \quad (3.33)$$

$$E_{AB} + E_{BC} + E_{CA} = 0 \quad (3.34)$$

The individual voltage equations can be written as

$$E_{AB} = E_a - I_a Z_s - I_0(Z_{0s} - Z_s) - I_{ap} Z_p - I_D Z_{ss} \quad (3.35)$$

$$E_{BC} = E_b - I_b Z_s - I_0(Z_{0s} - Z_s) - I_{bp} Z_p - I_D Z_{ss} \quad (3.36)$$

$$E_{CA} = E_c - I_c Z_s - I_0(Z_{0s} - Z_s) - I_{cp} Z_p - I_D Z_{ss} \quad (3.37)$$

Solving the Eqns. (3.29) to (3.37) the phase inrush currents can be found as (the detailed solutions are given in Appendix-B),

$$I_a = I_{ma} \left( \frac{5Z_{ss} + 2Z_{0s}}{6Z_{ss} + 3Z_{0s}} \right) - I_{mc} \left( \frac{Z_{ss} + Z_{0s}}{6Z_{ss} - 3Z_{0s}} \right) \quad (3.38)$$

$$I_b = I_D = -(I_{ma} + I_{mc}) \left( \frac{Z_{ss} + Z_{0s}}{6Z_{ss} + 3Z_{0s}} \right) \quad (3.39)$$

$$I_c = I_{mc} \left( \frac{5Z_{ss} + 2Z_{0s}}{6Z_{ss} + 3Z_{0s}} \right) - I_{ma} \left( \frac{Z_{ss} + Z_{0s}}{6Z_{ss} + 3Z_{0s}} \right) \quad (3.40)$$

The above equations were developed on the assumption that

the inrush occurred in phase 'a' and in phase 'c', whereas the inrush in phase 'b' is zero. For other conditions, similar set of equations can be developed.

Eqn. (3.39) yields an oscillatory-type wave whenever  $I_{ma}$  and  $I_{mc}$  are of opposite polarity and are shifted in the time-phase with respect to each other.

The boundary value of Eqns. (3.38) to (3.40) will depend upon the values of the sequence impedances. Two extreme conditions which yielded simplified results are considered.

I. When zero sequence impedance is zero

With the limit,  $Z_{0s} \rightarrow 0$ ,

$$I_a = \frac{5}{6} I'_{ma} - \frac{1}{6} I_{mc} \quad (3.41)$$

$$I_b = -\frac{1}{6} I'_{ma} - \frac{1}{6} I_{mc} \quad (3.42)$$

$$I'_c = \frac{5}{6} I_{mc} - \frac{1}{6} I'_{ma} \quad (3.43)$$

II. When zero-sequence impedance is infinity

With the limit,  $Z_{0s} \rightarrow \infty$ ,

$$I_a = \frac{2}{3} I'_{ma} - \frac{1}{3} I_{mc} \quad (3.44)$$

$$I_b = -\frac{1}{3} I'_{ma} - \frac{1}{3} I_{mc} \quad (3.45)$$

$$I_c = \frac{2}{3} I_{mc} - \frac{1}{3} I'_{ma} \quad (3.46)$$

Hence, the accuracy of the predicting inrush currents will

depend on the correct choice of sequence impedance values.

(B) Δ-connected Primary: The inrush phenomena of each phase of the delta-side will take place individually on a single-phase basis. So, the currents in each phase will be the instantaneous difference of the respective currents as shown in the Figure 3.10. Hence, the inrush currents in the three phases are as follows,

$$I_A = I_{ma} - I_{mc} \quad (3.47)$$

$$I_B = I_{mb} - I_{ma} \quad (3.48)$$

$$I_C = I_{mc} - I_{mb} \quad (3.49)$$

### 3.2.3 Analysis Taking Into Account The Mutual Inductive Couplings

The analysis of three-phase transformers carried out in the earlier subsections did not take into account the effect of mutual magnetic couplings between the various limbs of transformers. In other words, it was done as if the three phases are electrically connected but magnetically isolated. This is true if three isolated single-phase transformers are electrically connected for three-phase representation. The accuracy will be improved if mutual couplings are taken into account in the case of analysis of a 3-phase, 3-limb core-type transformer.

A configuration of a 3-limb transformer is shown in Figure 3.12, where the magnetic flux associated with the transformer can be subdivided for analysis into three different categories as follows:

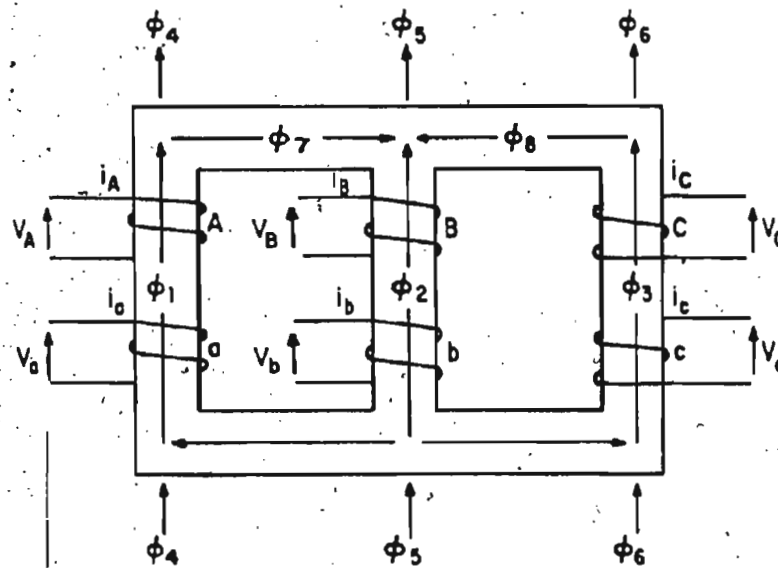


Fig. 3.12 Diagram of a 3-phase, 3-limb transformer showing assumed flux paths and reference directions



(a) Magnetic flux which links mainly the coils of the same phase and has a magnetic path which is mainly confined to the core material.

(b) Leakage flux which links with only one coil and has a magnetic path which is mainly in the air.

(c) Interphase leakage flux which couples the coils of the same phase and path of this flux is mainly through yoke sections of the transformer.

The fluxes can be split as shown in Fig. 3.12, accordingly,

$\phi_1, \phi_2, \phi_3$  - fluxes associated with limbs

$\phi_4, \phi_5, \phi_6$  - fluxes associated with phase-leakage paths

$\phi_7, \phi_8$  - fluxes associated with yokes

Now, if the secondary quantities of the transformer are referred to the primary side, the voltage equation of phase A can be written as

$$V_A = R_A i_A + L_A p i_A + N \frac{d\phi_1}{dt} \quad (3.50)$$

where  $V_A$ ,  $R_A$ ,  $L_A$  are the applied voltage, resistance of the coil and leakage inductance of phase-A respectively and 'N' is the number of turns in the primary. 'p' is the differential operator  $\frac{d}{dt}$ . Now,

$$\phi = B \times A = \frac{\mu N i}{l} \times A = \mu H A \quad (3.51)$$

where 'l' is the length. Hence, Eqn. 3.50 can be rewritten

in the form,

$$V_A = R_A i_A + l_A p i_A + N A_1 \mu_1 p H_1 \quad (3.52)$$

If the magnetizing current for the limb of coil 'A' is defined as  $i_1 = H_1 l_1 / N$ , then by substituting this value in Eqn. (3.52) gives:

$$V_A = R_A i_A + l_A p i_A + M_1 p i_1 \quad (3.53)$$

It is to be noted that Eqn. (3.53) is now modified with the mutual coupling term  $M_1$  here.

Similarly, for the other phases in the primary and all phases in the secondary side, the equations can be written as,

$$V_B = R_B i_B + l_B p i_B + M_2 p i_2 \quad (3.54)$$

$$V_C = R_C i_C + l_C p i_C + M_3 p i_3 \quad (3.55)$$

$$V_a = R_a i_a + l_a p i_a + M_1 p i_1 \quad (3.56)$$

$$V_b = R_b i_b + l_b p i_b + M_2 p i_2 \quad (3.57)$$

$$V_c = R_c i_c + l_c p i_c + M_3 p i_3 \quad (3.58)$$

In the above equations, the subscripts A, B, C and a, b, c refer to the primary and secondary respectively and subscript 1, 2, 3 refer to the respective limb section of Fig. 3.12. The resistance and inductance of the source can be added to  $R$  and  $l$  in the primary equations.

By applying the magnetic circuit equation,  $\oint H \cdot dl = 0$  at any junction, and expressing the resulting equations in terms of inductance and branch magnetising currents, the followings are obtained:

$$0 = M_1 p i_1 - M_4 p i_4 - M_7 p i_7 \quad (3.59)$$

$$0 = M_2 p i_2 - M_5 p i_5 + M_7 p i_7 + M_8 p i_8 \quad (3.60)$$

$$0 = M_3 p i_3 - M_6 p i_6 - M_8 p i_8 \quad (3.61)$$

Applying the magnetic circuit law,

$$NI = \oint H d \ell,$$

gives,

$$i_4 = i_A + i_a - i_1 \quad (3.62)$$

$$i_5 = i_B + i_b - i_2 \quad (3.63)$$

$$i_6 = i_C + i_c - i_3 \quad (3.64)$$

$$i_7 = i_A + i_a - i_B - i_b - i_1 + i_2 \quad (3.65)$$

$$i_8 = i_C + i_c - i_B - i_b - i_3 + i_2 \quad (3.66)$$

The above Eqns. (3.53 to (3.61) consist of nine differential equations and Eqns. (3.62) to (3.66) consist of five algebraic equations. Solving these fourteen equations, a generalized matrix equation can be found as

$$[H][pI] = [Z][V] - [Y][I] \quad (3.67)$$

The derivation of Eqns. (3.67) is shown in Appendix B, for no load condition. The different matrix elements of Eqn. 3.67, for no load condition are as follows,

$$[H] = \begin{bmatrix} l_A & 0 & 0 & M_1 & 0 & 0 \\ 0 & l_B & 0 & 0 & M_2 & 0 \\ 0 & 0 & l_C & 0 & 0 & M_3 \\ -(M_4 + M_7) & M_7 & 0 & (M_1 + M_4 + M_7) & -M_7 & 0 \\ M_7 & (M_5 + M_7 + M_8) & M_8 & -M_7 & (M_2 + M_5 + M_7 + M_8) & -M_8 \\ 0 & M_8 & -(M_6 + M_8) & 0 & -M_8 & (M_3 + M_6 + M_8) \end{bmatrix}$$

$$[pI] = \begin{bmatrix} pI_A \\ pI_B \\ pI_C \\ pI_1 \\ pI_2 \\ pI_3 \end{bmatrix}$$

$$[V] = \begin{bmatrix} V_A \\ V_B \\ V_C \\ 0 \\ 0 \\ 0 \end{bmatrix}$$

$$[I] = \begin{bmatrix} I_A \\ I_B \\ I_C \\ 0 \\ 0 \\ 0 \end{bmatrix}$$

$$[Z] = \begin{bmatrix} 1 & 0 & 0 & 0 & 0 & 0 \\ 0 & 1 & 0 & 0 & 0 & 0 \\ 0 & 0 & 1 & 0 & 0 & 0 \\ 0 & 0 & 0 & 1 & 0 & 0 \\ 0 & 0 & 0 & 0 & 1 & 0 \\ 0 & 0 & 0 & 0 & 0 & 1 \end{bmatrix}$$

$$[Y] = \begin{bmatrix} R_A & 0 & 0 & 0 & 0 & 0 \\ 0 & R_B & 0 & 0 & 0 & 0 \\ 0 & 0 & R_C & 0 & 0 & 0 \\ 0 & 0 & 0 & 0 & 0 & 0 \\ 0 & 0 & 0 & 0 & 0 & 0 \\ 0 & 0 & 0 & 0 & 0 & 0 \end{bmatrix}$$

Eqn. (3.67) can be written in the following form,

$$[pI] = [H]^{-1}[Z][V] - [X]^{-1}[Y][I] \quad (3.68)$$

If the right hand side matrices are known in the above equation, then magnetizing currents can be found.

For a system, where the secondary is connected to a load, the system Eqn. (3.97) is valid but the dimension of the matrices change as follows,

[H]=

$l_A$	0	0	0	0	0	$M_1$	0	0
0	$l_B$	0	0	0	0	0	$M_2$	0
0	0	$l_C$	0	0	0	0	0	$M_3$
0	0	0	$l_a$	0	0	$M_1$	0	0
0	0	0	0	$l_b$	0	0	$M_2$	0
0	0	0	0	0	$l_c$	0	0	$M_3$
$-(M_4 + M_7)$	$M_7$	0	$-(M_4 + M_7)$	$M_7$	0	$(M_1 + M_4 + M_7)$	$-M_7$	0
$M_7$	$-(M_5 + M_7 + M_8)$	$M_8$	$M_7$	$-(M_5 + M_7 + M_8)$	$M_8$	$-M_7$	$(M_2 + M_5 + M_7 + M_8)$	$-M_8$
0	$M_8$	$-(M_6 + M_8)$	0	$M_8$	$-(M_6 + M_8)$	0	$-M_8$	$(M_3 + M_6 + M_8)$

$$[pI] = \begin{bmatrix} pi_A \\ pi_B \\ pi_C \\ pi_a \\ pi_b \\ pi_c \\ pi_1 \\ pi_2 \\ pi_3 \end{bmatrix}$$

$$[V] = \begin{bmatrix} v_A \\ v_B \\ v_C \\ v_a \\ v_b \\ v_c \\ 0 \\ 0 \\ 0 \end{bmatrix}$$

$$[I] = \begin{bmatrix} i_A \\ i_B \\ i_C \\ i_a \\ i_b \\ i_c \\ i_1 \\ i_2 \\ i_3 \end{bmatrix}$$

$$[z] = \begin{bmatrix} 1 & 0 & 0 & 0 & 0 & 0 & 0 & 0 & 0 \\ 0 & 1 & 0 & 0 & 0 & 0 & 0 & 0 & 0 \\ 0 & 0 & 1 & 0 & 0 & 0 & 0 & 0 & 0 \\ 0 & 0 & 0 & 1 & 0 & 0 & 0 & 0 & 0 \\ 0 & 0 & 0 & 0 & 1 & 0 & 0 & 0 & 0 \\ 0 & 0 & 0 & 0 & 0 & 1 & 0 & 0 & 0 \\ 0 & 0 & 0 & 0 & 0 & 0 & 1 & 0 & 0 \\ 0 & 0 & 0 & 0 & 0 & 0 & 0 & 1 & 0 \\ 0 & 0 & 0 & 0 & 0 & 0 & 0 & 0 & 1 \end{bmatrix}$$



$$[Y] = \begin{bmatrix} R_A & 0 & 0 & 0 & 0 & 0 & 0 & 0 & 0 \\ 0 & R_B & 0 & 0 & 0 & 0 & 0 & 0 & 0 \\ 0 & 0 & R_C & 0 & 0 & 0 & 0 & 0 & 0 \\ 0 & 0 & 0 & R_a & 0 & 0 & 0 & 0 & 0 \\ 0 & 0 & 0 & 0 & R_b & 0 & 0 & 0 & 0 \\ 0 & 0 & 0 & 0 & 0 & R_c & 0 & 0 & 0 \\ 0 & 0 & 0 & 0 & 0 & 0 & 0 & 0 & 0 \\ 0 & 0 & 0 & 0 & 0 & 0 & 0 & 0 & 0 \\ 0 & 0 & 0 & 0 & 0 & 0 & 0 & 0 & 0 \end{bmatrix}$$

### 3.3 Experiemental Results and Computer Simulations

#### 3.3.1 Single-Phase Case

For modelling the inrush current waveform, a 1KVA, 120/120 volts, 60HZ transformer is selected. The parameters have been determiped from standard O.C and S.C., tests. The transformer parameters are as follows:

Full load current in Primary,	$I_A = 8.33A$
Full load current in secondary,	$I_a = 8.33A$
Magnetizing current (steady state),	$I_0 = 1.15A$
Core Resistance, $R_m$	$= 600 \Omega$
Core Reactance, $X_m$	$= 105.96 \Omega$
Equivalent Winding Resistance referred to primary $R_{01}$	$= 0.3174 \Omega$
Equivalent Winding Reactance referred to primary $X_{01}$	$= 0.4374 \Omega$

For modelling the current for a particular value of ' $\lambda$ ', a point-on-wave switch is required. Such a switch using a simple circuit consisting of a single-phase thyristor bridge and a contactor arrangement is shown in Fig. 3.13. If a particular switching angle ' $\lambda$ ' is desired, either in the positive or in the negative direction, it can be set in the bridge circuit accordingly. As soon as the thyristors fire at the specified angle on the voltage waveform, the transformer primary gets energized. Also, the coil 'X' gets energized and changes contact X-1 from NO to NC and contact X-2 from NC to NO. The conduction through thyristors stop and the current is bypassed through the shorted path via X-1.

Fig. 3.14(a) shows the switching of the transformer at  $\lambda=0^\circ$ . Fig. 3.14(b) shows the corresponding inrush for the first five cycles. The applied voltage waveform is to be seen actually inverted because of necessary oscilloscope arrangement to keep a common grounding. The first inrush peak is 24.60A. Fig. 3.15 shows the inrush at the same switching angle,  $\lambda=0^\circ$ , whereas the peaks can be seen as different from those of Fig. 3.14(b). Here, the first peak is 36.40A and it shows that even the transformer is switched on at the same angle, the inrush may vary due to the variation in residual magnetism. Fig. 3.16(a) shows switching at an angle  $\lambda=180^\circ$  (the applied voltage to be seen as inverted) and the corresponding inrush in Fig. 3.16(b)

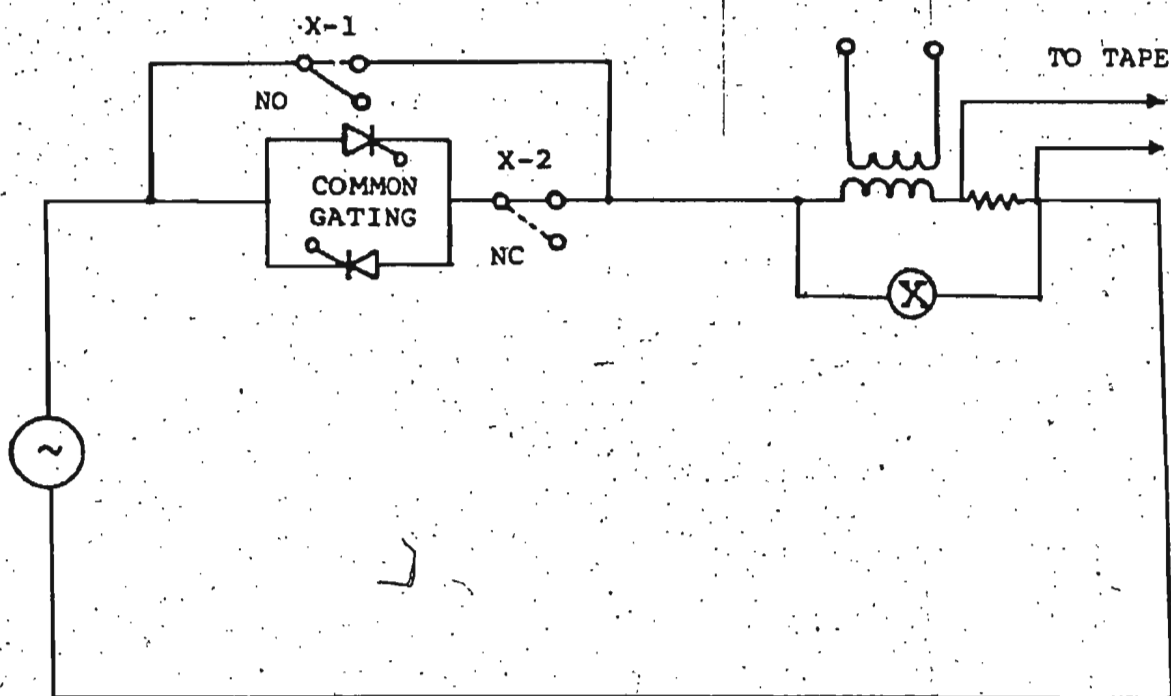


Fig. 3.13 Circuit diagram of single-phase point-on-wave switch

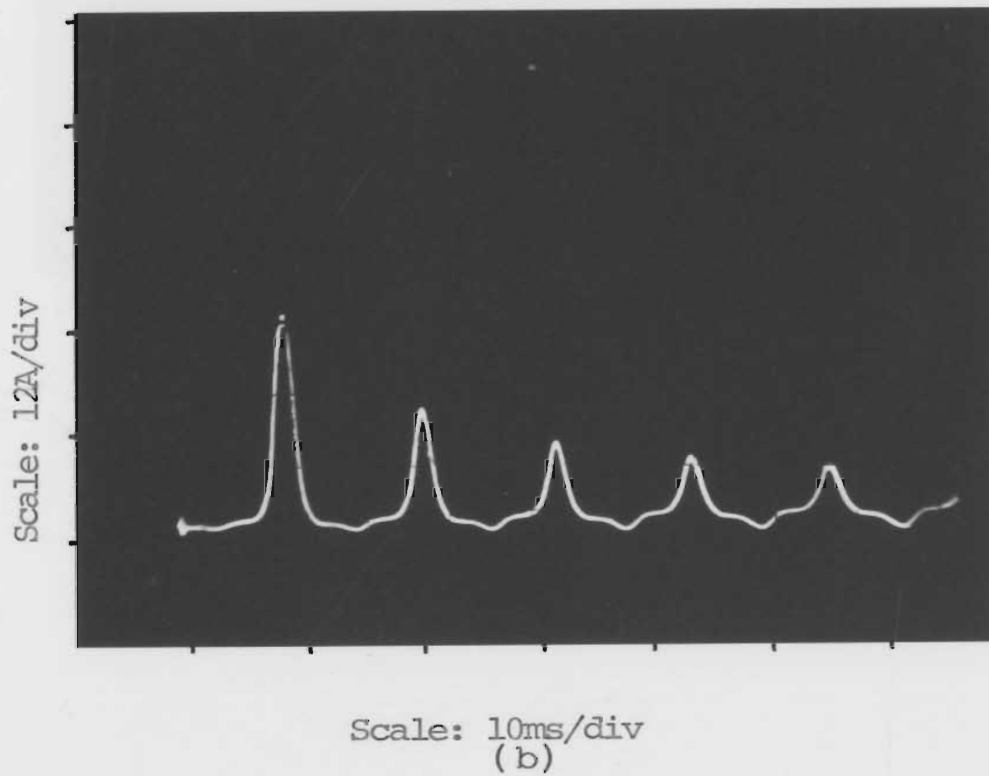
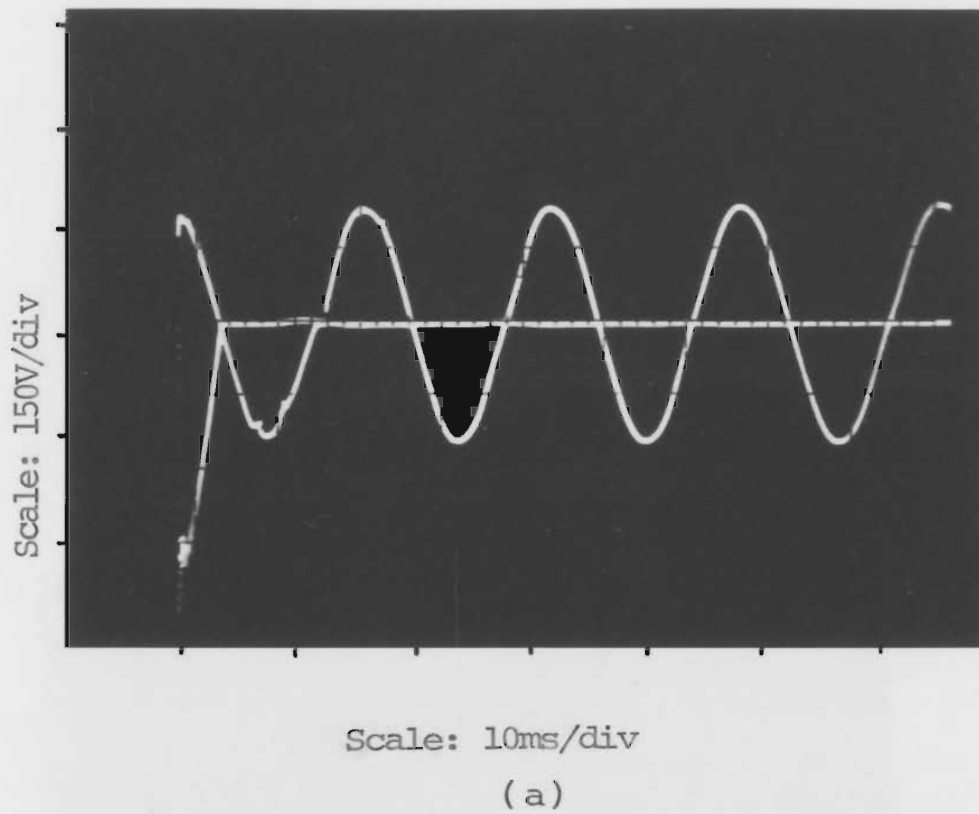


Fig. 3.14 (a) Switching at  $\lambda=0^\circ$   
(applied voltage inverted)  
(b) Positive Inrush

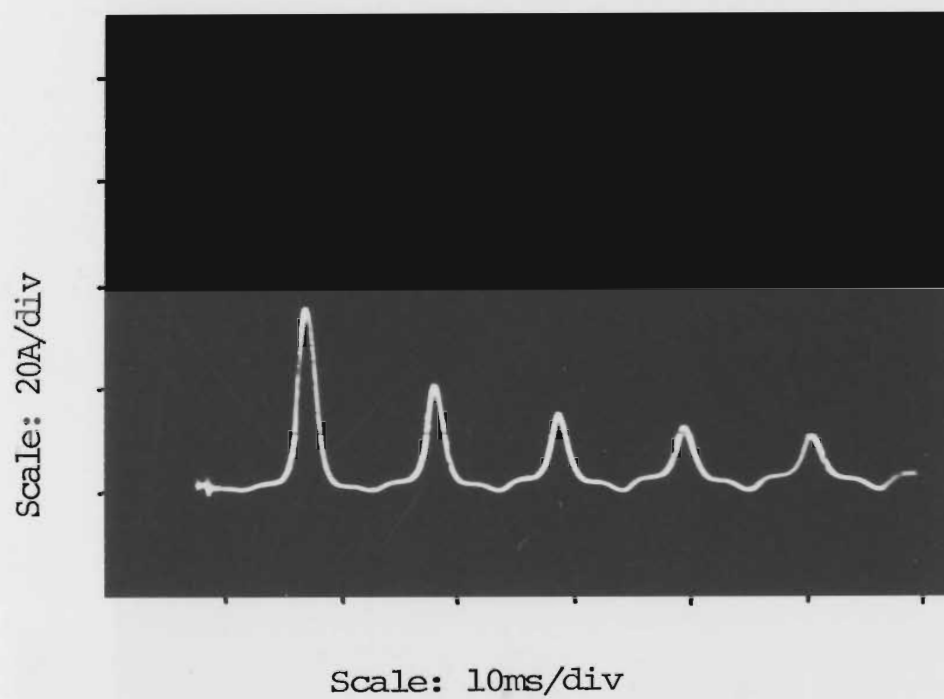
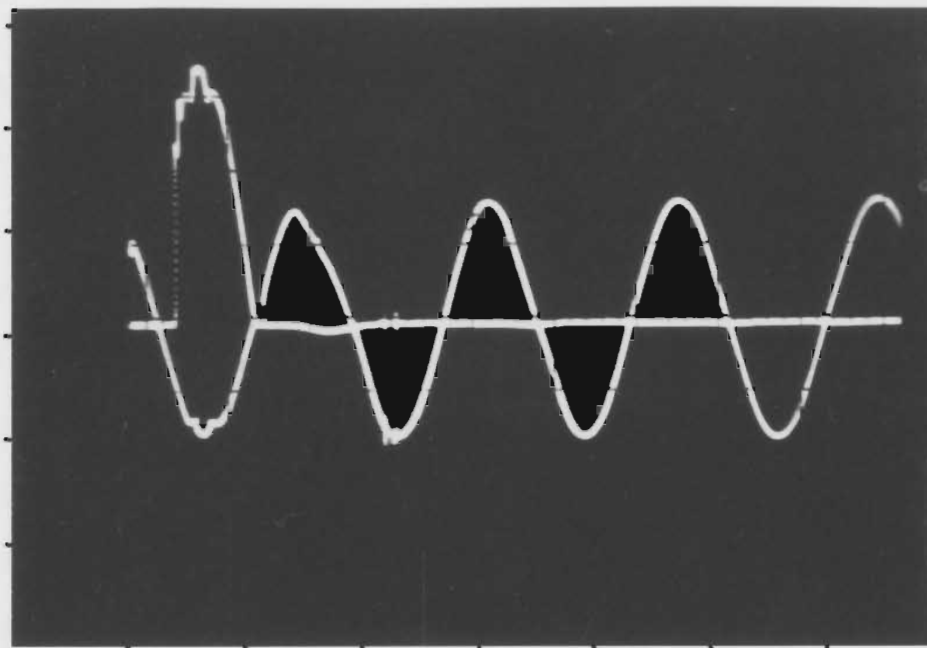


Fig. 3.15 Positive Inrush at same  $\lambda=0^\circ$

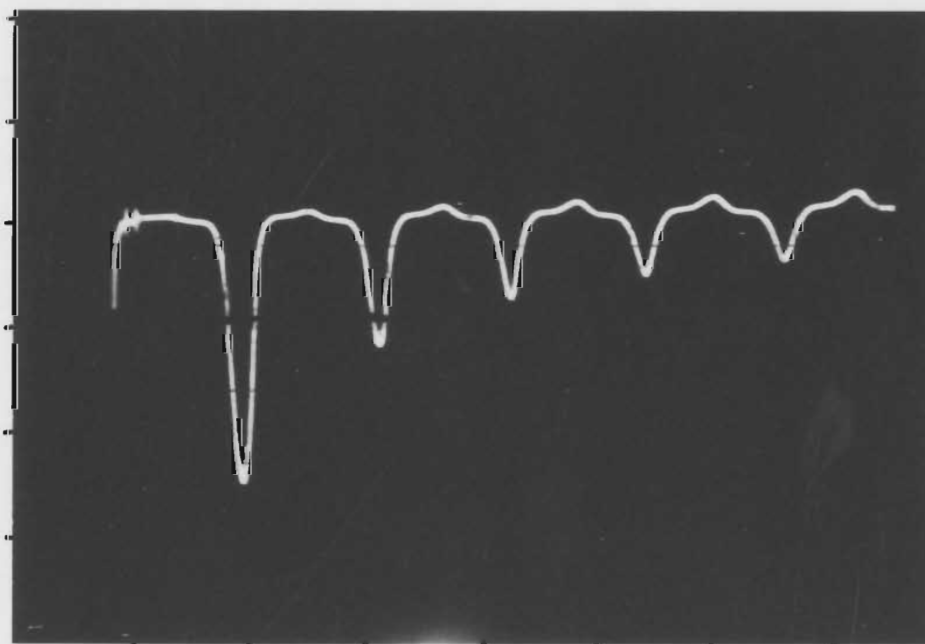
Scale: 150V/div



Scale: 10ms/div

(a)

Scale: 17A/div



Scale: 10ms/div  
(b)

Fig. 3.16 (a) Switching at  $\lambda-180^\circ$   
(applied voltage inverted)

(b) Negative Inrush

which is obviously in negative direction. The magnitude of the first peak is  $-44.3A$ .

It is important that inrush values to be simulated digitally stay within a given accuracy, so that algorithms for digital relay can be tested first on these simulated data. For any cycle of experimental inrush waveform, the current can be calculated using either Eqn. (3.9) or Eqn. 3.24 depending on the value of the switching angle ' $\lambda$ '. In a generalized way, Eqn. (3.24) may be used so that in case of  $\lambda=0^\circ$ , it reduces to Eqn. (3.9). The value of ' $R$ ' is the resistance of the winding to which the source resistance can be added depending on the particular system. If the KVA of the transformer is small in comparison to the KVA of the system from which it is energized, the source resistance and inductance may be assumed as zero [33]. In equation 3.24 ' $X$ ' is not the normal leakage reactance of the transformer. During each of the inrush cycle, the excursion of the flux path is not through the core beyond saturation region. Also, in subsequent cycles, the current damps out. It is difficult to find out the value of the saturation angle  $\theta_s$  which depends upon the amount of residual flux due to previous turn-off of the transformer. An attempt has been made to ascertain these values theoretically using the derived equations. An iterative program is developed accordingly with different values of  $R/X$  ratio. The flow chart of the

program is shown in Fig. 3.17, where it is seen that the only parameters to be known are ' $\lambda$ ' and ' $\gamma$ ', from which the program generates different sets of values for  $I_{pmax}$ ,  $\theta_s$ ,  $X$ ,  $\alpha$  and  $\beta$ . These sets of values for different parameters are utilized to simulate the inrush currents for various cycles. Normally, the first four to five cycles of simulation for inrush current is sufficient as the inrush decays down to a considerable lower value after that. Obviously, it depends upon the rating of a transformer. Also the choice is left while designing a particular system and the limiting values for  $I_{pmax}$ ,  $\theta_s$ ,  $X$ ,  $\alpha$ , and  $\beta$  are being calculated accordingly. Fig. 3.18 shows the flow chart of the programming for simulation where the subroutine calculates the transcendental function for current using Eqn. (3.24). This program calculates the positive value of inrush. For negative inrush currents, the expression for the negative current is to be used.

For simulation purposes, a typical waveform from the test transformer was recorded on a magnetic tape and the trace was reproduced from a Hewlett Packard Fourier Analyzer - 5451B system. This is shown in Fig. 3.19(a). The trace is for a positive inrush at  $\lambda=0^\circ$ . The relative magnitudes can be compared from the left hand side scale, where the first peak is 1.38V. It corresponds to 24.60A. The simulation of the respective current cycles are shown in Fig. 3.19(b). The



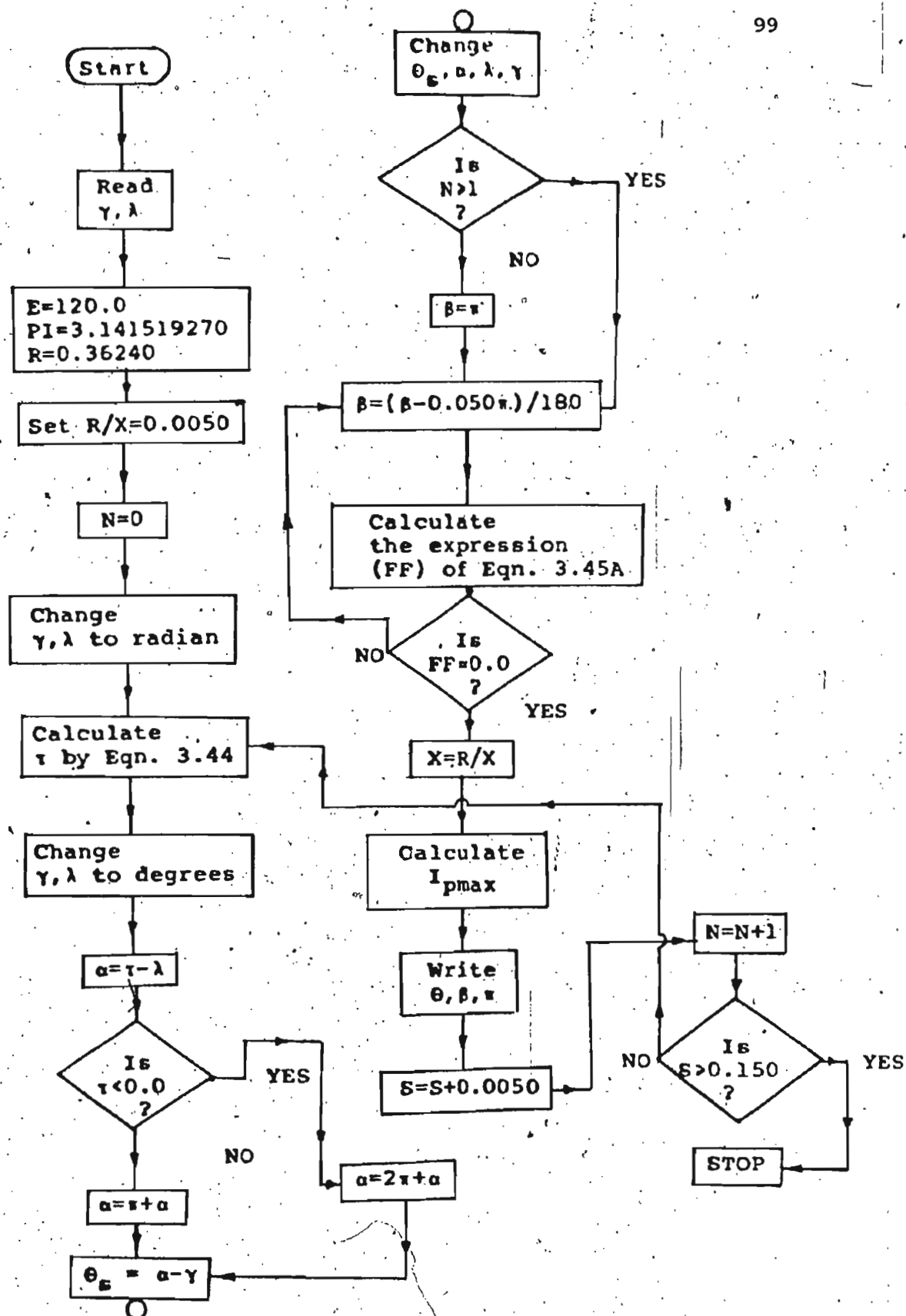


Fig. 3.17 Flow chart of program for calculating various parameters of transformer under switching transient

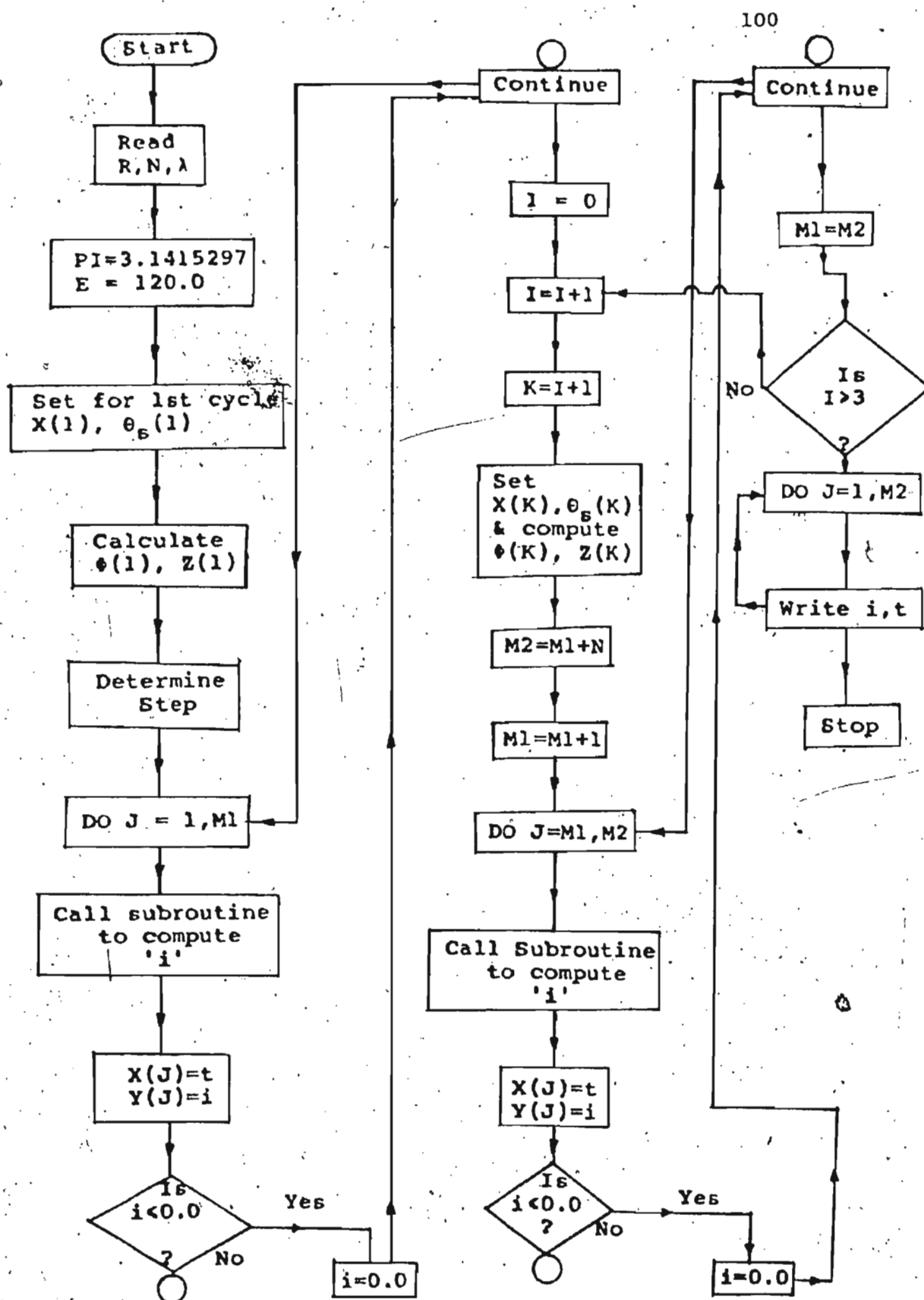


Fig. 3.18 Flow chart of program for digital simulation of single-phase inrush

magnitudes of the respective current peaks for the first 4 cycles are compared in Table 3.1.

$\theta_s$  and  $\gamma$  vary from cycle to cycle according to the change in other parameters. The program for which the flowchart is shown in Fig. 3.18, determines  $\theta_s$  and  $\gamma$  from cycle to cycle. A typical case is simulated here. Fig. 3.20(a) shows the reproduced trace of the inrush current at  $\lambda=0^\circ$  from Fourier Analyzer. The time scale is different from that of Fig. 3.19(a). The first peak is 1.08 V which corresponds to 19.22A. Fig. 3.20(b) shows its simulation with the respective conduction angles. Table 3.2 compares the peak magnitudes and the conduction angles of both the actual and simulated waves.

However, keeping the conduction angle constant at the value for the first cycle, does not affect the operation of the relay as will be seen in a later chapter. In such a case, the program also becomes simplified to certain extent as ' $\theta_s$ ' is also can be taken as constant.

Similarly, a negative inrush is recorded for which  $\lambda=180^\circ$  and reproduced in Fig. 3.21(a). Fig. 3.21(b) shows the simulation of the same waveform for 4 cycles in bigger scale. Table 3.3 compares the peak magnitudes and conduction angles of the measured and simulated waveforms. The conduction angles of the measured waveforms are found from the amplified lobes of the 1st, 2nd, 3rd and 4th cycles of

the inrush which are shown in Figs. 3.21(c) to 3.21(f) respectively.

One will be most interested in the harmonic components of the waveforms, because the algorithms block the relay from operation during inrush on the 2nd harmonic restraint principle. An attempt was made to analyze the harmonics of the individual cycles for both the measured as well as the simulated waveforms. For an example, the harmonic components of the first four cycles of the individual peaks shown in Figs. 3.21(c) to 3.21(f) are compared in Table 3.4 with the corresponding simulated cycles. The individual peaks are again amplified in Figs. 3.22(b) to 3.22(e). Fig. 3.22(a) shows the same output trace of Fig. 3.21(b), this time reproduced from Fourier Analyzer. The left hand scales of Fig. 3.21(a) and Fig. 3.22(b) are not compatible as the input to the Fourier system for the measured and the simulated data are different. Figs. 3.23(a) to 3.23(b) show the continuous and discrete frequency spectrums from the 1st to the 4th cycle of the measured data respectively. Similarly Figs. 3.24(a) to 3.24(h) show the continuous and discrete frequency spectrums of the corresponding simulated cycles respectively.

The discrepancy in the respective harmonic contents of the measured and the simulated waveforms can be explained due to two reasons. The prime reason for the discrepancy is

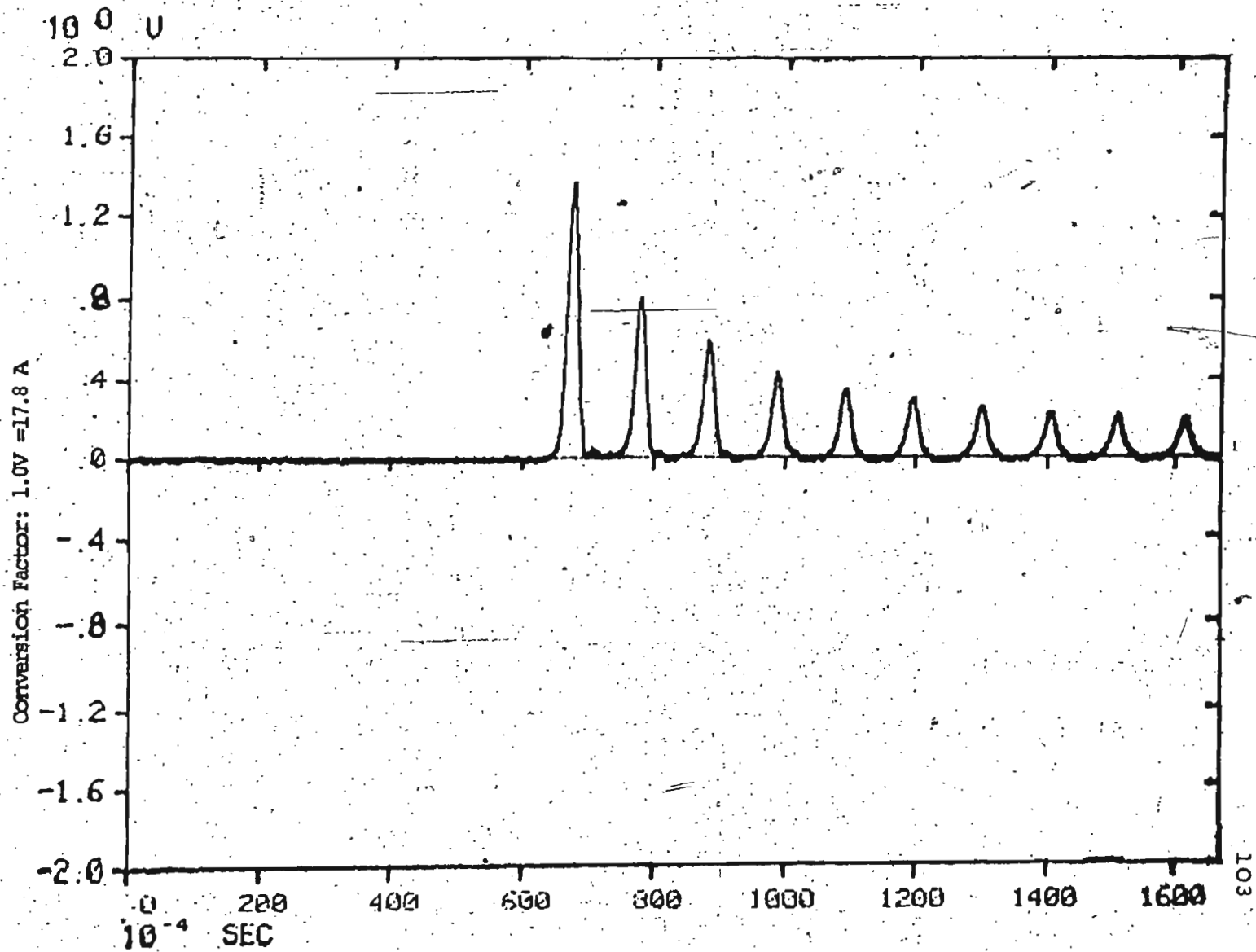


Fig. 3.19 (a) Recorded waveform of a positive inrush current in a single-phase transformer

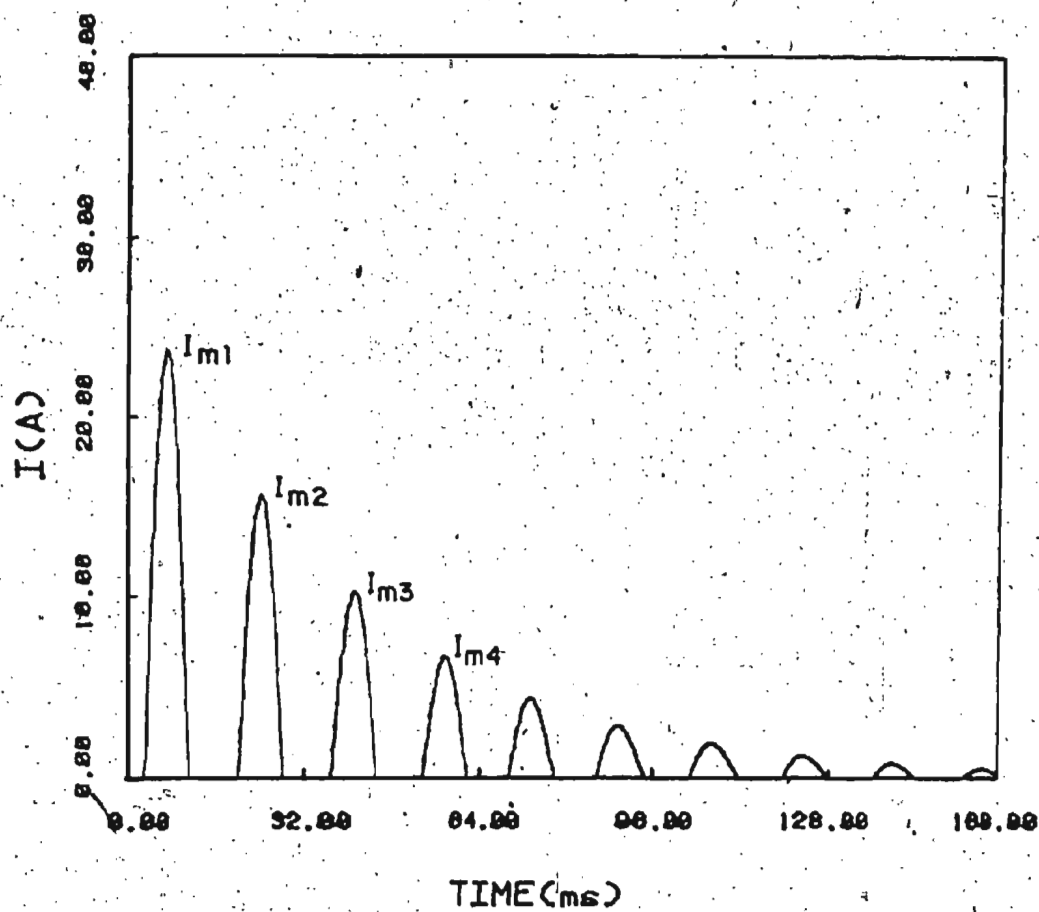


Fig. 3.19 (b) Digital simulation of positive inrush current shown in (a)

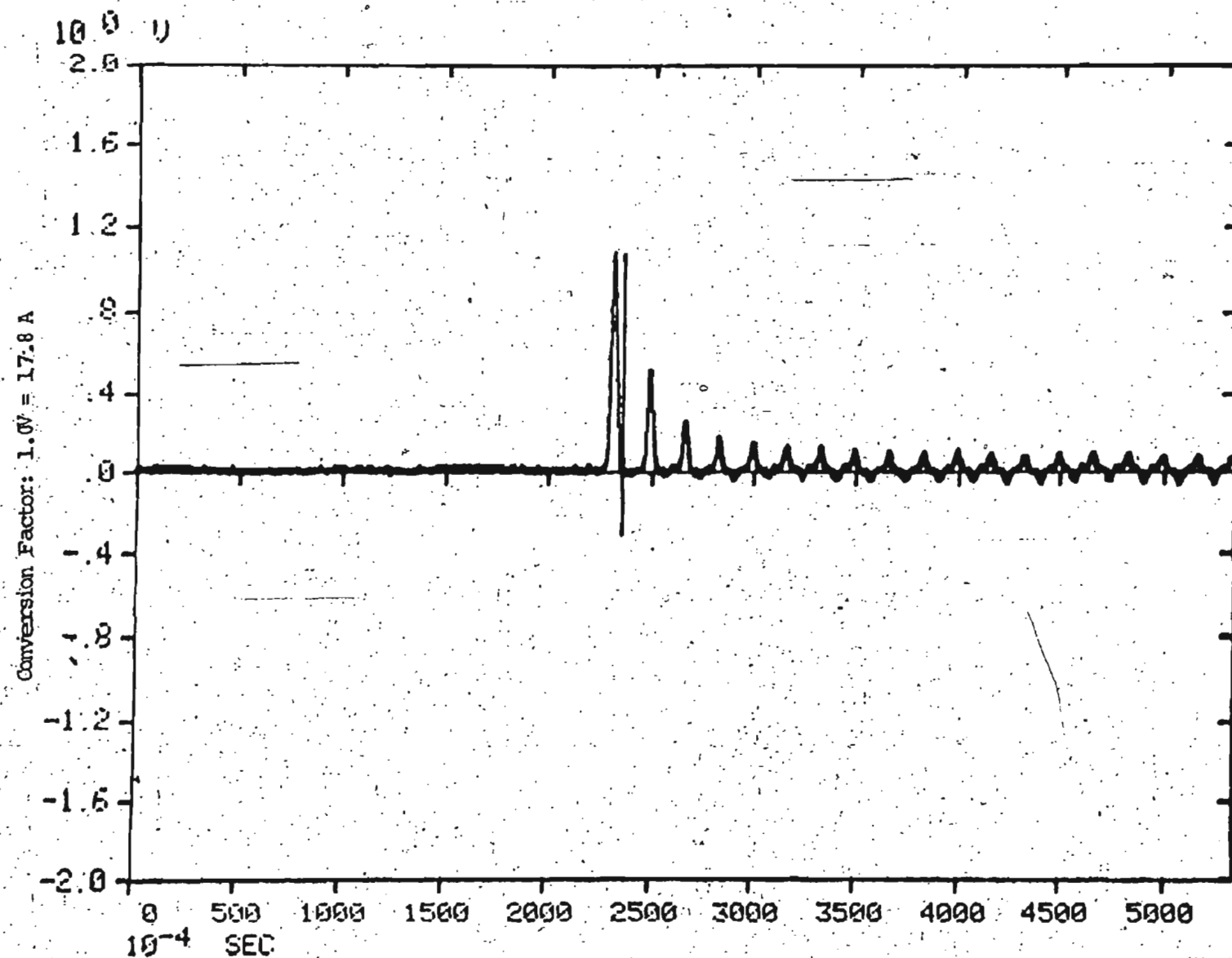


Fig. 3.20 (a) Recorded waveform of a positive inrush at ( $\lambda=0^\circ$ )

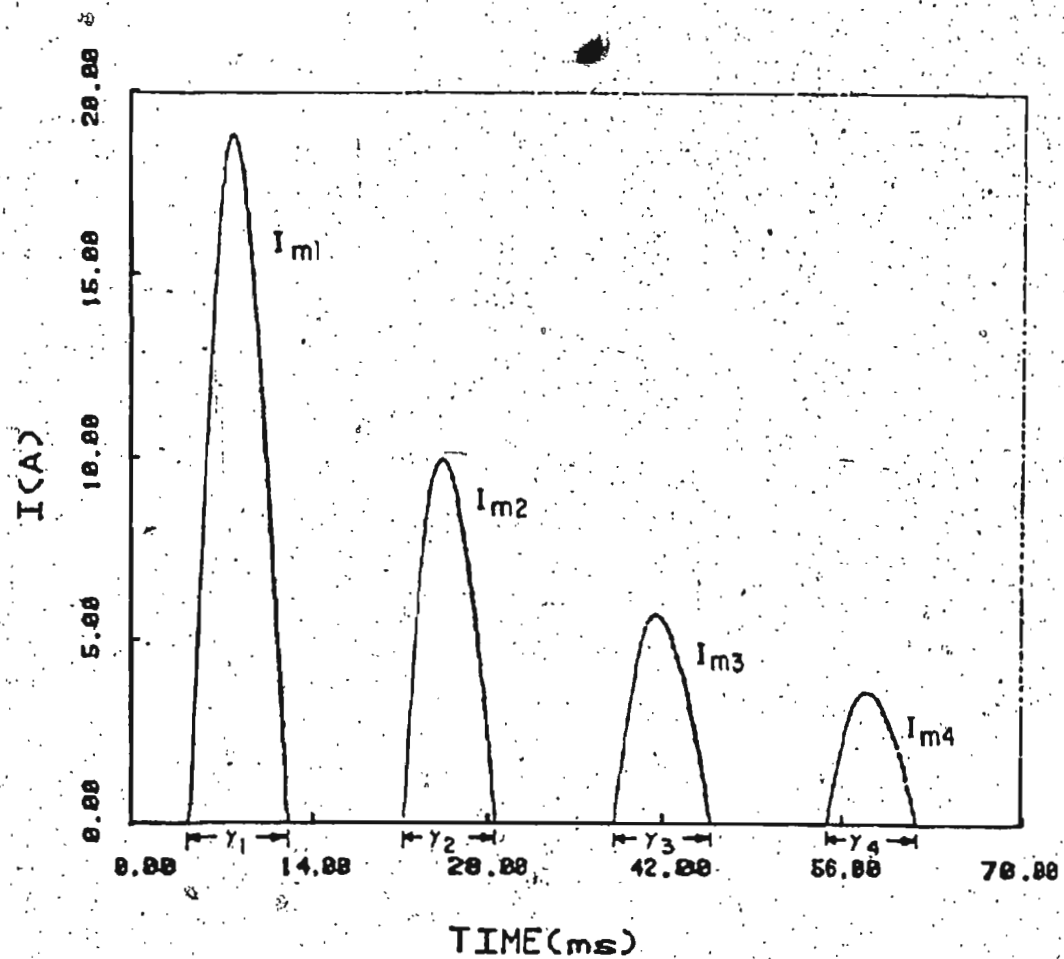


Fig. 3.20 (b) Simulation of inrush current shown in (a) for the first four cycles.



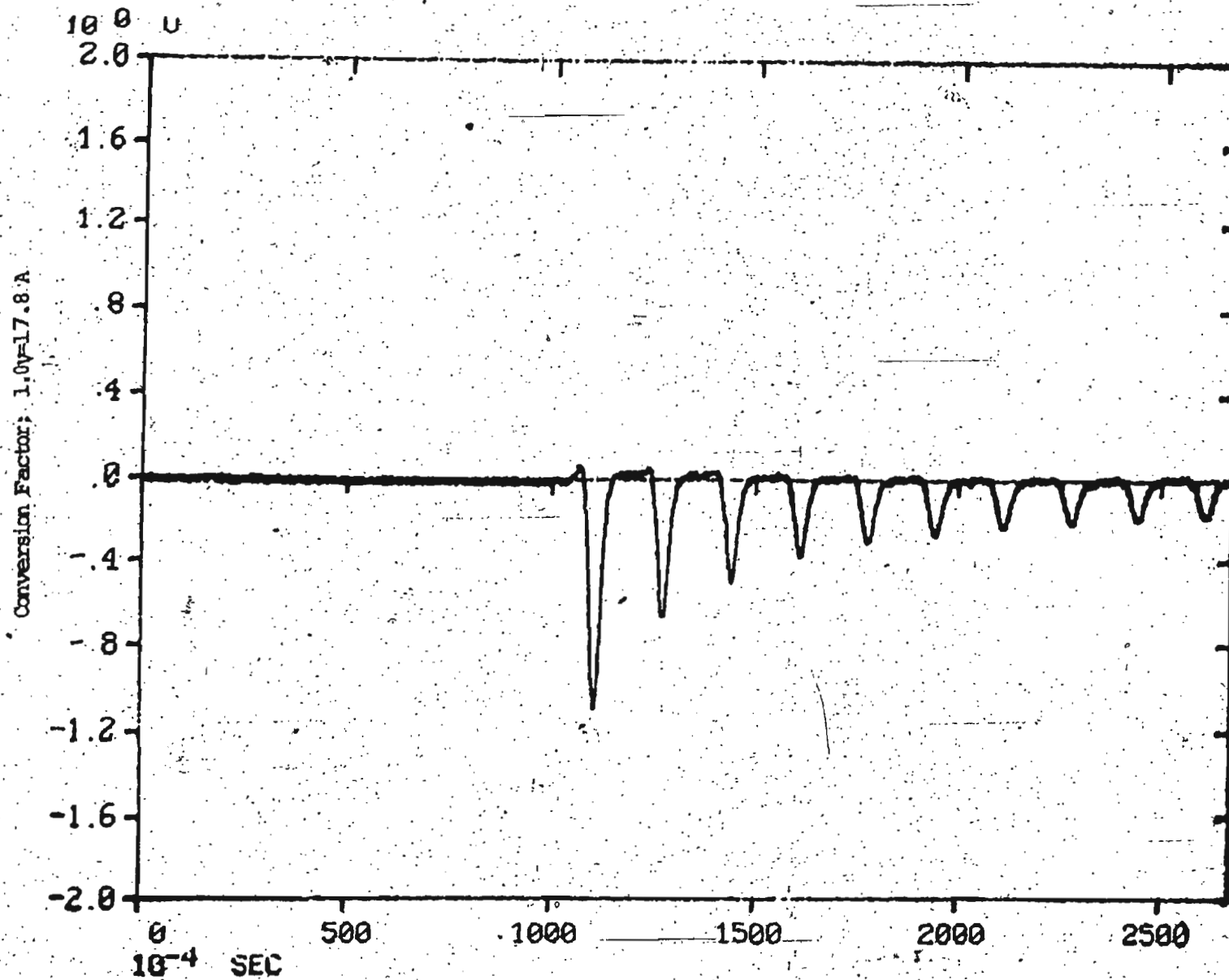


Fig. 3.21 (a) Recorded waveform of a negative inrush  
( $\lambda=180^\circ$ )

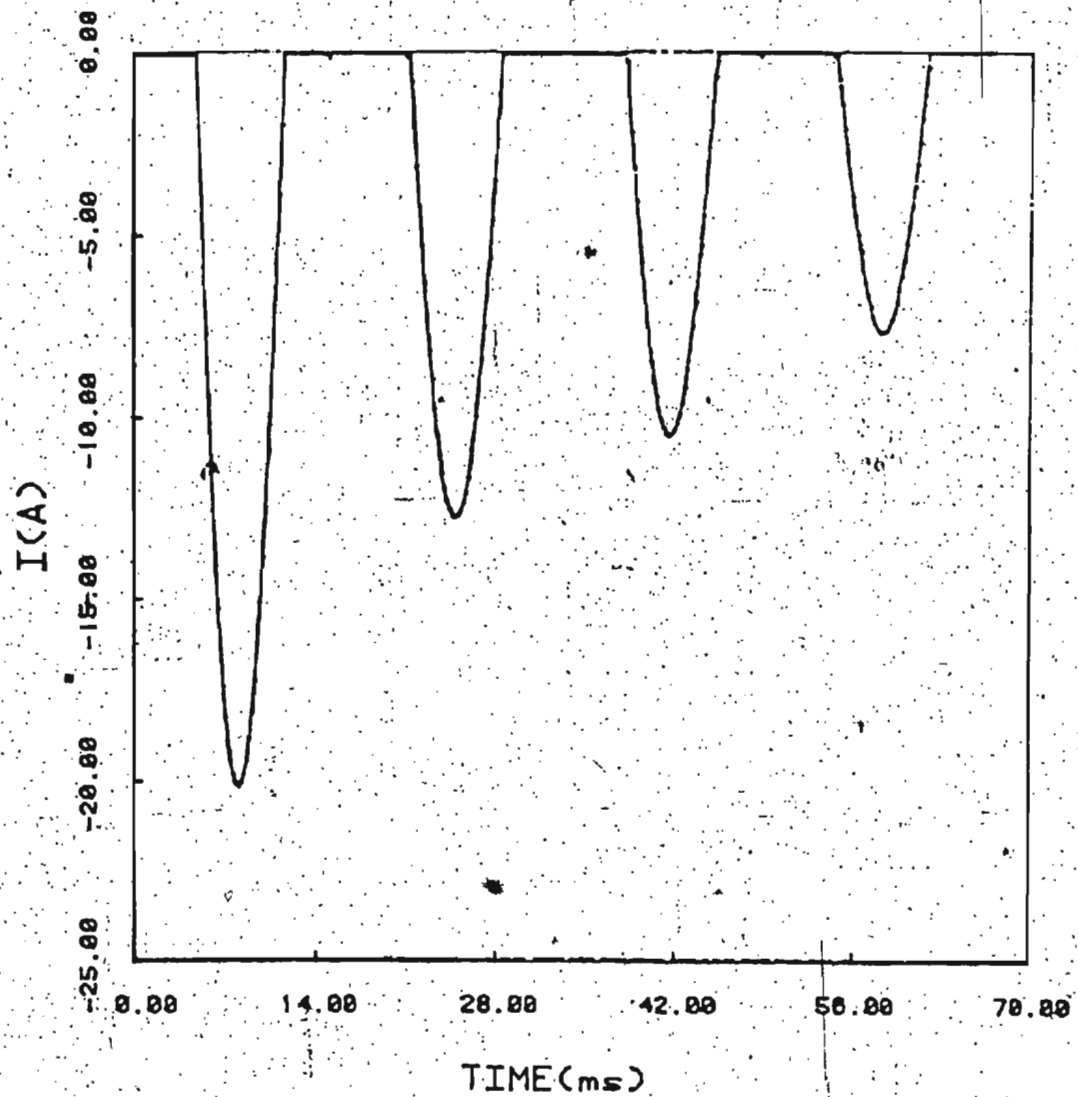


Fig. 3.21 (b) Simulation of inrush current shown in (b) for the first four cycles

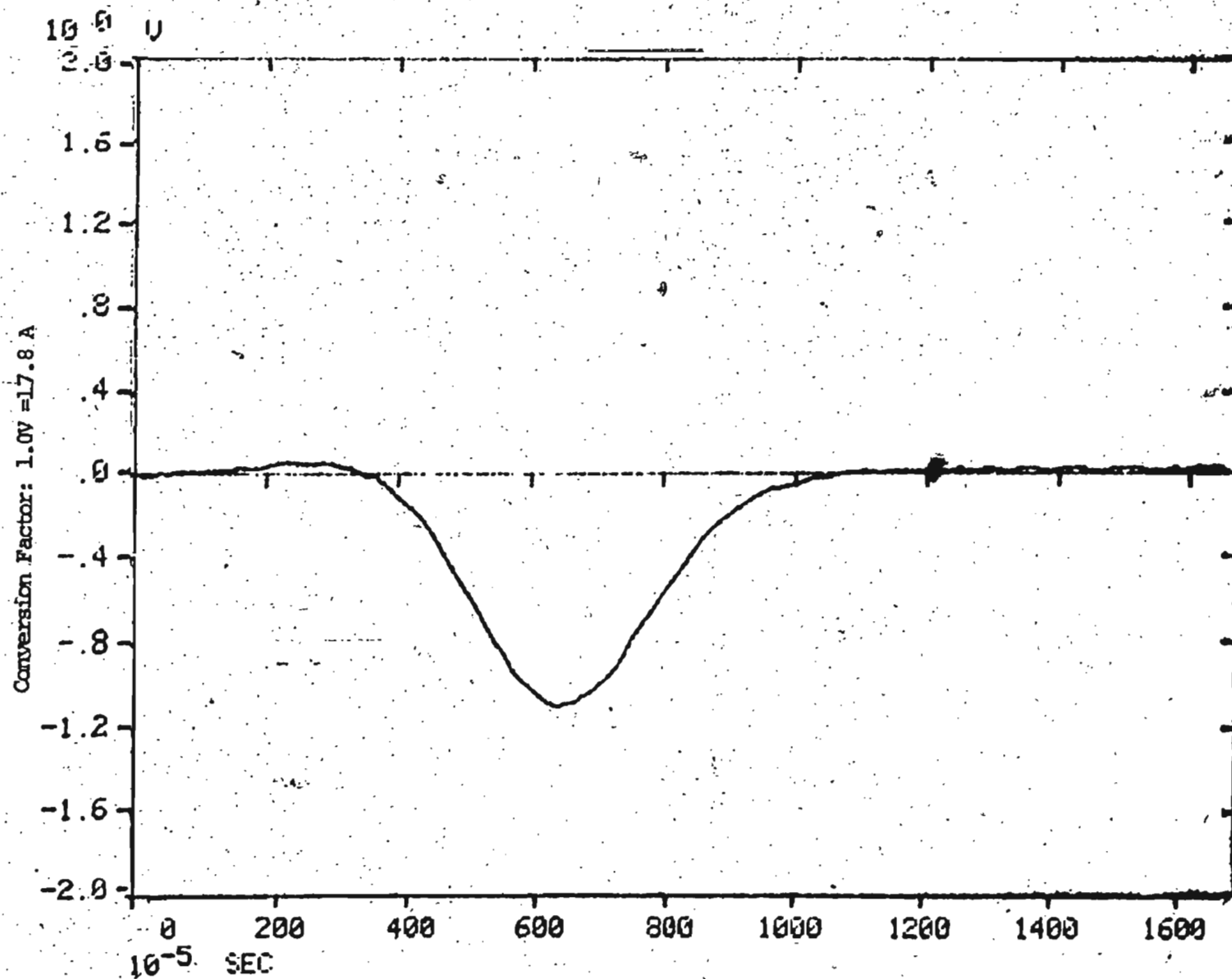


Fig. 3.21 (c) Amplified 1st cycle of inrush current shown in (a)

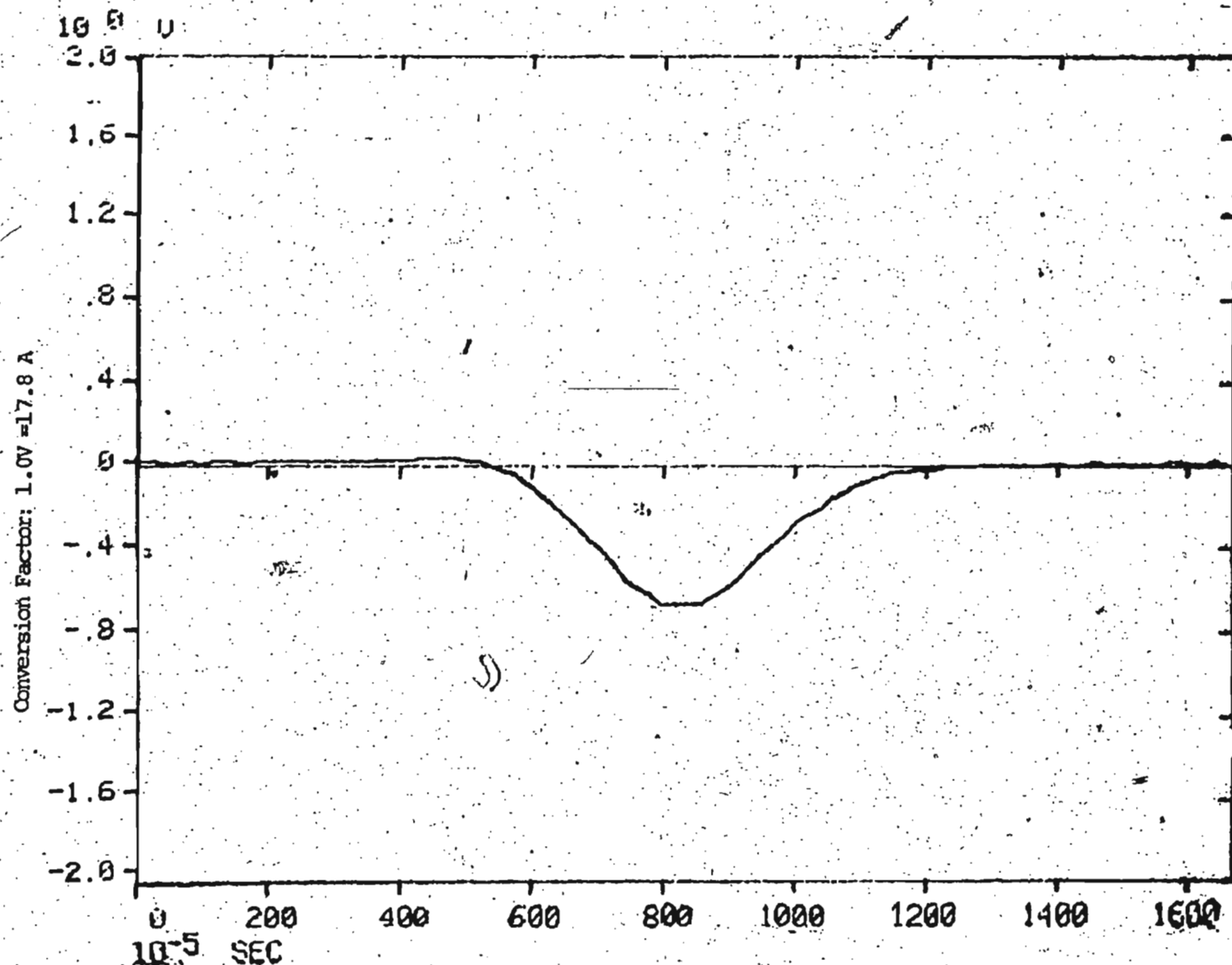


Fig. 3.21 (d) Amplified 2nd cycle of inrush currents shown in (a)

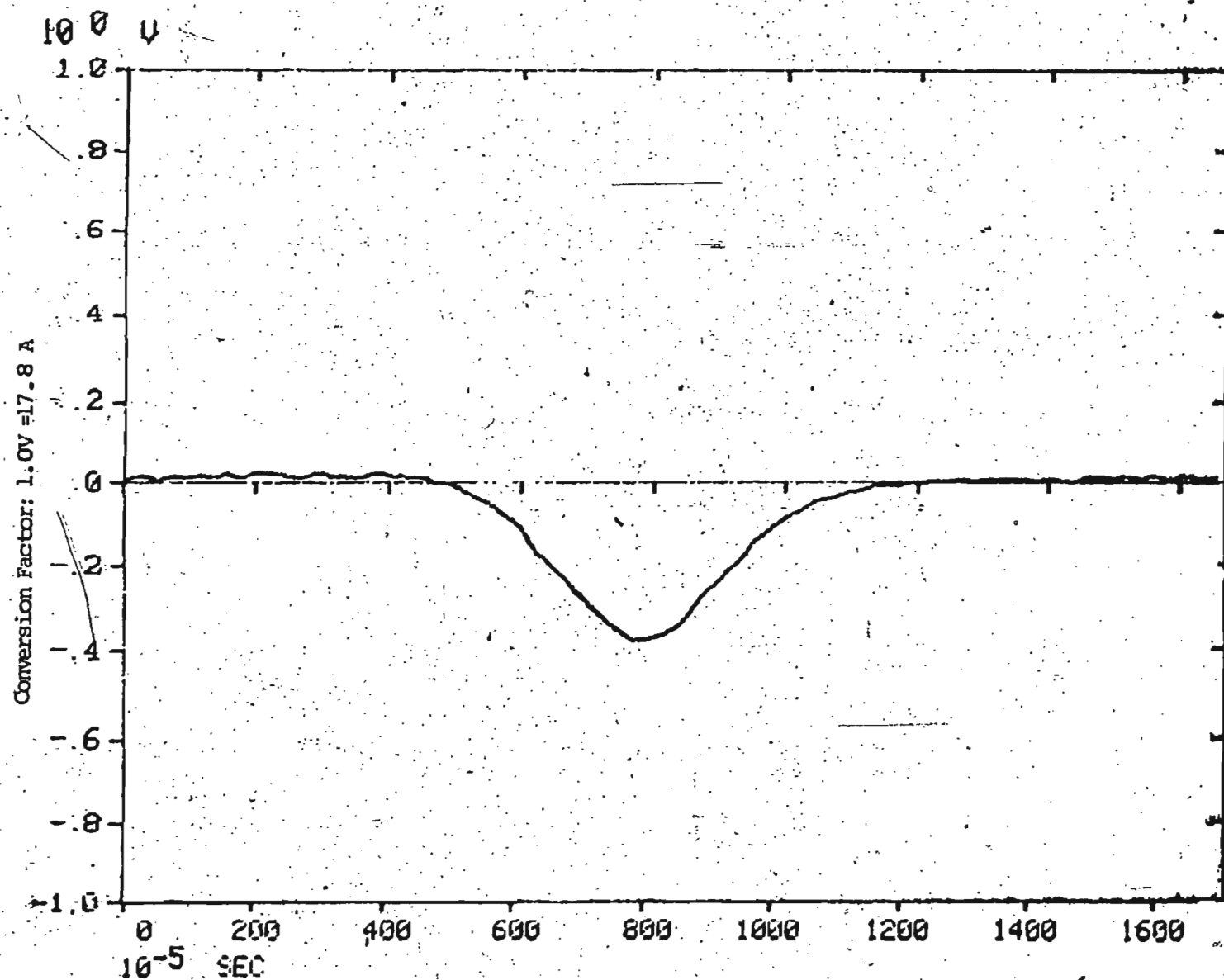


Fig. 3.21 (e) Amplified 3rd cycle of inrush current shown in (a).

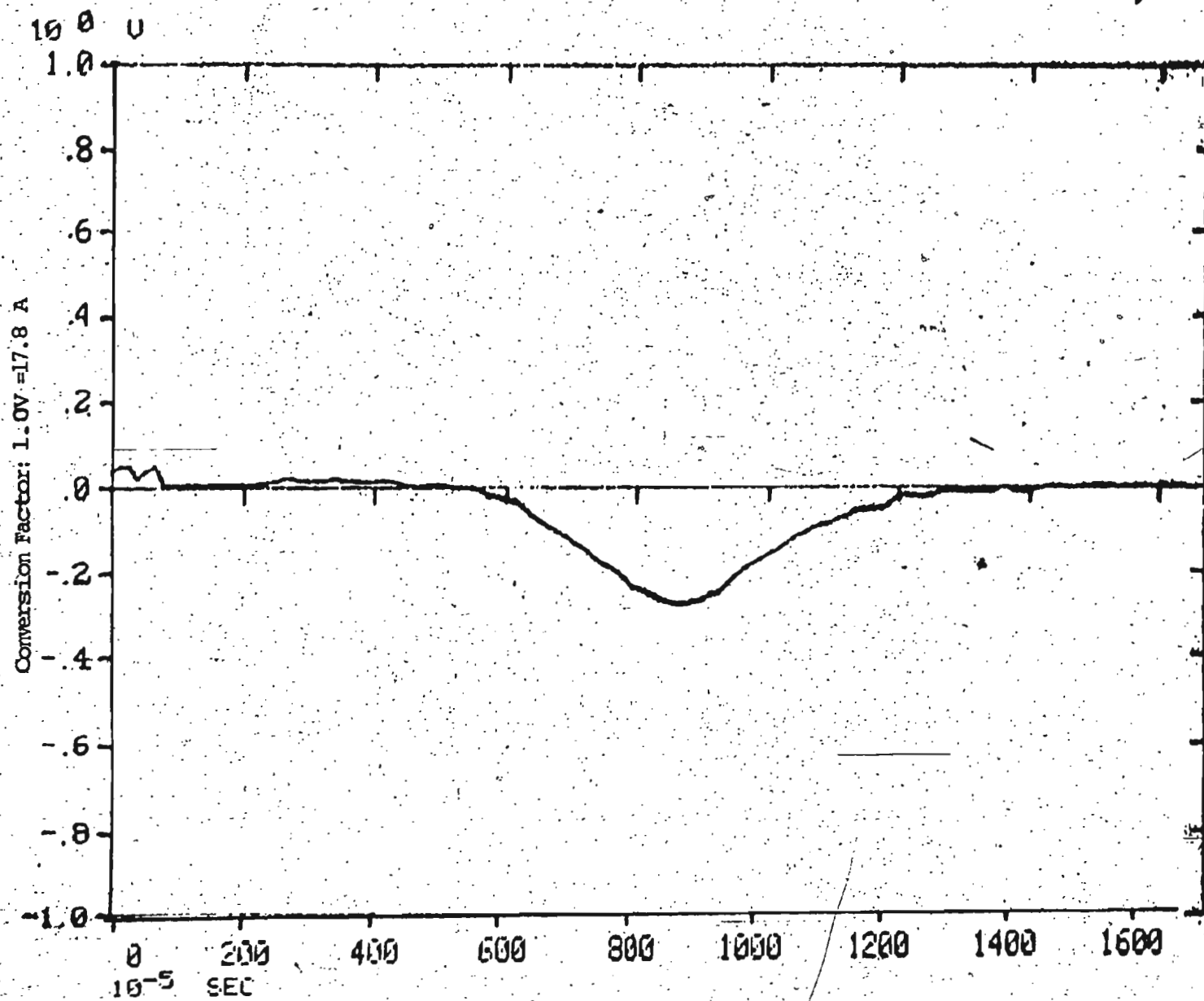


Fig. 3.21 (f) Amplified 4th cycle of inrush current shown in (a)

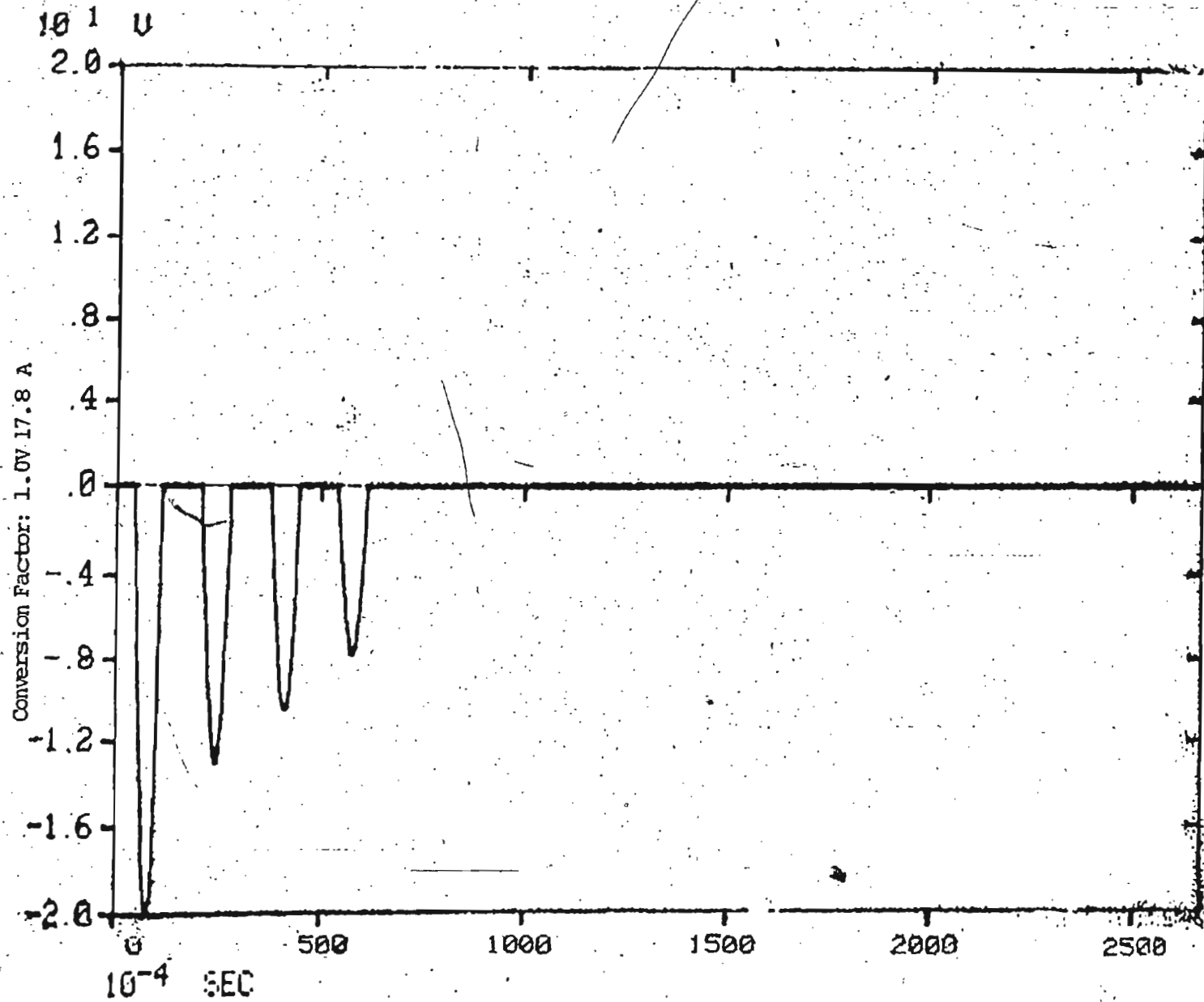


Fig. 3.22 (a) Simulation of negative inrush reproduced from  
Fourier Analyzer

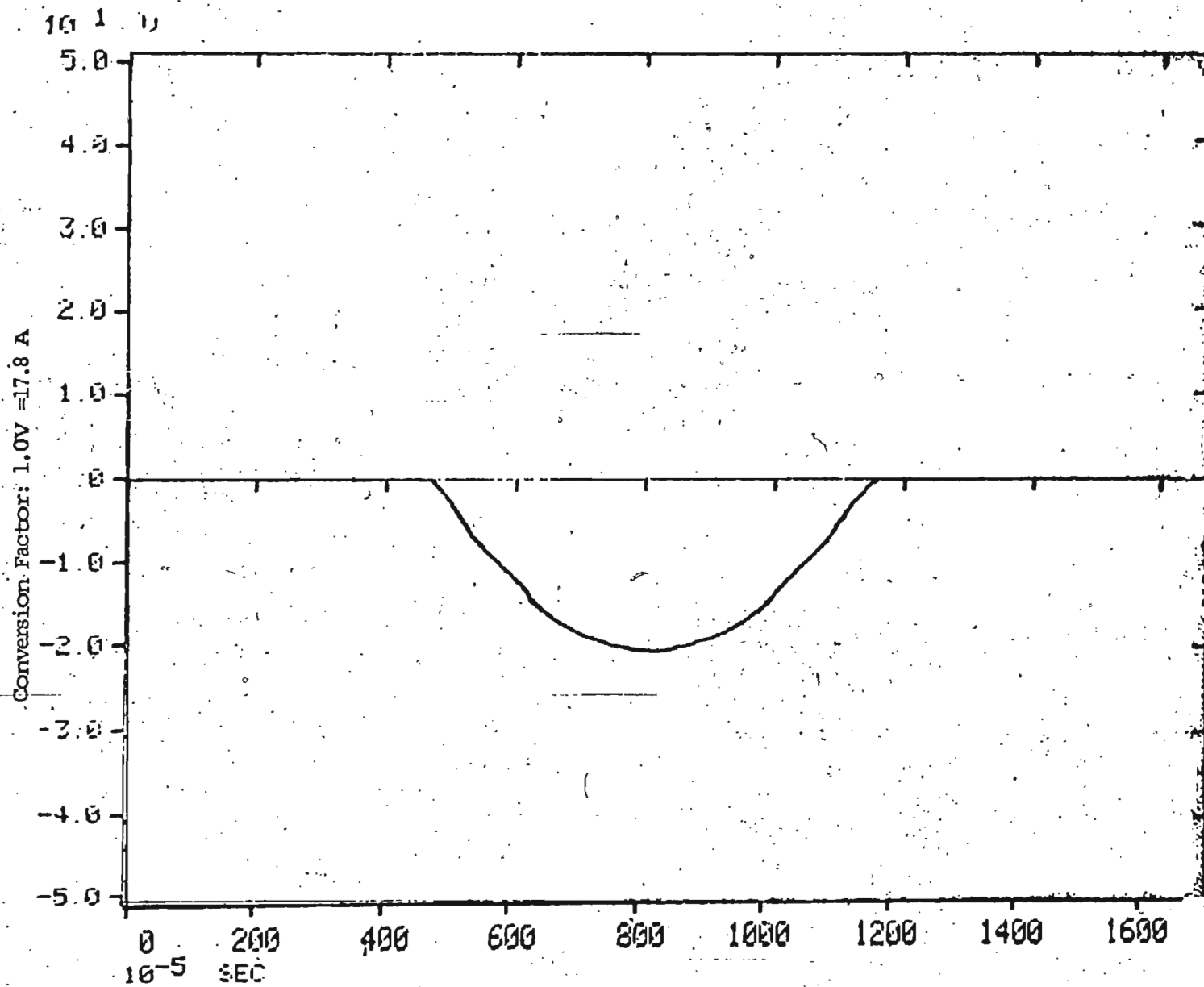


Fig. 3.22 (b) Amplified 1st cycle of inrush current shown in (a)



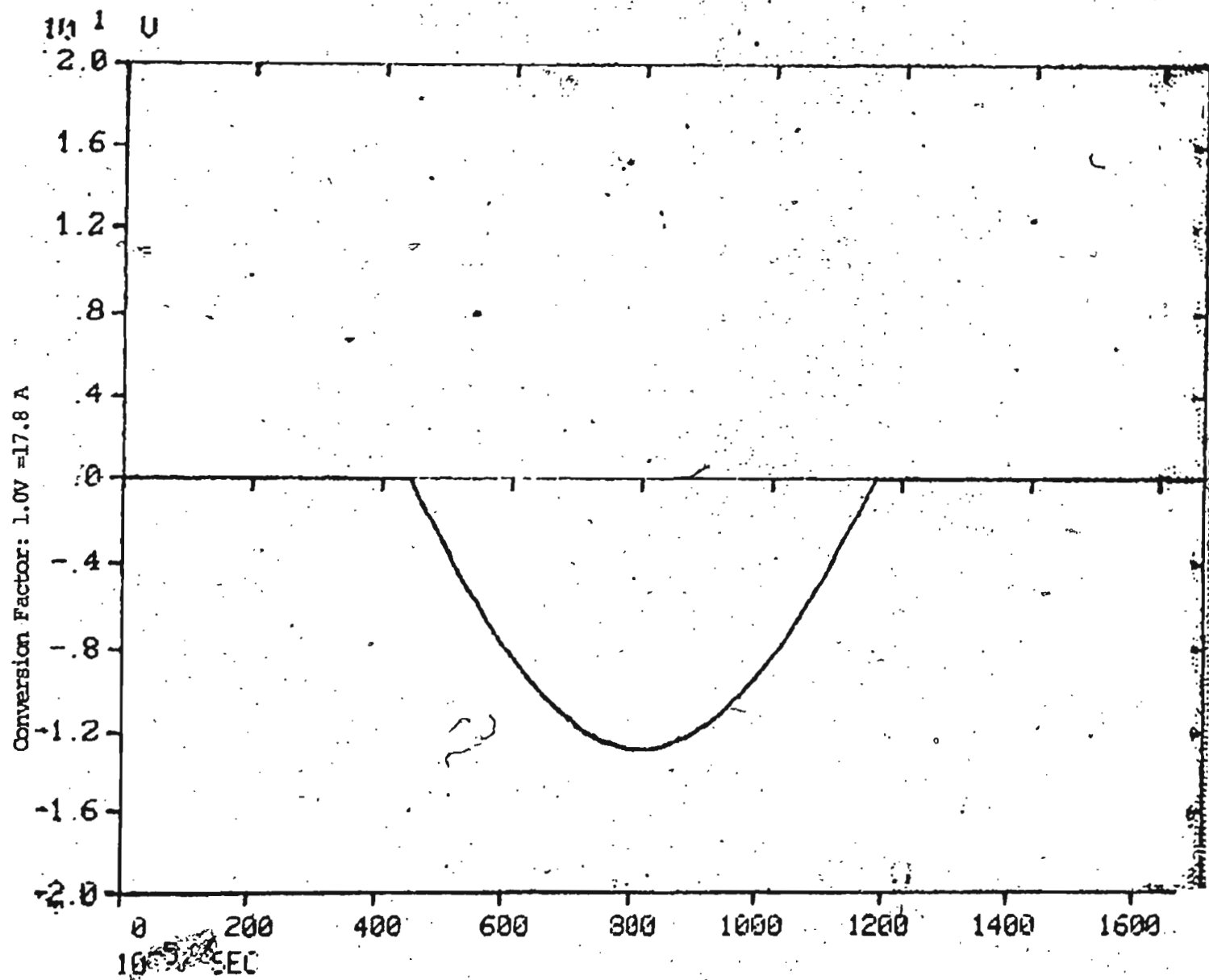


Fig. 3.22 (c) Amplified 2nd cycle of inrush current shown in (a)

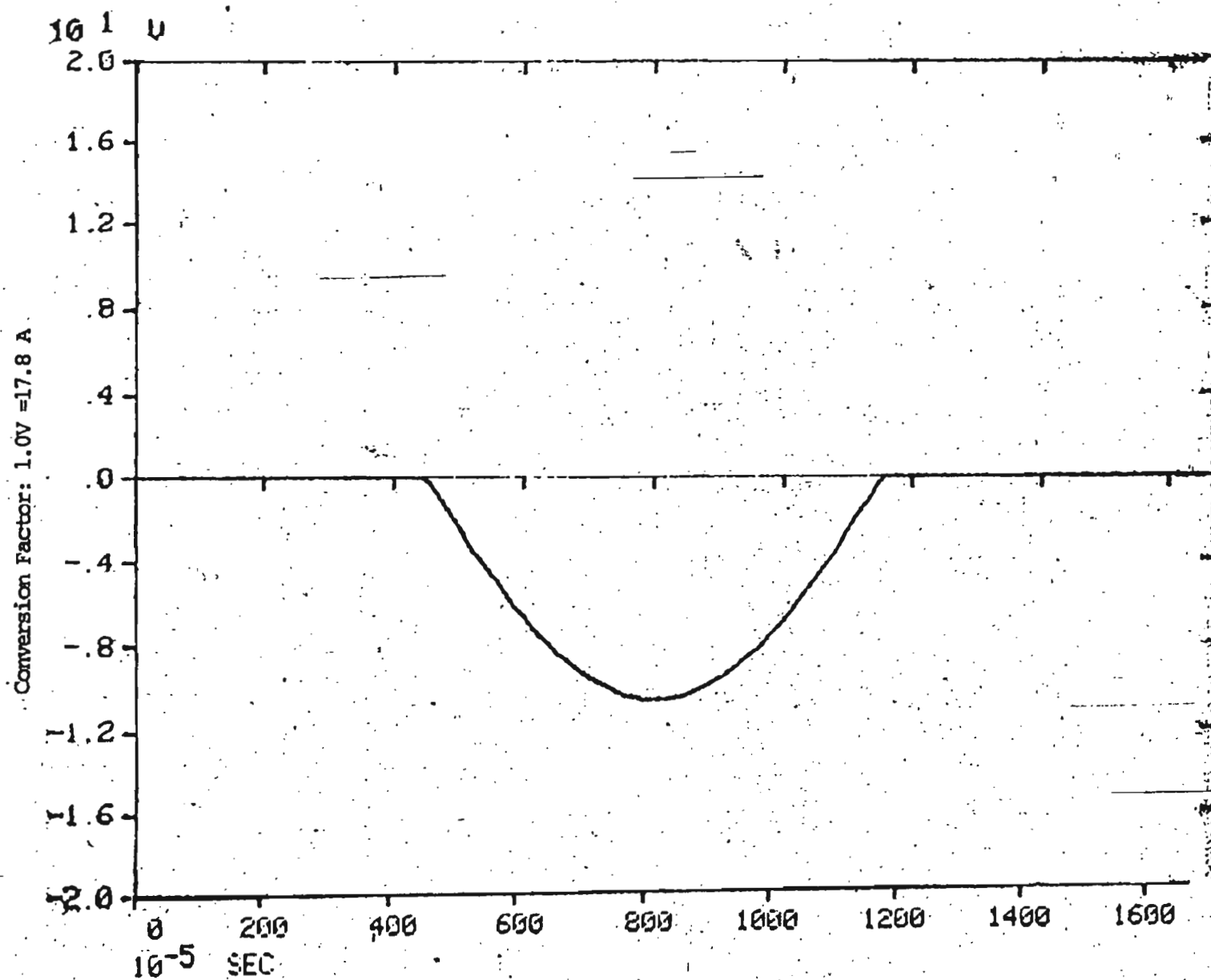


Fig. 3.22 (d) Amplified 3rd cycle of inrush current shown in (a)

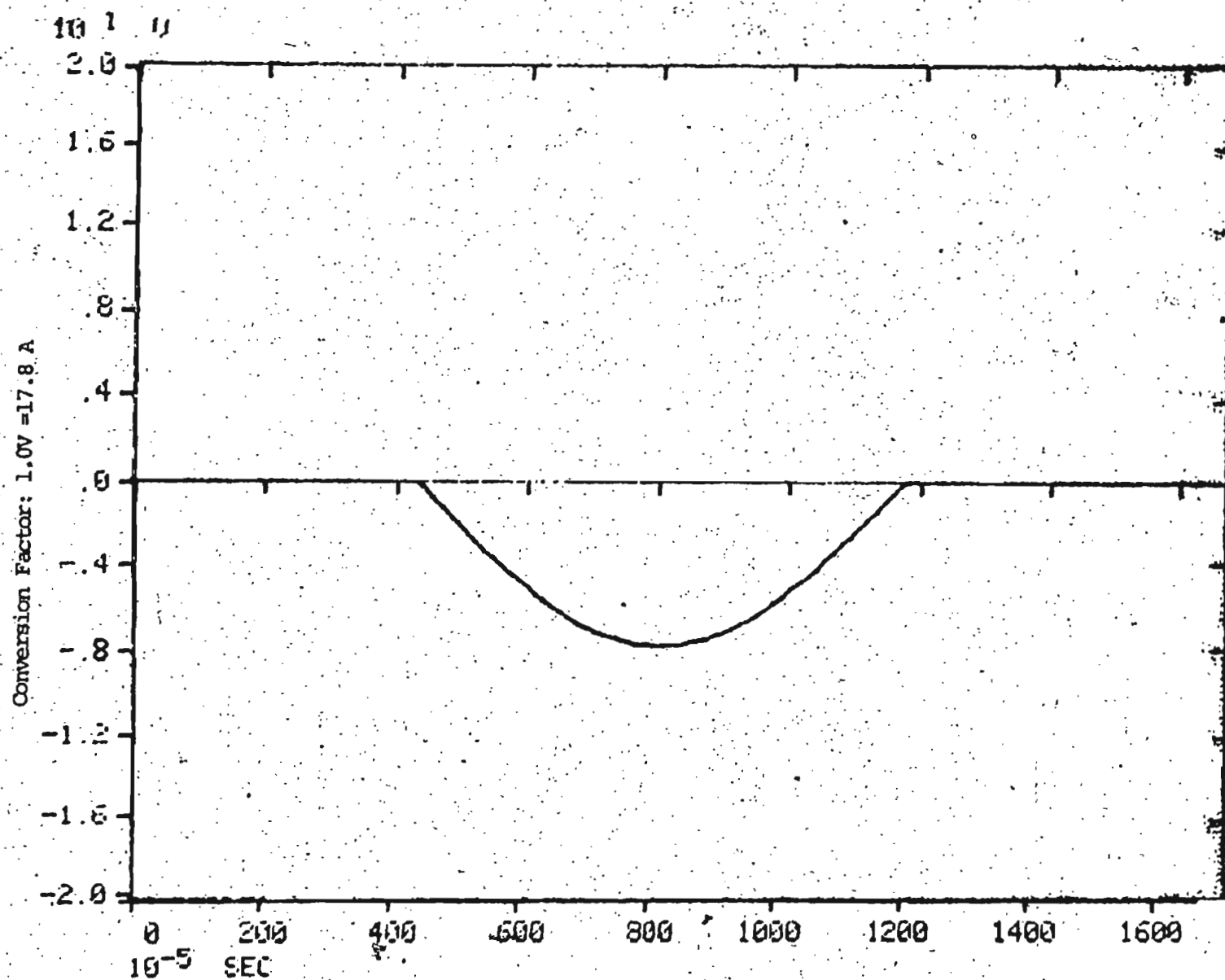


Fig. 3.22 (e) Amplified 4th cycle of inrush current shown in (a)

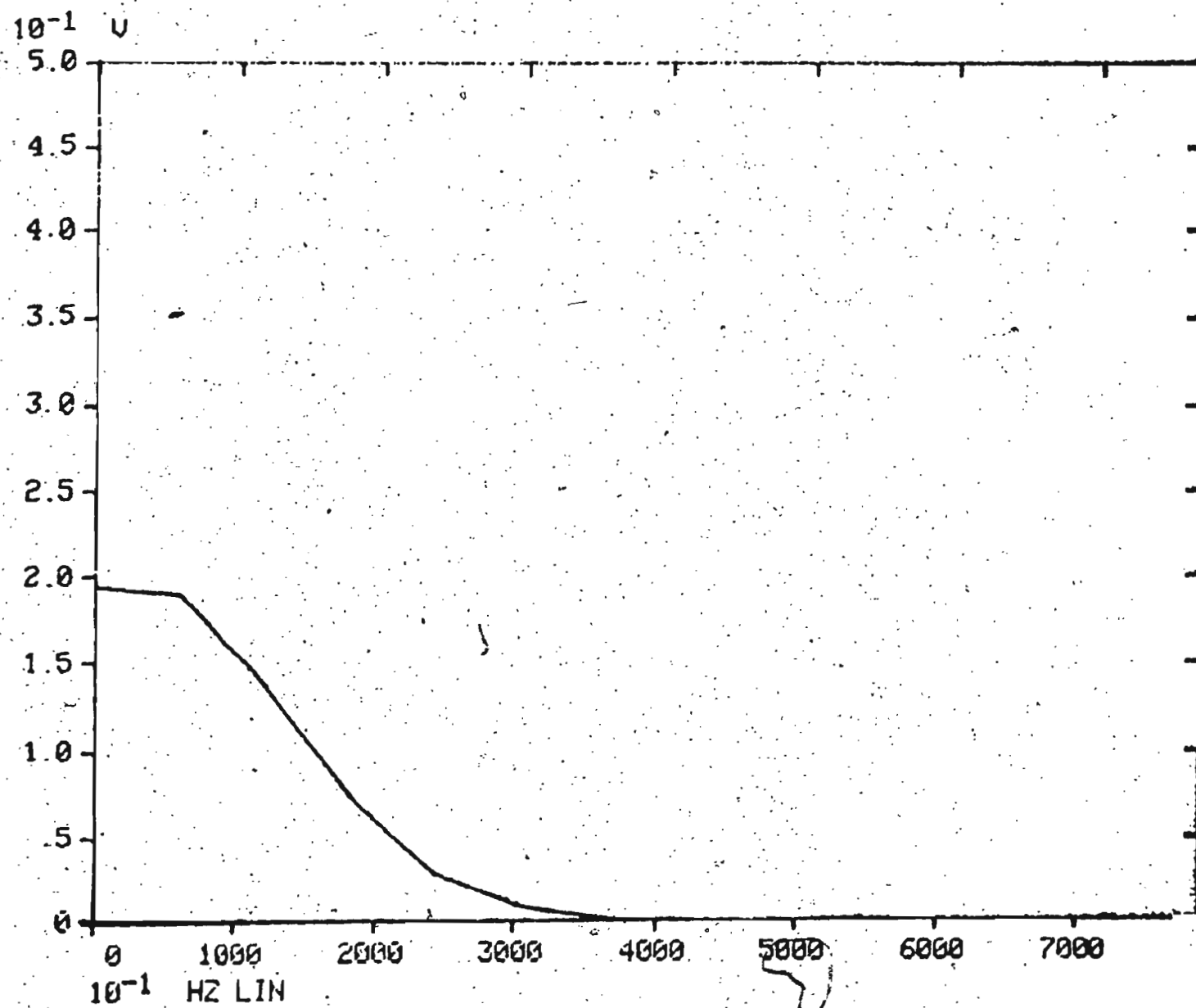


Fig. 3.23 (a) Continuous frequency spectrum of 1st cycle of inrush shown in Fig. 3.21 (c).

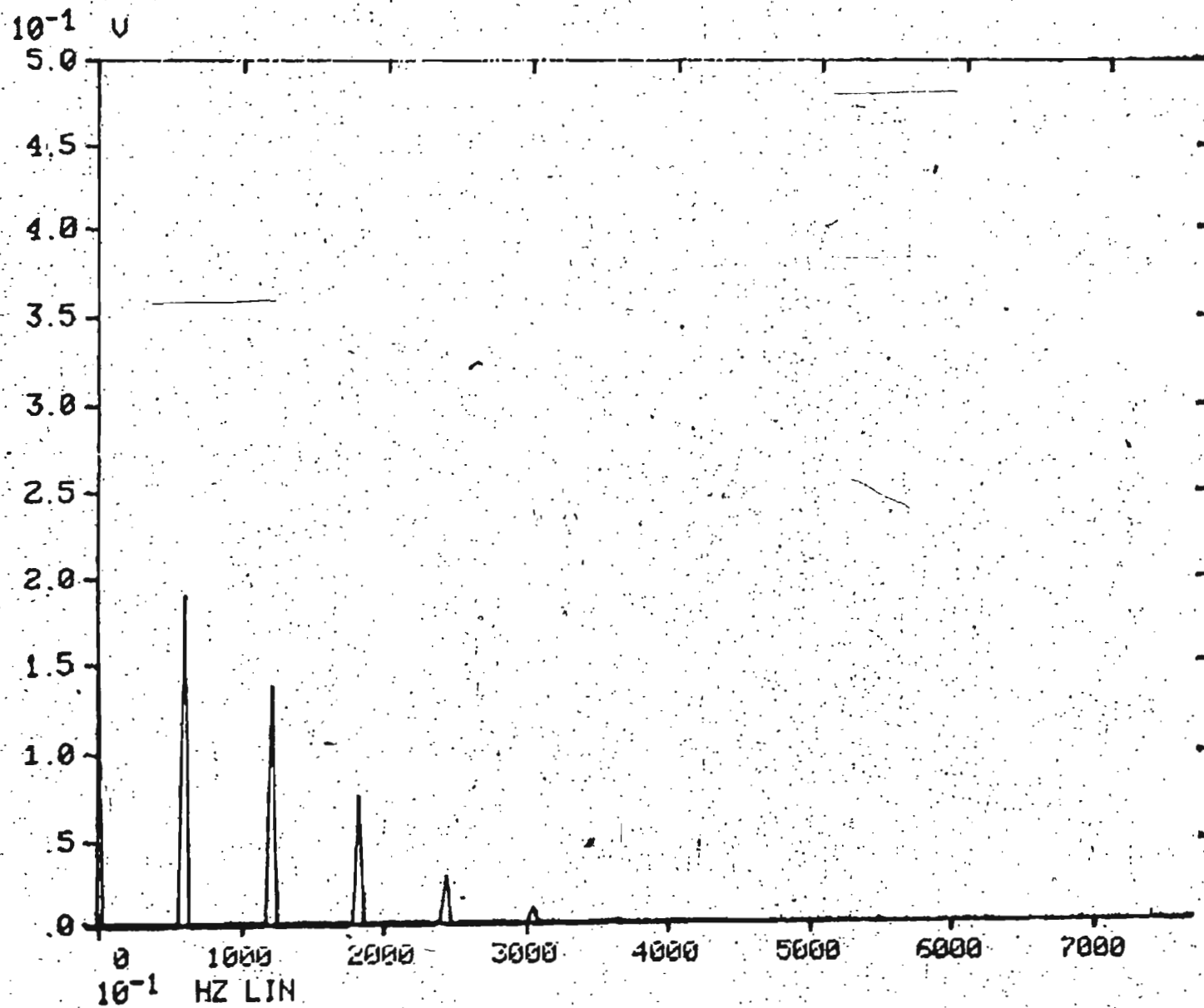


Fig. 3.23 (b) Discrete frequency spectrum of 1st cycle of inrush shown in Fig. 3.21(c)

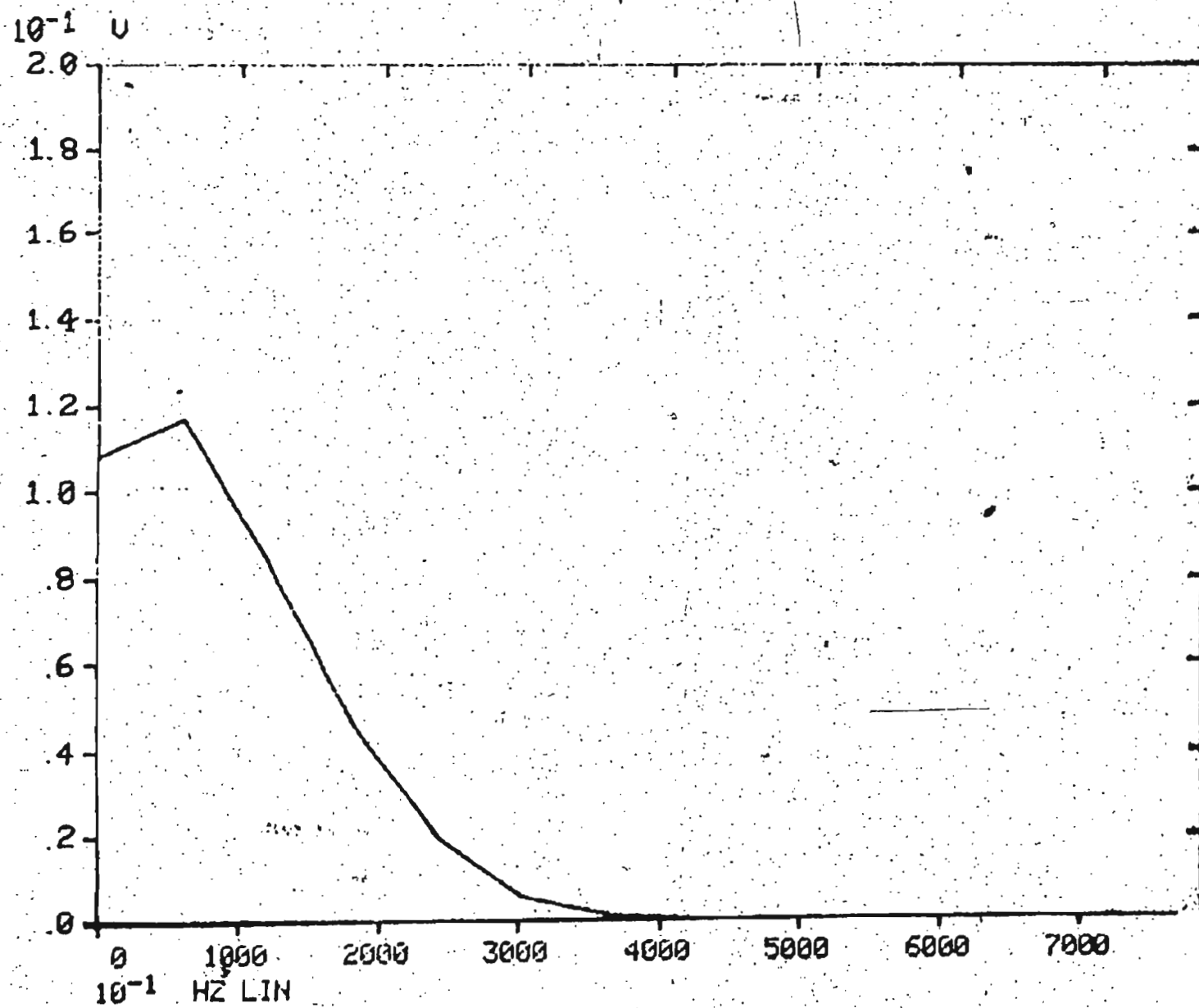


Fig. 3.23 (c) Continuous frequency spectrum of 2nd cycle of inrush shown in Fig. 3.21(d)

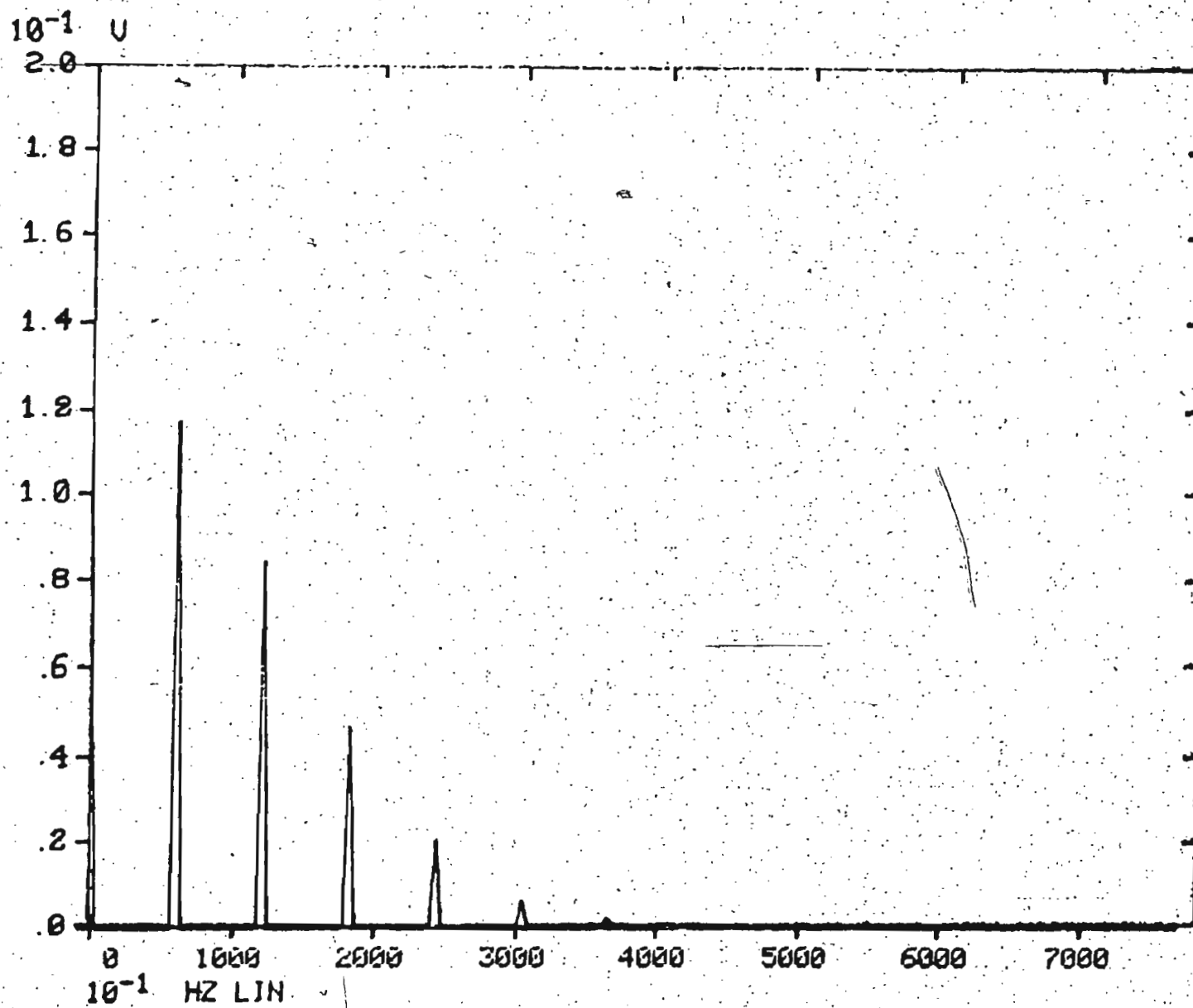


Fig. 3.23 (d) Discrete frequency spectrum of 2nd cycle of inrush shown in Fig. 3.21 (d)

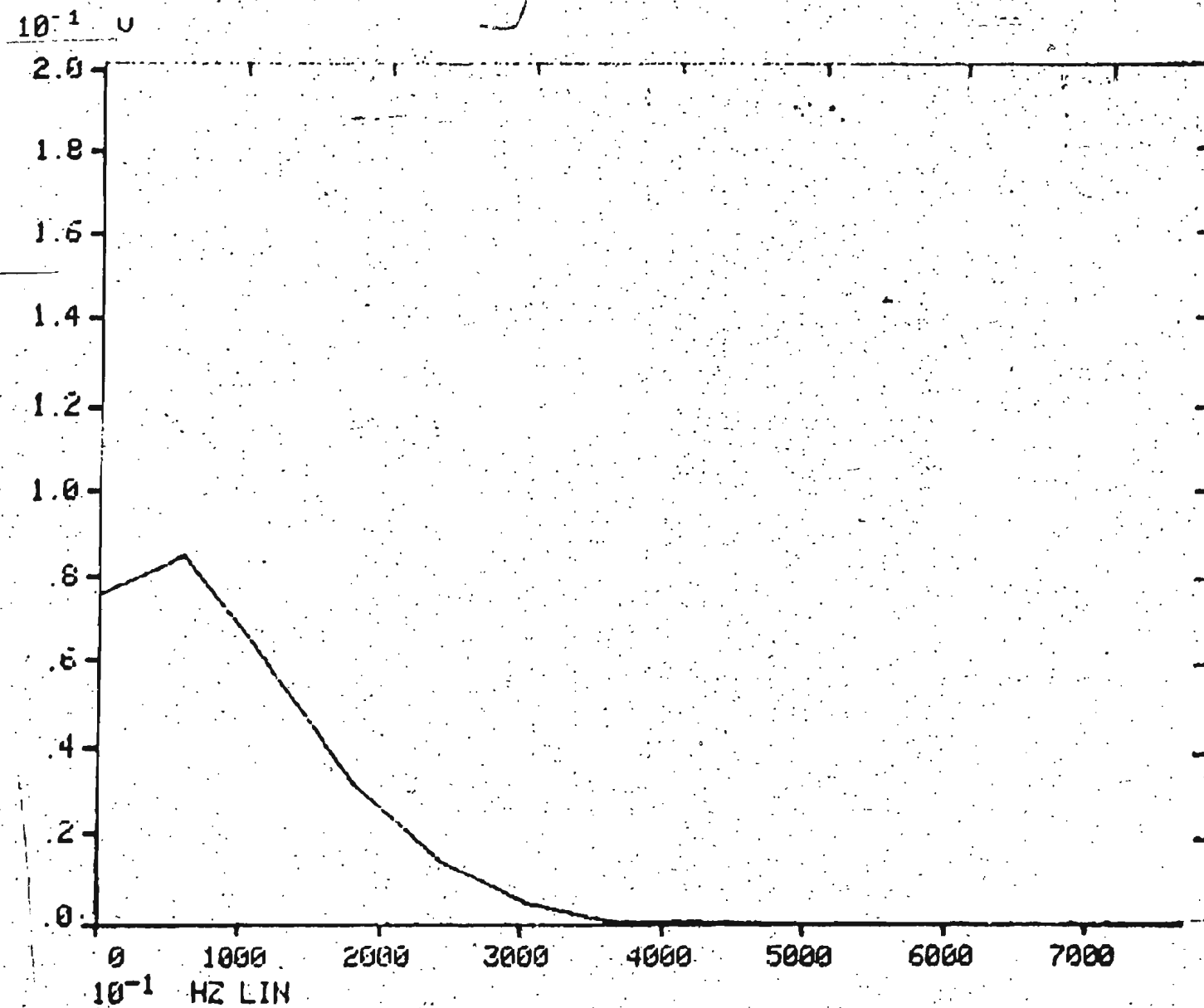


Fig. 3.23 (e) Continuous frequency spectrum of 3rd cycle of inrush shown in Fig. 3.21(e)



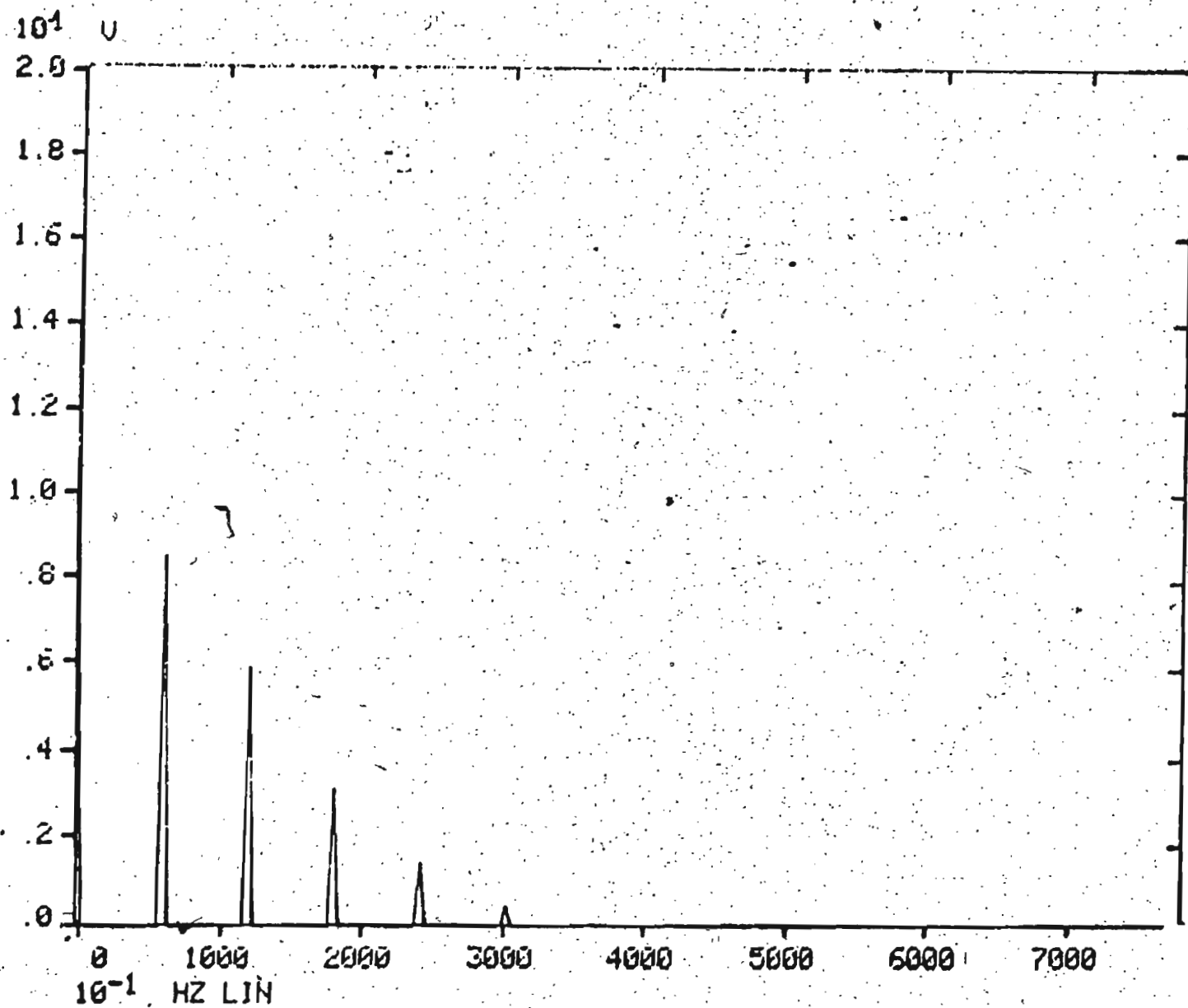


Fig. 3.23 (f) Discrete frequency spectrum of 3rd cycle of inrush shown in Fig. 3.21(e)

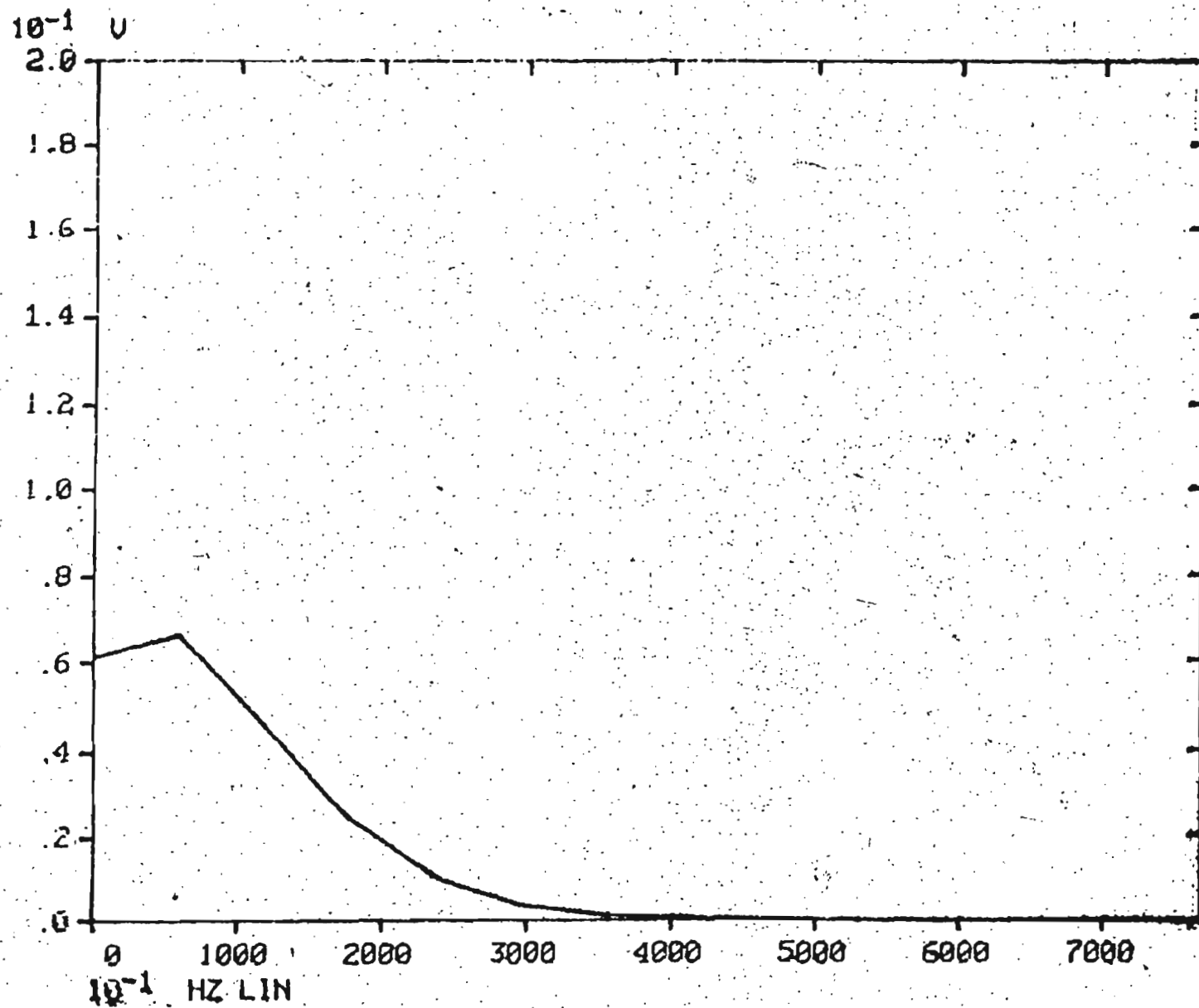


Fig. 3.23 (g) Continuous frequency spectrum of 4th cycle of inrush shown in Fig. 3.21 (f)

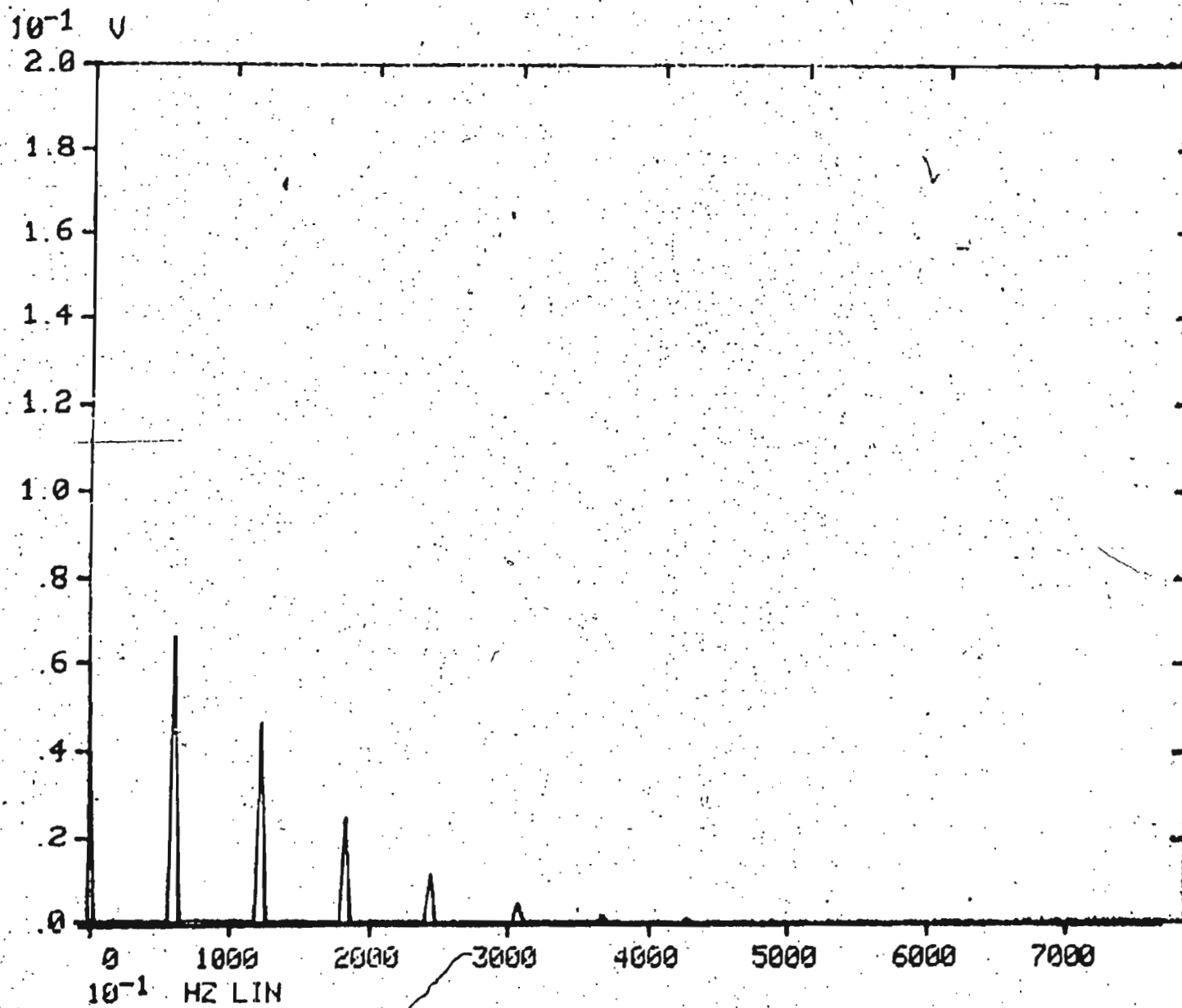


Fig. 3.23 (h) Discrete frequency spectrum of 4th cycle of inrush shown in Fig. 3.21 (f)

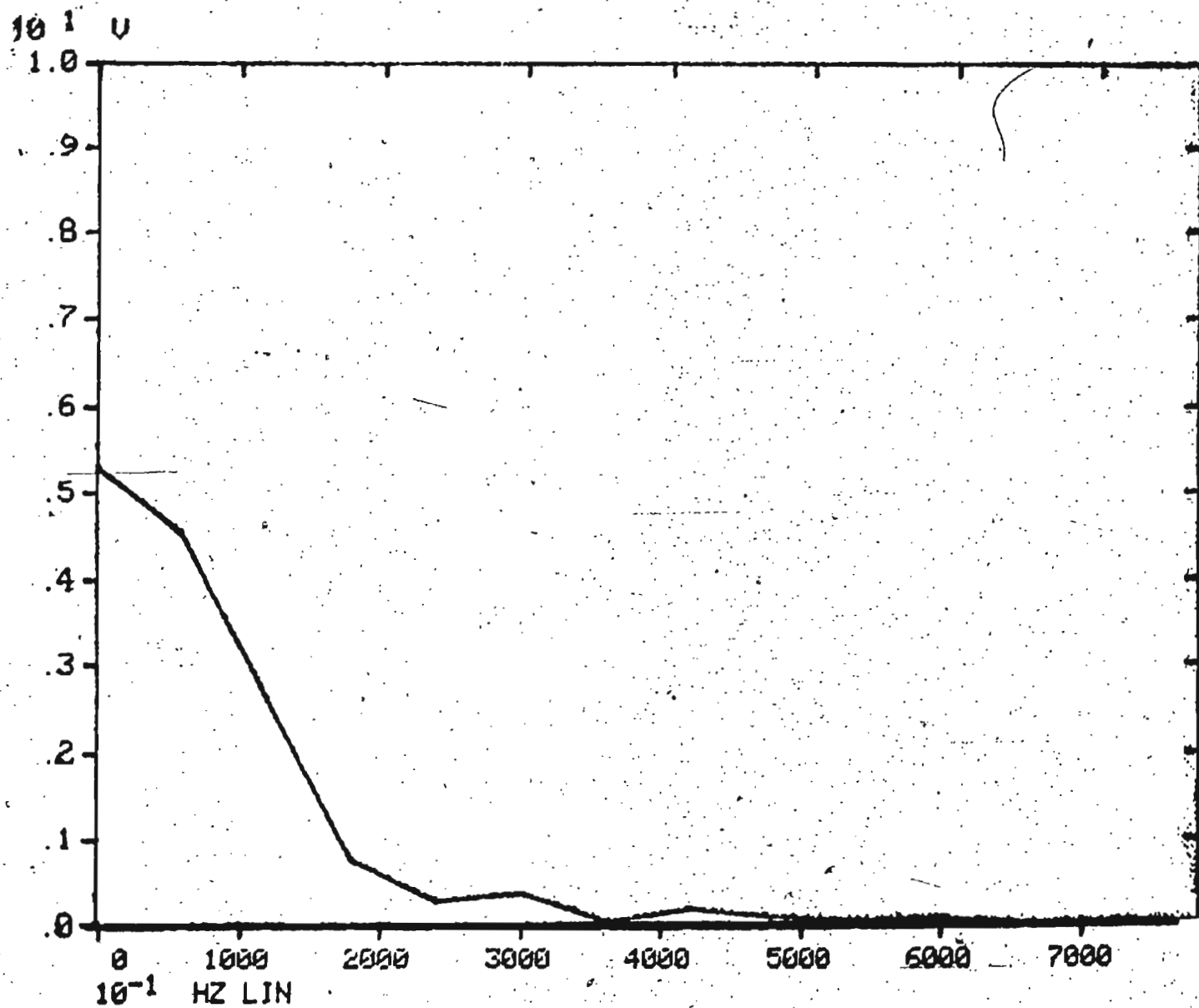


Fig. 3.24 (a) Continuous Frequency Spectrum of 1st Cycle of inrush shown in Fig. 3.22 (b)

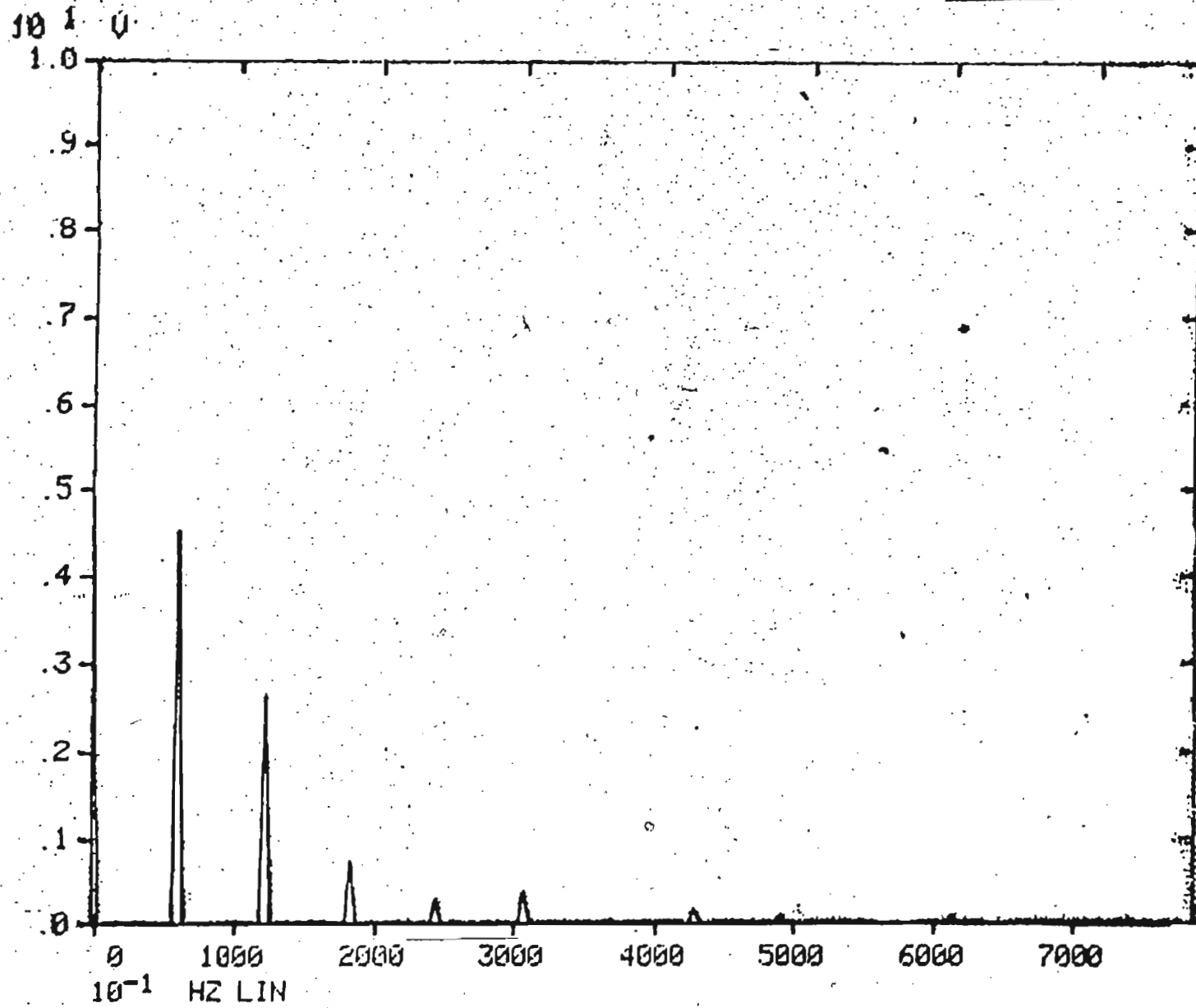


Fig. 3.24 (b) Discrete frequency spectrum of 1st cycle of intrush shown in Fig. 3.22 (b)

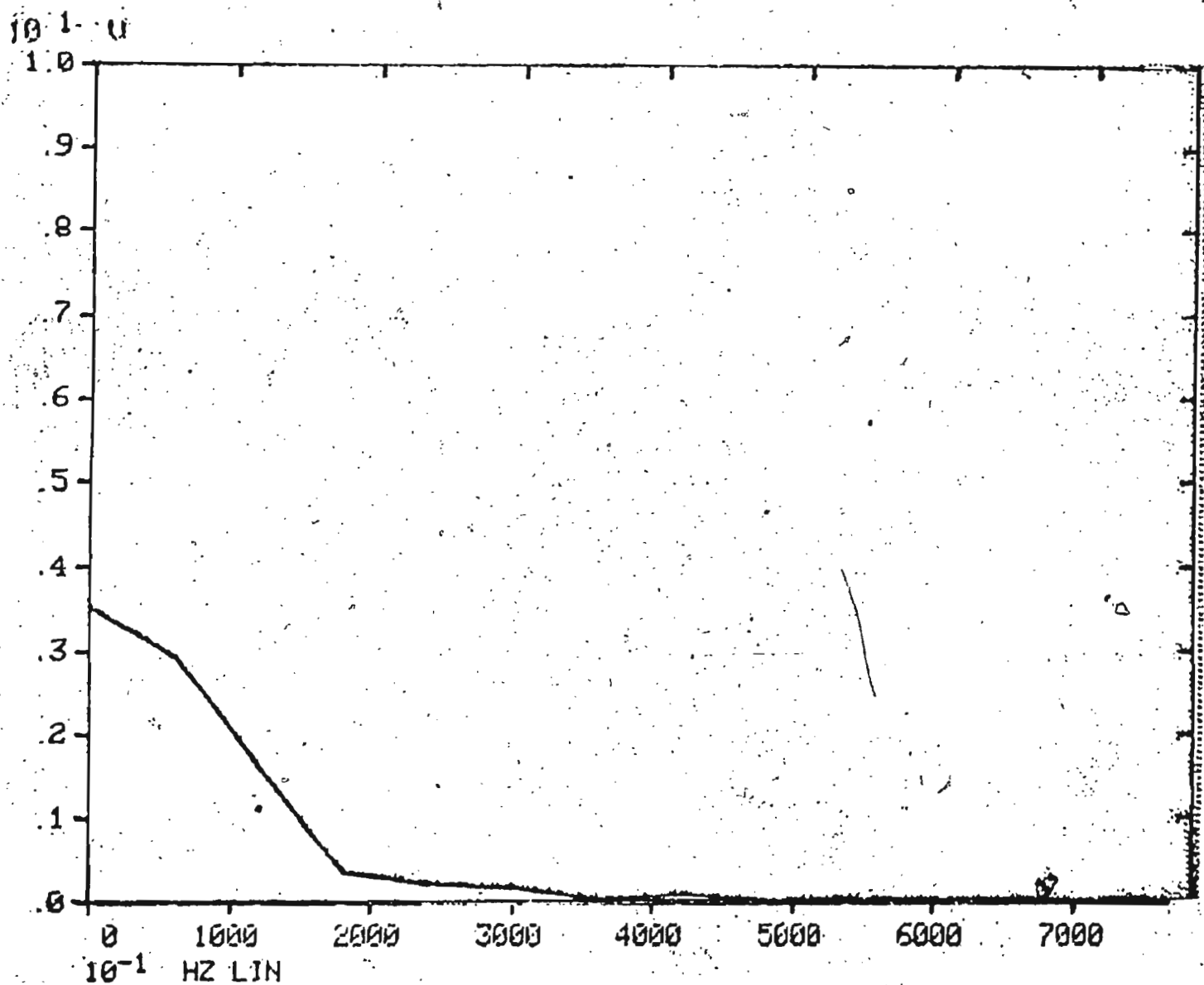


Fig. 3.24 (c) Continuous frequency spectrum of 2nd cycle of inrush shown in Fig. 3.22 (c)

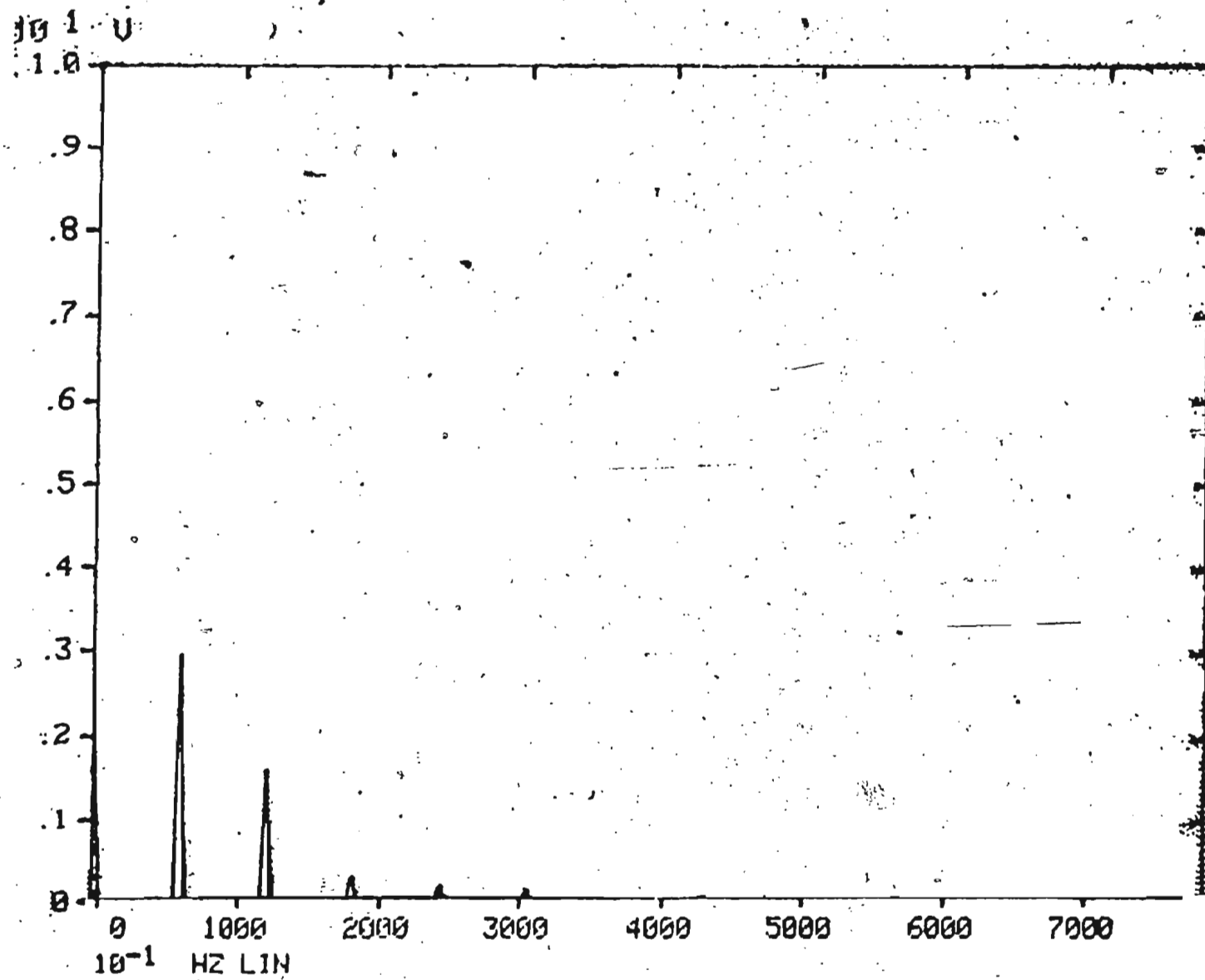


Fig. 3.24 (d) Discrete frequency spectrum of 2nd cycle of inrush shown in Fig. 3.22(c)

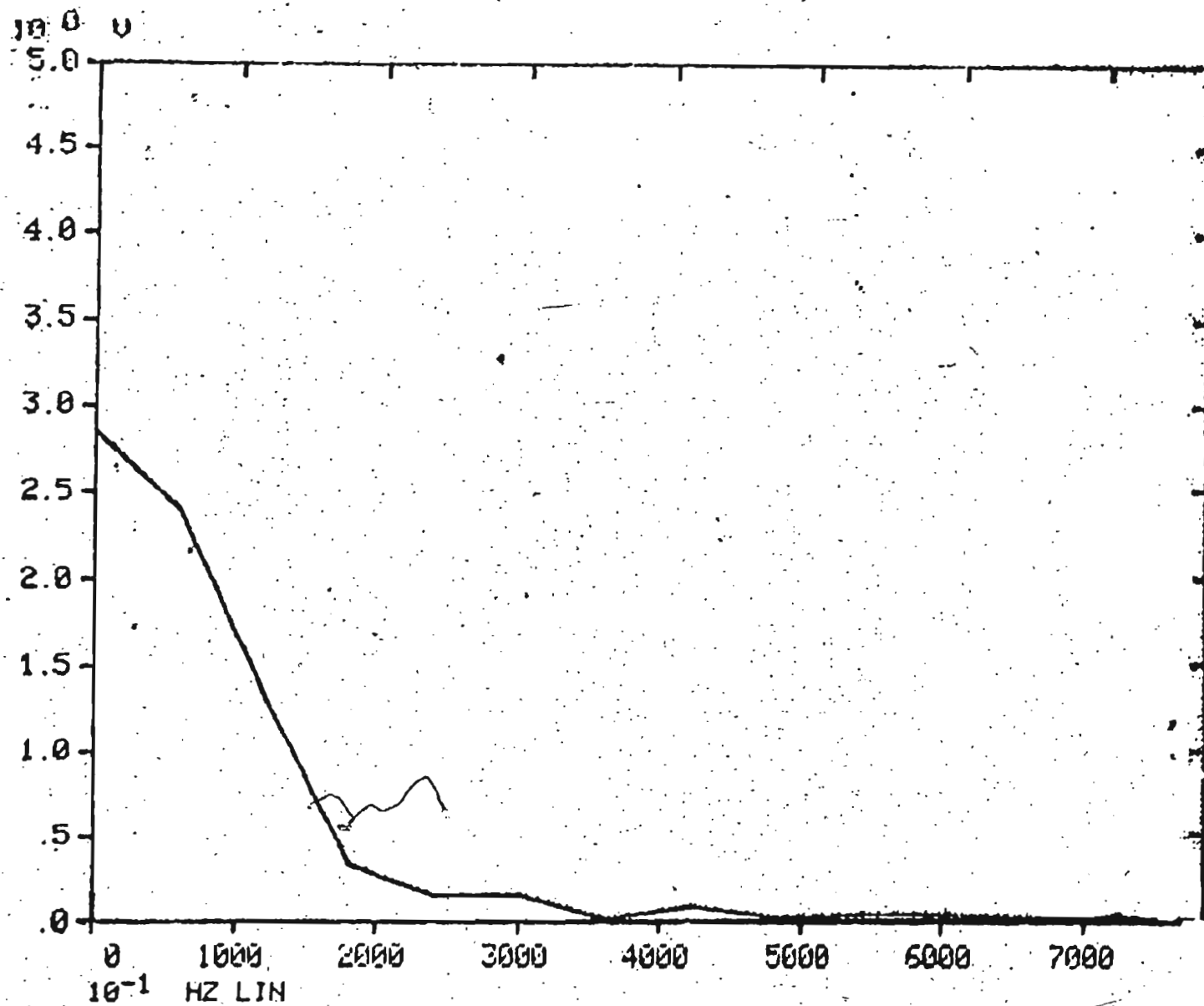


Fig. 3.24 (e) Continuous frequency spectrum of 3rd cycle of inrush shown in Fig. 3.22 (d)



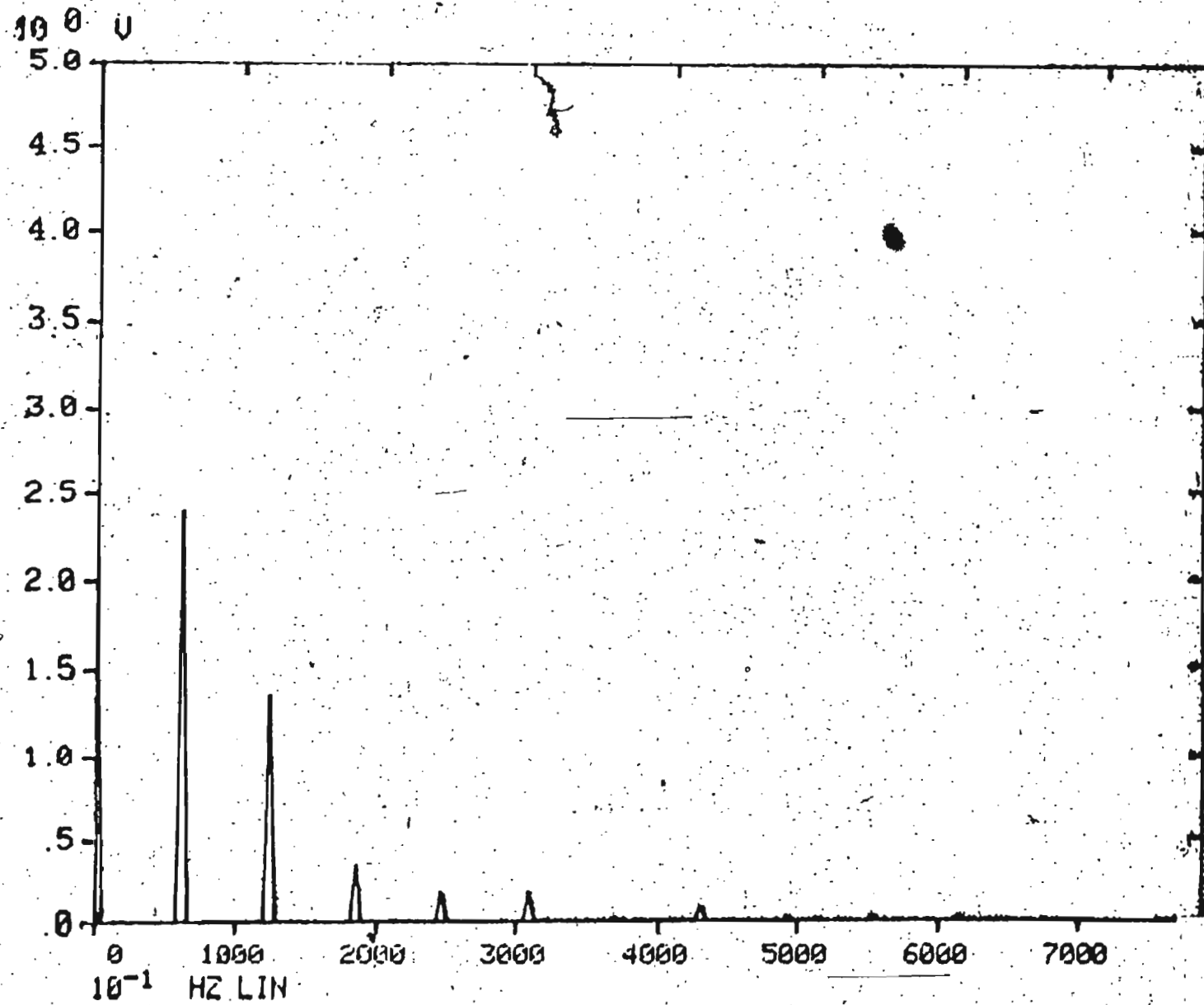


Fig. 3.24 (f) Discrete frequency spectrum of 3rd cycle of inrush shown in Fig. 3.22(d)

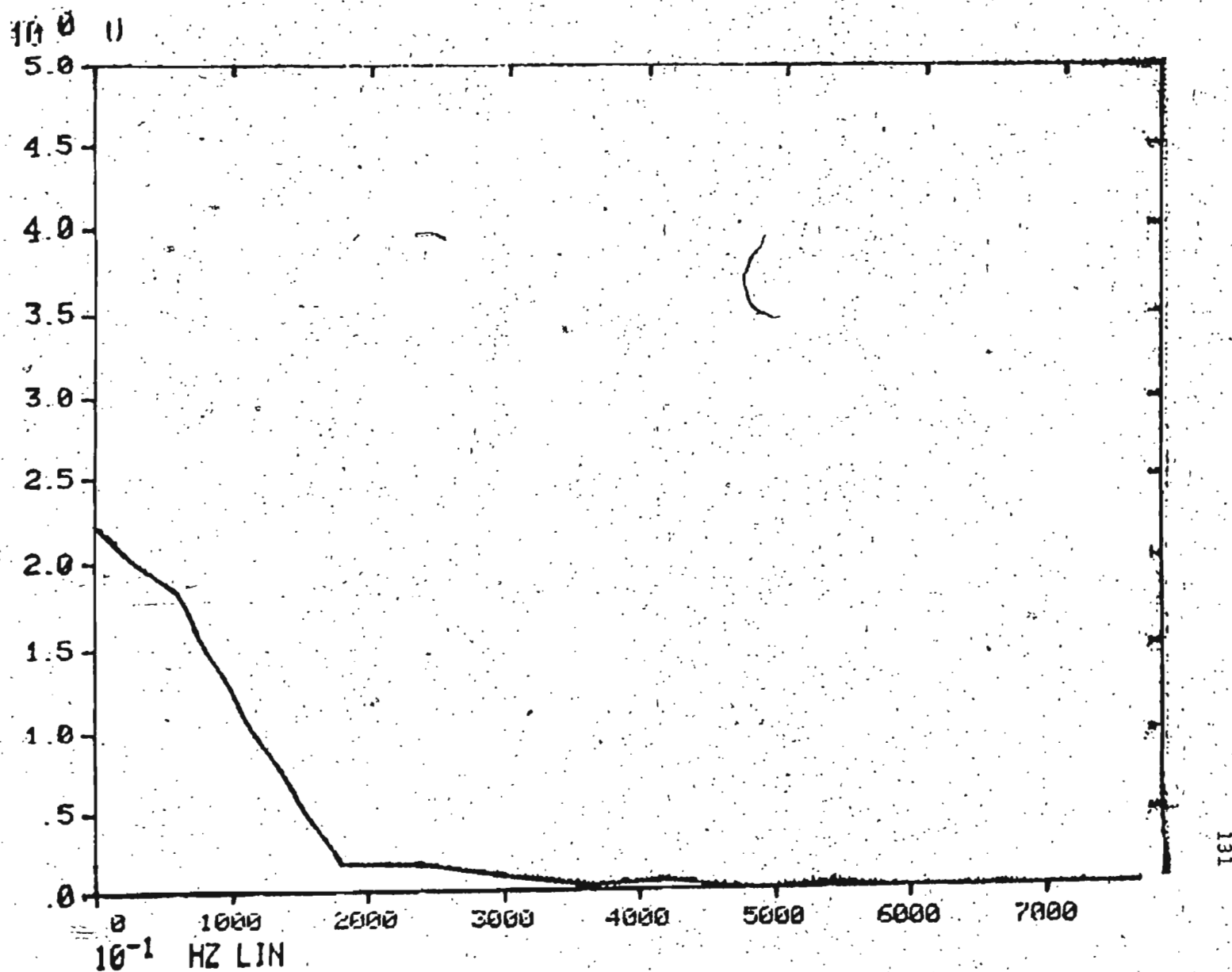


Fig. 3.24 (g) Continuous frequency spectrum of 4th cycle of  
inrush shown in Fig. 3.22 (e)

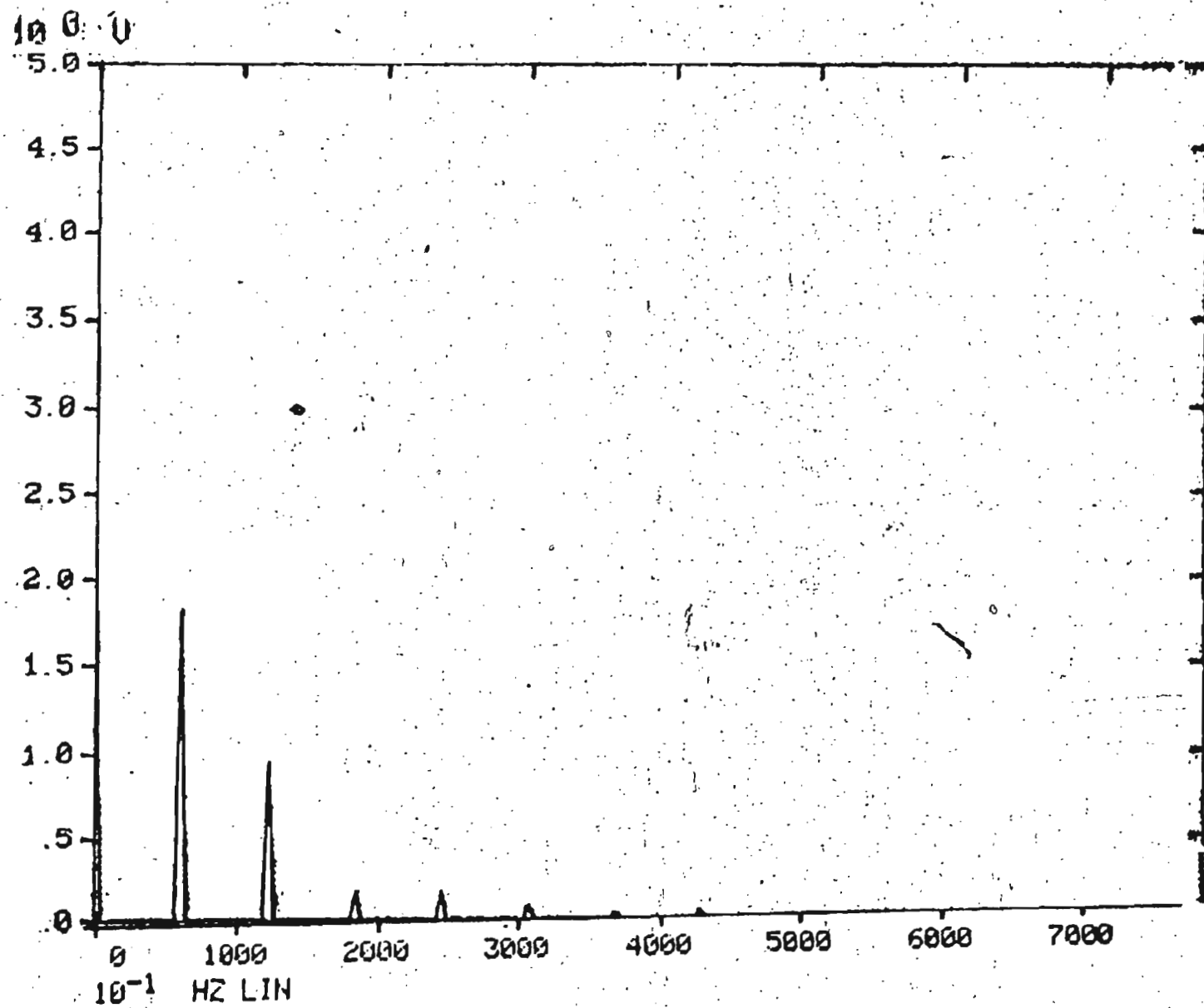


Fig. 3.24 (h) Discrete frequency spectrum of 4th cycle of inrush shown in Fig. 3.22 (e)

the shape of the waveforms. When amplified, the individual peaks are found to have irregular trace while the simulated waveforms are quite regular. These asymmetries between measured and simulated waveforms change the respective harmonic components of each cycle. Another reason is the distortion of the actual waveforms due to the noise introduced while recording the waveforms on a tape recorder. It is not much prominent in the results for lower harmonics, but while going towards higher harmonics, the effect is quite prominent due to the fairly high signal to noise ratio. As it is seen from Table 3.4, percentile discrepancy is higher as one goes for the higher harmonics.

However, practically, after the 5th harmonic, the effect of the other harmonics in protection algorithms are insignificant. All the algorithms described in the next chapter operate on the 2nd harmonic restraint principle. In such a case, if the algorithm restrains the relay during inrush with simulated data, it will surely restrain in case of actual inrush as, those will contain more 2nd harmonic content. Numerous tests were made for recording inrush and corresponding computer simulation of inrush were carried out. Subsequent successful tests of the algorithms on these simulated data proved the usefulness of accurate modelling of the inrush waveforms.

### 3.3.2 Three-phase Cases

Three-phase inrush currents can be simulated in two ways following the expressions described in the text. If it is chosen to simulate inrush following equations 3.44 to 3.46 or Eqn. 3.47 to 3.49 depending on whether the transformer is connected in Y/ $\Delta$  or  $\Delta$ /Y, it is important to calculate the individual phase inrush as is done in single phase case. But the choice of parameters in simulating the individual phases is not as simple as in the single phase case. As the steady-state flux wave varies in the three limbs with  $120^\circ$  phase differences, the apparent reactance of the core seen by the magnetizing current is also different in different phases. Also, those are different in different connections. This phenomena has been described in Appendix C, and the various parameters in Table 3.5 have been determined by O.C and S.C tests of the phases as described therein.

It was described in earlier section that the inrush phenomena of the Y/ $\Delta$  transformer is complicated rather than in  $\Delta$ /Y transformer while energized from the primary. Tests were carried out on a 3-phase, 120/120 V transformer with full load current rating of 4.55A both in the primary and secondary. The parameters of this transformer are shown in Table 3.5. A particular case of a Y/ $\Delta$  transformer energized from primary is considered here. A 3-phase point-on-wave switch using a 3-phase thyristor bridge is designed as was

done in single-phase case. The parameters used for the simulation, taken from Table 3.5, are

Equivalent resistance

referred to Primary side = 1.376  $\Omega$

for Phase-A

Equivalent resistance

referred to Primary side = 0.857  $\Omega$

for Phase-C

The individual simulation of A-phase and C-phase depends on the determination of the conduction angles of the individual cycles of respective phases. The simulation of B-phase is dependent on the inrush of the A and C phases respectively, if the ' $\lambda$ ' for A-phase is  $0^\circ$ . The accuracy of simulation, however, depends on choice of the value of the zero sequence impedance of the system. Rockefeller [33] arbitrarily suggested a zero sequence impedance equal to 10 times the value of  $Z_{ss}$ . However, this value is not a fixed one and the constants related to Eqn. 3.46 to 3.48 are changed accordingly for simulation of a particular waveform.

The program developed for a numerical solution is much alike to that of the single-phase case. A flow-chart is shown in Fig. 3.25 which is a generalized version for the 3-phase programming. The major difference is that it calls two different subroutines for the individual phase inrush calculations. It also finds out the resultant inrush for

any of the three phases.

However, for protection purpose, the 'A' and 'C' phase currents for 'A'-phase switching being done at  $\lambda=0^\circ$  can also be simulated using single-phase programming with the appropriate values of the parameters. For the B-phase simulation using the single phase programming approach is comparatively difficult to achieve result up to the desired perfection. Figs. 3.26(a), (b) and (c) show the measured wave-traces of inrush currents in phases A, B and C respectively. The switching angle  $\lambda$  for phase 'A' is  $0^\circ$ . Figs. 3.27(a), (b), and (c) show the simulation for the first four cycles of inrush in A, B and C phase respectively. Figs. 3.28(a), (b) and (c) show the same simulated data reproduced from the Fourier Analyzer. Figs. 3.29(a), (b) and (c) show the discrete frequency spectra of the first cycles for the measured waveforms of A, B and C phases respectively. Figs. 3.30(a), (b) and (c) show the discrete frequency spectra of the same for the simulated waveforms. Table 3.6 compares the respective current peaks for both the measured and simulated data waveforms for four cycles.

The harmonic contents of the respective cycles are shown in Table 3.7. The discrepancies in the harmonic contents are evident as can be found from the amplified first cycles for both the measured and the simulated waveforms shown in Figs. 3.31(a), (b) and (c) and Figs. 3.32(a), (b) and (c) respectively. As explained earlier, the main reason

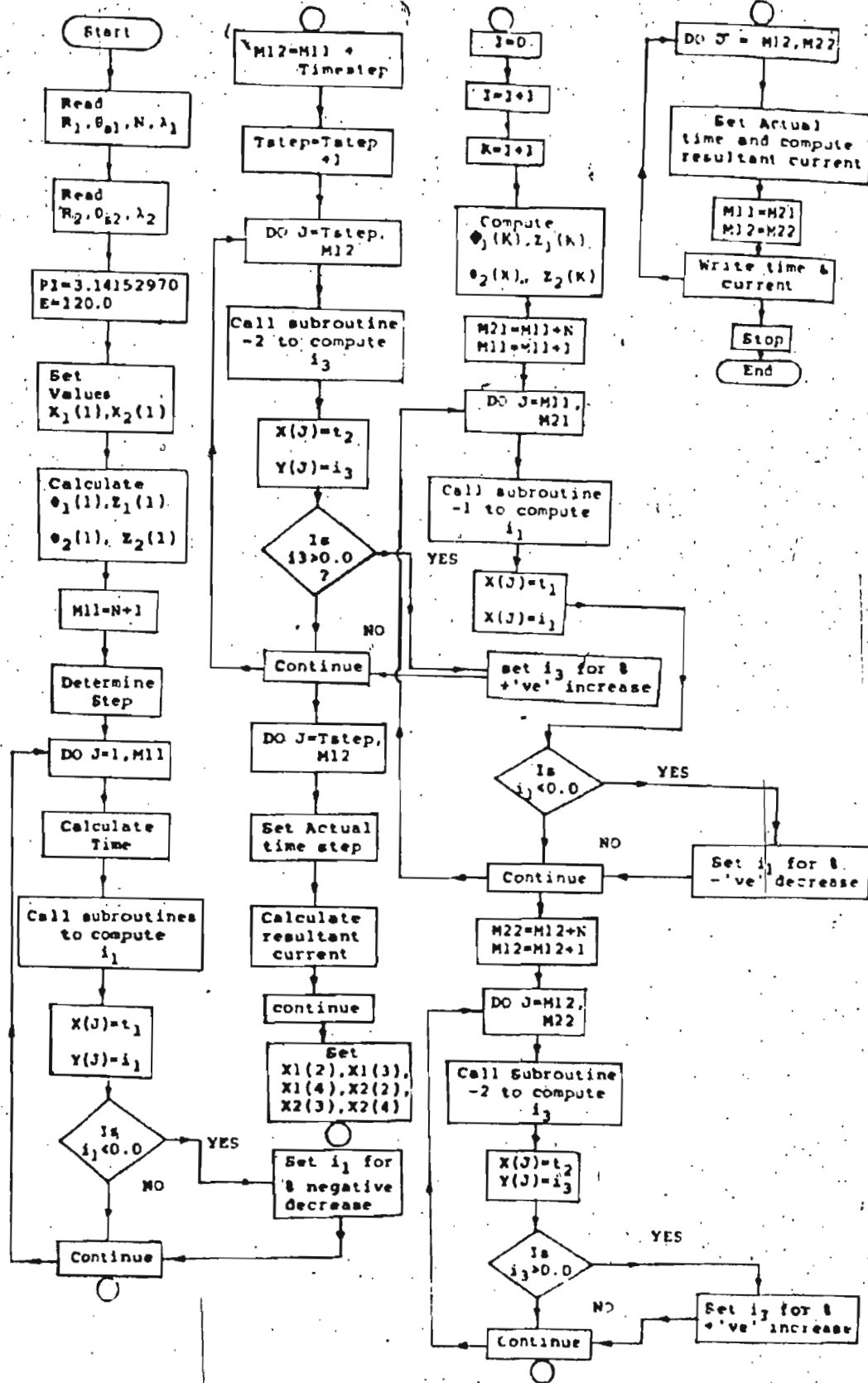


Fig. 3.25

Flow chart of the program for simulation of oscillatory inrush in Y-Δ transformer



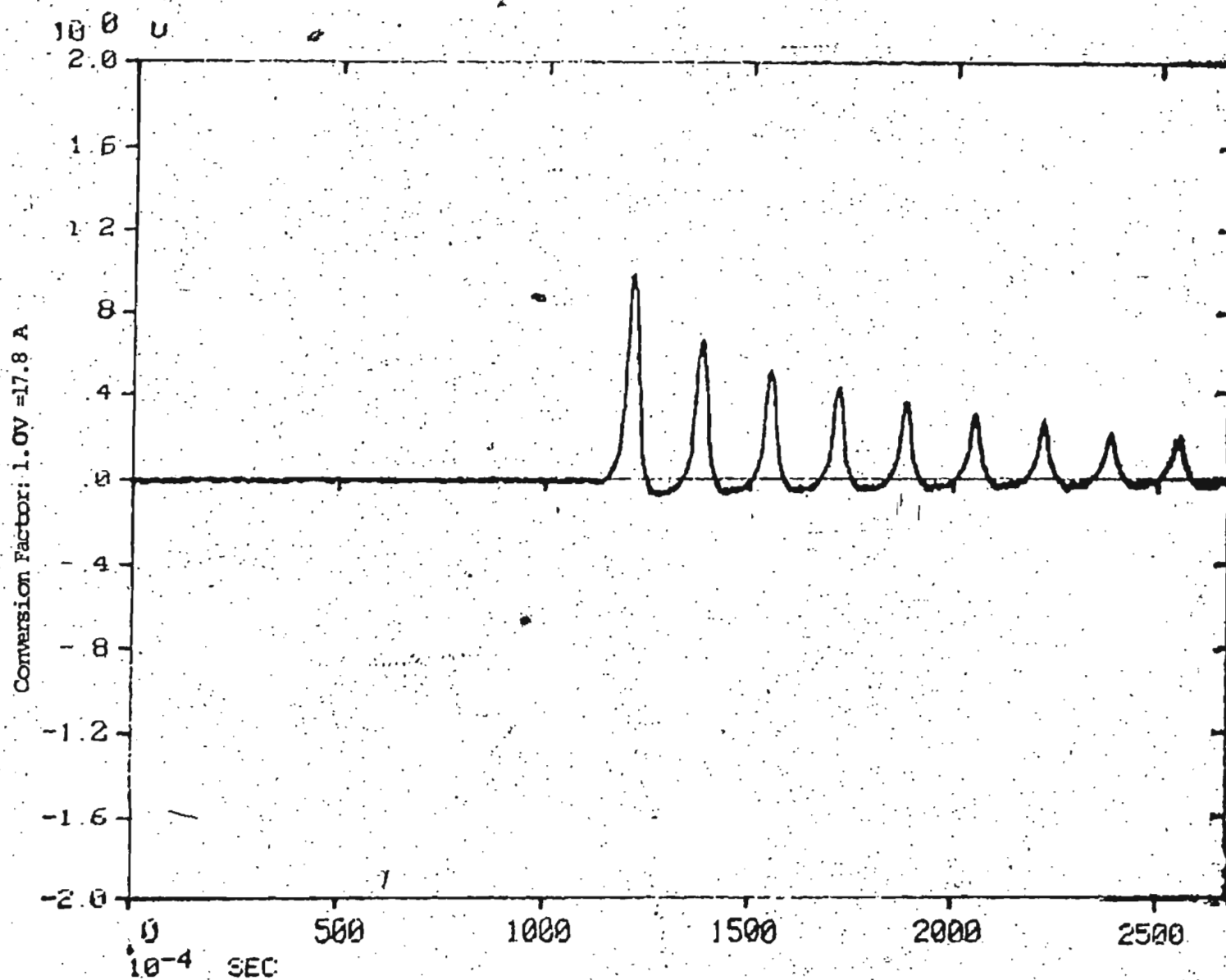


Fig. 3.26 (a) Recorded waveform of phase-a inrush of a Y-Δ transformer energized from Y-side ( $\lambda=0^\circ$ )

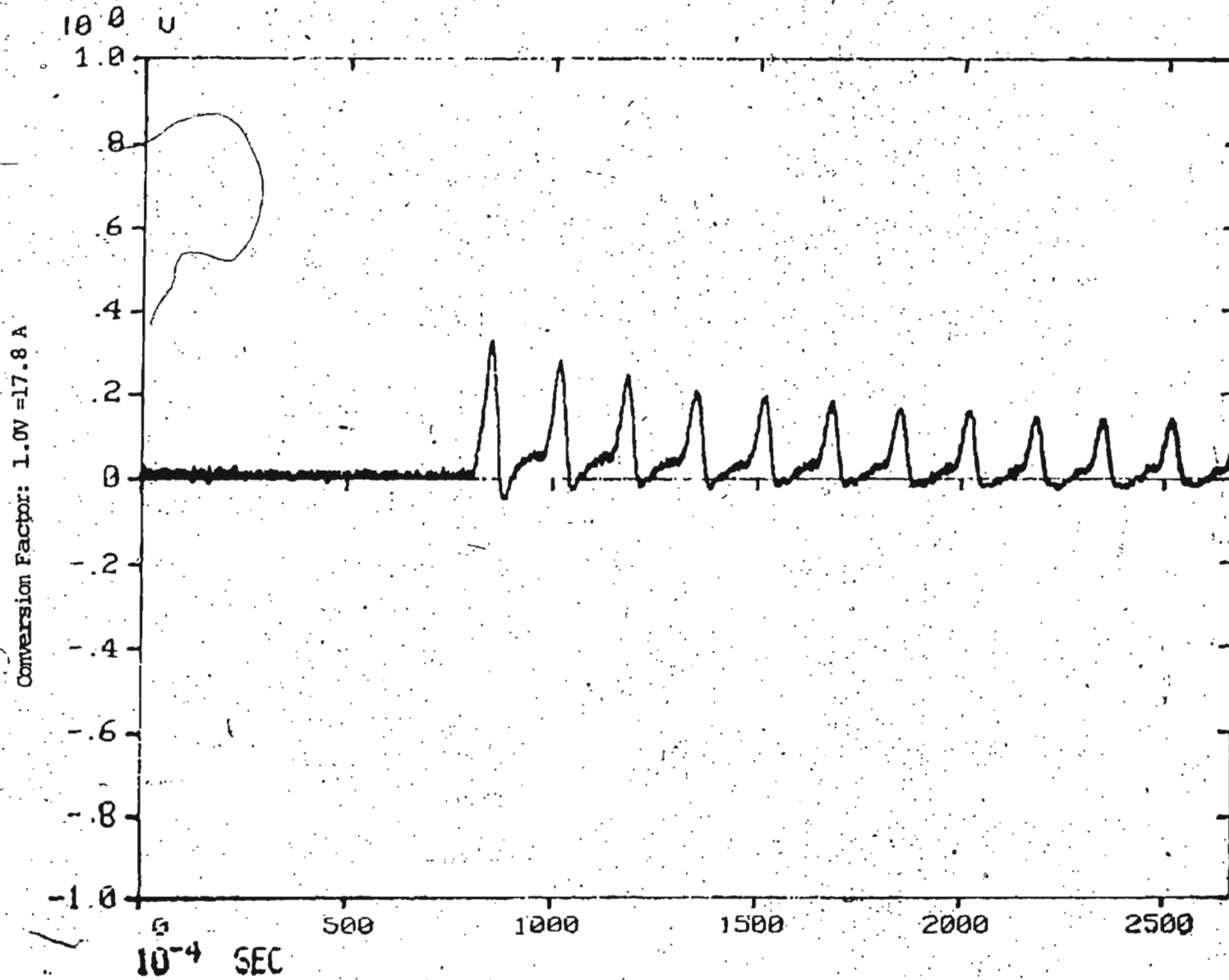


Fig. 3.26 (b) Recorded waveform of phase-b inrush of a Y-Δ transformer energized from Y-side

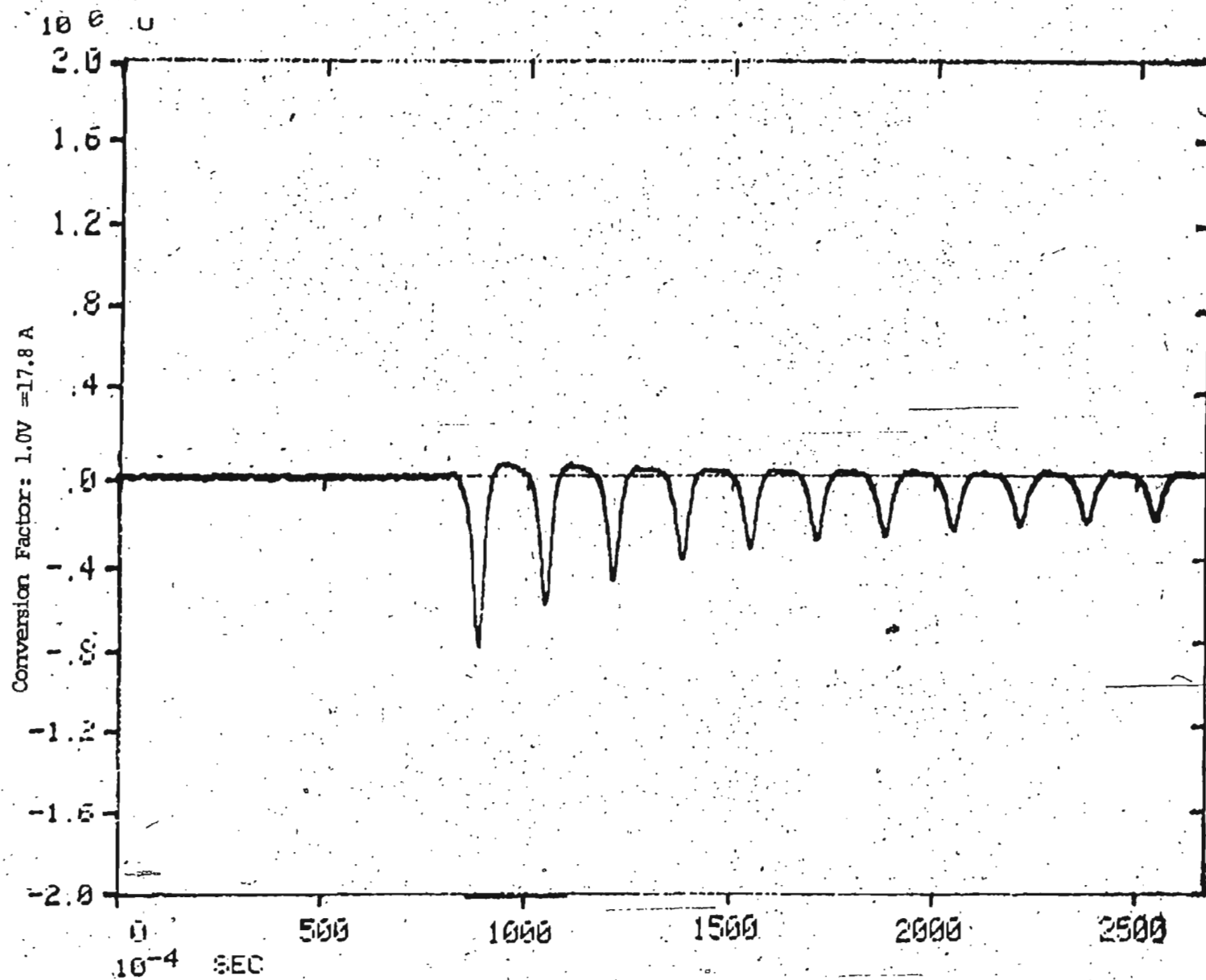


Fig. 3.26 (c) Recorded waveform of phase-c inrush of a Y-Δ transformer energized from Y-side

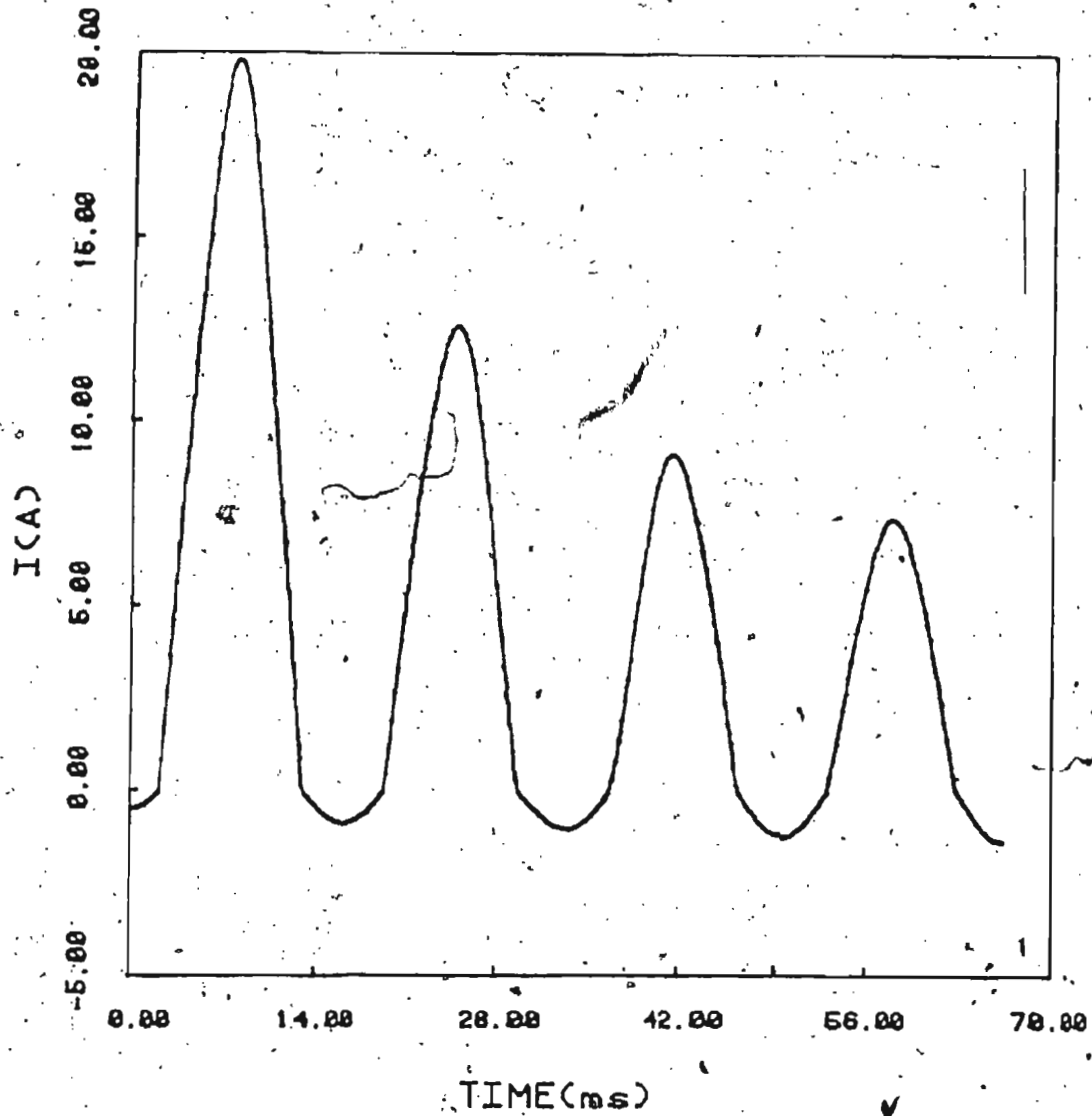


Fig. 3.27 (a) Simulation of phase-a inrush shown in Fig. 3.26(a)

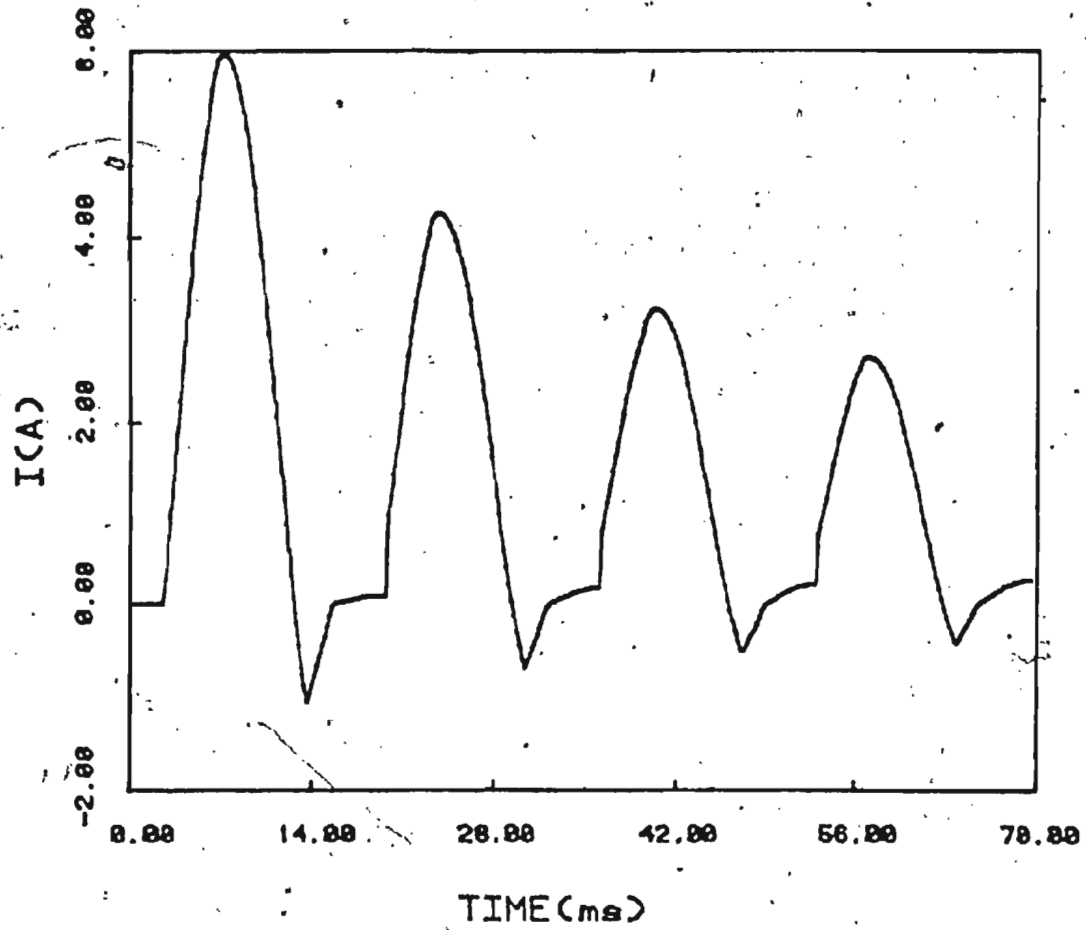


Fig. 3.27 (b) Simulation of phase-b inrush shown in Fig. 3.26(b)

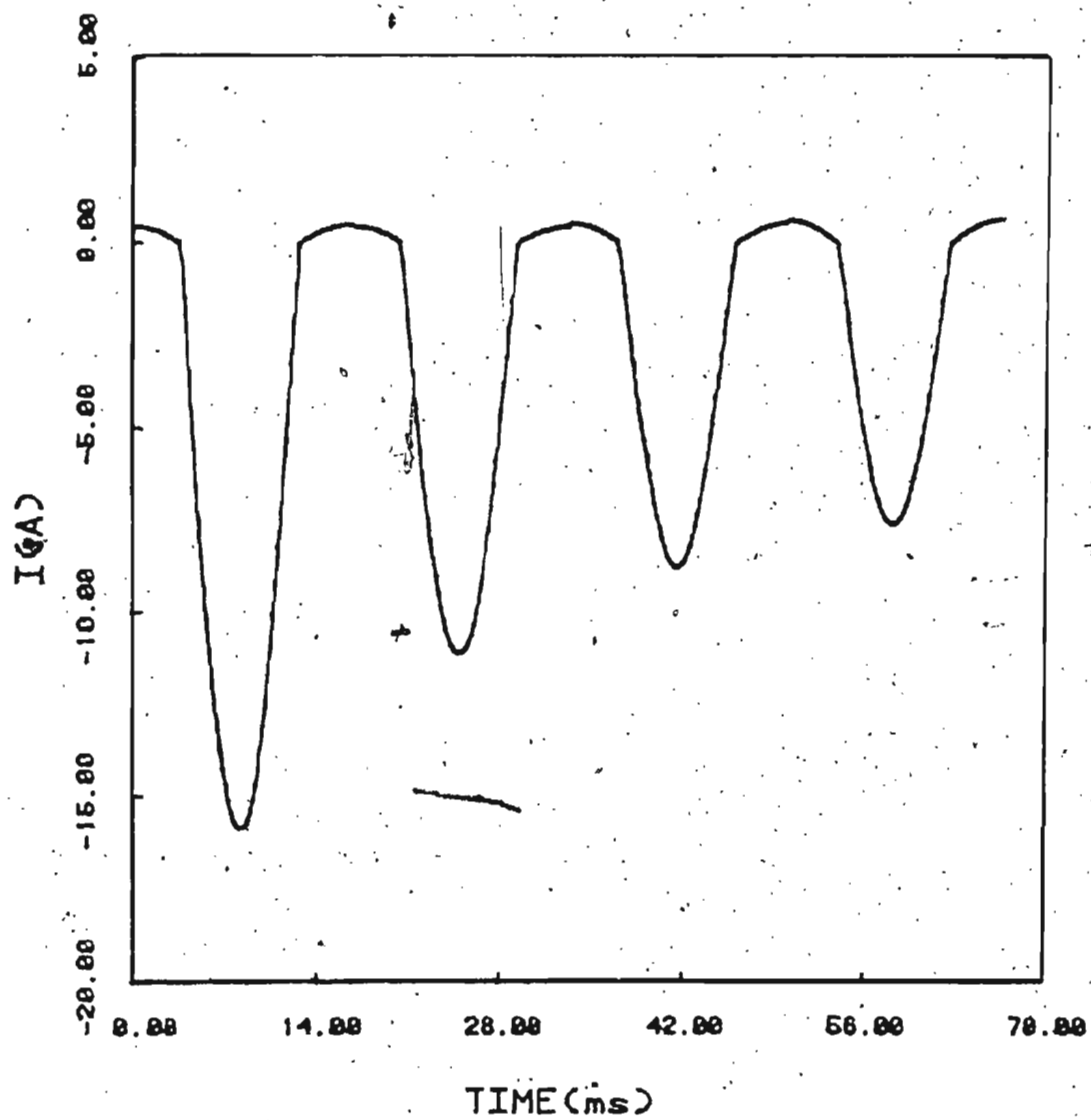


Fig. 3.27 (c) Simulation of phase-c inrush shown in Fig. 3.26(c)

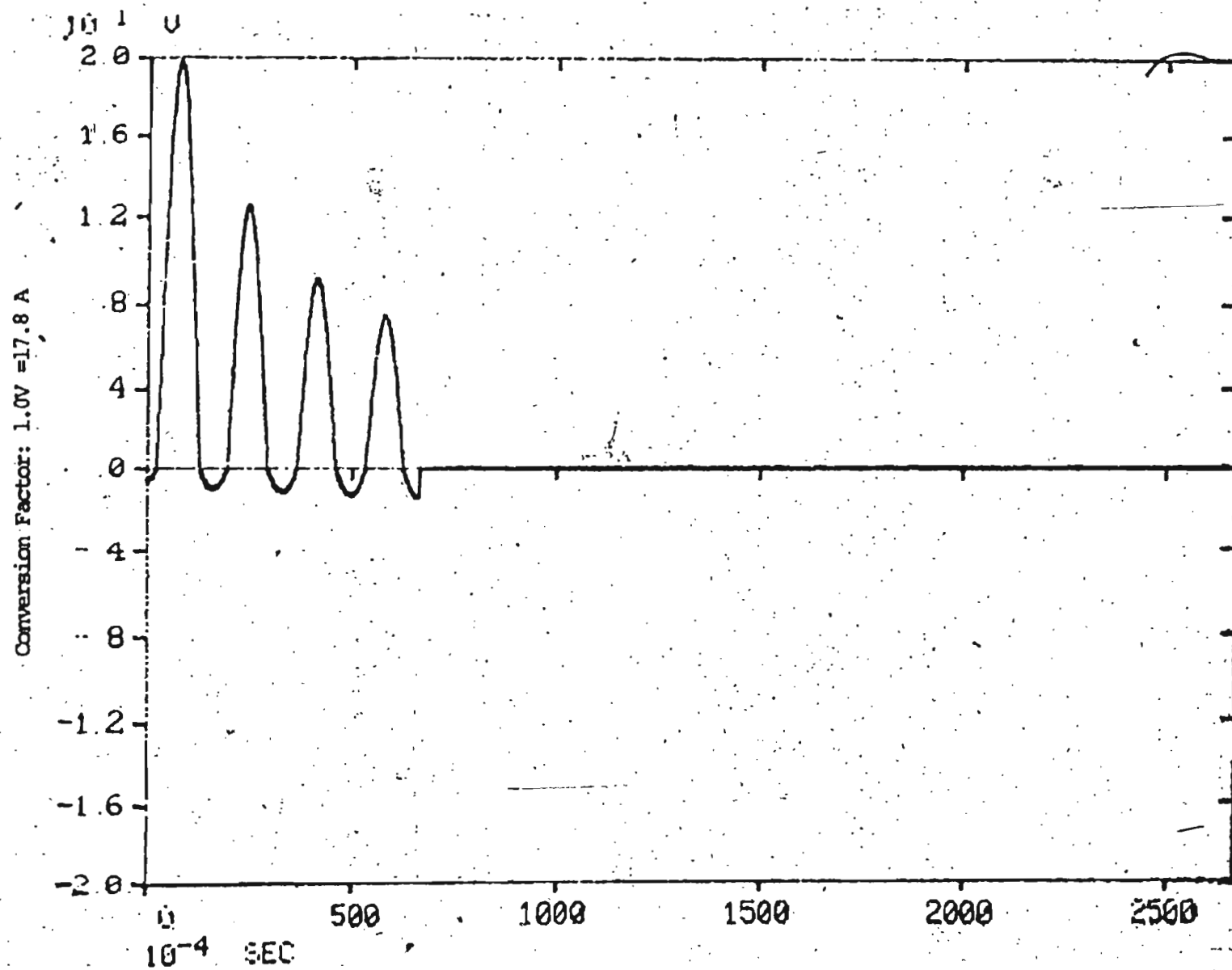


Fig. 3.28 (a) Simulation of Fig. 3.27(a) reproduced from Fourier Analyzer

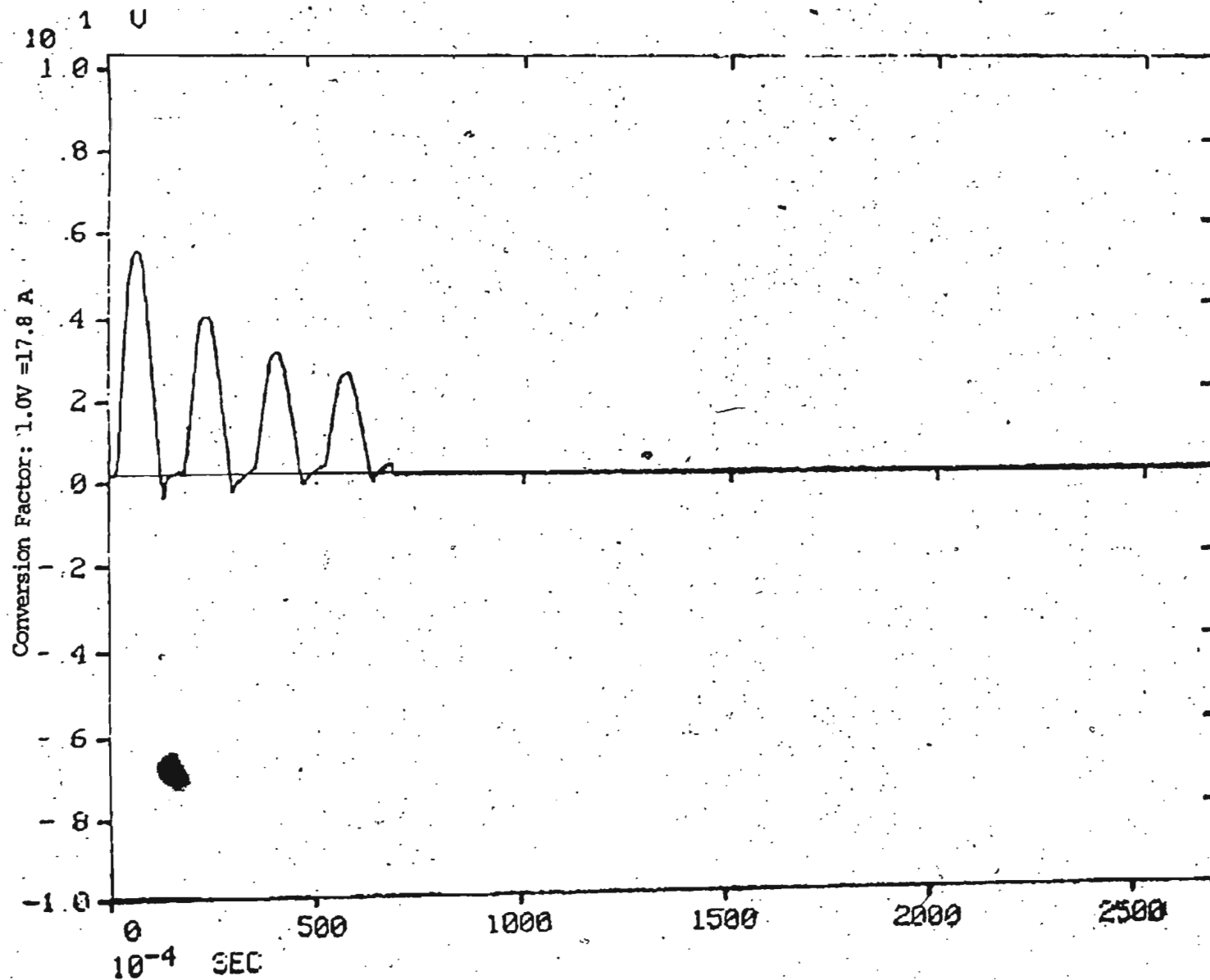


Fig. 3.28 (b) Simulation of Fig. 3.27(b) reproduced from Fourier Analyzer



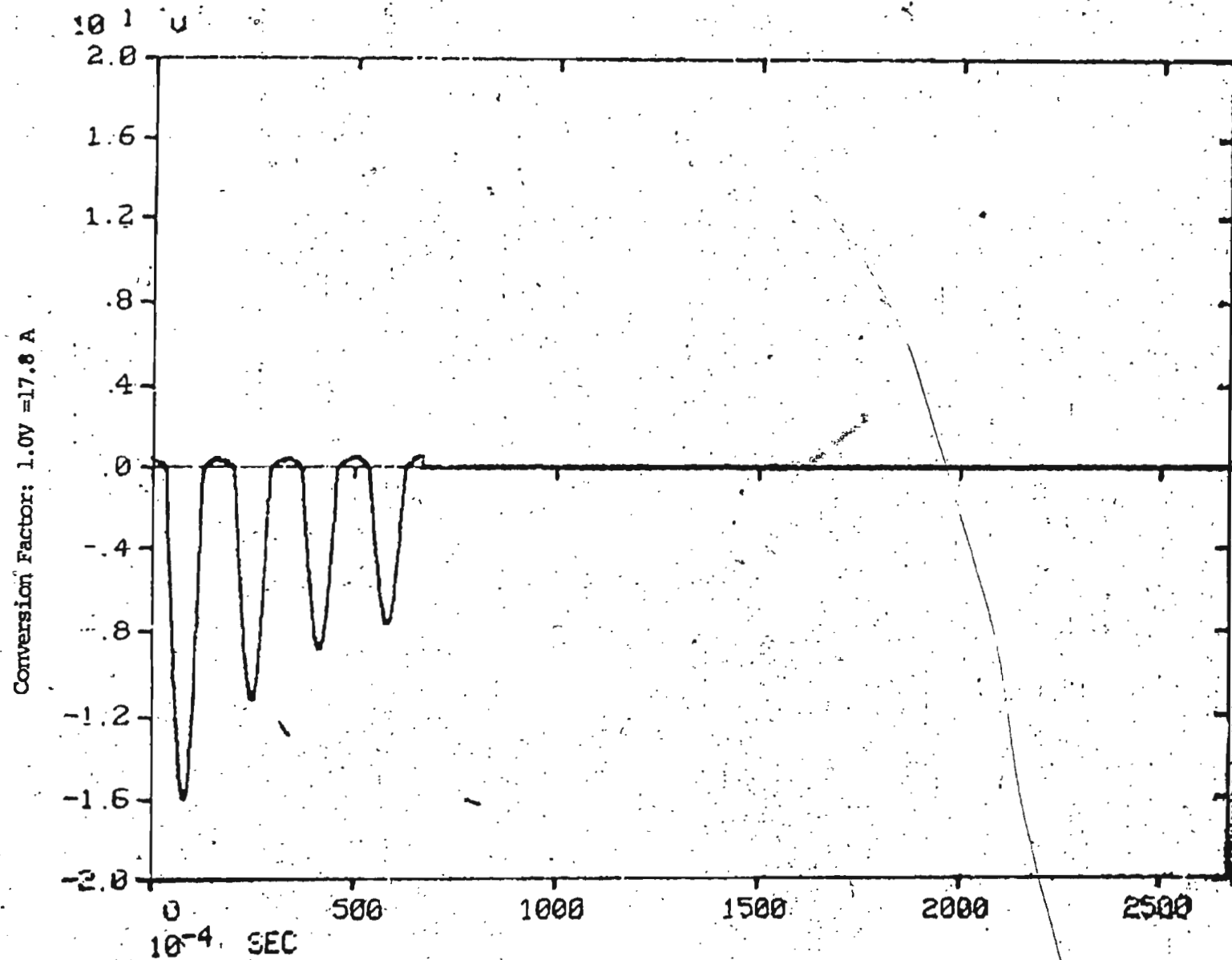


Fig. 3.28 (c) Simulation of Fig. 3.27(c) reproduced from Fourier Analyzer

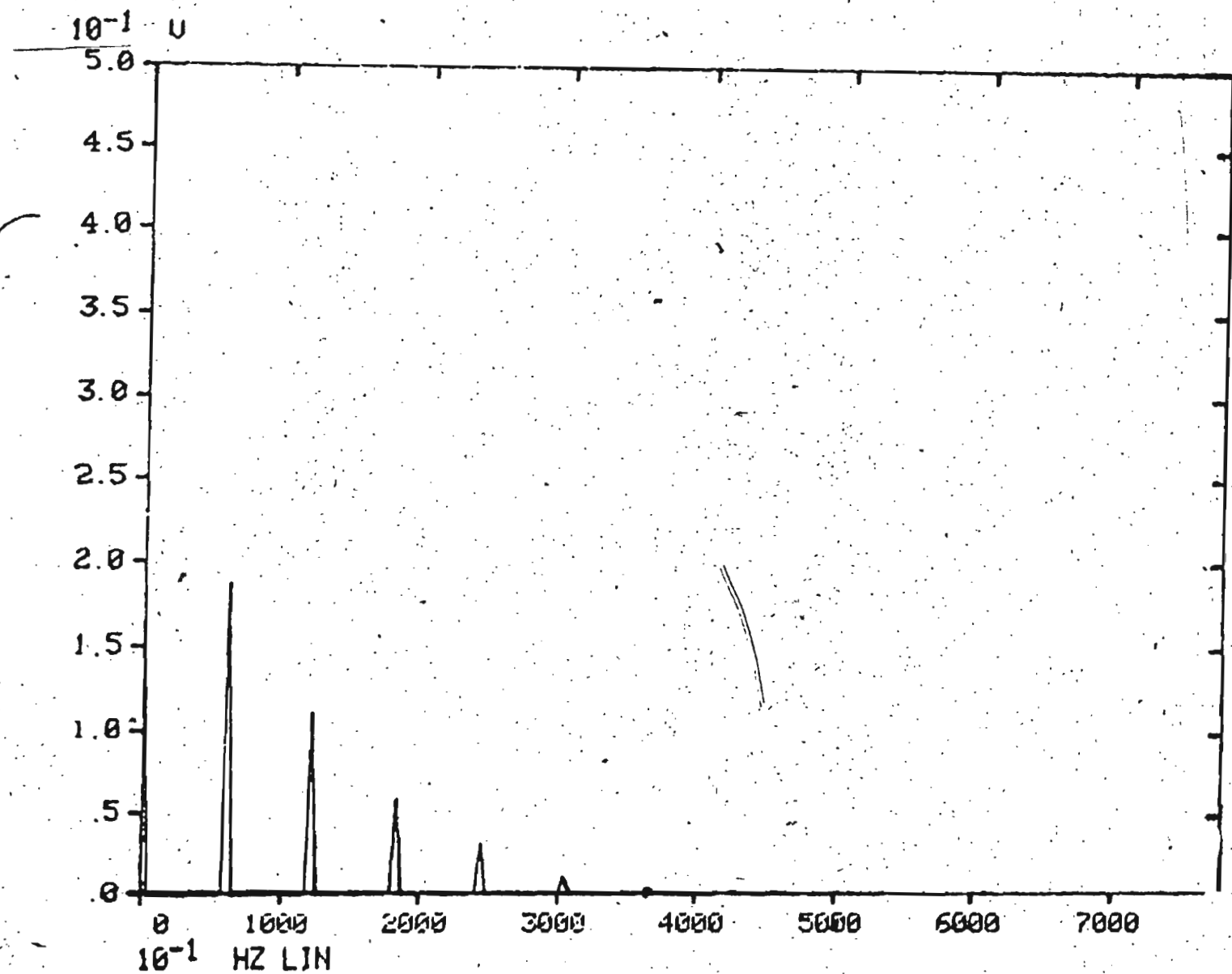


Fig. 3.29 (a) Discrete frequency spectrum of 1st cycle of inrush shown in Fig. 3.26 (a)

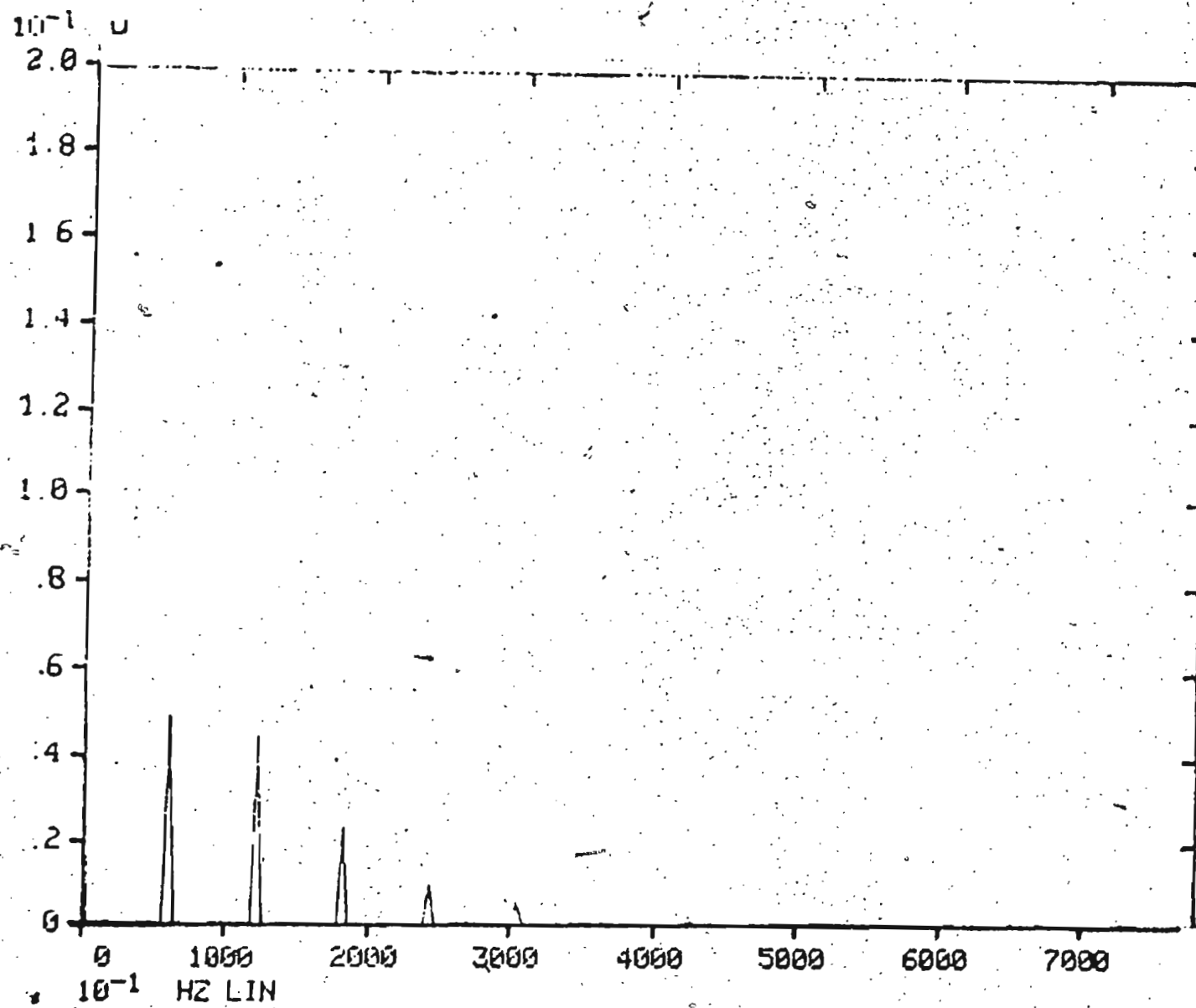


Fig. 3.29 (b) Discrete frequency spectrum of 1st cycle of inrush shown in Fig. 3.26(b)

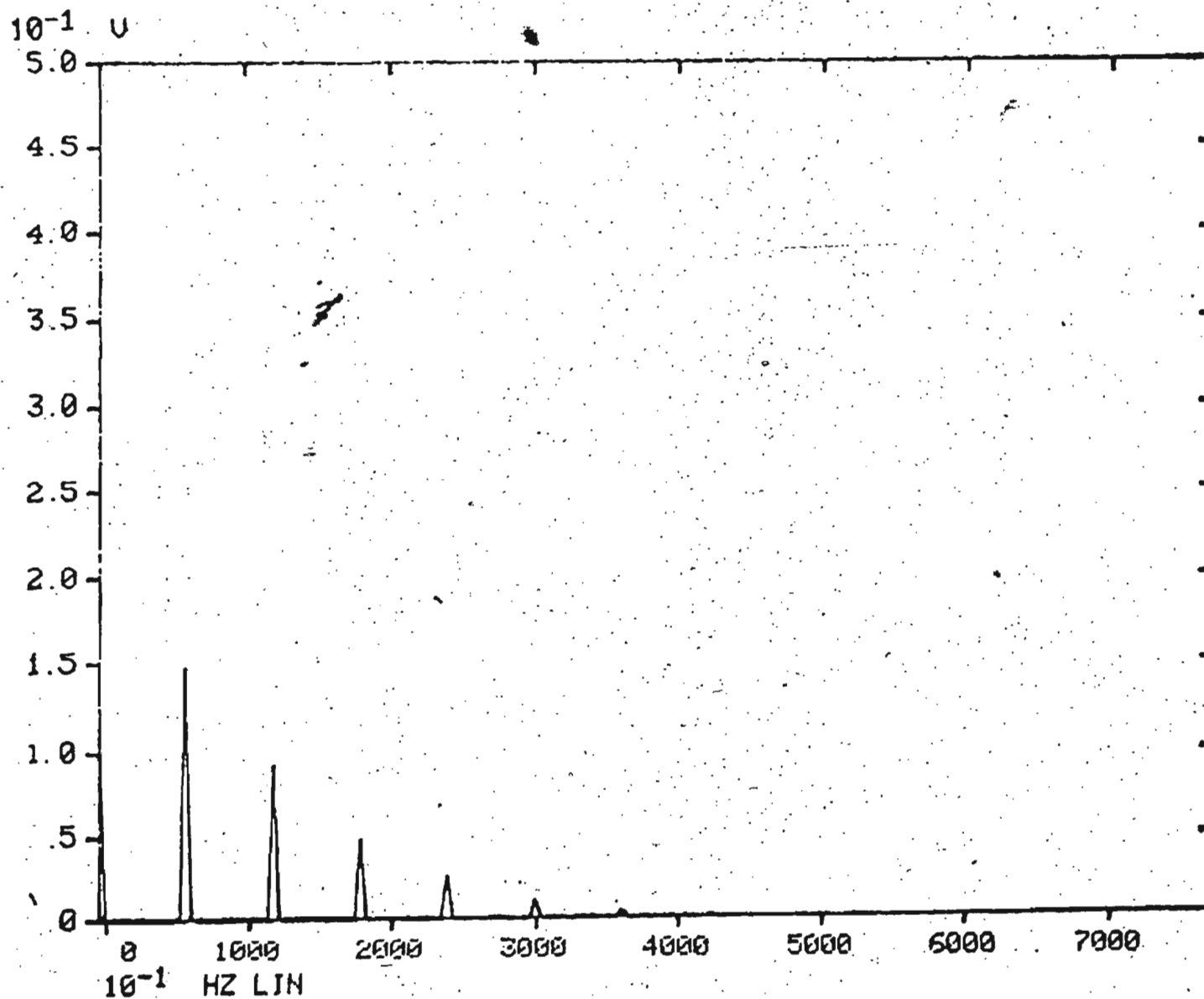


Fig. 3.29 (c) Discrete frequency spectrum of 1st cycle of  
inrush shown in Fig. 3.26 (c)

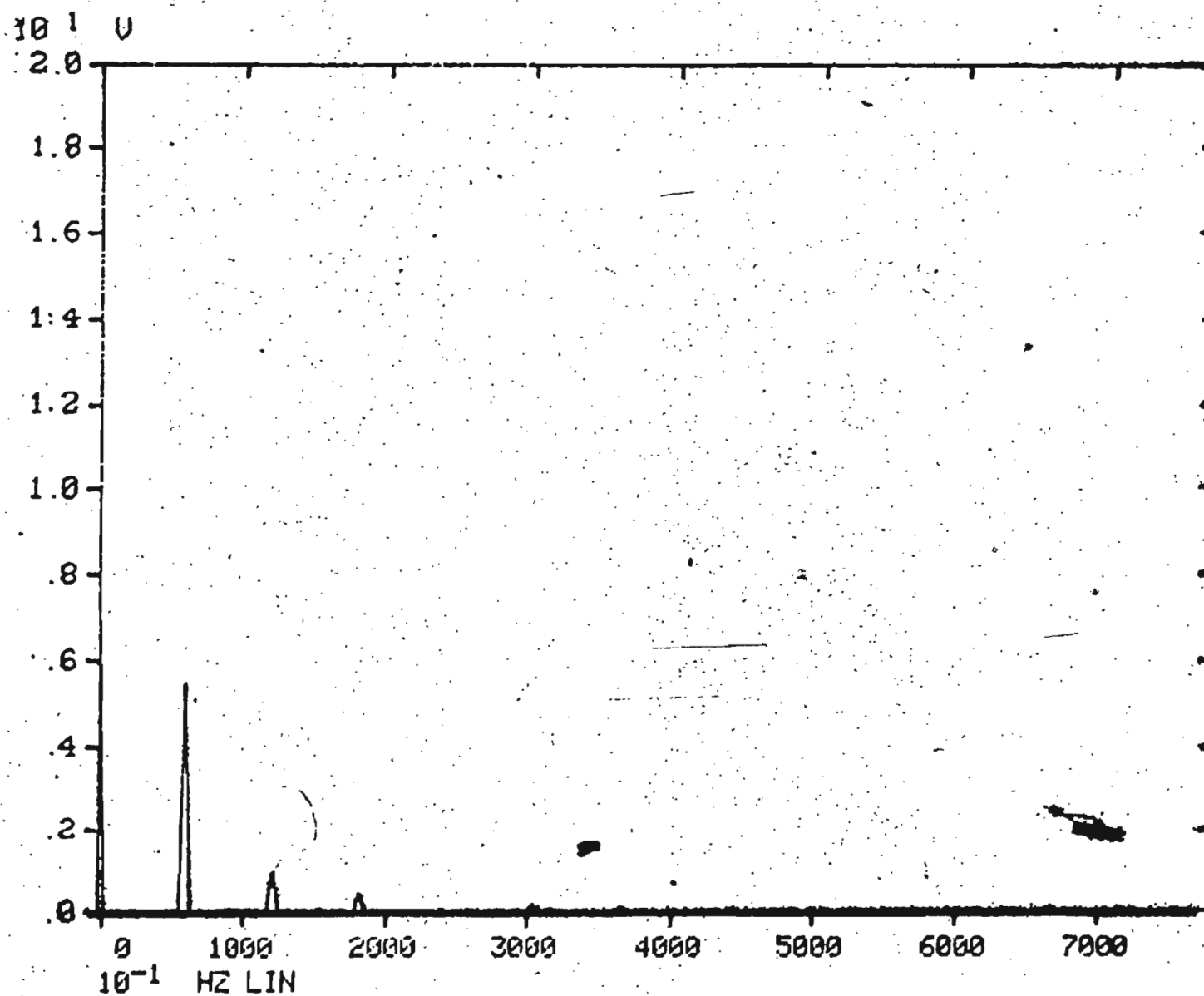


Fig. 3.30 (a) Discrete frequency spectrum of 1st cycle of  
inrush shown in Fig. 3.27(a)

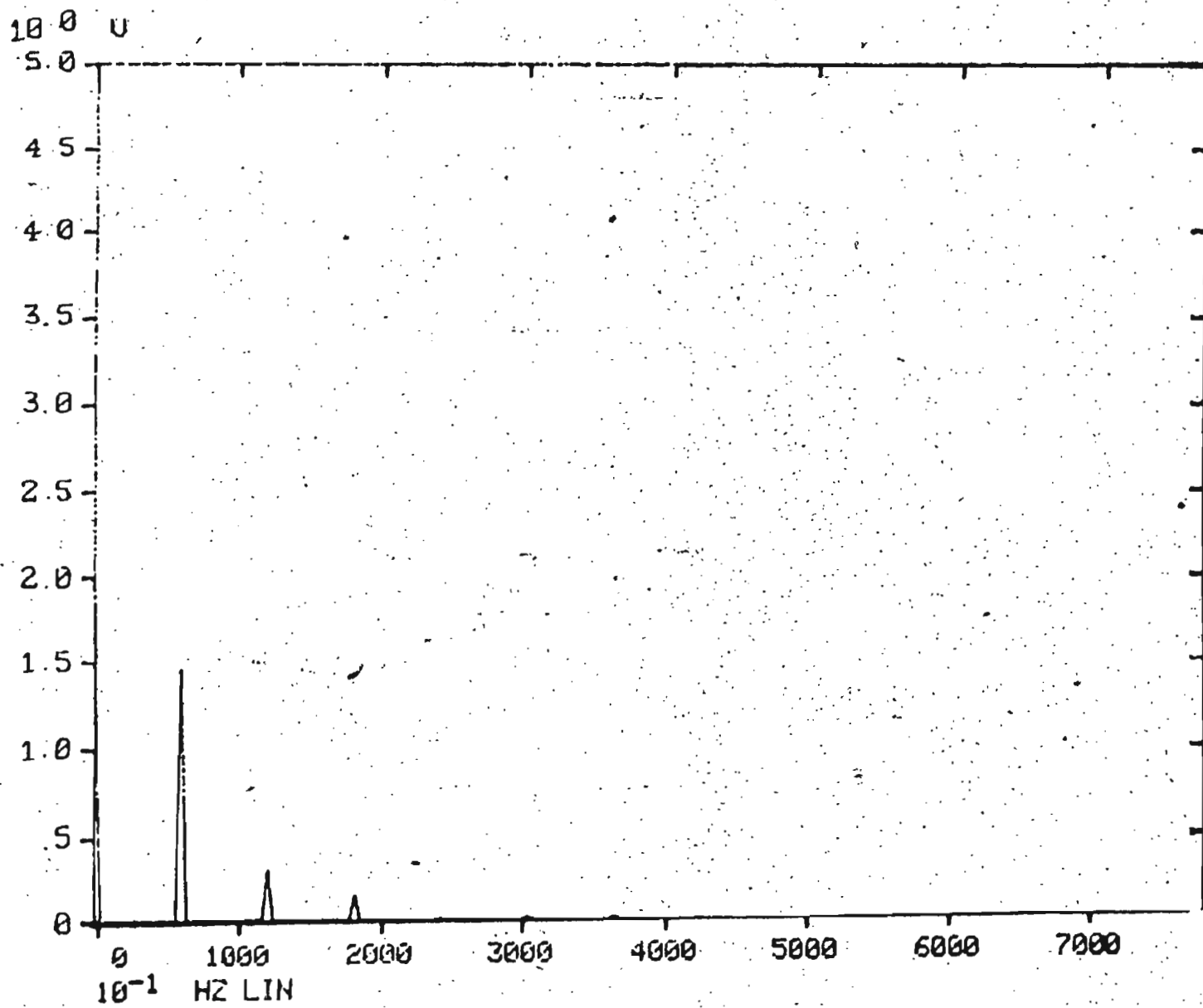


Fig. 3.30 (b) Discrete frequency spectrum of 1st cycle of inrush shown in Fig. 3.28(b)

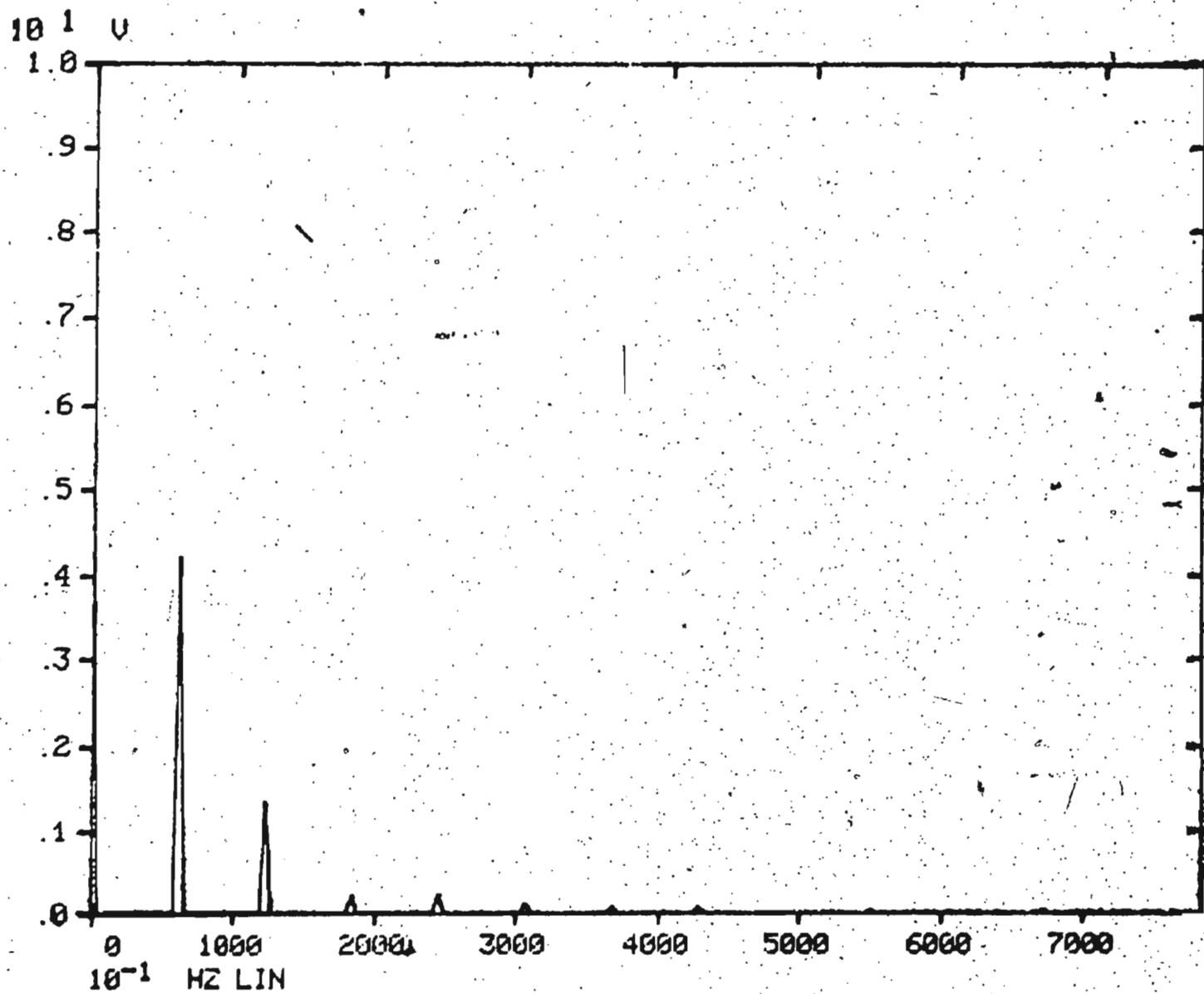


Fig. 3.30 (c) Discrete frequency spectrum of 1st-cycle of  
inrush shown in Fig. 3.28(c)

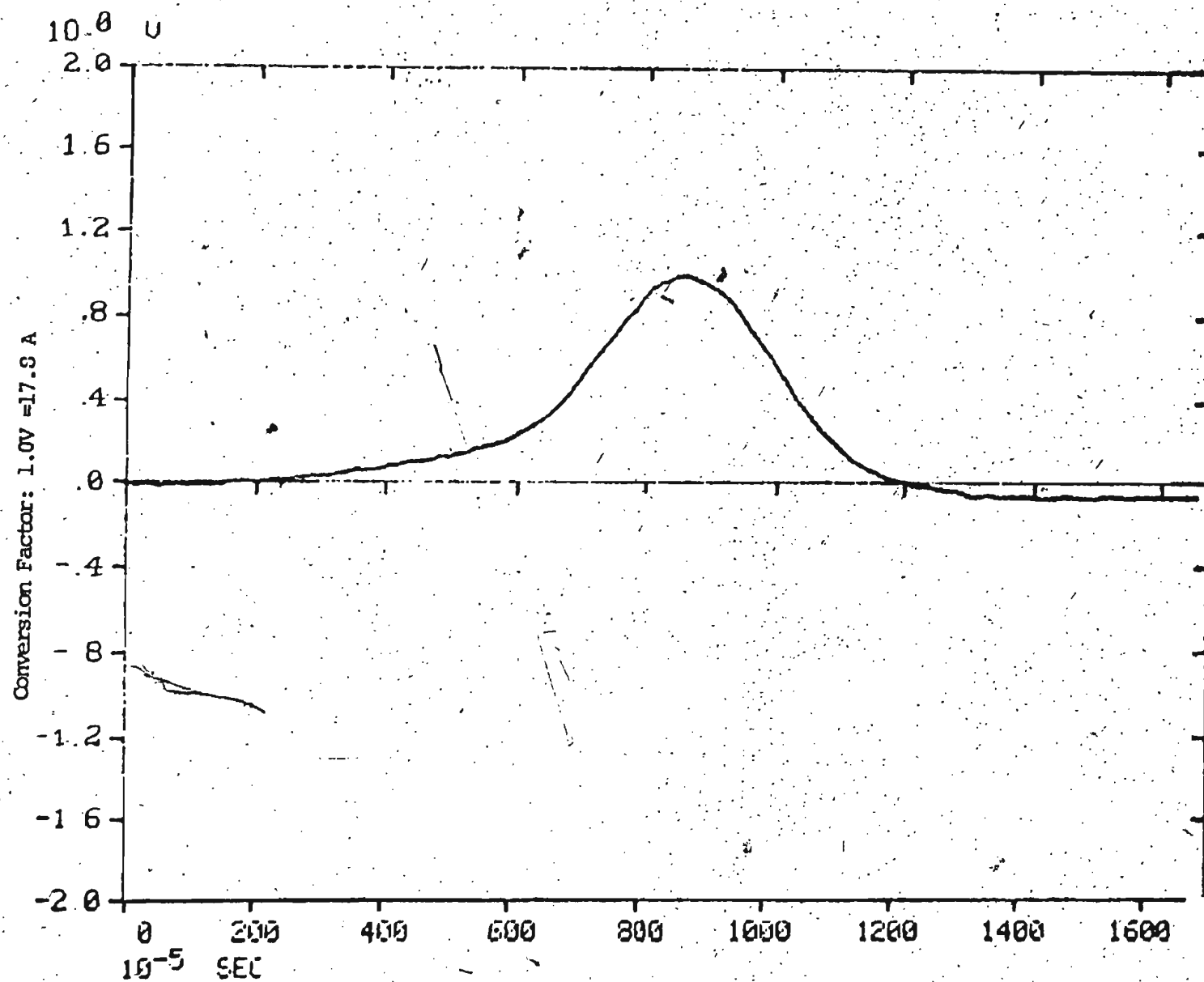


Fig. 3.31 (a) Amplified 1st cycle of inrush current in phase-a shown in Fig. 3.26(a)



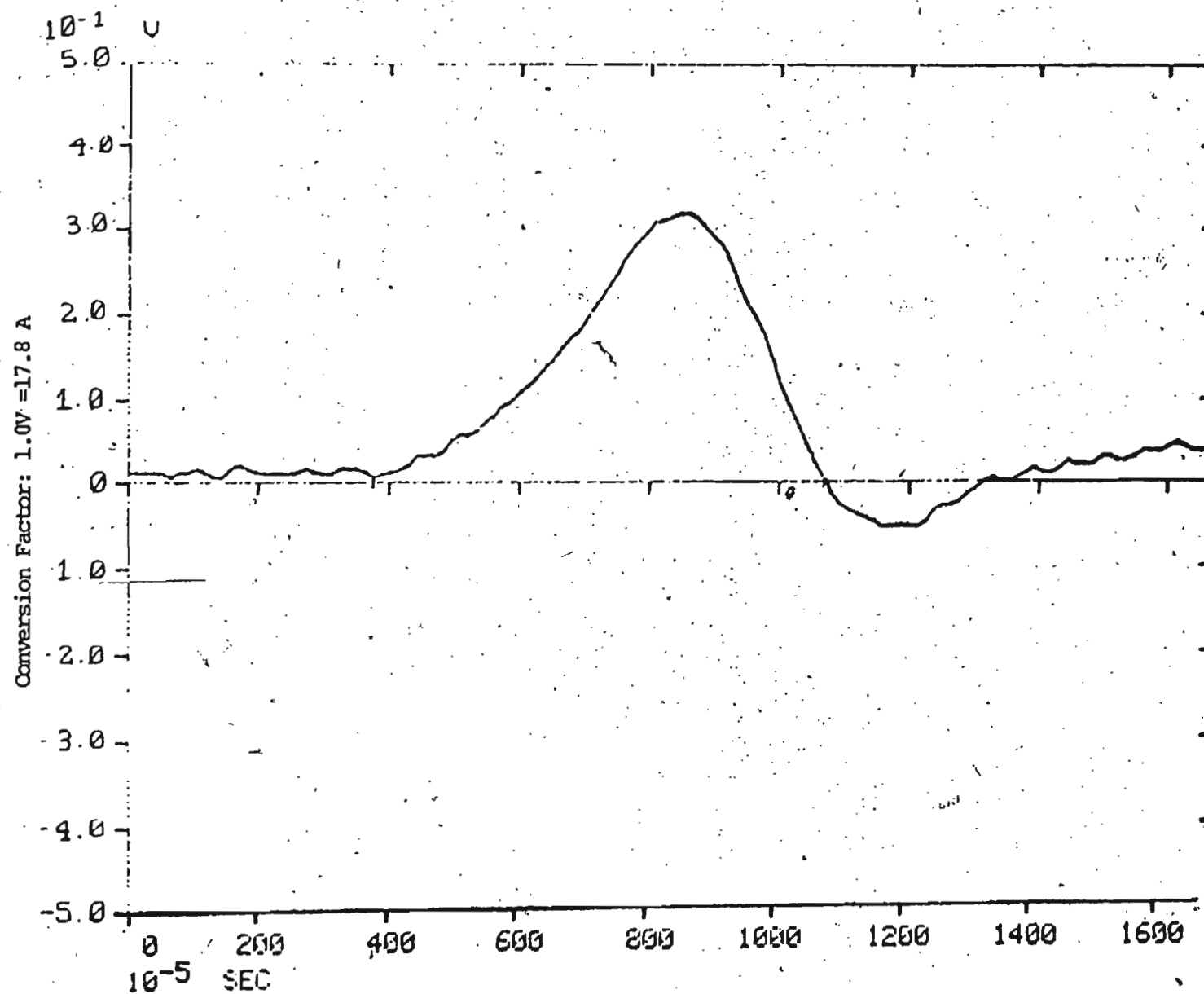


Fig. 3.31 (b) Amplified 1st-cycle of inrush current in phase-b shown in Fig. 3.26(b)

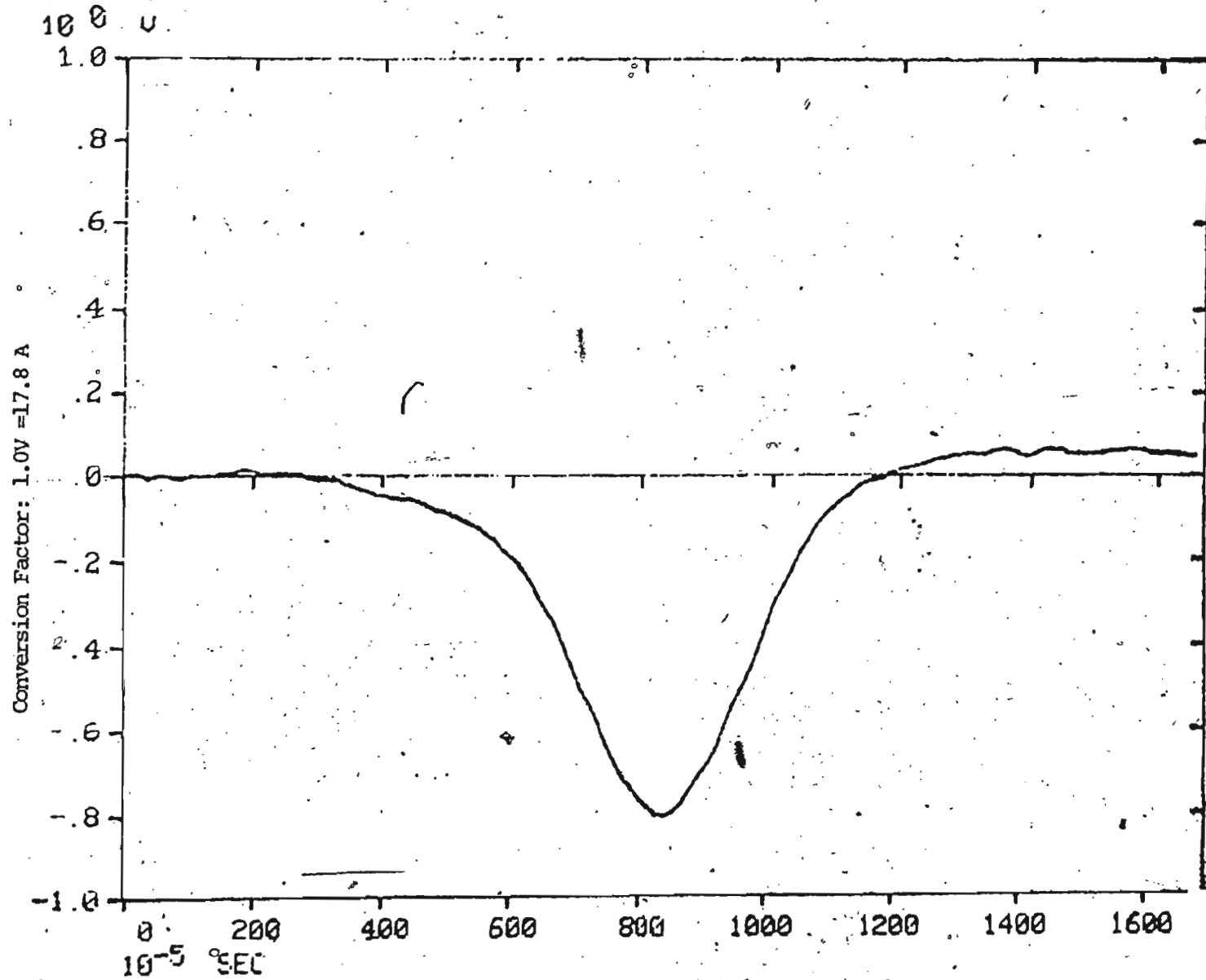


Fig. 3.31 (c) Amplified 1st cycle of inrush current in phase-c shown in Fig. 3.26(c)

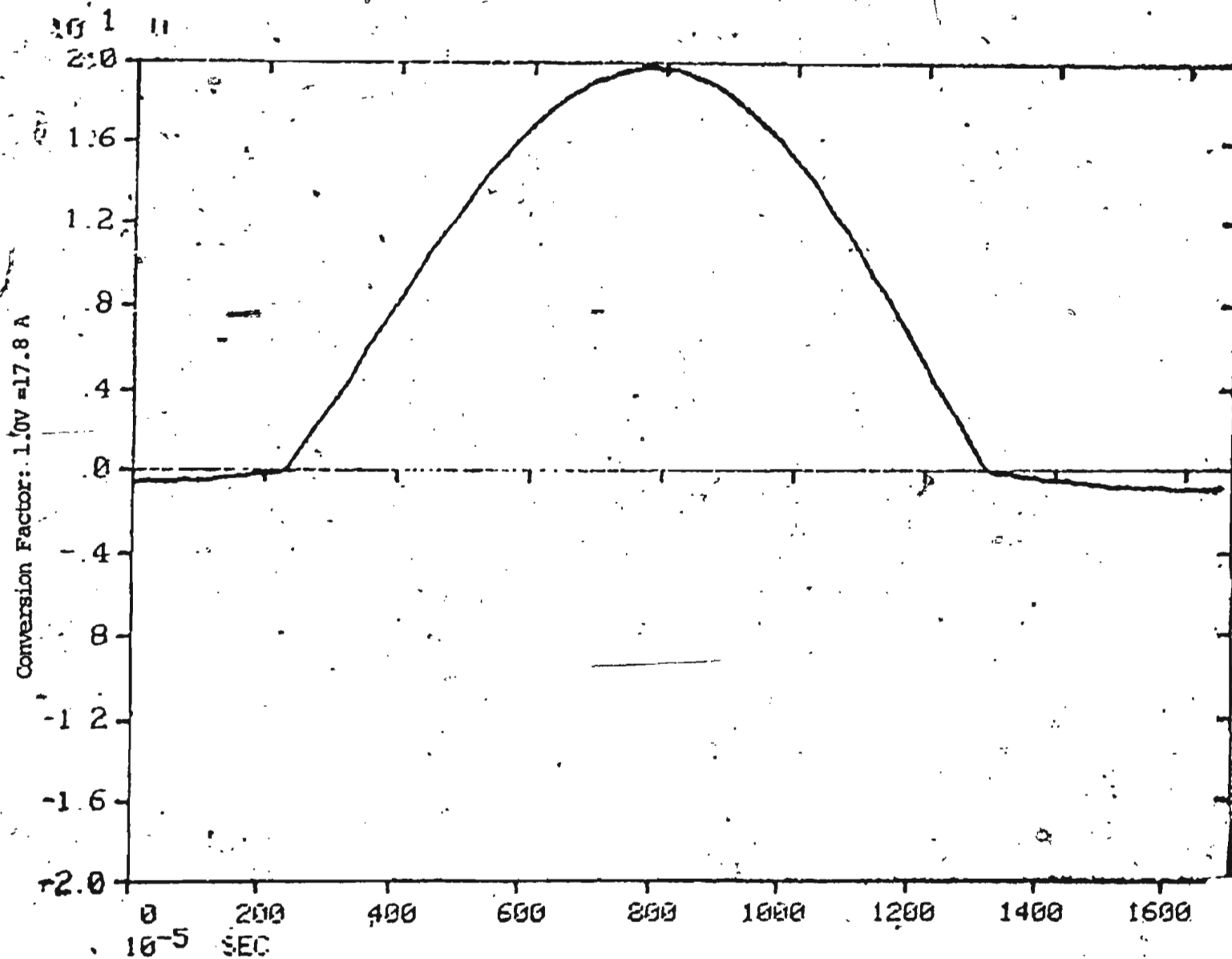


Fig. 3.32 (a) Amplified 1st cycle of inrush current in phase-a shown in Fig. 3.28(a)

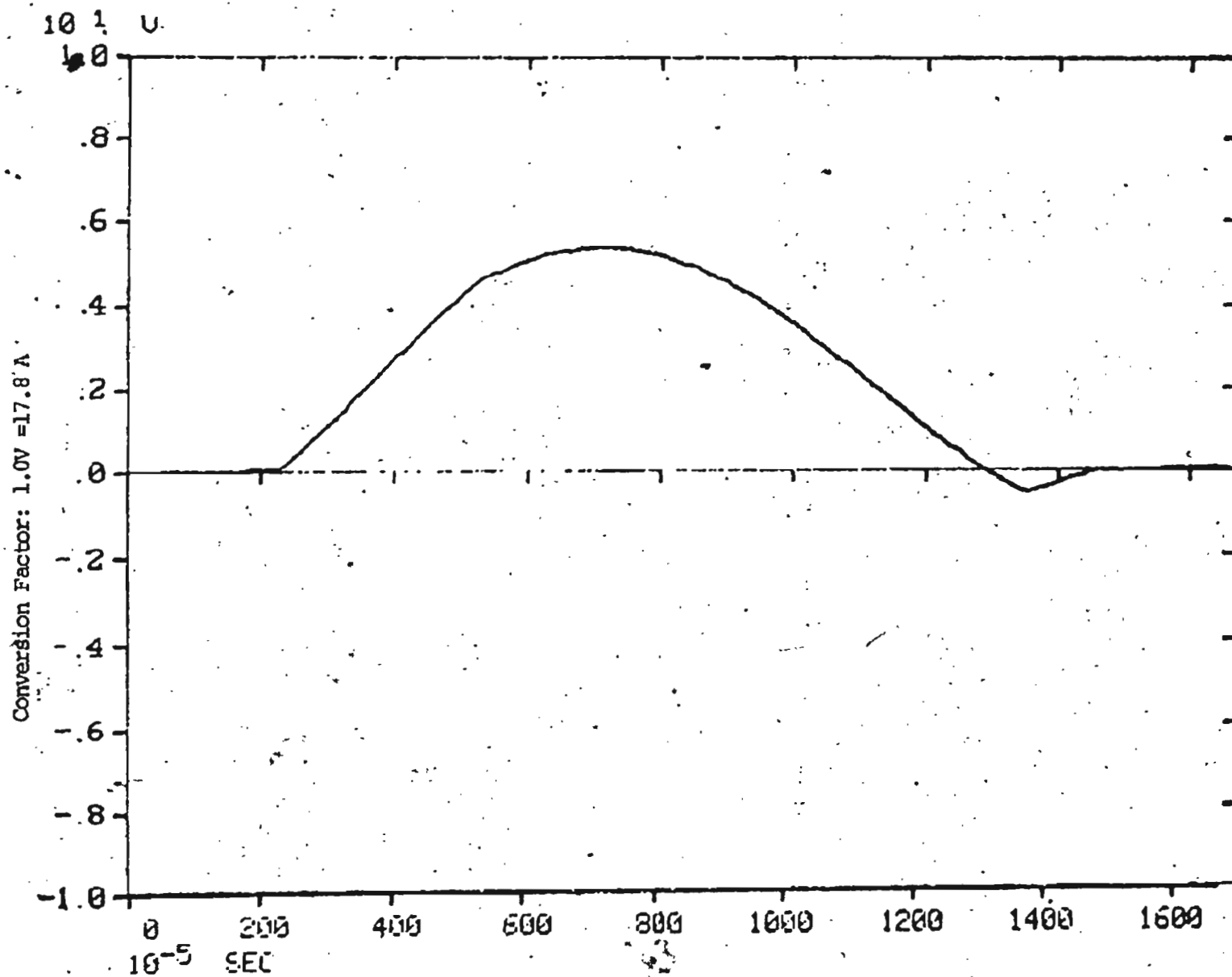


Fig. 3.32 (b) Amplified 1st cycle of inrush current  
in phase-b shown in Fig. 3.28(b)

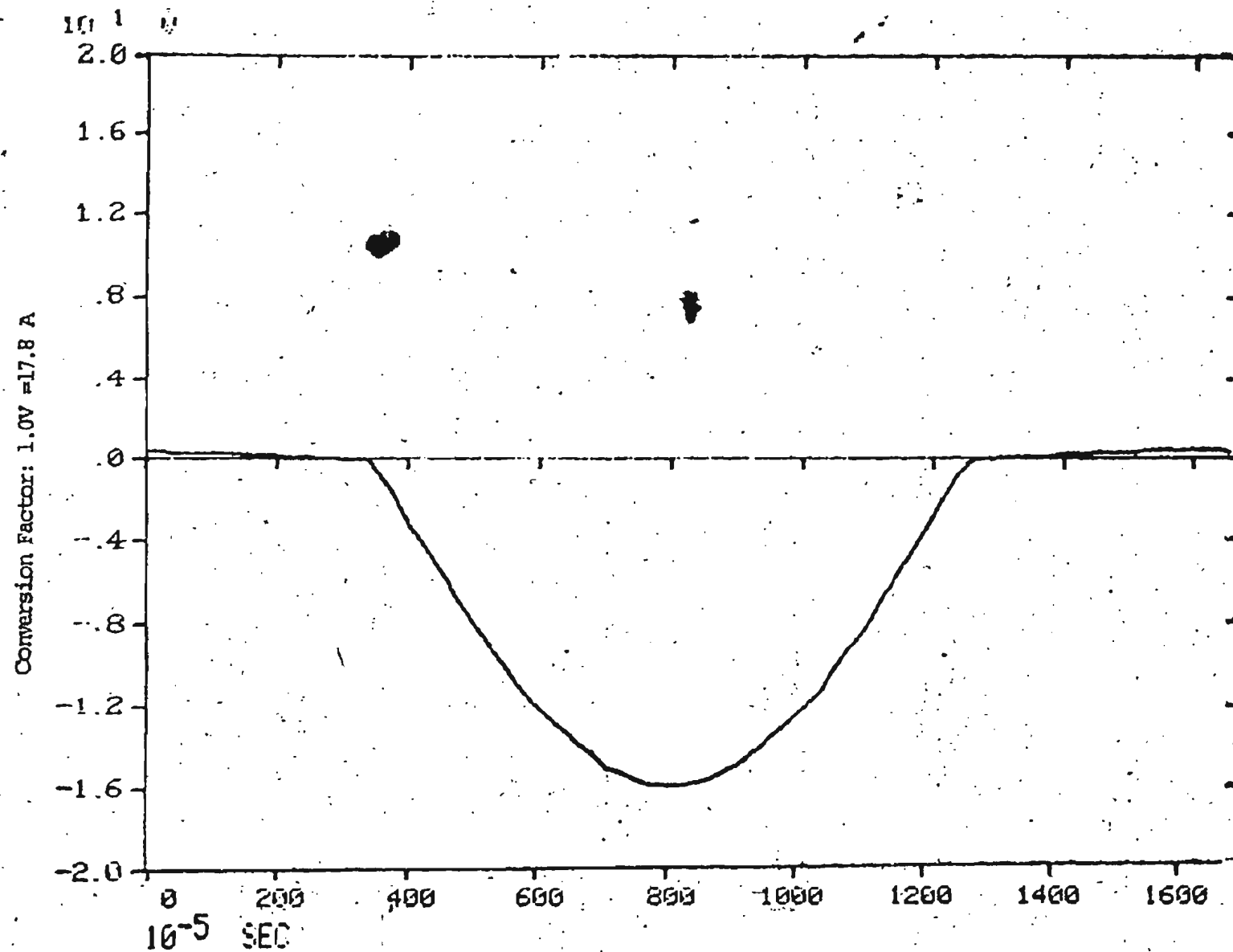


Fig. 3.32 (c) Amplified 1st cycle of inrush current in phase-c shown in Fig. 3.28(c)

for the discrepancy arises out of the fact that simulated waveforms are more regular thus containing lesser amount of harmonics than measured ones. The irregularities in the measured waveforms are difficult to achieve in the simulation as is reflected in Figs. 3.32(a), (b) and (c) for phases A, B and C respectively.

Simulation of the magnetizing current for three-phase transformers can also be carried out using Eqn. 3.68, provided that the parameters pertaining to the different matrix elements are known. A flow chart of the programming using Runge-Kutta-IV method is shown in Fig. 3.33. The advantage of this method is all the three-phase magnetizing inrush currents can be obtained by this method.

A particular case, while switching is done on a 120/120 V,  $\Delta/Y$  transformer is considered here. The angle of switching  $\lambda$  is  $0^\circ$ . The parameters used are as follows,

$$L_A = 0.00620 \text{ H}, L_B = 0.0060 \text{ H}, L_C = 0.0060 \text{ H}.$$

$$R_A = 0.8650 \text{ } \Omega, R_B = 0.48910 \text{ } \Omega, R_C = 0.60280 \text{ } \Omega$$

$$M_1 = 1.360 \text{ H}, M_2 = 1.790 \text{ H}, M_3 = 1.120 \text{ H}$$

$$M_4 = M_5 = M_6 = 0 \text{ [18]},$$

$$M_7 = 2.1760 \text{ H}, M_8 = 1.7920 \text{ H}.$$

The values of  $M_7$  and  $M_8$  are taken as 1.6 times  $M_1$  and  $M_3$  respectively from the design consideration. The measured waveforms are shown in Figs. 3.34(a), (b), (c) for the phase

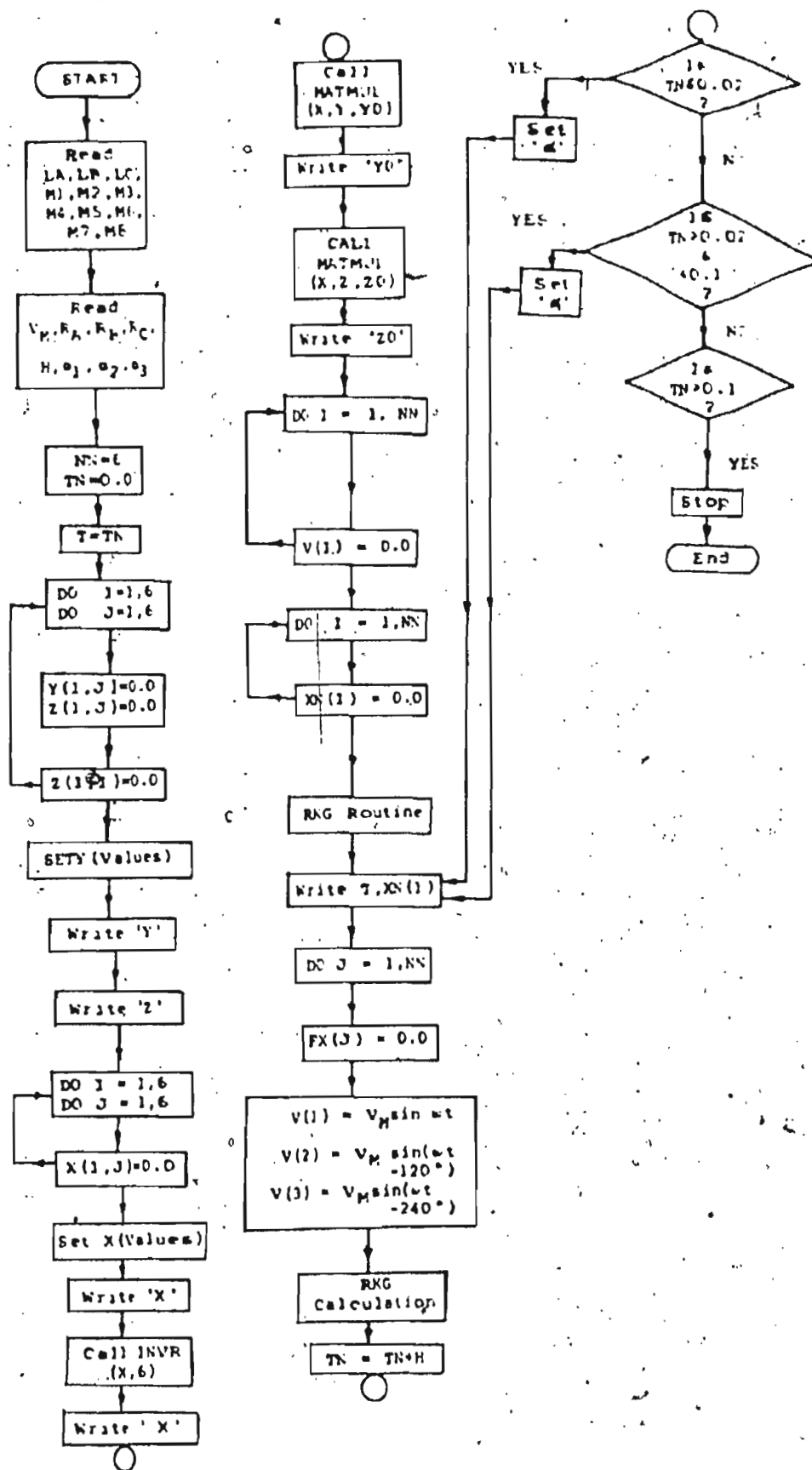


Fig. 3.33 Flow chart of programming three-phase inrush currents by mutual inductive coupling method

A, B and C respectively. Corresponding simulations for the phase A, B and C are shown in Figs. 3.35(a), (b) and (c) respectively. The magnitudes are compared up to 4th cycles in Table 3.8.

As it is clear from the table, the simulated peaks are not as accurate as the previous method. The reason for this is, the values of the self as well as the mutual inductances do not remain constant from cycle to cycle and to ascertain the values of mutual inductance above saturation levels is a very difficult task. An exponentially decaying constant has been used for this reason in the programming. The accuracy obviously will depend on selecting the correct values of these parameters. Whereas, in the other method, all the parametric values can be determined numerically before hand, and the flexibility is more in simulating inrush in different conditions. However, for protection purpose, as shown in the next chapter, the algorithms are tested on both type of simulations to find out their suitabilities.

#### 3.4 Discussion on Application of Simulated Results

As it was indicated in Section 1.4 earlier, the simulation of magnetizing inrush current is very important from protection point of view. For designing a digital differential protection system of power transformers using microcomputers, it is absolutely necessary to test the relay



on digitally simulated data for both the fault and magnetizing inrush currents. To test the restraining characteristics of any algorithm during inrush current of a transformer, accurate simulation of the inrush currents for different conditions are necessary. Hence, for accurate simulations, proper understanding of the magnetizing inrush phenomenon and their mathematical formulations are required. These have been carried out in sections 3.1 and 3.2 of this chapter. Performance of various algorithms on these simulated data will be shown in the next chapter. Obviously C. T. saturation effect distort the original signals to a large extent. This is to be taken into consideration while designing a practical protective scheme and is not considered here.

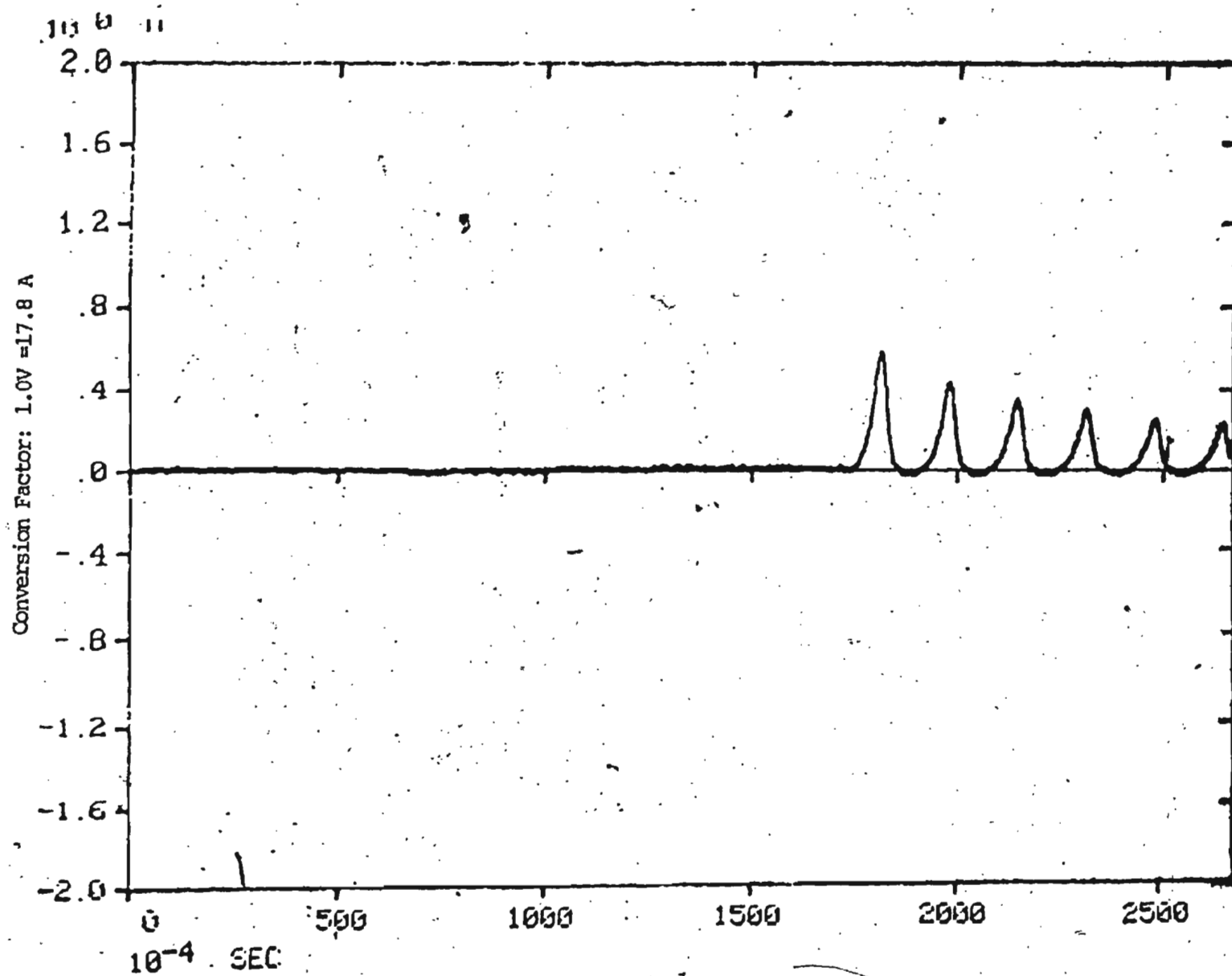


Fig. 3.34 (a) Recorded waveforms of phase-a inrush of a  $\Delta$ -Y transformer energized from  $\Delta$ -side ( $\lambda=0^\circ$ )

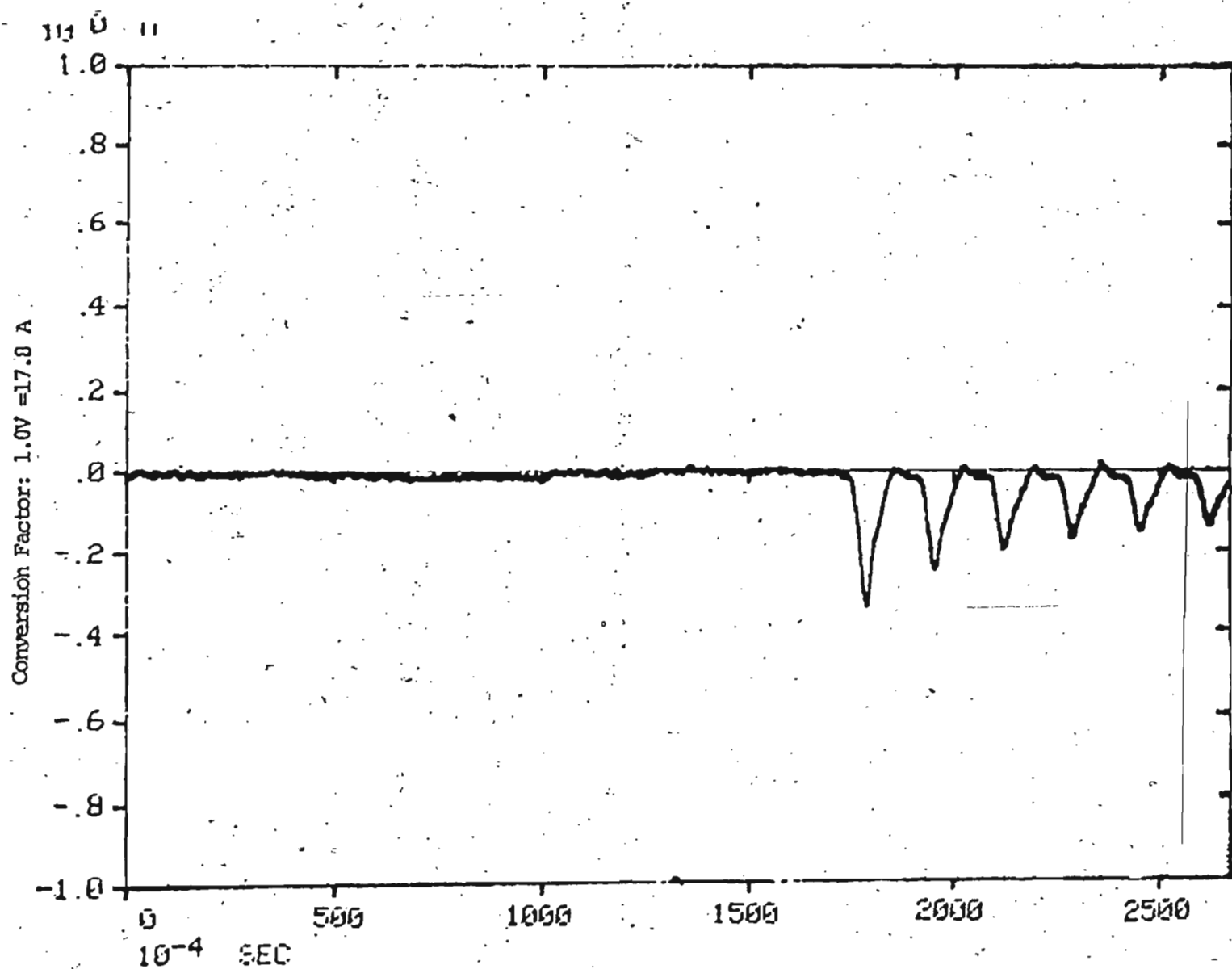


Fig. 3.94 (b) Recorded waveform of phase-b inrush of a  $\Delta$ -Y transformer energized from  $\Delta$ -side

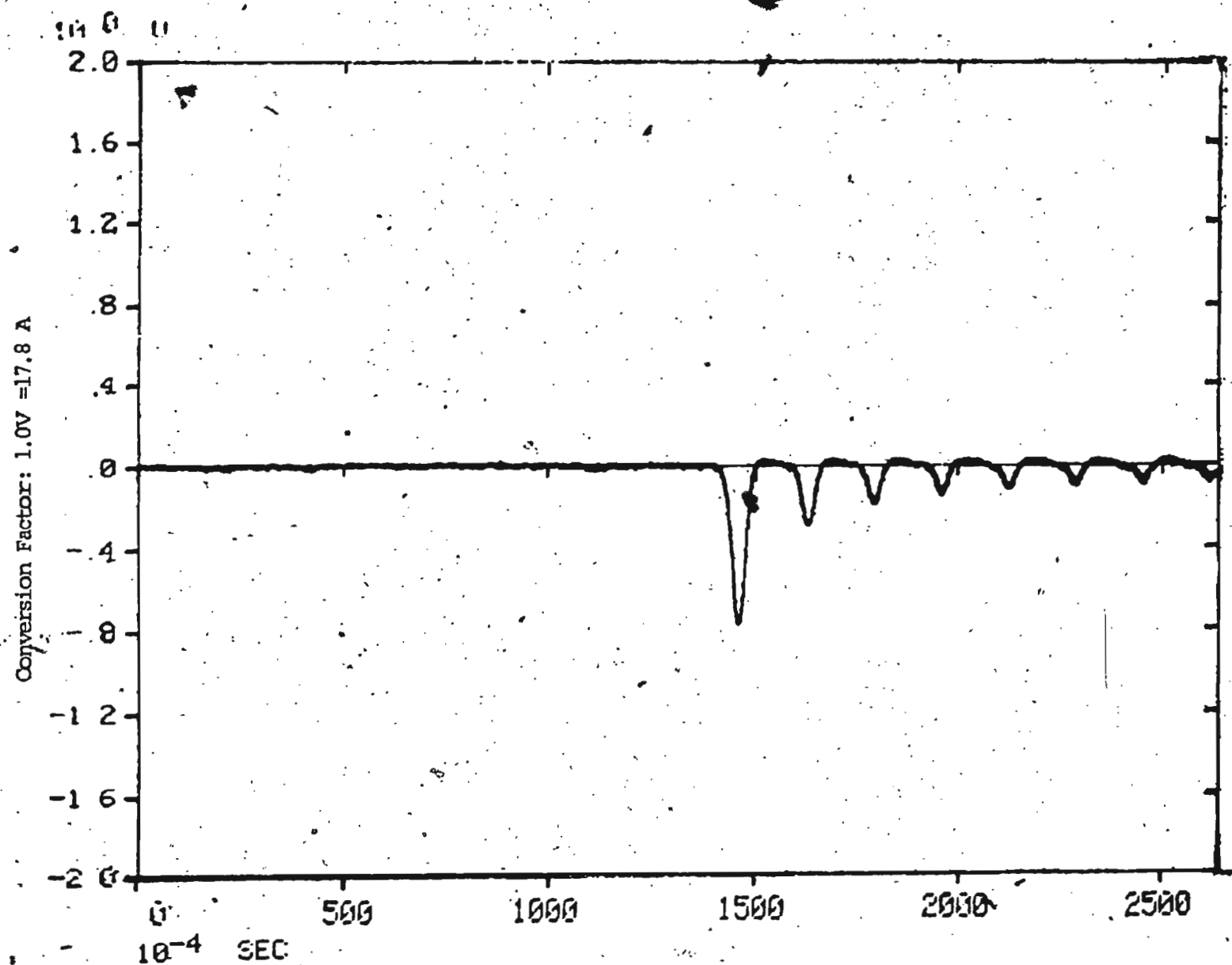


Fig. 3.34 (c) Recorded waveform of phase-c inrush of a Δ-Y transformer energized from Δ-side

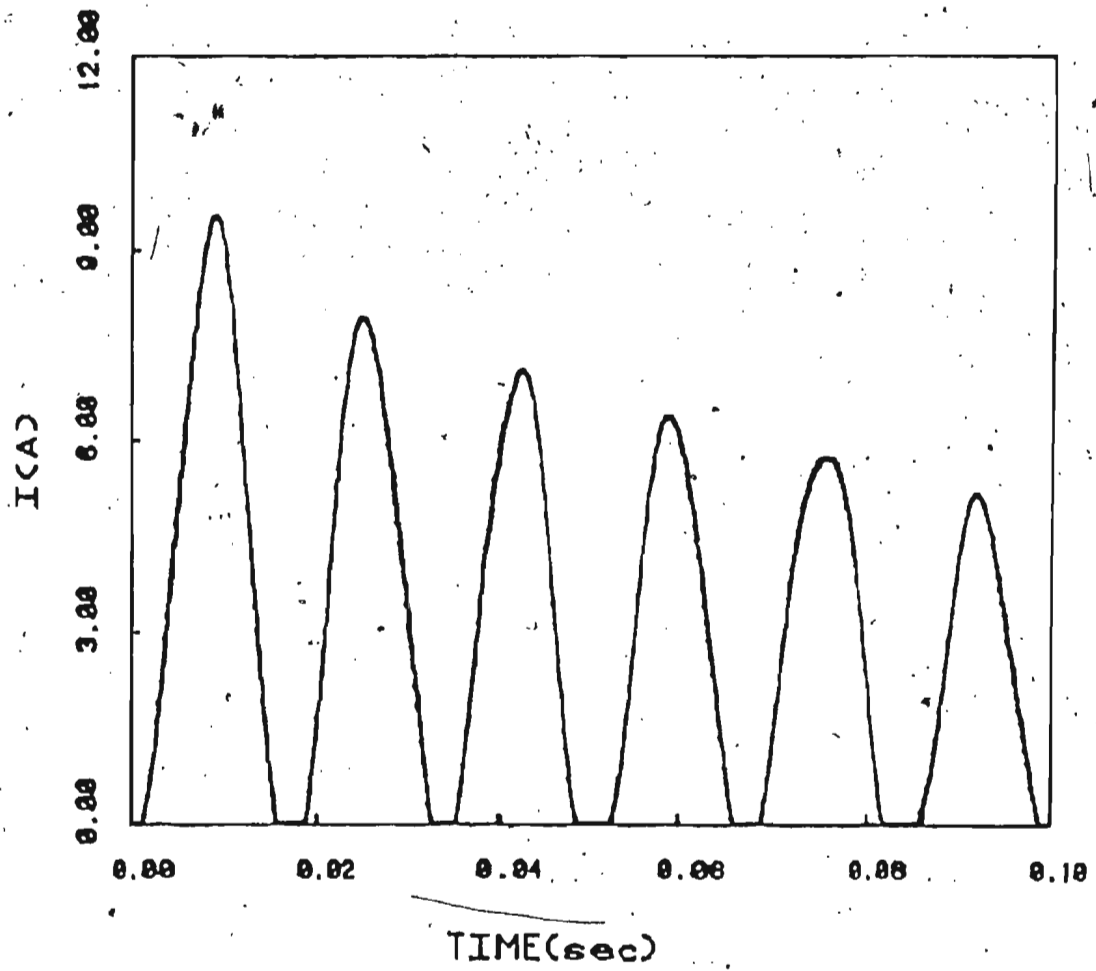


Fig. 3.35 (a) Simulation of phase-a inrush shown in Fig. 3.34(a).

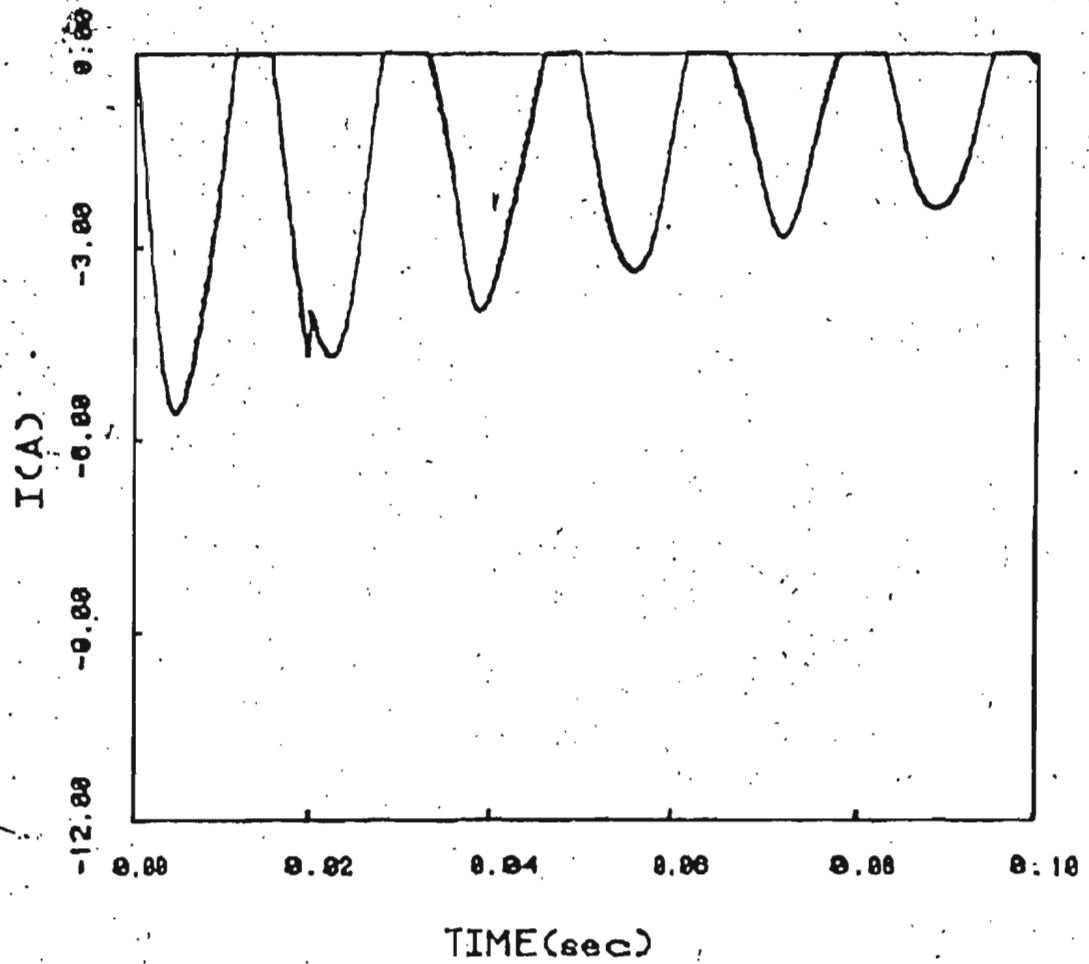


Fig. 3.35 (b) Simulation of phase-b inrush shown in Fig. 3.35 (b)

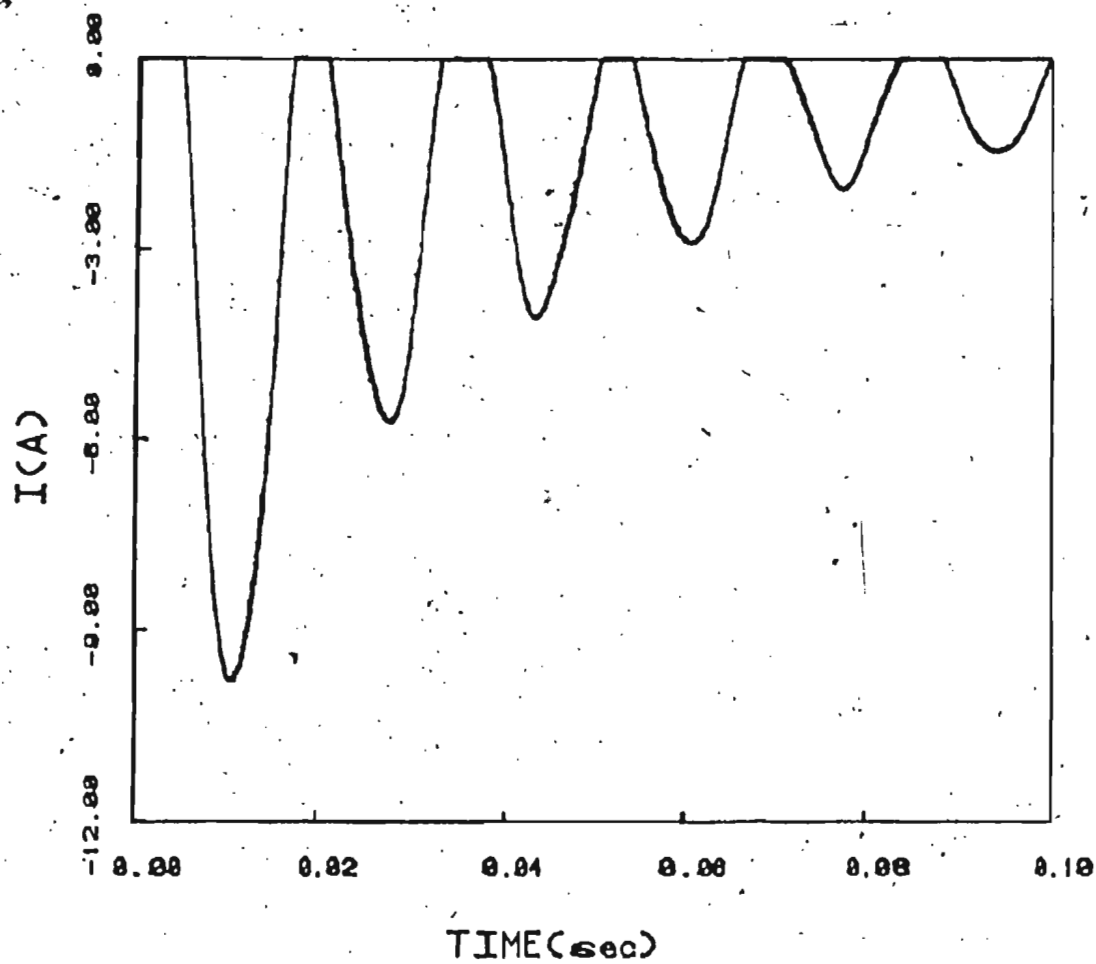


Fig. 3.35 (c) Simulation of phase-c inrush shown in Fig. 3.34 (c)

Table 3.1 Comparison of Measured and Simulated Positive  
Inrush Current Peaks In A Single-Phase Transformer

Current Peaks	$I_{m1}$ (A)	$I_{m2}$ (A)	$I_{m3}$ (A)	$I_{m4}$ (A)
Measured	24.60	14.62	9.98	7.84
Simulated	23.80	15.65	10.30	6.79



Table 3.2 Comparison of Peaks and Conduction Angles of Measured And Simulated Positive Inrush Currents in a Single-Phase Transformer

Current Peaks	$I_{m1}$ (A)	$I_{m2}$ (A)	$I_{m3}$ (A)	$I_{m4}$ (A)
Measured	19.22	9	4.2	2.61
Simulated	18.84	9.97	5.72	3.62

Conduction Angles	$\gamma_1$	$\gamma_2$	$\gamma_3$	$\gamma_4$
Measured	167.89°	160.04°	154.14°	148.25°
Simulated	172.77°	164°	155°	151°

Table 3.3 Comparison of Peaks and Conduction Angles of Measured and Simulated Negative Inrush Currents In A Single-Phase Transformer

Current Peaks	$I_{m1}$ (A)	$I_{m2}$ (A)	$I_{m3}$ (A)	$I_{m4}$ (A)
Measured	-19.56	-11.82	-8.15	-6.11
Simulated	-20.18	-12.79	-10.54	-7.71

Conduction Angles	$\gamma_1$	$\gamma_2$	$\gamma_3$	$\gamma_4$
Measured	147.33°	148.25°	137.37°	150.22°
Simulated	138.77°	151.78°	147.44°	157.11°

Table 3.4 Comparison of Harmonics in Measured and Simulated Inrush Waveforms in a Single-Phase Transformer

Harmonics (%)		Fund.	2nd	3rd	4th	5th
1st Cycle	Measured	100.00	74.42	39.15	16.30	4.37
	Simulated	100.00	58.01	16.31	6.11	7.74
2nd Cycle	Measured	100.00	71.49	39.91	17.02	5.11
	Simulated	100.00	54.58	12.00	7.77	6.29
3rd Cycle	Measured	100.00	70.09	38.08	17.76	5.84
	Simulated	100.00	56.21	14.00	7.06	7.02
4th Cycle	Measured	100.00	69.42	37.33	16.79	6.30
	Simulated	100.00	52.15	9.24	8.53	5.12

Table 3.5: A three-phase transformer parameters under different mode of connections

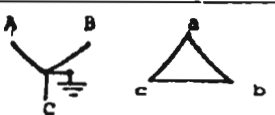
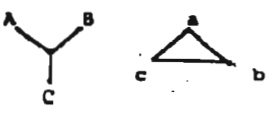

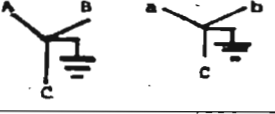
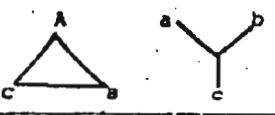
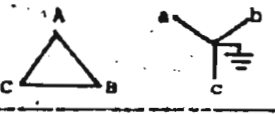
Mode of Connections (not according to vector group)	$X_{mA,B,C}$ =Core Reactance $X_{mAB,BC,CA}$ /Phase	$R_{mA,B,C}$ =Core Resistance $R_{mAB,BC,CA}$ /Phase	$X_{01A,B,C}$ =Equivalent Reactance referred $X_{01AB,BC,CA}$ to primary/phase	$R_{01A,B,C}$ =Equivalent Resistance referred $R_{01AB,BC,CD}$ to primary/phase
A 	$X_{mA}=533\Omega$	$R_{mA}=781\Omega$	$X_{01A}=2.128\Omega$	$R_{01A}=1.1$
	$X_{mB}=803\Omega$	$R_{mB}=3780\Omega$	$X_{01B}=2.243\Omega$	$R_{01B}=0.917\Omega$
	$X_{mC}=505\Omega$	$R_{mC}=3606\Omega$	$X_{01C}=2.36\Omega$	$R_{01C}=0.76\Omega$
B 	$X_{mA}=579\Omega$	$R_{mA}=853\Omega$	$X_{01A}=1.917\Omega$	$R_{01A}=1.376\Omega$
	$X_{mB}=840\Omega$	$R_{mB}=2200\Omega$	$X_{01B}=2.17\Omega$	$R_{01B}=1.11\Omega$
	$X_{mC}=481\Omega$	$R_{mC}=4846\Omega$	$X_{01C}=2.113\Omega$	$R_{01C}=0.857\Omega$
C 	$X_{mA}=578\Omega$	$R_{mA}=853\Omega$	$X_{01A}=2.122\Omega$	$R_{01A}=1.115\Omega$
	$X_{mB}=778\Omega$	$R_{mB}=2200\Omega$	$X_{01B}=2.332\Omega$	$R_{01B}=0.870\Omega$
	$X_{mC}=481\Omega$	$R_{mC}=4400\Omega$	$X_{01C}=2.17\Omega$	$R_{01C}=0.738\Omega$
D 	$X_{mA}=510\Omega$	$R_{mA}=755\Omega$	$X_{01A}=2.148\Omega$	$R_{01A}=1.11\Omega$
	$X_{mB}=860\Omega$	$R_{mB}=4661\Omega$	$X_{01B}=2.249\Omega$	$R_{01B}=0.9299$
	$X_{mC}=532\Omega$	$R_{mC}=3035\Omega$	$X_{01C}=2.1307$	$R_{01C}=0.7505\Omega$
E 	$X_{mAB}=512\Omega$	$R_{mAB}=672\Omega$	$X_{01AB}=4.6488\Omega$	$R_{01AB}=1.173\Omega$
	$X_{mBC}=676\Omega$	$R_{mBC}=2245\Omega$	$X_{01BC}=4.5417\Omega$	$R_{01BC}=0.9789\Omega$
	$X_{mCA}=424\Omega$	$R_{mCA}=10091\Omega$	$X_{01CA}=4.5385\Omega$	$R_{01CA}=0.7815\Omega$
F 	$X_{mAB}=540\Omega$	$R_{mAB}=682\Omega$	$X_{01AB}=4.7091\Omega$	$R_{01AB}=1.2056\Omega$
	$X_{mBC}=676\Omega$	$R_{mBC}=2240\Omega$	$X_{01BC}=4.5132\Omega$	$R_{01BC}=0.96607\Omega$
	$X_{mCA}=423\Omega$	$R_{mCA}=10082\Omega$	$X_{01CA}=4.5385\Omega$	$R_{01CA}=0.7815\Omega$

Table 3.6 Comparison of Measured and Simulated Inrush Current Peaks In All Three-Phases of a Y- $\Delta$  Transformer Energized From Y-side

Current Peaks		$I_{m1}$ (A)	$I_{m2}$ (A)	$I_{m3}$ (A)	$I_{m4}$ (A)
Measured	A	17.81	12.10	9.39	7.58
	B	5.70	4.79	4.37	3.68
	C	-14.26	-10.41	-8.32	-6.88
Simulated	A	19.83	12.58	9.11	7.39
	B	5.97	4.26	3.24	2.72
	C	-15.87	-11.12	-8.79	-7.60

Table 3.7 Comparison of Harmonics in Measured and Simulated Inrush Waveforms in all Three Phases of a Y- $\Delta$  Transformer Energized From Y-side.

Harmonics (%)		Fund	2nd	3rd	4th	5th
Measured	A	100.00	58.71	31.03	16.31	5.63
	B	100.00	89.92	47.37	19.96	11.09
	C	100.00	62.73	32.93	18.33	7.40
Simulated	A	100.00	18.28	7.49	0.37	2.74
	B	100.00	21.28	11.05	1.09	2.18
	C	100.00	32.24	4.81	5.60	2.73

Table 3.8 Comparison of Measured and Simulated Inrush Current Peaks In All Three Phases of A  $\Delta$ -Y Transformer Energized From  $\Delta$ -side

Current Peaks		$I_{m1}$ (A)	$I_{m2}$ (A)	$I_{m3}$ (A)	$I_{m4}$ (A)
Measured	A	11	8.56	7.13	6.06
	B	-5.81	-4.08	-3.21	-2.50
	C	-13.19	-4.1	-2.05	-1.34
Simulated	A	9.52	7.10	6.38	5.16
	B	-5.59	-4.71	-4.00	-3.38
	C	-9.80	-4.09	-2.91	-2.07

## CHAPTER 4

ALGORITHMS FOR TRANSFORMER PROTECTION4.1 Classification of Algorithms

As was stated in an earlier section, the algorithm to be used for transformer protection must have two basic characteristics, namely:

(1) they should be able to clearly distinguish between the magnetizing inrush and fault currents of a transformer.

(2) they should be simple enough so that computational burdens on the microcomputer is less and a fast detection of fault is achieved.

Three different algorithms are described here,

- (1) Discrete Fourier Transform
- (2) Rectangular Transform
- (3) Walsh Transform

All the above three algorithms distinguish between the magnetizing inrush and fault currents using the second harmonic restraint principle. Fourier coefficients generated in the Discrete Fourier Transform (D.F.T.) algorithm are utilized in the fault classification routine. Rectangular and Walsh Transform Algorithms generate the Rectangular and Walsh Coefficients respectively, from which ultimately, Fourier coefficients are extracted. These coefficients are



then used in the fault classification routine.

The algorithms are tested on simulated fault data of a laboratory transformer. Their performances are compared for both inrush and internal fault conditions. Discrete Fourier Transform is the basis of major protection algorithms and discussed here as reference. However, its high computational burden makes it incompetent for microprocessor applications without special arrangements. That is why, this algorithm is tested here on simulated data with a sampling rate of 16 samples/cycle to show its performance in comparison to the other two algorithms. The Rectangular and Walsh transform have been tested with sampling rates of both 16 and 8 samples/cycle.

#### 4.2 Discrete Fourier Transform Technique

Ramamoorthy [26] was one of the first authors to propose that the desired fundamental voltage or current can be extracted from the fault transients by correlating one cycle of data samples with the stored samples of reference fundamental sine and cosine waves.

##### Theory:

It is known that any continuous waveform  $g(t)$ , having a finite energy in the interval  $(0, T)$  can be expressed in this interval as a Fourier series,

$$g(t) = \frac{a_0}{2} + \sum_{K=1}^{\infty} (C_K \cos k\omega t + S_K \sin k\omega t) \quad (4.1)$$

where

$$\begin{aligned} \frac{a_0}{2} &= \frac{1}{T} \int_0^T g(t) dt \\ C_K &= \frac{2}{T} \int_0^T g(t) \cos k\omega t dt \\ S_K &= \frac{2}{T} \int_0^T g(t) \sin k\omega t dt \end{aligned} \quad (4.2)$$

Here  $\frac{a_0}{2}$  is the average value and  $C_K$  and  $S_K$  are the respective cosine and sine components of the Fourier coefficients. In a discrete mode, if the waveform is sampled at equispaced intervals of time  $t_j$ , spaced  $\Delta t$  apart, so that there are  $n=T/\Delta t$  samples, then the expression for  $C_K$  becomes,

$$\begin{aligned} C_K &= \frac{2}{T} \sum_{j=0}^{n-1} x(t_j) \cos \left( \frac{2\pi jk}{n} \right) \Delta t \\ &= \frac{2}{n} \sum_{j=0}^{n-1} x(t_j) \cos \left( \frac{2\pi jk}{n} \right) \end{aligned} \quad (4.3)$$

$j=0,1,2,\dots,n-1$

where  $x(t_j)$  are the discrete samples at the times  $t_j$ .

Similarly, the sine coefficients  $S_K$  are given by

$$S_K = \frac{2}{n} \sum_{j=0}^{n-1} x(t_j) \sin \left( \frac{2\pi jk}{n} \right) \quad (4.4)$$

$j=0,1,2,\dots,n-1$

For transformer protection,  $X(t_j)$  are current samples. For samples 1 to  $n$ , the coefficients will be extracted after correlation as

$$C_k = \frac{2}{n} \{x(1) \cos\left(\frac{2\pi \cdot 1 \cdot k}{n}\right) + x(2) \cos\left(\frac{2\pi \cdot 2 \cdot k}{n}\right) + \dots + x(n) \cos\left(\frac{2\pi \cdot n \cdot k}{n}\right)\}$$

and

$$S_k = \frac{2}{n} \{x(1) \sin\left(\frac{2\pi \cdot 1 \cdot k}{n}\right) + x(2) \sin\left(\frac{2\pi \cdot 2 \cdot k}{n}\right) + \dots + x(n) \sin\left(\frac{2\pi \cdot n \cdot k}{n}\right)\} \quad (4.5)$$

Hence, for a full cycle data window with 16 samples/cycle, 16

Fourier coefficients will be an array of dimension  $16 \times 1$ .

The system matrix is represented by Eqns. 4.6a and 4.6b.

$$\begin{array}{c}
 \begin{bmatrix} S_1 \\ S_2 \\ \vdots \\ S_{15} \\ S_{16} \end{bmatrix} = \frac{2}{16} \begin{bmatrix} \sin(\frac{2\pi \cdot 1 \cdot 1}{16}) & \sin(\frac{2\pi \cdot 2 \cdot 1}{16}) & \dots & \sin(\frac{2\pi \cdot 16 \cdot 1}{16}) \\ \sin(\frac{2\pi \cdot 1 \cdot 2}{16}) & \sin(\frac{2\pi \cdot 2 \cdot 2}{16}) & \dots & \sin(\frac{2\pi \cdot 16 \cdot 2}{16}) \\ \vdots & \vdots & \ddots & \vdots \\ \sin(\frac{2\pi \cdot 1 \cdot 15}{16}) & \sin(\frac{2\pi \cdot 2 \cdot 15}{16}) & \dots & \sin(\frac{2\pi \cdot 16 \cdot 15}{16}) \\ \sin(\frac{2\pi \cdot 1 \cdot 16}{16}) & \sin(\frac{2\pi \cdot 2 \cdot 16}{16}) & \dots & \sin(\frac{2\pi \cdot 16 \cdot 16}{16}) \end{bmatrix} \begin{bmatrix} x(1) \\ x(2) \\ \vdots \\ x(15) \\ x(16) \end{bmatrix}
 \end{array}$$

16x1                                  16x16                                  16x1

(4.6 a)

and

$$\begin{array}{c}
 \begin{bmatrix} C_1 \\ C_2 \\ \vdots \\ C_{15} \\ C_{16} \end{bmatrix} = \frac{2}{16} \begin{bmatrix} \cos(\frac{2\pi \cdot 1 \cdot 1}{16}) & \cos(\frac{2\pi \cdot 2 \cdot 1}{16}) & \dots & \cos(\frac{2\pi \cdot 16 \cdot 1}{16}) \\ \cos(\frac{2\pi \cdot 1 \cdot 2}{16}) & \cos(\frac{2\pi \cdot 2 \cdot 2}{16}) & \dots & \cos(\frac{2\pi \cdot 16 \cdot 2}{16}) \\ \vdots & \vdots & \ddots & \vdots \\ \cos(\frac{2\pi \cdot 1 \cdot 15}{16}) & \cos(\frac{2\pi \cdot 2 \cdot 15}{16}) & \dots & \cos(\frac{2\pi \cdot 16 \cdot 15}{16}) \\ \cos(\frac{2\pi \cdot 1 \cdot 16}{16}) & \cos(\frac{2\pi \cdot 2 \cdot 16}{16}) & \dots & \cos(\frac{2\pi \cdot 16 \cdot 16}{16}) \end{bmatrix} \begin{bmatrix} x(1) \\ x(2) \\ \vdots \\ x(15) \\ x(16) \end{bmatrix}
 \end{array}$$

16x1                                  16x16                                  16x1

(4.6 b)

The closed matrix form of Eqn. (4.6) enables one to utilize it in the fault classification routine. The constants of sine and cosine matrix are stored in the memory and the sequency bandlimited fault signal is correlated with corresponding sine and cosine coefficients. The coefficients  $S_k$  and  $C_k$  thus generated will give an amplitude value of

$$F_k = \sqrt{(S_k^2 + C_k^2)} \quad (4.7)$$

where

$F_k$  = Fourier coefficients,  $k = 1, 2, \dots, n$ .

According to Eqn. (4.7),  $F_1$  and  $F_2$  represents the Fourier Coefficients of Fundamental and 2nd harmonic components of the waveform respectively. In the case of magnetizing inrush, the value of  $F_2$  is usually higher than the value of  $F_1$  for a fault. A weighting factor is needed to multiply with  $F_2$ , so that  $F_2$  remains always higher than  $F_1$  in case of inrush.  $F_2$  will always be lower in case of a fault. A weighting factor of the order 4 is found suitable. This value is not a fixed one and depends on the transformer equivalent circuit parameters. Again this also depends on the number of samples/cycle as well as the window size. If the value of this constant is increased, the algorithm used will provide good restraining feature during inrush but the operating time during internal fault may be affected. So, the value of this constant is to be chosen, based on the data

both for the inrush as well as internal fault for any particular transformer.

The nature of a transformer internal fault current is usually an undamped sinusoid. Fault current data were simulated on the basis of a current expression [24] is given by:

$$i(t) = A \sin(\omega t + \lambda - \phi) - B e^{-Ct} \sin(\lambda - \phi - D) \quad (4.7a)$$

where

$$\phi = \tan^{-1} \frac{X}{R}$$

and

$$\lambda = \text{switching angle}$$

A, B, C, D are constants which depend upon the transformer parameters and the type of fault.

The current based on Eqn. 4.7 can be considered as the C.T. secondary output of the post fault current by choosing the appropriate values of the constants.

#### Results:

A recursive programming is carried out so that the algorithm reads equally-spaced data from data-file to select 16 samples/cycle and calculate the fundamental and 2nd harmonic components from the inrush or fault data. A trip or no-trip decision is initiated by the relay from the generated Fourier coefficients. A flow-chart of the programming for computing above is shown in Fig. 4.1. The flow-chart will be

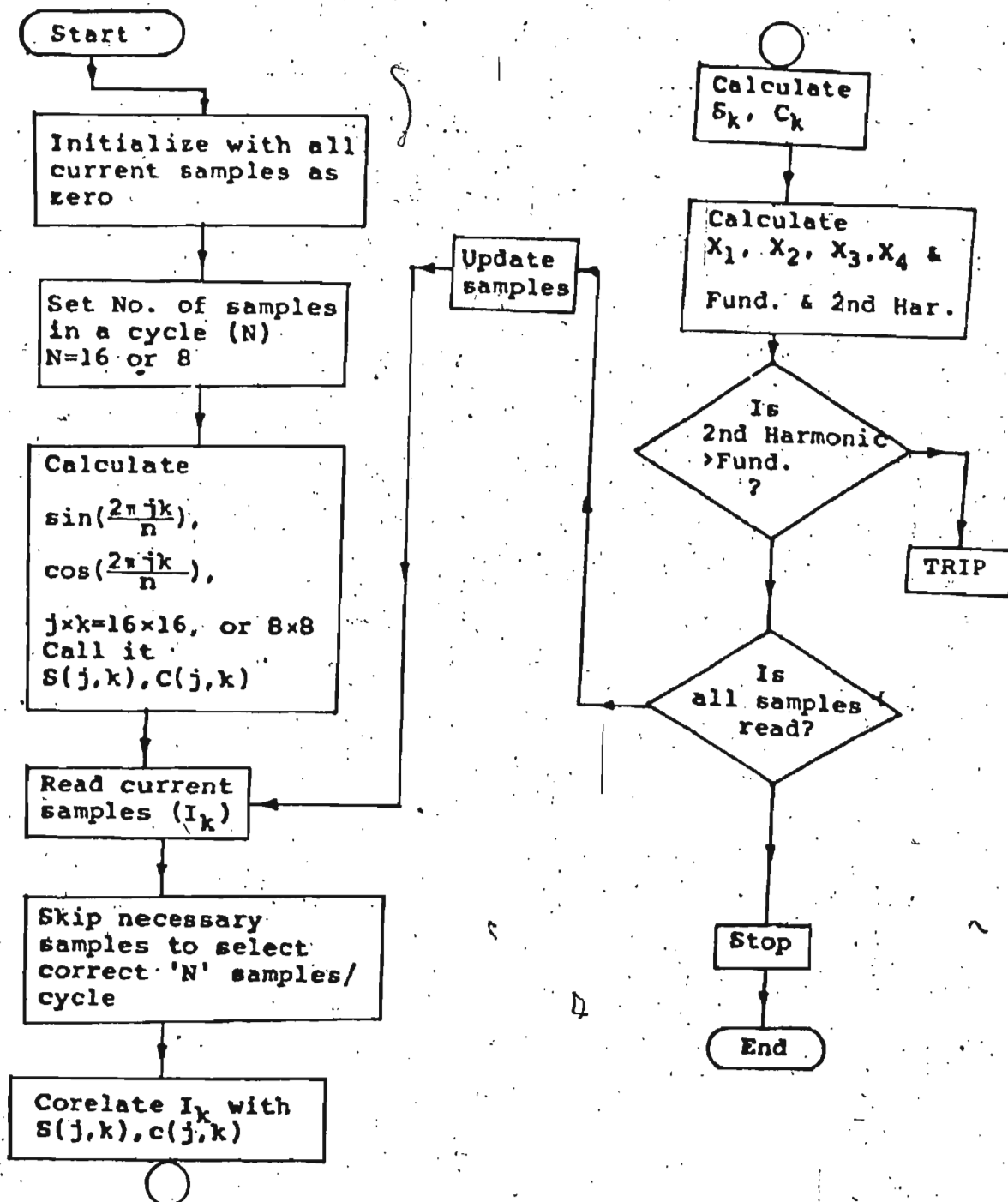


Fig. 4.1 Flow chart of programming logic of digital differential relay by Discrete Fourier algorithm

slightly different in a real-time processor relay. It is shown in Fig. 4.1 that the program stops after computing from a finite data file and there is no trip command. The transform performance is being computed from the programming. The data-train is continuous once the transformer is switched on, unless an internal fault causes the relay to trip. The right hand column vector of Eqn. (4.6) is the continuous data train and the relay continuously monitors the system, irrespective of fault or steady state condition. A threshold limit is also to be chosen in actual practice to distinguish the faulty system with its steady state condition, as  $F_2$  will be less than  $F_1$  in both steady state and internal fault conditions.

The performance characteristic of the transform with 16 samples/cycle is shown through Fig. 4.2 to Fig. 4.4. Figs. 4.2(a) - 4.2(c) show the comparison of the restraining property of the algorithm with operating quantity during magnetizing inrush in the three phases of a Y/ $\Delta$  transformer energized from the Y-side. The simulation of the magnetizing inrush is done for  $\lambda=0^\circ$  switching of A-phase. The following data are used for Phase-A and Phase-C.

$$R_{01A} = 1.3760 \, \Omega \quad \theta_{sA} = 81.2^\circ$$

$$R_{01C} = 0.857 \, \Omega \quad \theta_{sC} = 78.3^\circ$$

The B-phase inrush is due to the "helping effect" of A and C phases. The figures show that the algorithm develops enough restraining force to block the relay from operation due to



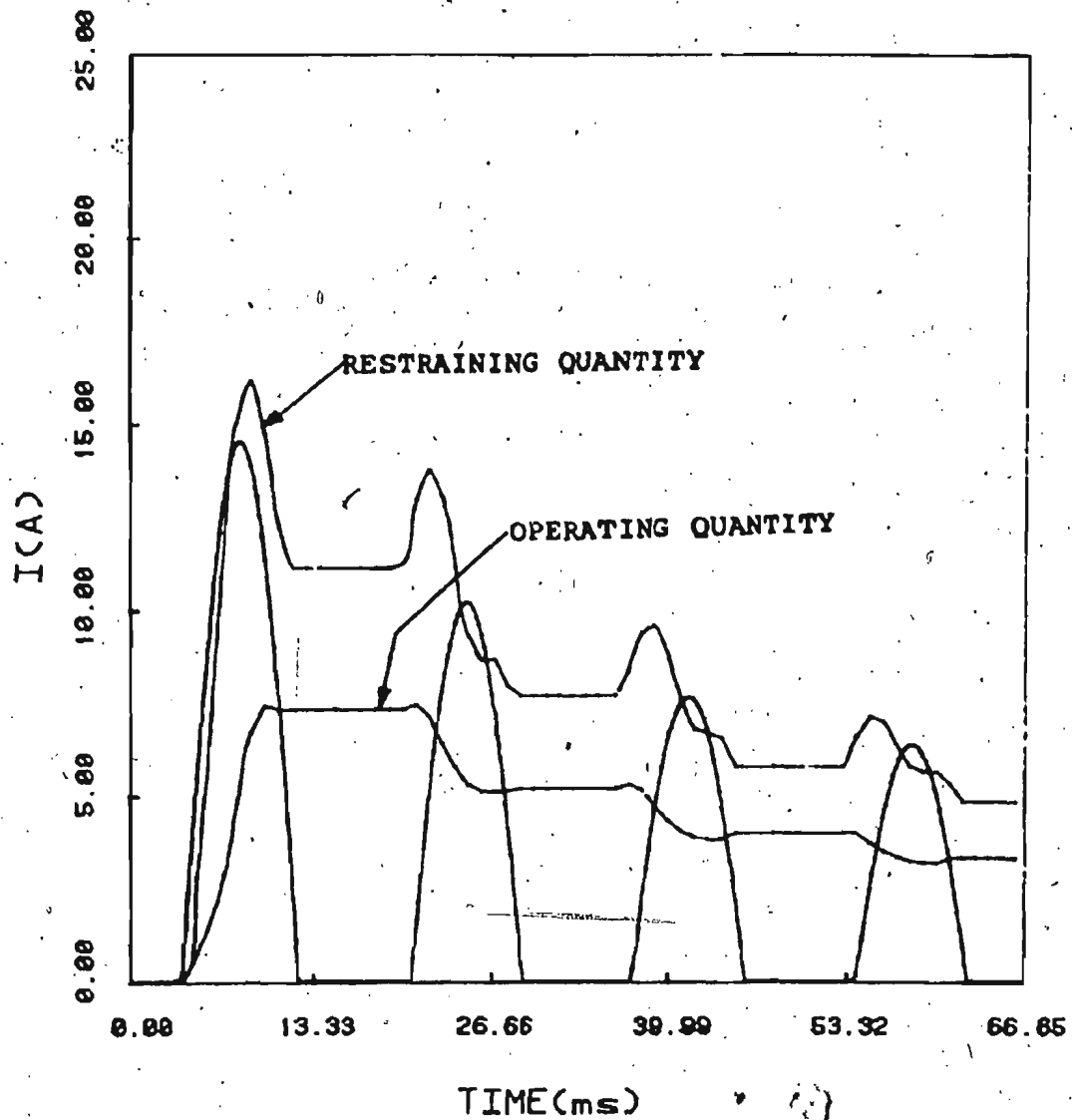


Fig. 4.2 (a) Performance of Discrete Fourier algorithm with 16 samples/cycle during inrush in phase-a of a Y-Δ transformer

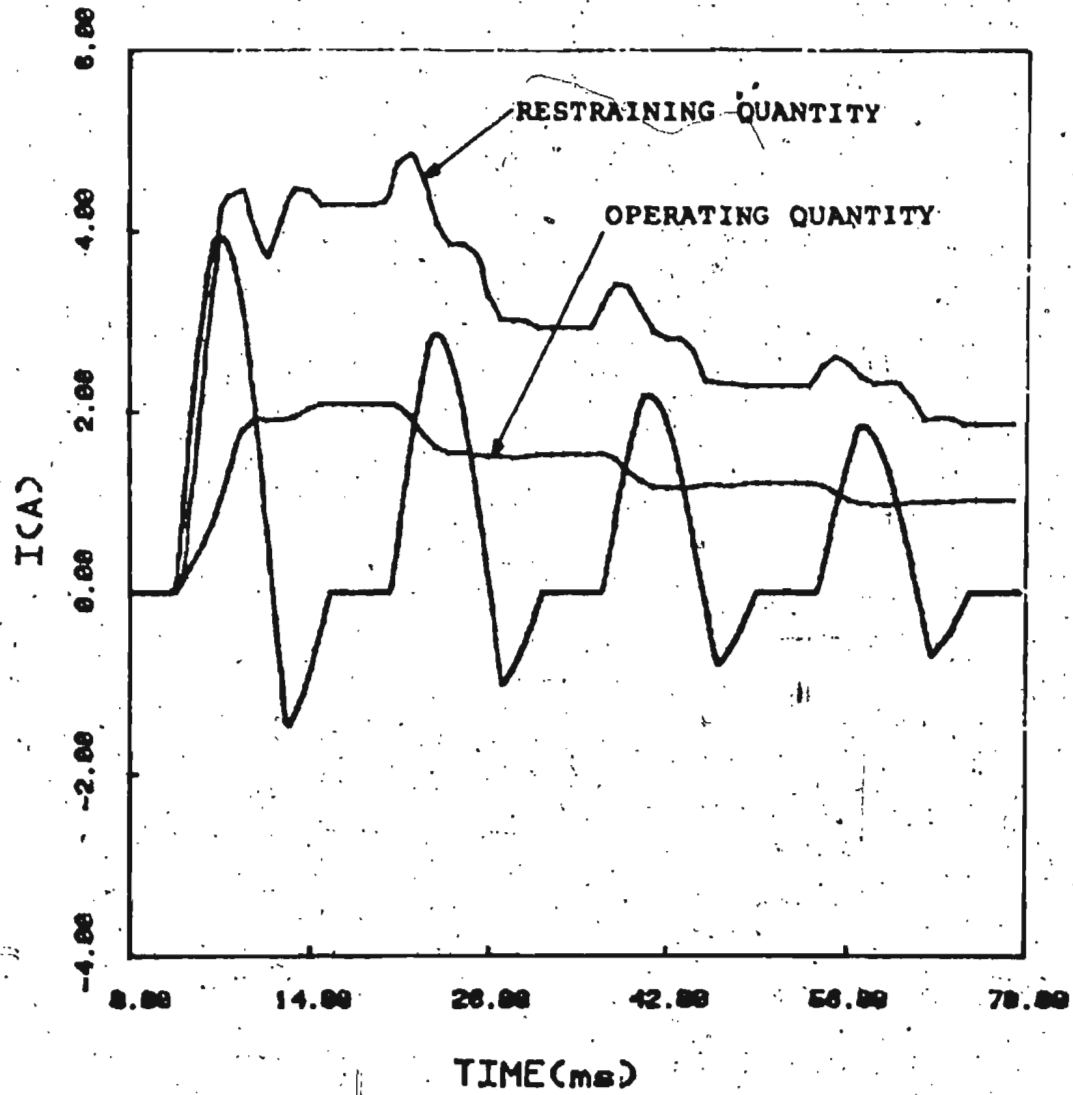


Fig. 4.2 (b) Performance of Discrete Fourier algorithm with 16 samples/cycle inrush in phase-b of a Y-Δ transformer

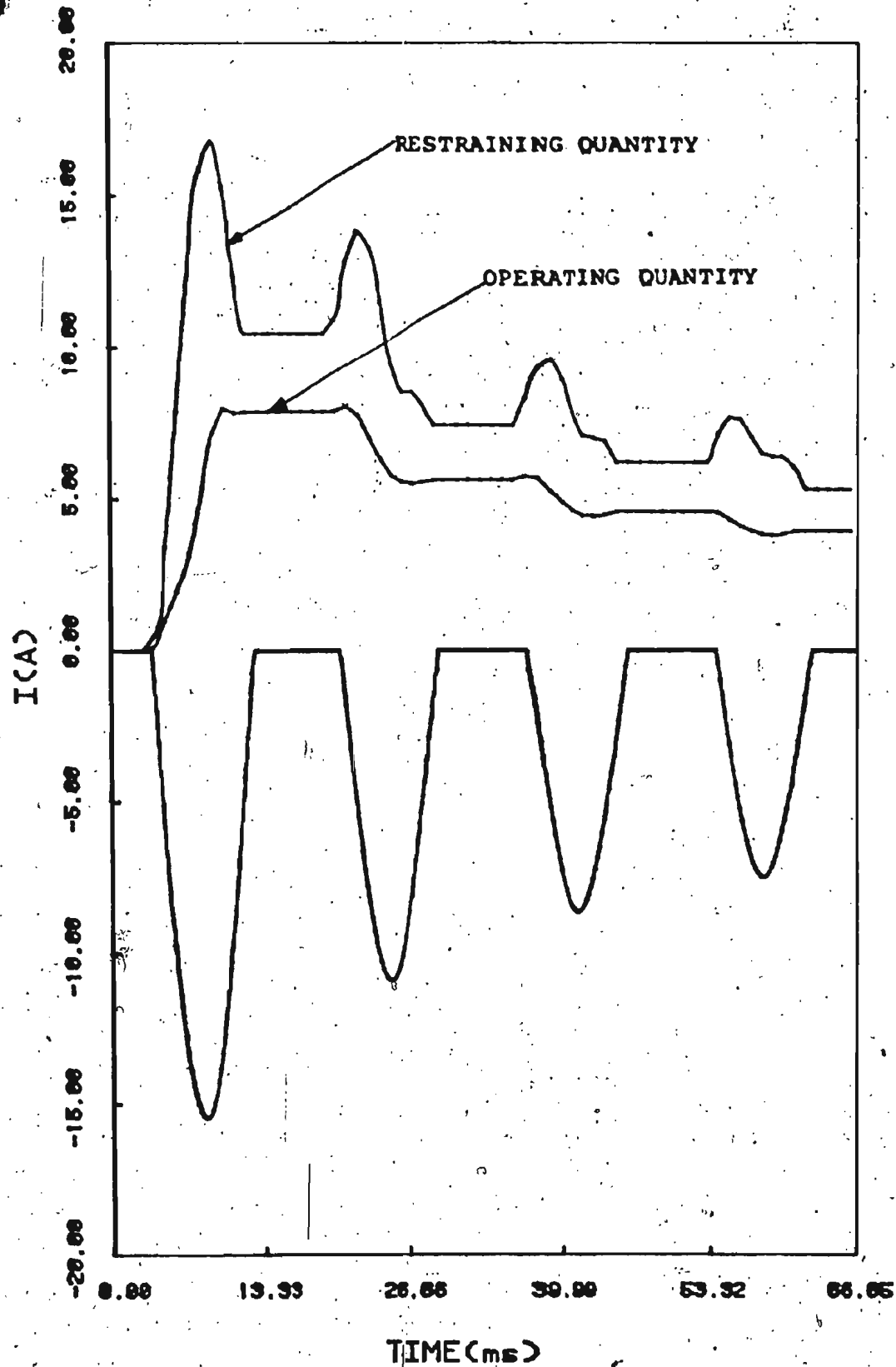


Fig. 4.2 (c) Performance of Discrete Fourier algorithm with 16 samples/cycle during inrush in phase-c of a Y- $\Delta$  transformer

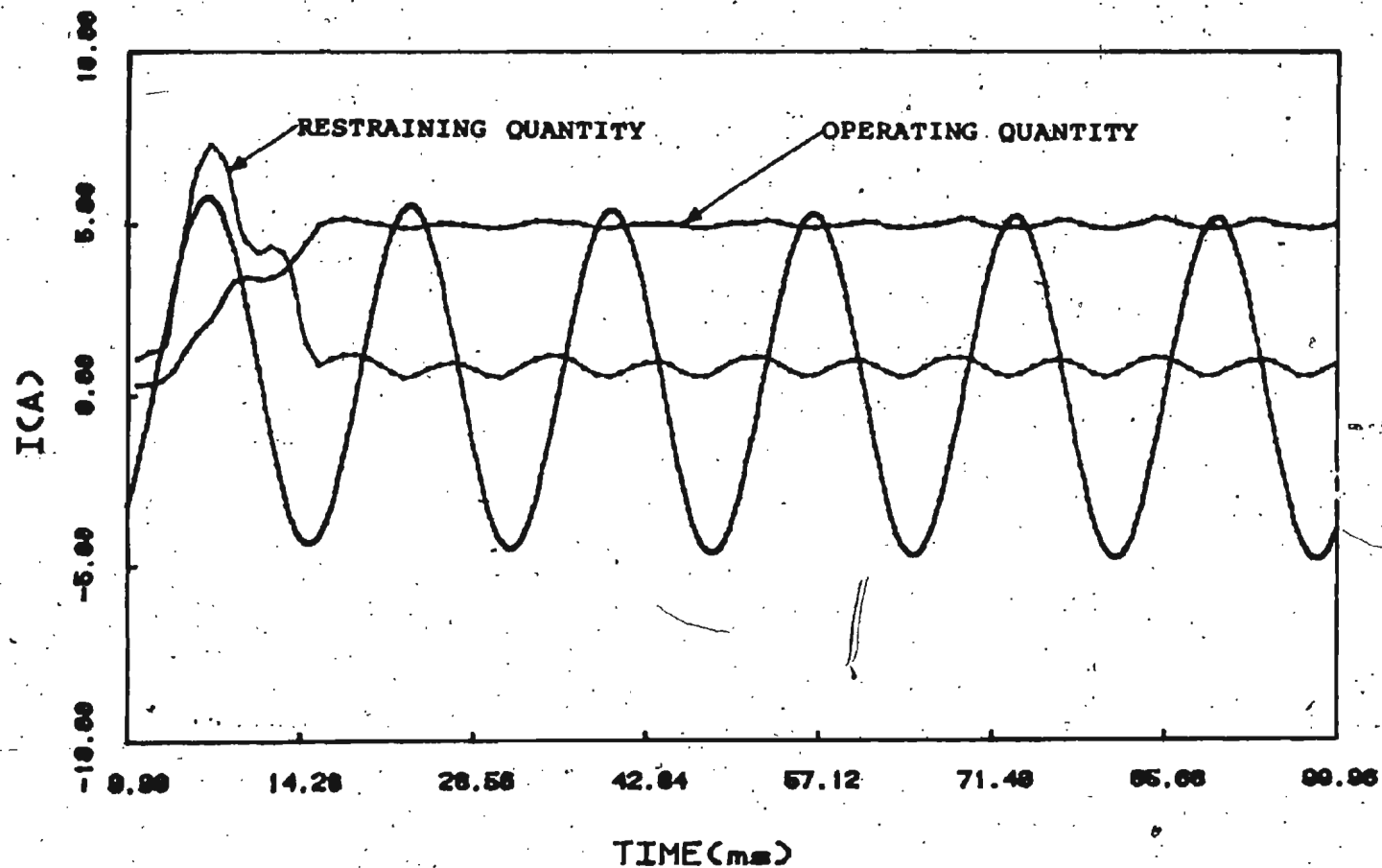


Fig. 4.3 (a) Performance of Discrete Fourier algorithm with 16 samples/cycle during an internal fault (fault initiation angle -  $0^\circ$ )

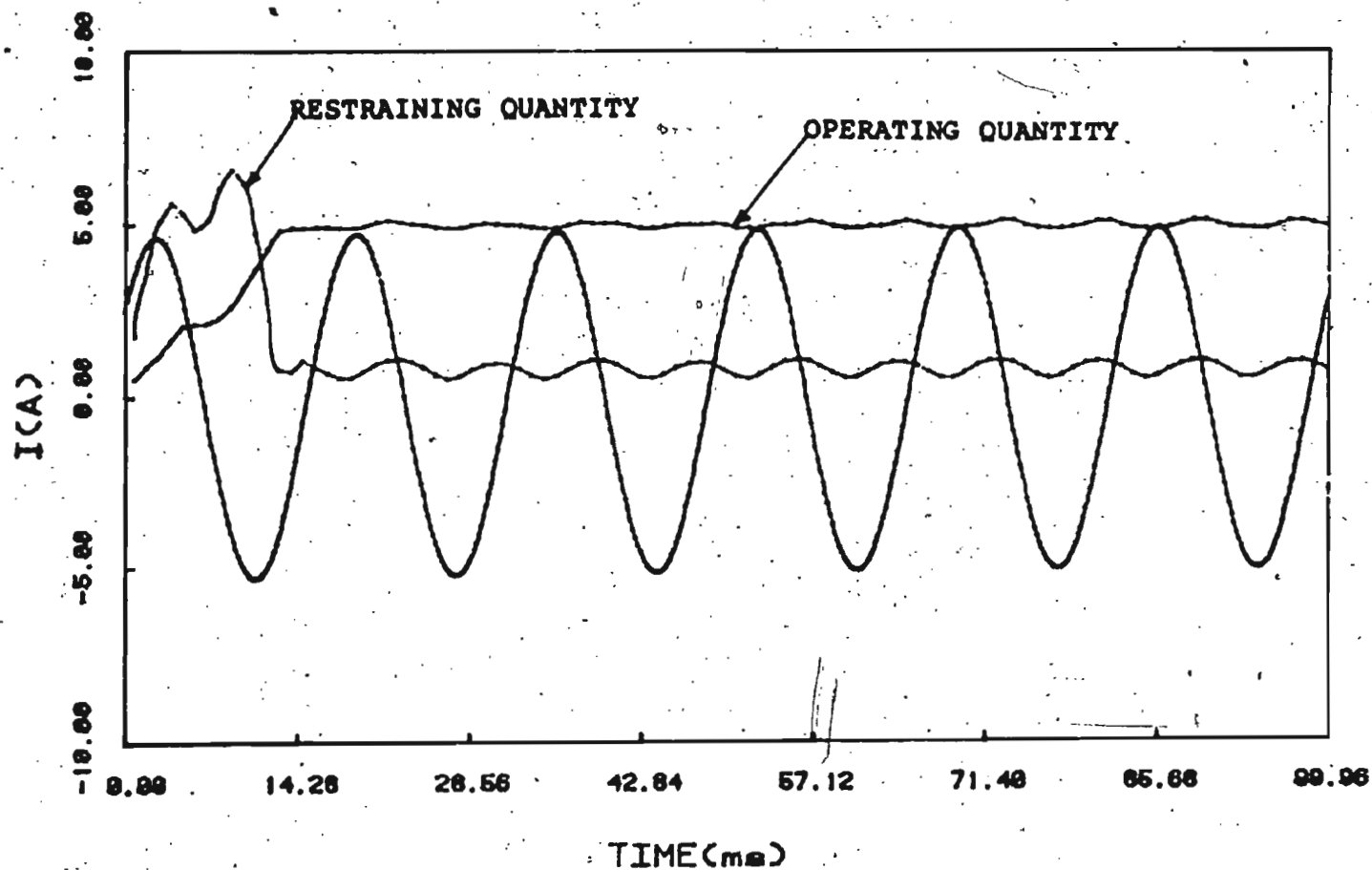


Fig. 4.3 (b) Performance of Discrete Fourier algorithm with 16 samples/cycle during an internal fault (fault initiation angle -  $90^\circ$ )

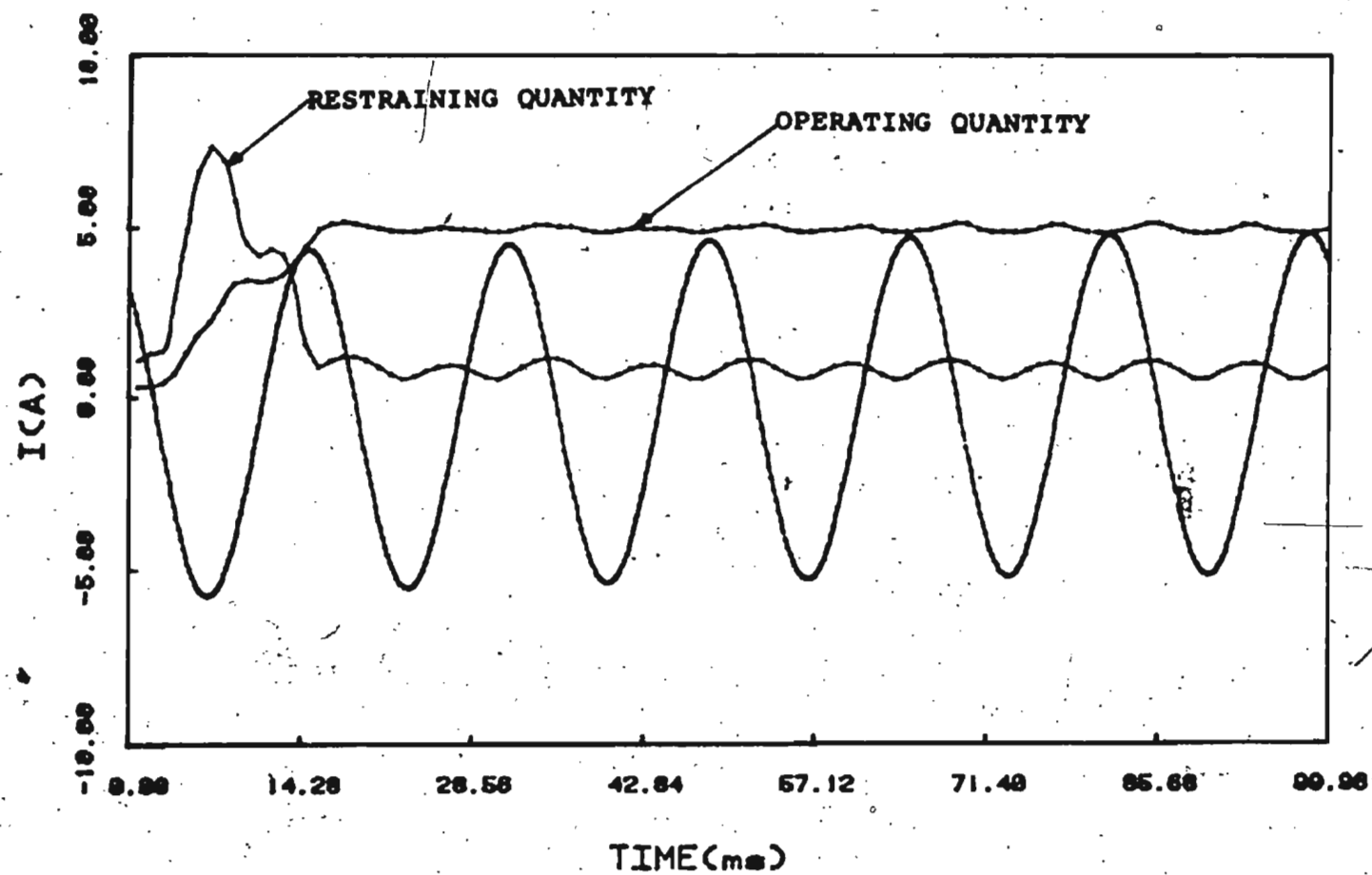


Fig. 4.3 (c) Performance of Discrete Fourier algorithm with 16 samples/cycle during an internal fault (fault initiation angle -  $180^\circ$ )

inrush in all the three phases.

The transform is applied to the case of an internal fault at all the possible angles of inception of fault at current waveform from  $0^\circ$  to  $180^\circ$  at a step of  $30^\circ$  intervals.

The convergence time of the transform varies from 11.8 msec to 13.8 msec depending on the angle of the current waveform where the fault is initiated. The time is minimum if the fault occurs at  $90^\circ$  of the current waveform. Figs. 4.3(a), (b) and (c) show the performance of the algorithm during an internal fault at fault initiation angle of  $0^\circ$ ,  $90^\circ$  and  $180^\circ$  respectively. The transform converges at 13.8, 11.8 and 13.8 msec respectively. For a three phase fault, the transform convergence in three phases will be different because of the  $120^\circ$  phase shift between phases. But whichever phase the transform converges earlier, the tripping will be initiated.

An asymmetrical fault current is considered in Fig. 4.4 where it is assumed that the fault initiation angle is  $0^\circ$ . The performance of the algorithm is shown in the same figure where, it is seen that the transform converges in 8.8 msec.

In all cases, the performance of the algorithm is less than a cycle in case of an internal fault and the maximum time of convergence is a little over  $3/4$ th of a cycle.

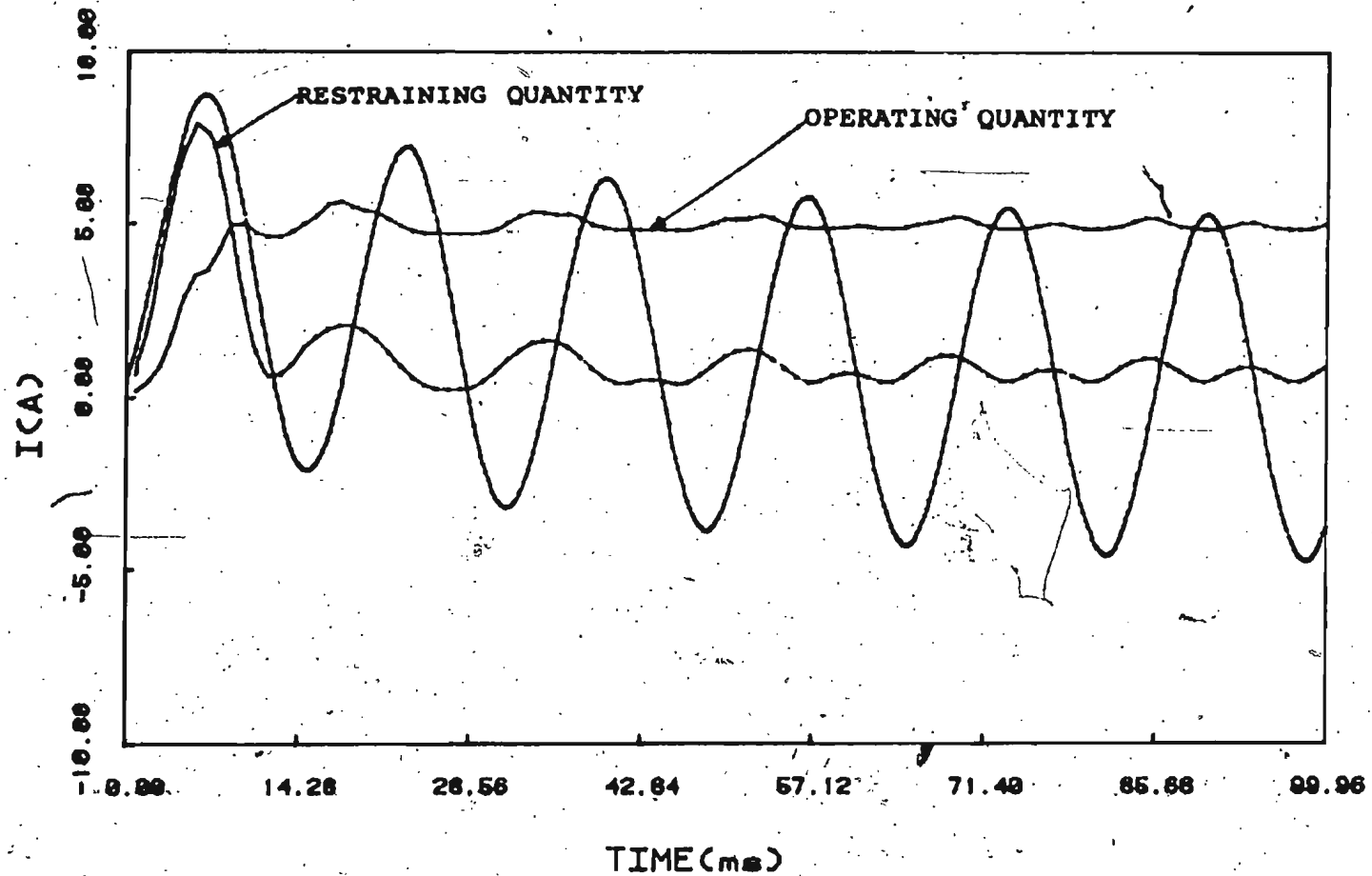


Fig. 4.4 Performance of Discrete Fourier algorithm with 16 samples/ cycle during an assymetrical internal fault (fault initiation angle  $-0^\circ$ )



### 4.3 Rectangular Transform Technique

In this method, the sinusoidal waveforms used in the Fourier Technique described in the previous section are replaced by equivalent rectangular waveforms. The fact that these periodic rectangular waveforms can be directly expressed as Fourier Series can then be used to relate the coefficient of the Fourier series of a block of data to the coefficients obtained from the rectangular wave transforms. It turns out that the column matrix defining the coefficients generated by replacing sinusoidal functions with the rectangular waves, can be equated to a sparse infinite matrix multiplied by a vector containing the true Fourier coefficients. Although, this equation contains infinite matrices, the Fourier coefficients are negligible at high frequency, and it is permissible to truncate the equations to a finite set. The infinite matrix equation can be inverted in a closed form [25] and the true Fourier coefficients can be extracted.

#### Theory

Let the terms  $S_k$  and  $C_k$  of Eqn. 4.4 and 4.3 be denoted as  $S_k^*$  and  $C_k^*$  and the rectangular coefficients will be denoted as  $S_k$  and  $C_k$ . If the sine and cosine terms in Eqns. 4.4 and 4.3 are replaced with the equivalent rectangular functions [12],

$$\begin{aligned} \sin \gamma t(x) &= \operatorname{sgn}(\sin x) \\ \cos \gamma t(x) &= \operatorname{sgn}(\cos x) \end{aligned} \quad (4.8)$$

where,

$$\begin{aligned} \operatorname{sgn}(y) &= y/|y|, \text{ for } y \neq 0, \\ &= 0 \quad \text{for } y=0 \end{aligned} \quad (4.9)$$

Then the corresponding rectangular transform coefficients,  $S_k$  and  $C_k$  are defined as

$$S_k = S(\omega_k) = \sum_{j=0}^{n-1} X(t_j) \operatorname{sgn} \sin\left(\frac{2\pi jk}{n}\right) \quad (4.10)$$

$$C_k = C(\omega_k) = \sum_{j=0}^{n-1} X(t_j) \operatorname{sgn} \cos\left(\frac{2\pi jk}{n}\right) \quad (4.11)$$

For a band limited signal  $X(t_j)$ , these rectangular coefficients are related to the Fourier sine and cosine coefficients as,  $S = [A]S^*$

$$(4.12) \quad C = [B]C^*$$

where,

$$S = [S_k]^T, \quad C = [C_k]^T \quad (4.13)$$

$T$  = transpose of a quantity

$[A]$  and  $[B]$  are infinite sparse matrices. The elements of  $[A]$  and  $[B]$  are formed by the following Fourier series expansion of  $\sin \gamma t(x)$  and  $\cos \gamma t(x)$ :

$$\begin{aligned} [A] = [A_{ij}] &= \frac{4}{\pi} [\delta\{(2m-1), j/i\} i/j] \\ &\quad \text{for } (i, j > 0) \\ &= \delta(i, j) \text{ for } (i=0, \text{ or } j=0) \end{aligned} \quad (4.14)$$

and

$$[B] = [B_{ij}] = \frac{4}{\pi} [(-1)^{m+1} \delta\{(2m-1), j/i\} i/j]$$

for  $(i, j > 0)$

$$= \delta(i, j) \text{ for } (i \neq 0 \text{ or } j = 0) \quad (4.15)$$

where  $m$  is any positive integer,  $\delta(i, j)$  is the Kronecker delta, such that  $\delta(i, j) = 1$ , if  $i = j$  and  $\delta(i, j) = 0$ , if  $i \neq j$ . The matrices  $A$  and  $B$  are of the form,

$$[A] = \frac{4}{\pi} \begin{bmatrix} 1 & 0 & \frac{1}{3} & 0 & \frac{1}{5} & 0 & \frac{1}{7} & 0 & \frac{1}{9} & 0 & \frac{1}{11} \\ 0 & 1 & 0 & 0 & 0 & \frac{1}{3} & 0 & 0 & 0 & \frac{1}{5} & 0 \\ 0 & 0 & 1 & 0 & 0 & 0 & 0 & 0 & \frac{1}{3} & 0 & 0 \\ 0 & 0 & 0 & 1 & 0 & 0 & 0 & 0 & 0 & 0 & 0 \\ 0 & 0 & 0 & 0 & 1 & 0 & 0 & 0 & 0 & 0 & 0 \\ 0 & 0 & 0 & 0 & 0 & 1 & 0 & 0 & 0 & 0 & 0 \\ 0 & 0 & 0 & 0 & 0 & 0 & 1 & 0 & 0 & 0 & 0 \\ 0 & 0 & 0 & 0 & 0 & 0 & 0 & 1 & 0 & 0 & 0 \\ 0 & 0 & 0 & 0 & 0 & 0 & 0 & 0 & 1 & 0 & 0 \\ 0 & 0 & 0 & 0 & 0 & 0 & 0 & 0 & 0 & 1 & 0 \\ 0 & 0 & 0 & 0 & 0 & 0 & 0 & 0 & 0 & 0 & 1 \end{bmatrix}$$

(4.16)

$$[B] = \frac{4}{\pi}$$

$$\begin{bmatrix} 1 & 0 & -\frac{1}{3} & 0 & \frac{2}{5} & 0 & -\frac{1}{7} & 0 & \frac{1}{9} & 0 & -\frac{1}{11} \\ 0 & 1 & 0 & 0 & 0 & -\frac{1}{3} & 0 & 0 & 0 & \frac{1}{5} & 0 \\ 0 & 0 & 1 & 0 & 0 & 0 & 0 & 0 & -\frac{1}{3} & 0 & 0 \\ 0 & 0 & 0 & 1 & 0 & 0 & 0 & 0 & 0 & 0 & 0 \\ 0 & 0 & 0 & 0 & 1 & 0 & 0 & 0 & 0 & 0 & 0 \\ 0 & 0 & 0 & 0 & 0 & 1 & 0 & 0 & 0 & 0 & 0 \\ 0 & 0 & 0 & 0 & 0 & 0 & 1 & 0 & 0 & 0 & 0 \\ 0 & 0 & 0 & 0 & 0 & 0 & 0 & 1 & 0 & 0 & 0 \\ 0 & 0 & 0 & 0 & 0 & 0 & 0 & 0 & 1 & 0 & 0 \\ 0 & 0 & 0 & 0 & 0 & 0 & 0 & 0 & 0 & 1 & 0 \\ 0 & 0 & 0 & 0 & 0 & 0 & 0 & 0 & 0 & 0 & 1 \end{bmatrix}$$

(4.17)

Both the matrices above are sparse matrices. In the absence of aliasing, the inverse of these matrices can be readily obtained as,

$$\begin{aligned} [A]^{-1} &= [A_{ij} \mu(j/i)] \text{ for } i, j > 0 \\ &= \delta(i, j) \text{ for } i=0, \text{ or } j=0 \end{aligned} \quad (4.18)$$

$$\begin{aligned} [B]^{-1} &= [B_{ij} (j/i)] \text{ for } i, j > 0 \\ &= \delta(i, j) \text{ for } i=0, \text{ or } j=0 \end{aligned} \quad (4.19)$$

where  $\mu(\tau)$  is the Moebius function, and  $\tau$  is any positive integer. The matrices  $[A]^{-1}$  and  $[B]^{-1}$  are given by,

$$[A]^{-1} = \frac{\pi}{4}$$

$$\begin{bmatrix} 1 & 0 & -\frac{1}{3} & 0 & \frac{1}{5} & 0 & -\frac{1}{7} & 0 & \frac{1}{9} & 0 & -\frac{1}{11} \\ 0 & 1 & 0 & 0 & 0 & -\frac{1}{3} & 0 & 0 & 0 & \frac{1}{5} & 0 \\ 0 & 0 & 1 & 0 & 0 & 0 & 0 & 0 & -\frac{1}{3} & 0 & 0 \\ 0 & 0 & 0 & 1 & 0 & 0 & 0 & 0 & 0 & 0 & 0 \\ 0 & 0 & 0 & 0 & 1 & 0 & 0 & 0 & 0 & 0 & 0 \\ 0 & 0 & 0 & 0 & 0 & 1 & 0 & 0 & 0 & 0 & 0 \\ 0 & 0 & 0 & 0 & 0 & 0 & 1 & 0 & 0 & 0 & 0 \\ 0 & 0 & 0 & 0 & 0 & 0 & 0 & 1 & 0 & 0 & 0 \\ 0 & 0 & 0 & 0 & 0 & 0 & 0 & 0 & 1 & 0 & 0 \\ 0 & 0 & 0 & 0 & 0 & 0 & 0 & 0 & 0 & 1 & 0 \\ 0 & 0 & 0 & 0 & 0 & 0 & 0 & 0 & 0 & 0 & 1 \end{bmatrix}$$

(4.20)

$$[B]^{-1} = \frac{\pi}{4}$$

$$\begin{bmatrix} 1 & 0 & \frac{1}{3} & 0 & \frac{1}{5} & 0 & \frac{1}{7} & 0 & \frac{1}{9} & 0 & \frac{1}{11} \\ 0 & 1 & 0 & 0 & 0 & \frac{1}{3} & 0 & 0 & 0 & \frac{1}{5} & 0 \\ 0 & 0 & 1 & 0 & 0 & 0 & 0 & 0 & \frac{1}{3} & 0 & 0 \\ 0 & 0 & 0 & 1 & 0 & 0 & 0 & 0 & 0 & 0 & 0 \\ 0 & 0 & 0 & 0 & 1 & 0 & 0 & 0 & 0 & 0 & 0 \\ 0 & 0 & 0 & 0 & 0 & 1 & 0 & 0 & 0 & 0 & 0 \\ 0 & 0 & 0 & 0 & 0 & 0 & 1 & 0 & 0 & 0 & 0 \\ 0 & 0 & 0 & 0 & 0 & 0 & 0 & 1 & 0 & 0 & 0 \\ 0 & 0 & 0 & 0 & 0 & 0 & 0 & 0 & 1 & 0 & 0 \\ 0 & 0 & 0 & 0 & 0 & 0 & 0 & 0 & 0 & 1 & 0 \\ 0 & 0 & 0 & 0 & 0 & 0 & 0 & 0 & 0 & 0 & 1 \end{bmatrix}$$

(4.21)

Again, both  $[A]^{-1}$  and  $[B]^{-1}$  are sparse matrices. Using these inverses, the Fourier coefficients can readily be calculated from the rectangular coefficients as

$$\hat{s}_k = [A]^{-1}[s_k] \quad (4.22)$$

$$\hat{c}_k = [B]^{-1}[c_k]$$

The above principle of Rectangular transform can be applied to a differential protection of transformers. For a sampling rate of 16 samples/cycle, the actual system matrix is as follows,

$$\begin{bmatrix} S_1 \\ S_2 \\ S_3 \\ \vdots \\ S_{15} \\ S_{16} \end{bmatrix} = \frac{2}{16} \begin{bmatrix} S_{1,1} & S_{1,2} & S_{1,3} & \cdots & S_{1,15} & S_{1,16} \\ S_{2,1} & S_{2,2} & S_{2,3} & \cdots & S_{2,15} & S_{2,16} \\ S_{3,1} & S_{3,2} & S_{3,3} & \cdots & S_{3,15} & S_{3,16} \\ \vdots & \vdots & \vdots & \ddots & \vdots & \vdots \\ S_{15,1} & S_{15,2} & S_{15,3} & \cdots & S_{15,15} & S_{15,16} \\ S_{16,1} & S_{16,2} & S_{16,3} & \cdots & S_{16,16} & S_{16,16} \end{bmatrix} \begin{bmatrix} x(1) \\ x(2) \\ x(3) \\ \vdots \\ x(15) \\ x(16) \end{bmatrix}$$

16x1

16x16

16x1

... (4.23)

Similarly,

$$\begin{array}{c}
 \begin{array}{|c|} \hline C_1 \\ \hline C_2 \\ \hline C_3 \\ \hline \vdots \\ \hline C_{15} \\ \hline C_{16} \\ \hline \end{array}
 \begin{array}{|c|} \hline \frac{2}{16} \\ \hline \end{array}
 \begin{array}{|c|} \hline C_{1,1} \quad C_{1,2} \quad C_{1,3} \quad \dots \quad C_{1,15} \quad C_{1,16} \\ \hline C_{2,1} \quad C_{2,2} \quad C_{2,3} \quad \dots \quad C_{2,15} \quad C_{2,16} \\ \hline C_{3,1} \quad C_{3,2} \quad C_{3,3} \quad \dots \quad C_{3,15} \quad C_{3,16} \\ \hline \vdots \\ \hline C_{15,1} \quad C_{15,2} \quad C_{15,3} \quad \dots \quad C_{15,15} \quad C_{15,16} \\ \hline C_{16,1} \quad C_{16,2} \quad C_{16,3} \quad \dots \quad C_{16,15} \quad C_{16,16} \\ \hline \end{array}
 \begin{array}{|c|} \hline x(1) \\ \hline x(2) \\ \hline x(3) \\ \hline \vdots \\ \hline x(15) \\ \hline x(16) \\ \hline \end{array}
 \end{array}
 \begin{array}{l}
 16 \times 1 \qquad \qquad \qquad 16 \times 16 \qquad \qquad \qquad 16 \times 1 \\
 \dots (4.24)
 \end{array}$$

In Eqn. (4.23) and (4.24) above, the  $S_k$  and  $C_k$  are the rectangular coefficients which correspond to the sine and cosine terms of the Fourier coefficients respectively.  $S_{k,k}$  and  $C_{k,k}$  are the elements of the rectangular matrices and are defined as,

$$\begin{aligned}
 S_{k,k} &= \text{sgn} [\sin (\beta_{k,k})] \\
 C_{k,k} &= \text{sgn} [\cos (\beta_{k,k})]
 \end{aligned}
 \quad (4.25)$$

where,

$$\beta_{k,k} = \frac{2 \pi j k}{n}$$

The right hand column matrix  $[x]$  contains the differential current samples which are correlated with the matrix elements  $S_{k,k}$  and  $C_{k,k}$  to form rectangular coefficients. For a sampling rate of 8 samples/cycle, the dimension of the

matrices is given by

$$[S_k] = [C_k] = 8 \times 1, [S_{k,k}] = 8 \times 8, [X_k] = 8 \times 1 \quad (4.26)$$

The Fourier coefficients can be obtained using the matrix relationship of Eqn. 4.20 and 4.21 as,

$$\begin{aligned} S_1^* &= S_1 - \frac{1}{3} S_3 - \frac{1}{5} S_5 \\ C_1^* &= C_1 + \frac{1}{3} S_3 - \frac{1}{5} S_5 \\ S_2^* &= S_2 \\ C_2^* &= C_2 \end{aligned} \quad (4.27)$$

The fundamental and second harmonic components are found to be,

$$\begin{aligned} F_1 &= \sqrt{(S_1^*)^2 + (C_1^*)^2} \\ F_2 &= \sqrt{(S_2^*)^2 + (C_2^*)^2} \end{aligned} \quad (4.28)$$

### Results

A recursive programming is carried out to compute the Fourier coefficients from the Rectangular coefficients using the Rectangular Transform algorithm. The flow-chart of the programming is shown in Fig. 4.5. The flow chart is quite similar to that of Discrete Fourier Transform shown in Fig. 4.1 except that the necessary constants of the matrices  $[A]^{-1}$  and  $[B]^{-1}$  is stored and the respective sine and cosine terms of the Fourier series are replaced with +1 and -1 depending on whether the values are positive or negative.



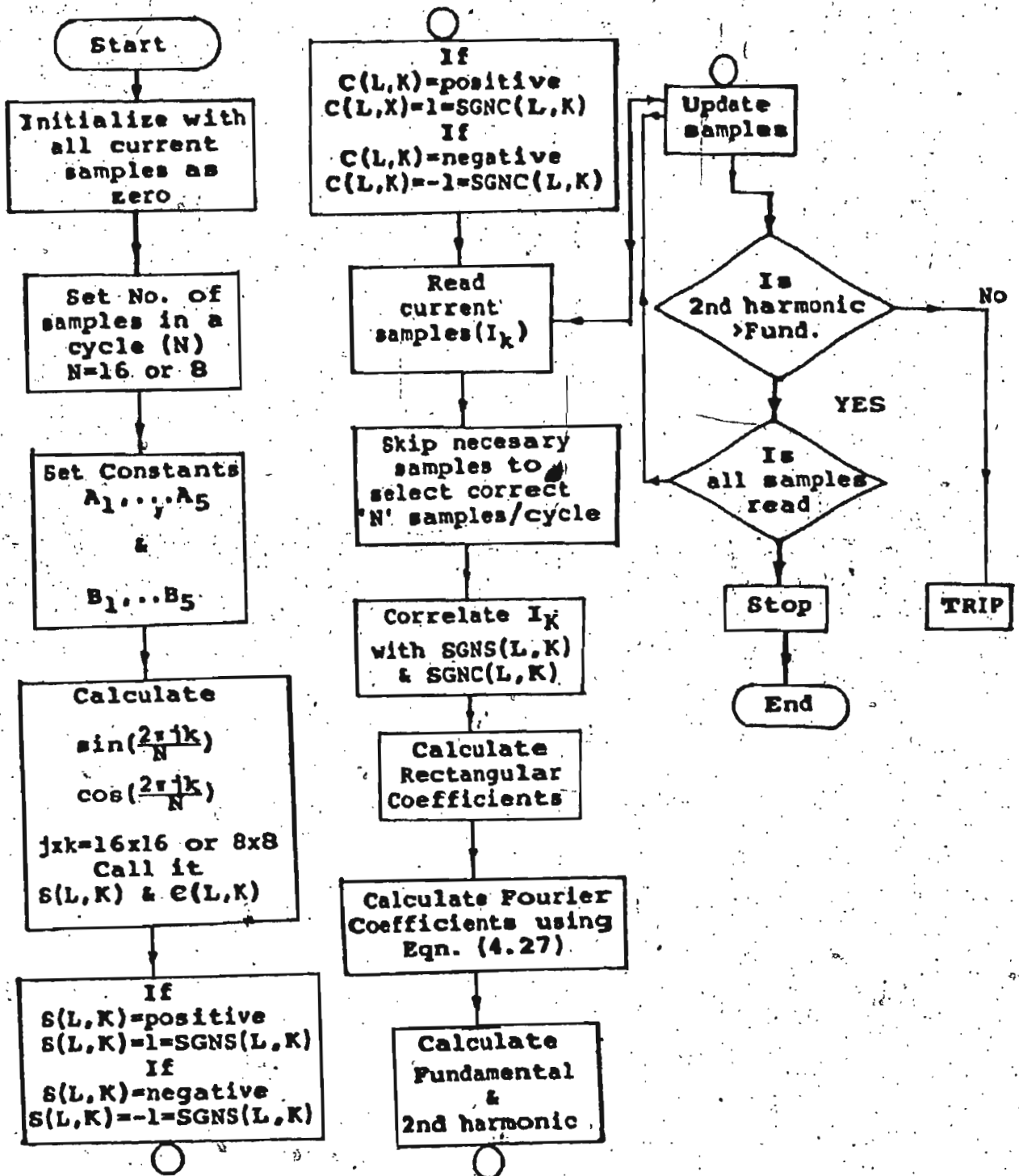


Fig. 4.5 Flow chart of programming logic of digital differential relay by Rectangular Transform

Zeros of the Fourier matrix are considered as zeros here again. Instead of correlating the samples with respective sine and cosine terms, they are correlated with +1, -1 and 0 here.

The algorithm is tested on the same sets of simulated magnetizing inrush data first, with a sampling rate of 16 samples/cycle. Figs. 4.6(a), (b) and (c) show the performance of the algorithm on the inrush for phases A, B and C respectively. It is observed that the restraint during inrush is quite adequate such that the relay remains in the blocking zone. Figs. 4.7(a), (b) and (c) show the performance of the algorithm during an internal fault at fault initiation angles of  $0^\circ$ ,  $90^\circ$  and  $180^\circ$  respectively. Similar cases were treated in the case of Discrete Fourier Transform algorithm, so that the performance of Rectangular Transform technique can be compared to that of D.F.T. Performance under similar conditions. It is seen that the rectangular transform converges to 12.8, 10.8 and 12.8 msec, if the fault is initiated at  $0^\circ$ ,  $90^\circ$  and  $180^\circ$  respectively. The inherent gain in the time convergence for the rectangular Transform is 1 msec over that required for the Discrete Fourier Transform under similar conditions. This is in addition to the simplicity of the Rectangular Transform as far as digital computation in a microprocessor is concerned.

An asymmetrical fault is also treated to find out

the performance of the algorithm like Fourier Transform. This is shown in Fig. 4.8, where it is observed that the transform converges at 8.8 msec which is the same with Fourier Transform shown in Fig. 4.4 earlier.

The algorithm is tried on the same sets of simulated data but with a sampling rate of 8 samples/cycle. Figs. 4.9(a), (b) and (c) show the performance of the algorithm during an inrush. It is observed that the restraint is quite adequate to block the relay during inrush.

During the second cycle, the restraining characteristic suddenly drops down, so that, the difference between the restraining and the operating quantity is less in comparison to those when tested with 16 samples/cycle. But the characteristic becomes stabilized in subsequent cycles if compared with Figs. 4.6(a), (b) and (c).

Figs. 4.10(a), (b) and (c) show the performance of the rectangular transform under the internal fault conditions. These performances are similar to those of Figs. 4.7(a), (b) and (c). Convergence times of the transform are 13.8, 11.8 and 13.8 msec for fault initiation angles of  $0^\circ$ ,  $90^\circ$  and  $180^\circ$  respectively. Fig. 4.11 shows the performance of the algorithm on an asymmetrical fault. The time of convergence is 9.8 msec.

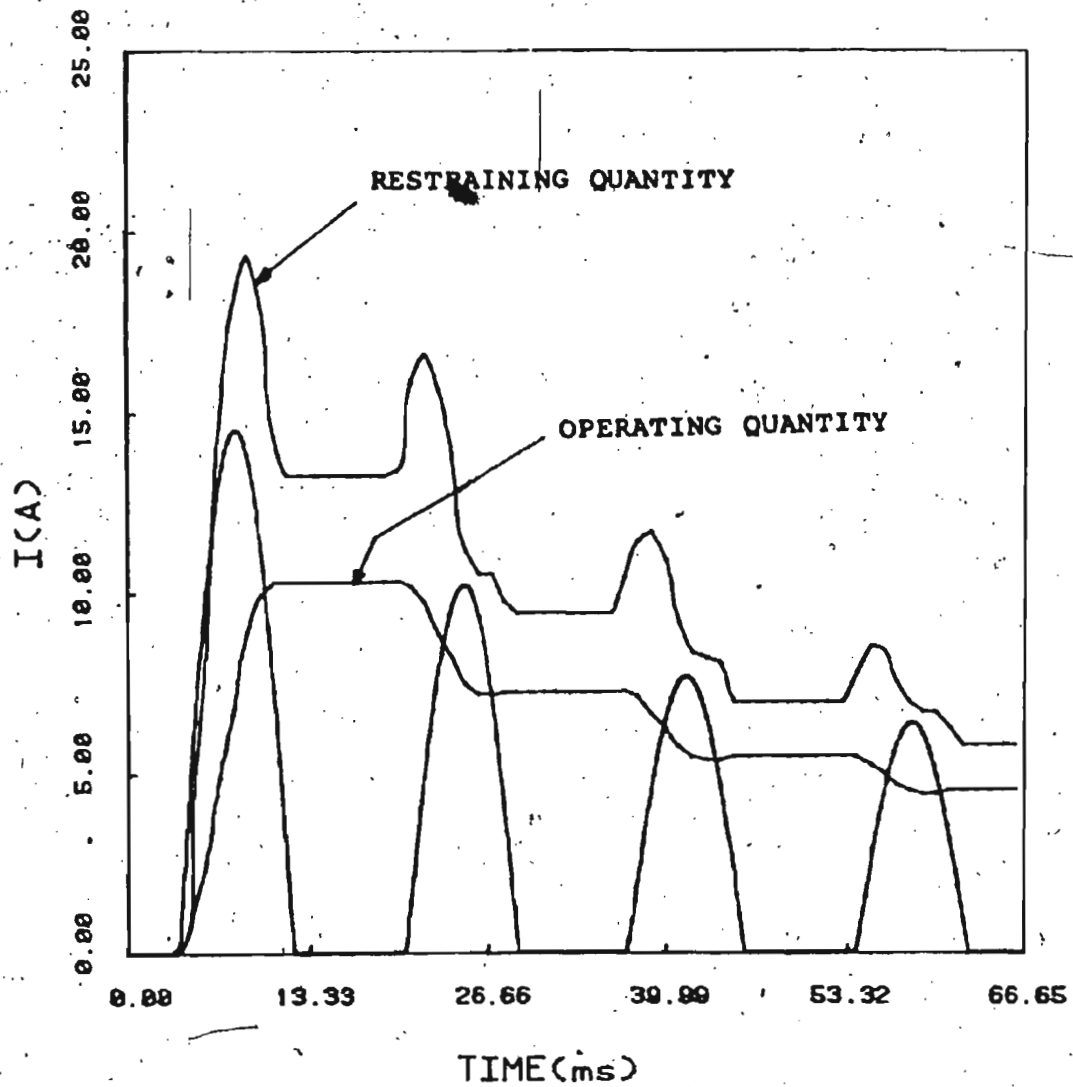


Fig. 4.6 (a) Performance of Rectangular Transform algorithm with 16 samples/cycle during inrush in phase-a of a Y-Δ transformer

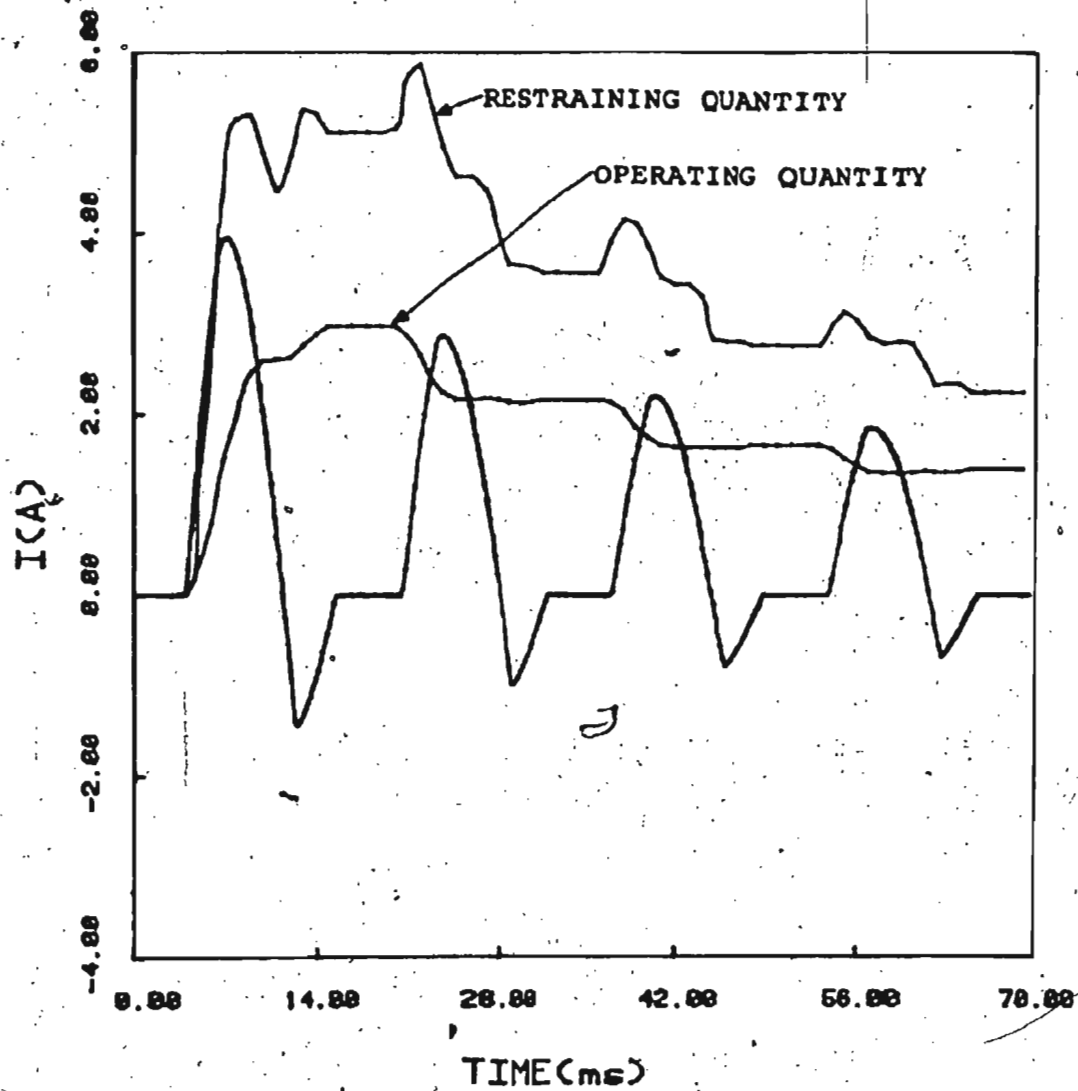


Fig. 4.6 (b) Performance of Rectangular Transform algorithm with 16 samples/cycle in phase-b of a Y- $\Delta$  transformer

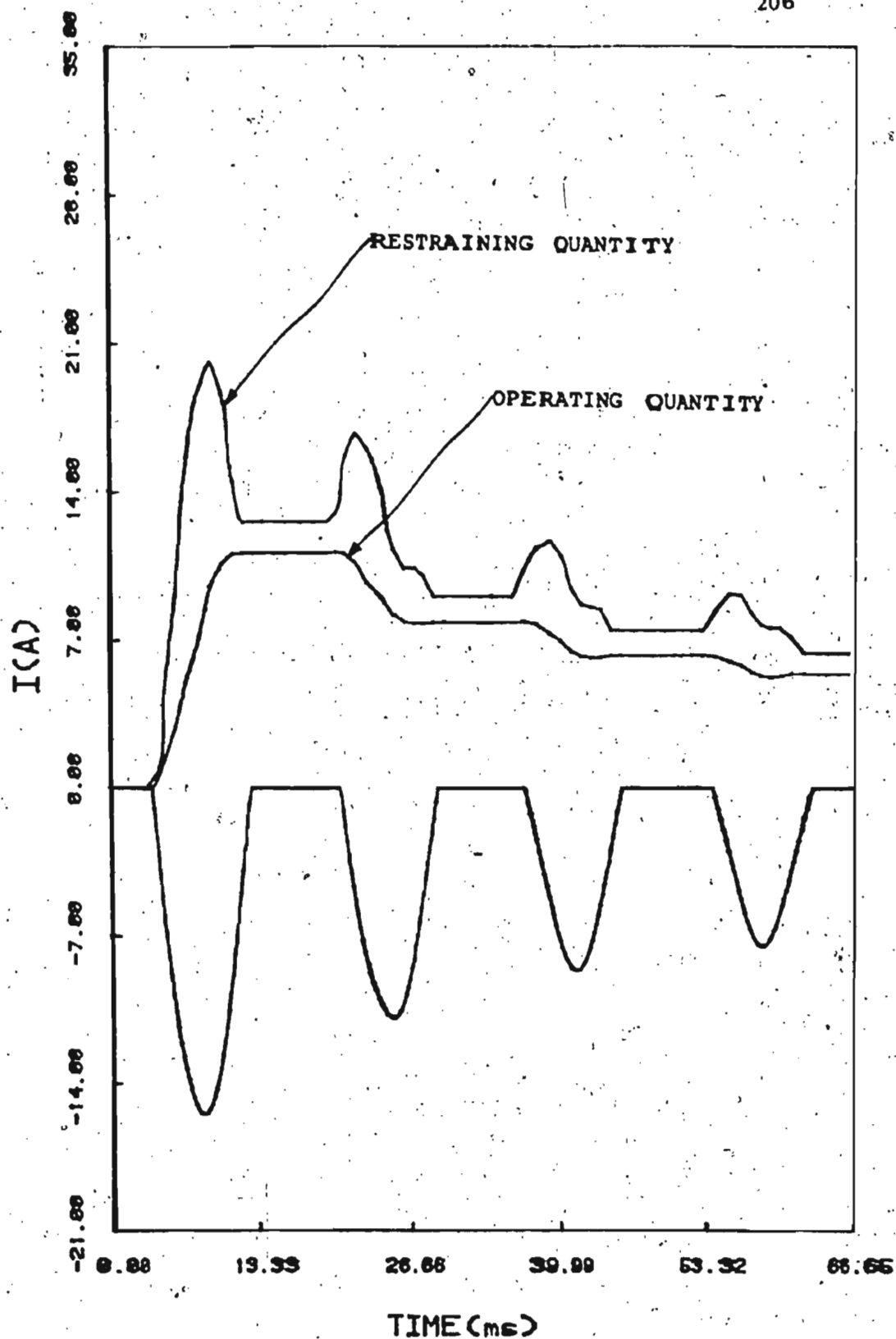


Fig. 4.6 (c) Performance of Rectangular Transform algorithm with 16 Samples/cycle inrush in phase-c of a Y-Δ transformer

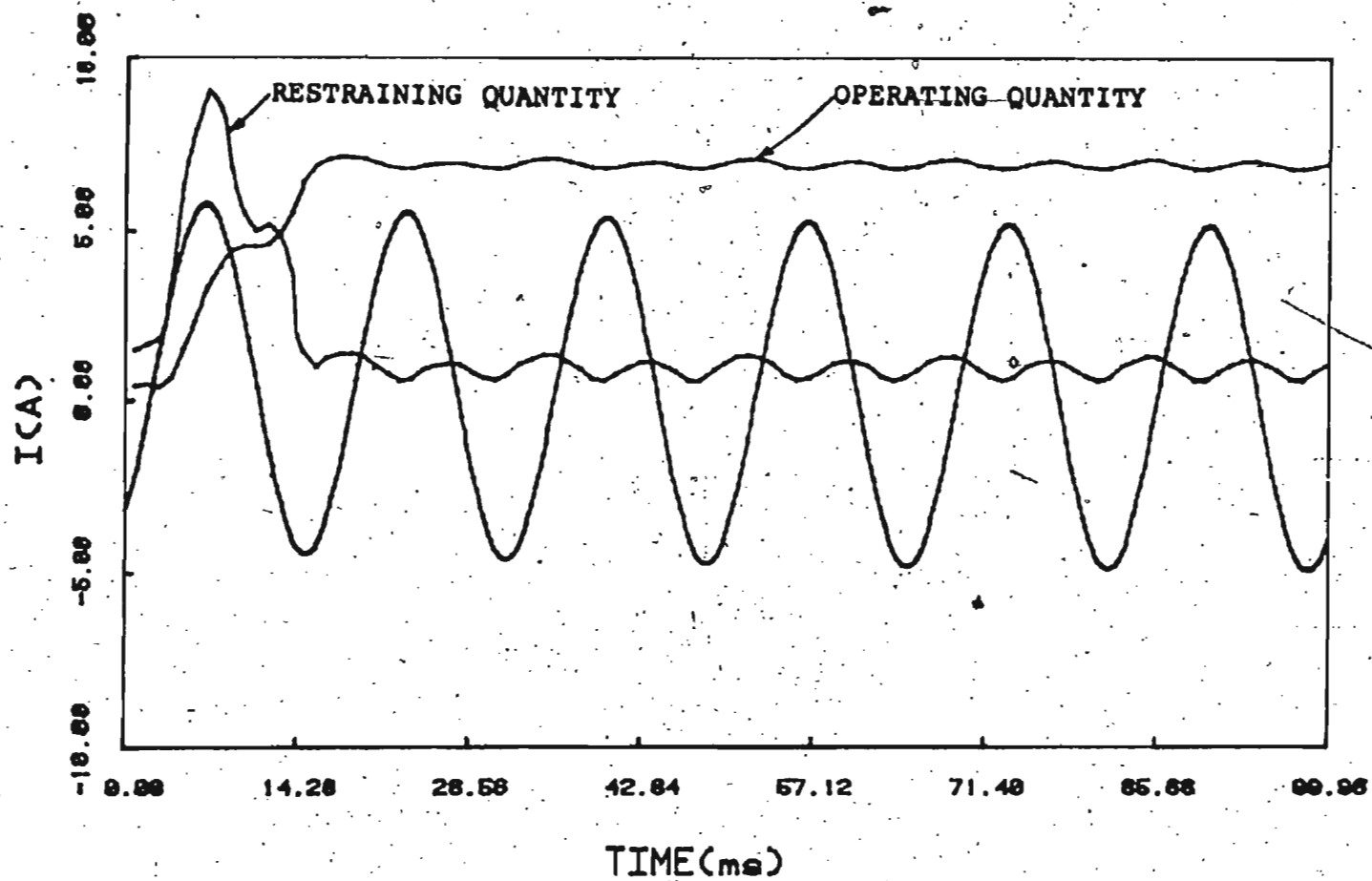


Fig. 4.7 (a) Performance of Rectangular Transform algorithm with 16 samples/cycle during an internal fault (fault initiation angle  $-0^\circ$ )

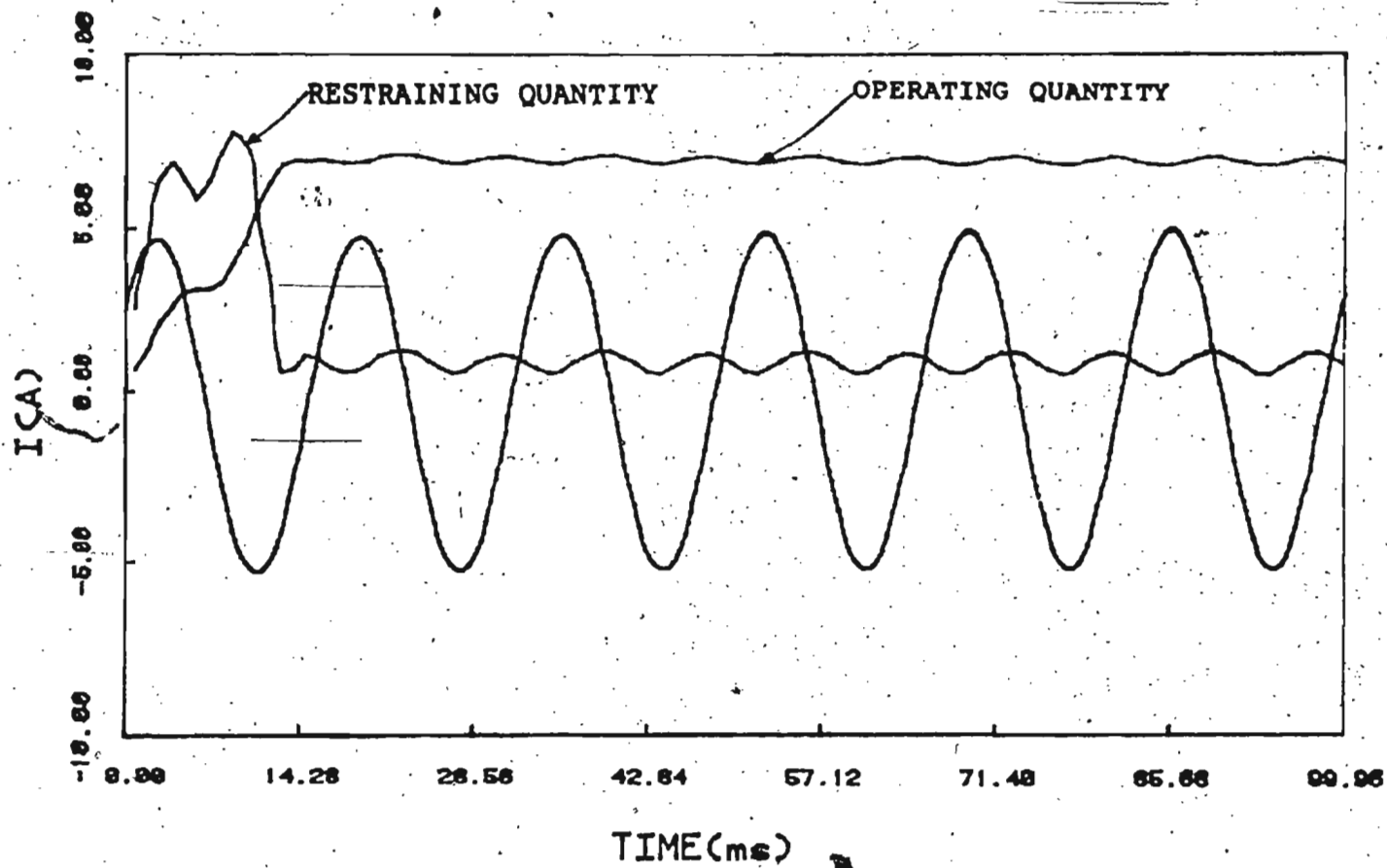


Fig. 4.7 (b) Performance of Rectangular Transform algorithm with 16 samples/cycle during an internal fault (fault initiation angle - 90°)



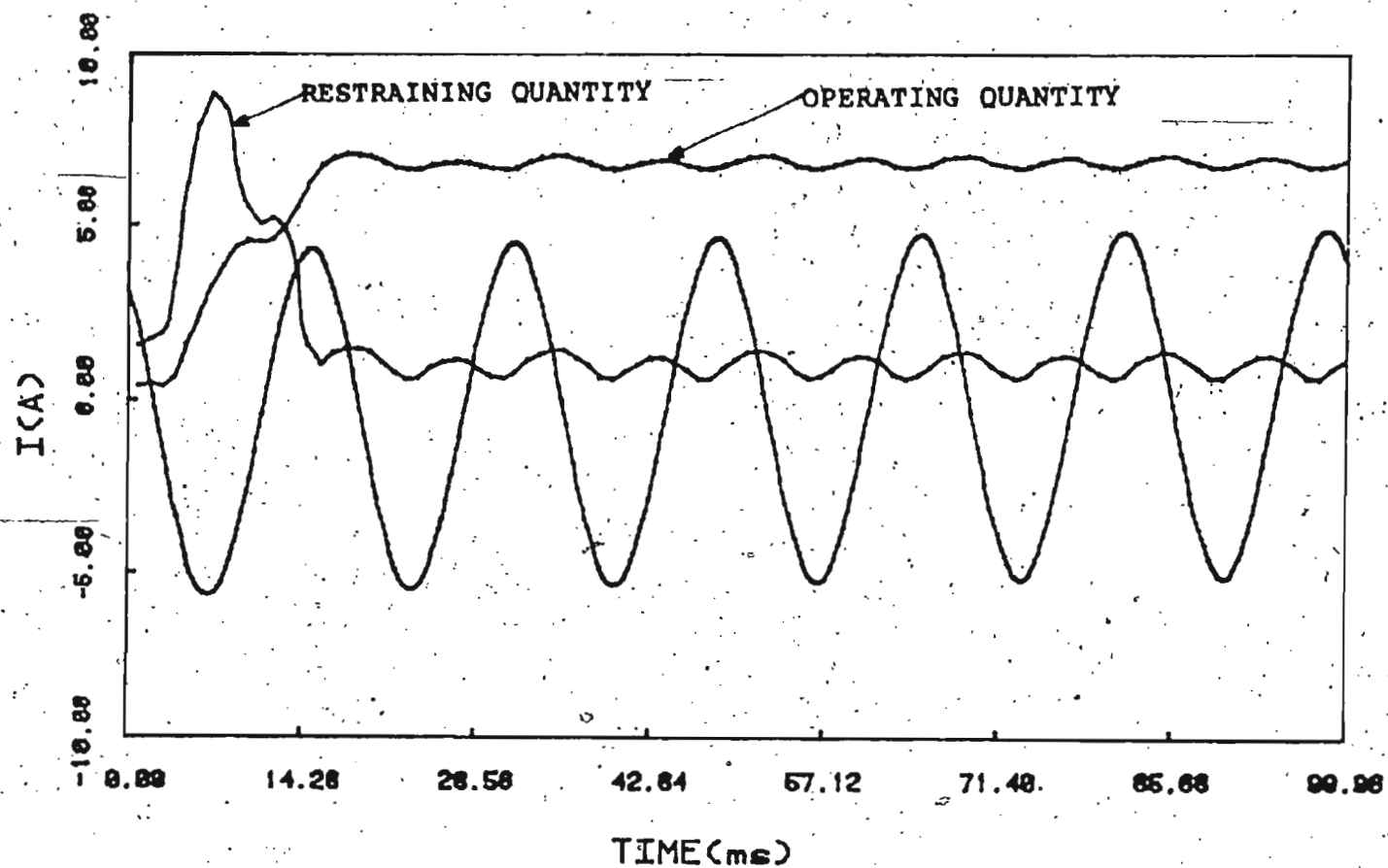


Fig. 4.7 (c) Performance of Rectangular Transform algorithm with 16 samples/cycle during an internal fault (fault initiation angle -  $180^\circ$ )

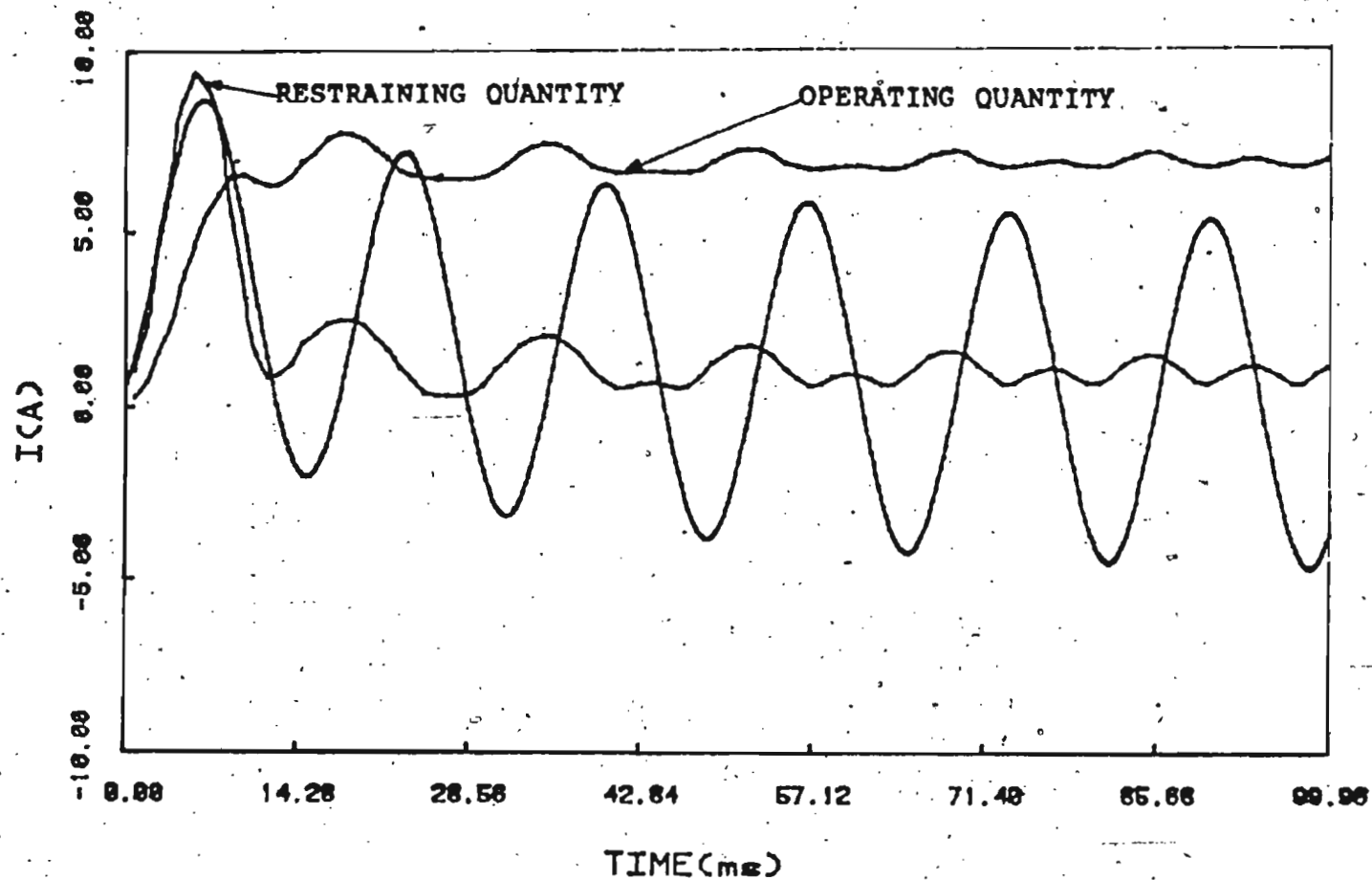


Fig. 4.8 Performance of Rectangular Transform algorithm with 16 samples/cycle during an asymmetrical internal fault (fault initiation angle -  $0^\circ$ )

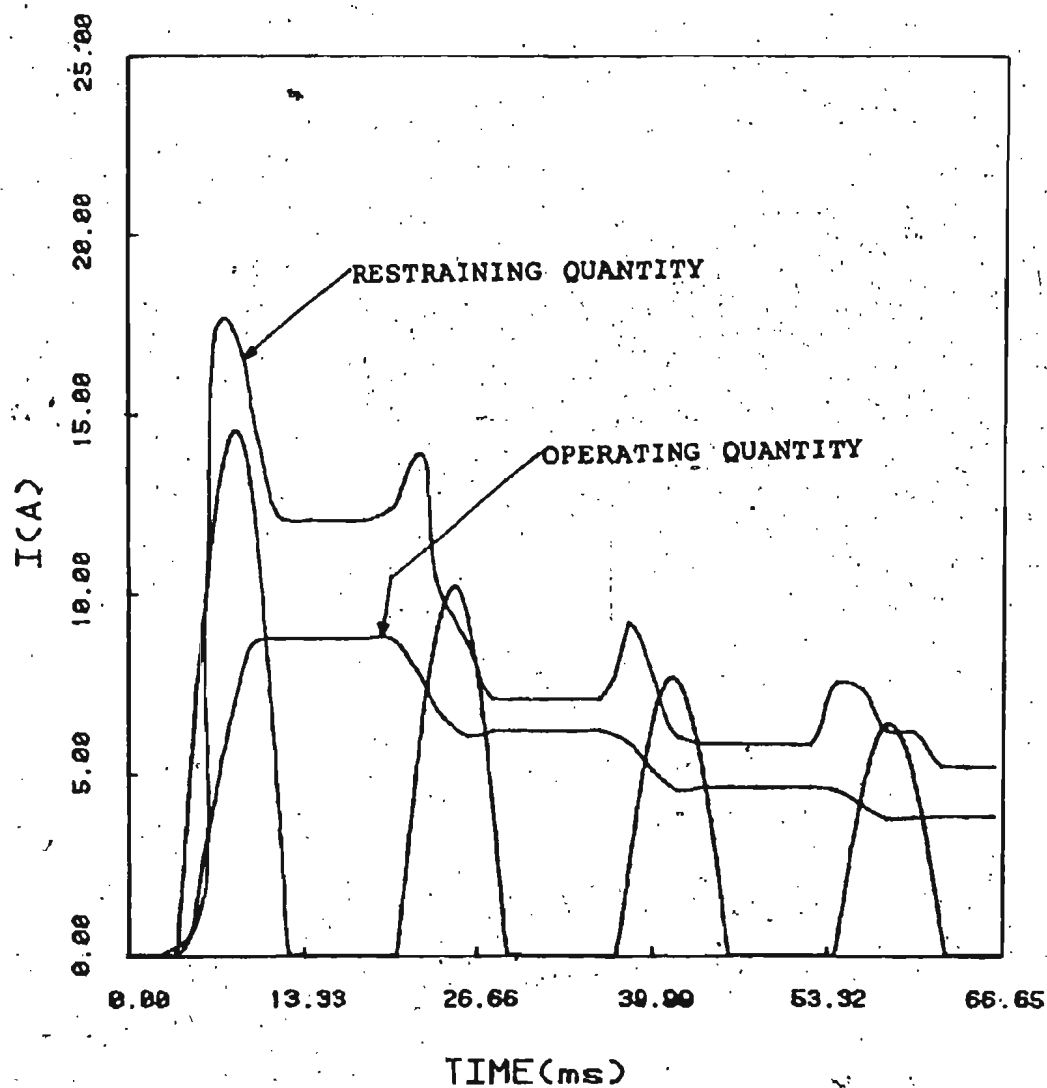


Fig. 4.9 (a) Performance of Rectangular Transform algorithm with 8 samples/cycle during inrush in phase-a of a Y-Δ transformer.

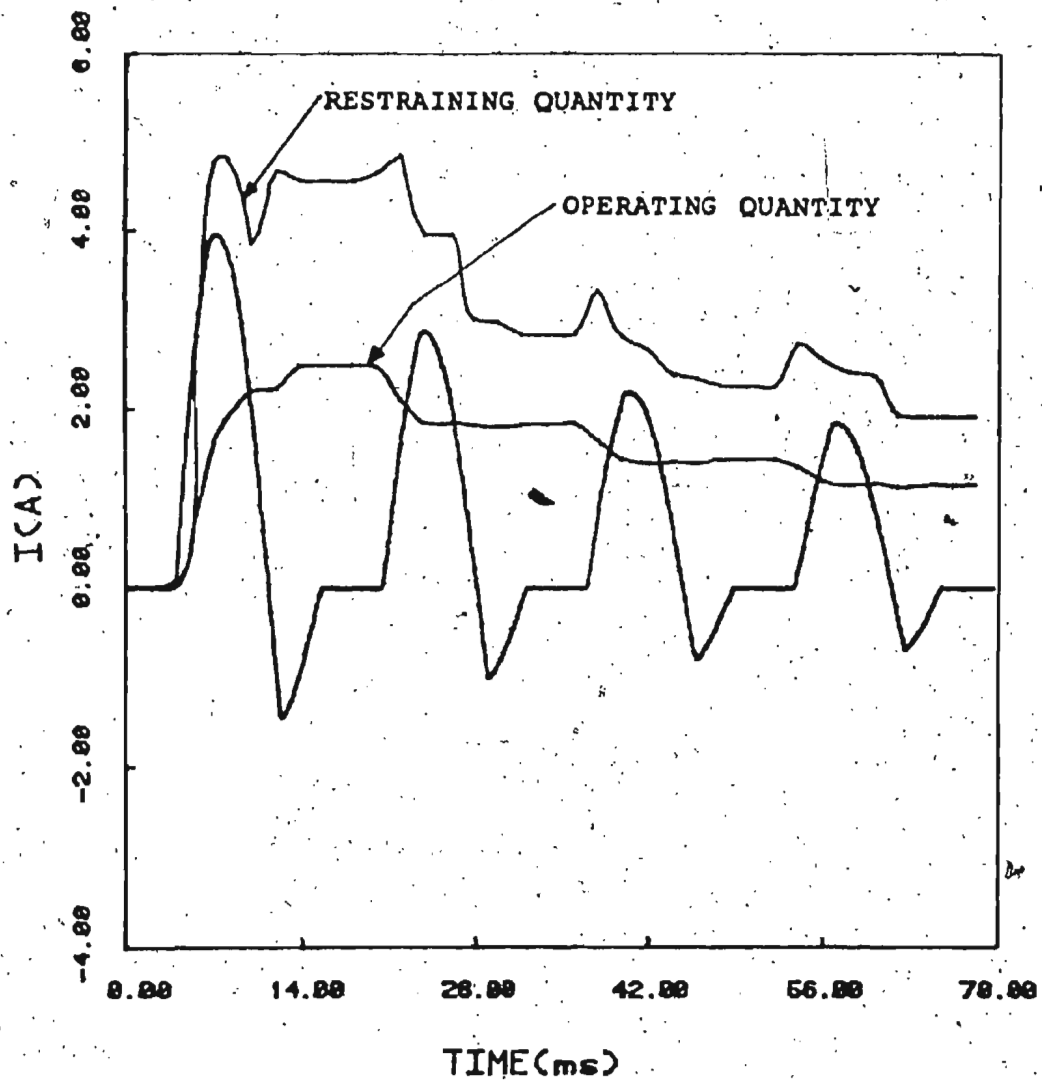


Fig. 4.9 (b) Performance of Rectangular Transform algorithm with 8 samples/cycle during inrush in phase-b of a Y-A transformer

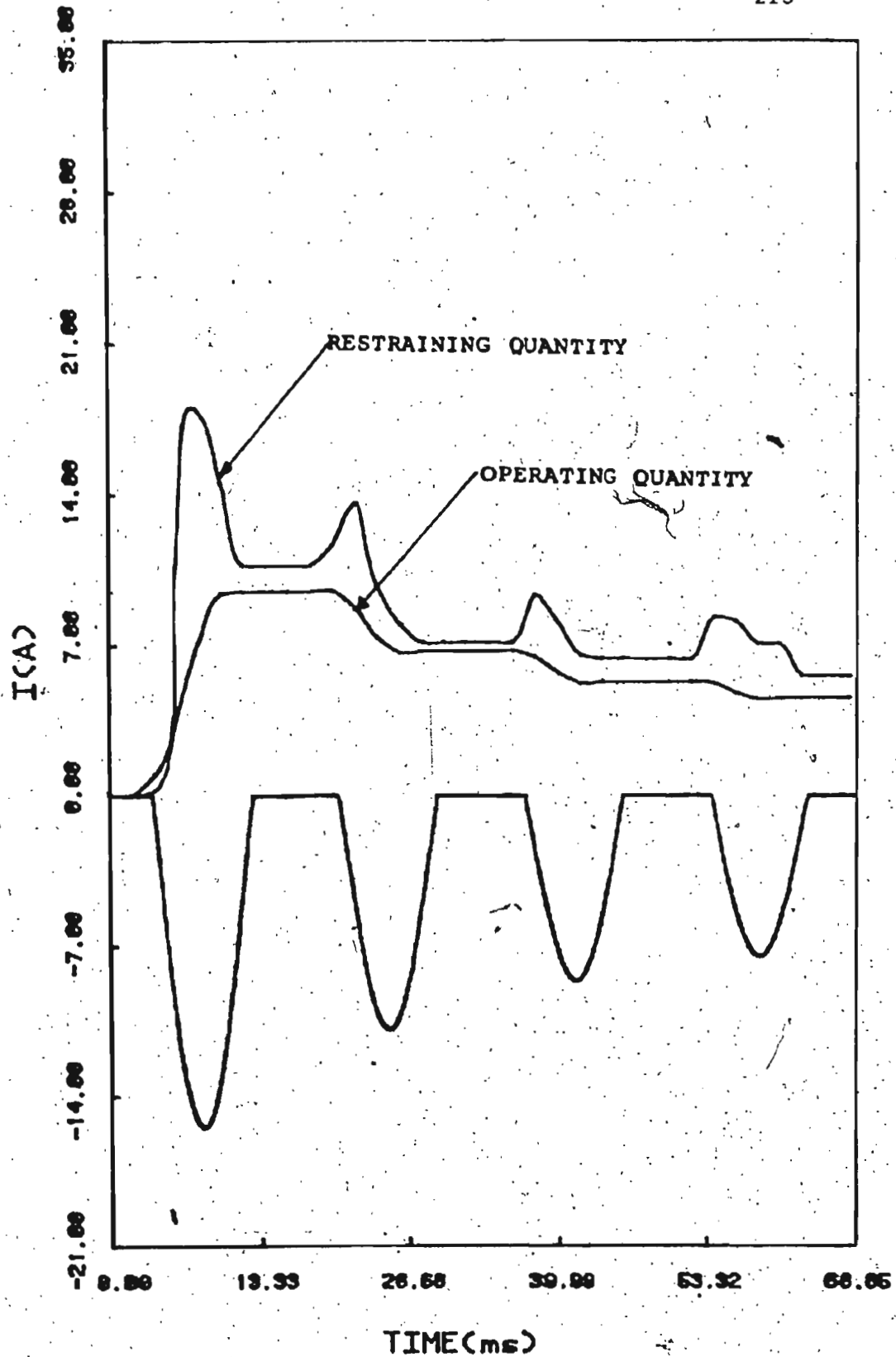


Fig. 4.9 (c) Performance of Rectangular Transform algorithm with 8 samples/cycle during inrush in phase-c of a Y-Δ transformer

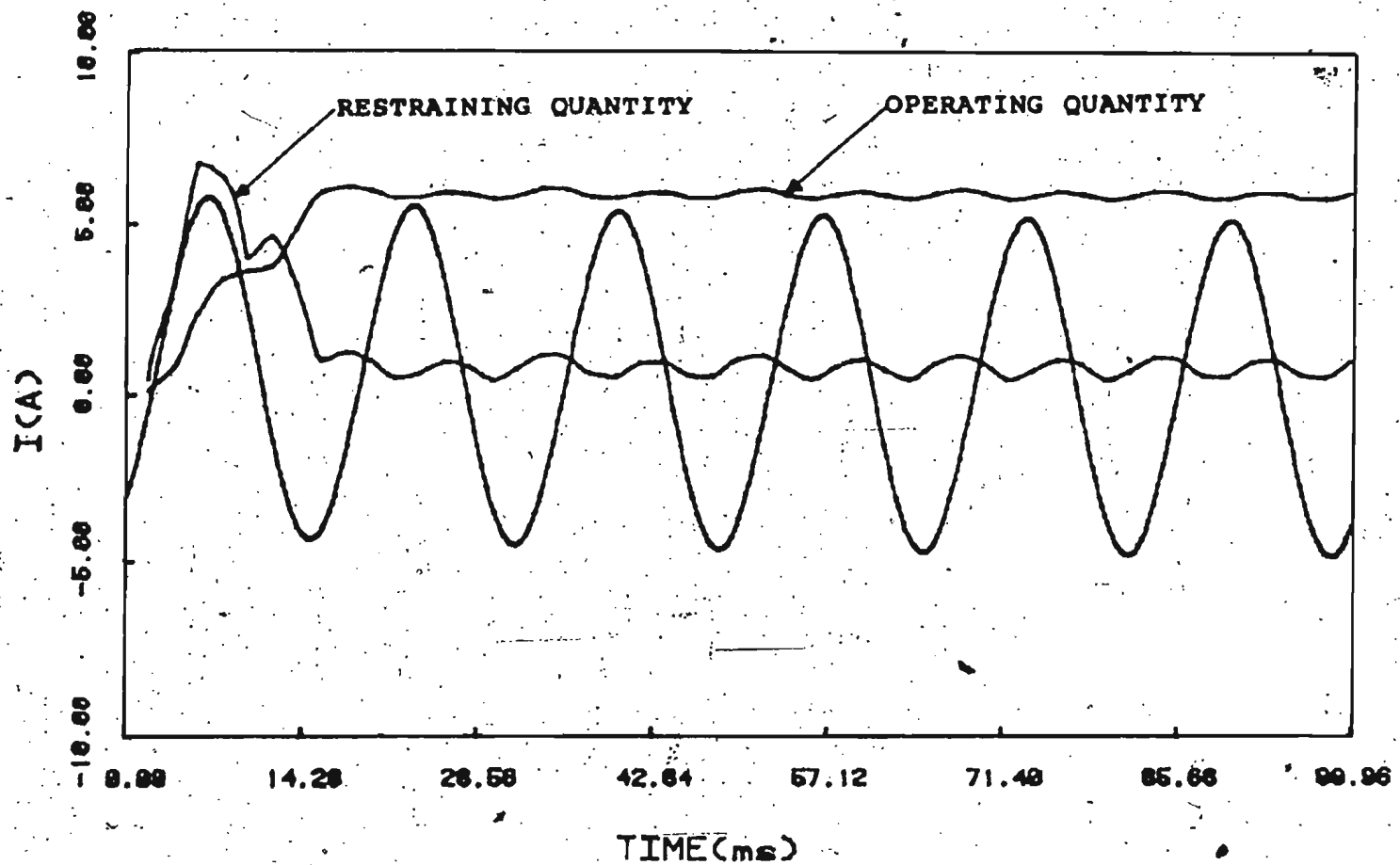


Fig. 4.10 (a) Performance of Rectangular Transform algorithm with 8 samples/ cycle during an internal fault (fault initiation angle -  $0^\circ$ )

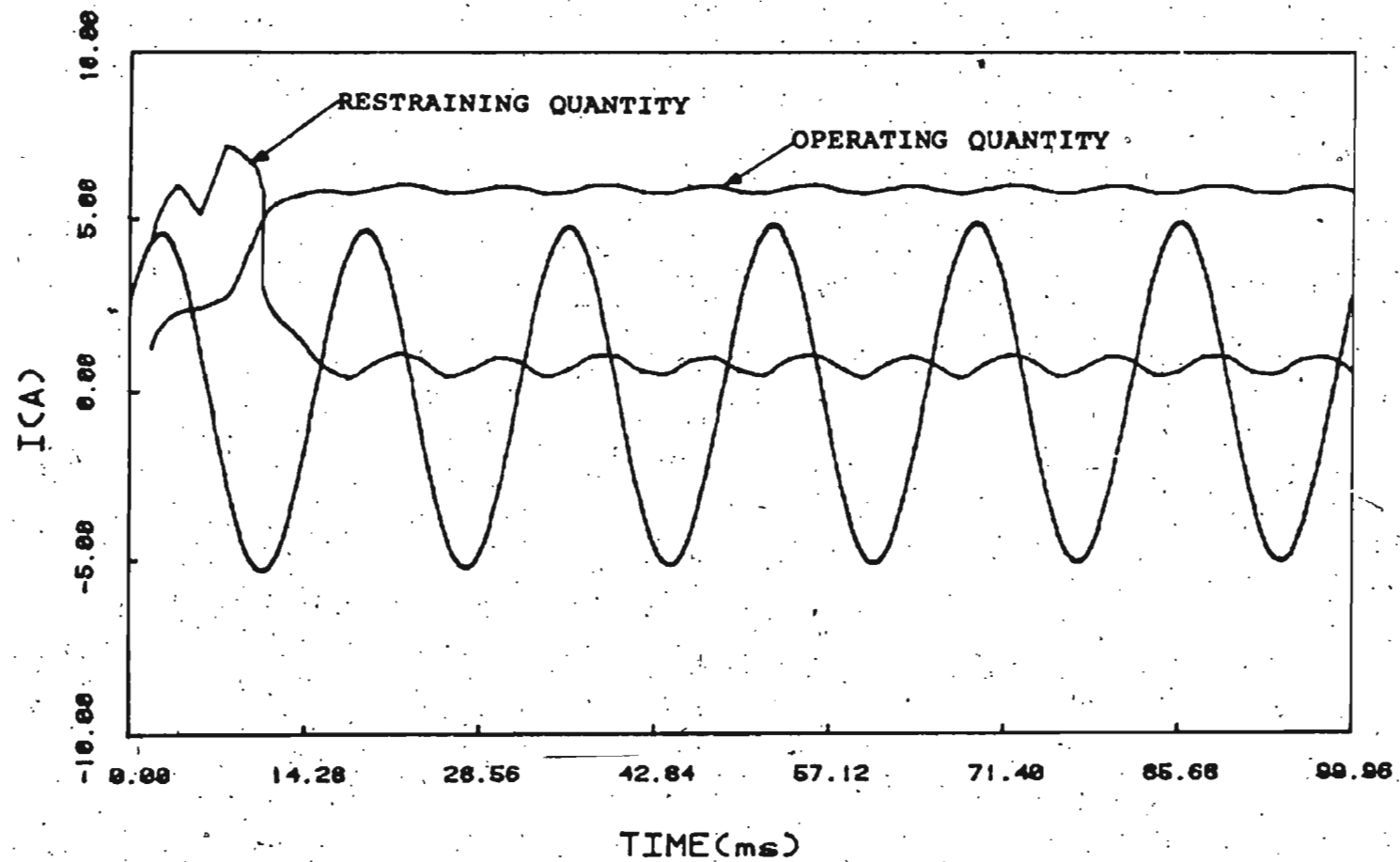


Fig. 4.10 (b) Performance of Rectangular algorithm with 8 samples/cycle during an internal fault (fault initiation angle - 90°)

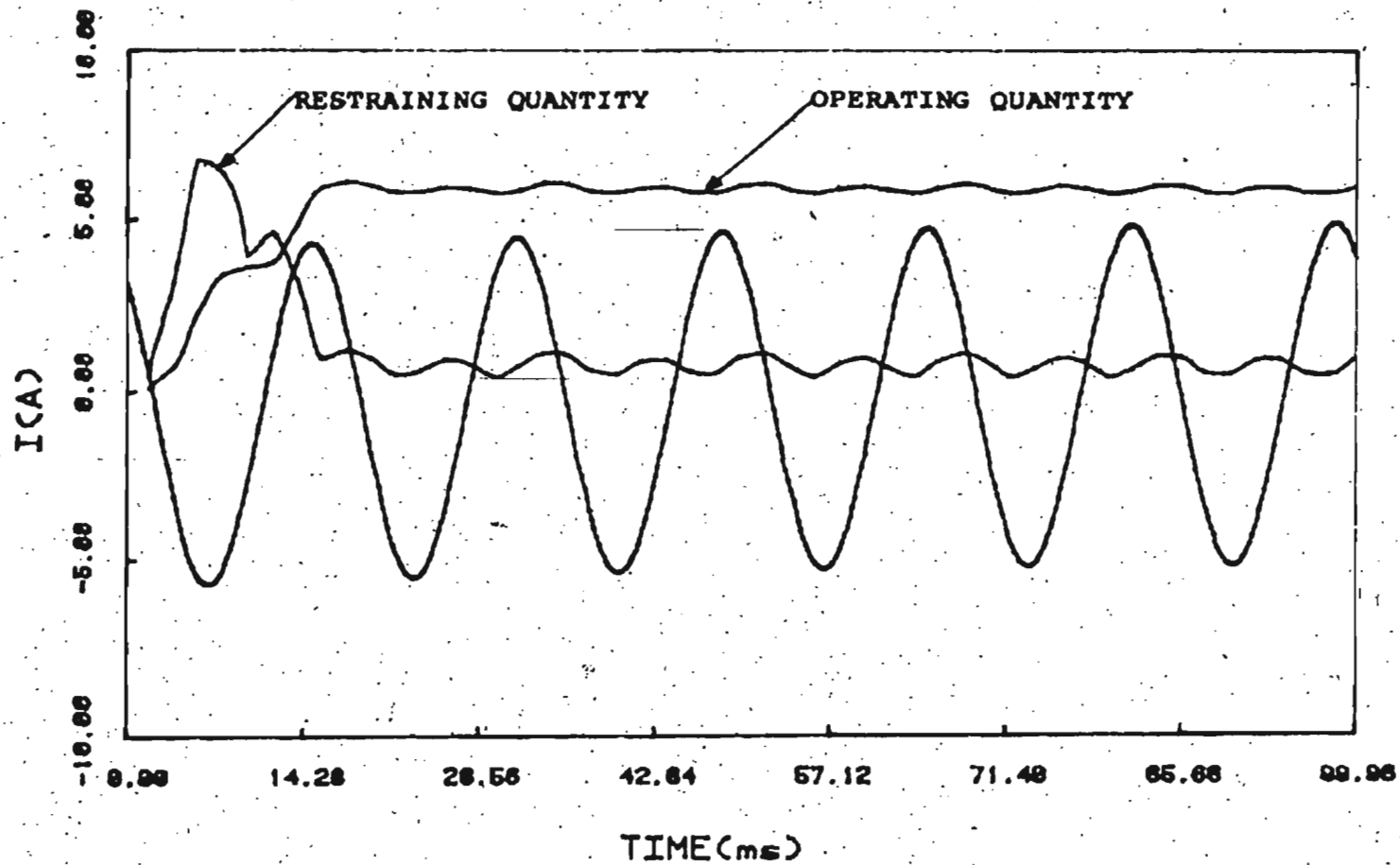


Fig. 4.10 (c) Performance of Rectangular Transform algorithm with 8 samples/cycle during an internal fault (fault initiation angle -  $180^\circ$ )



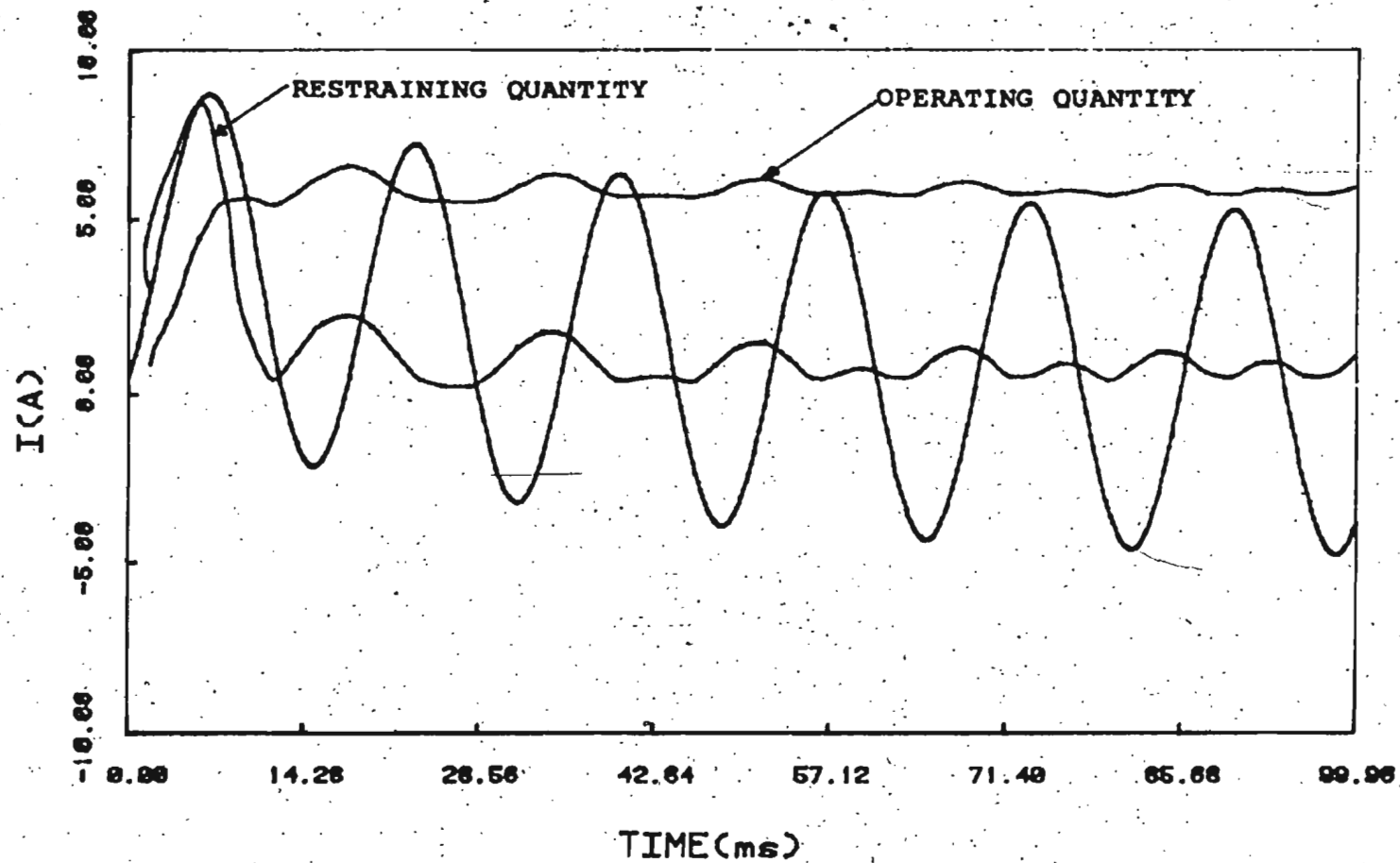


Fig. 4.11 Performance of Rectangular Transform algorithm with 8 samples/cycle during an asymmetrical internal fault (fault initiation angle  $0^\circ$ )

#### 4.4 Walsh Function Technique

In 1923, Joseph L. Walsh introduced a new complete set of orthonormal functions for a variable 't' in the interval (0,1)

$$\text{Wal}(K,t) = \prod_{i=0}^m \text{sgn}(\cos K_i 2^{i-1} \pi t) \quad (4.29)$$

where the integer 'K' has the binary expansion

$$K = K_0 2^0 + K_1 2^1 + K_2 2^2 + \dots + K_m 2^m \quad (4.30)$$

and where the binary coefficients  $K_j$  are either 0 or 1. The Walsh functions take only the values of  $\pm 1$  and they change sign only when 't' is a multiple of a power of 1/2. The index 'K', termed as the sequency of a Walsh Function, is analogous to frequency in Fourier analysis.

#### Theory

A function  $X(t)$  with finite energy and a finite number of discontinuities in the interval (0,T) may be expanded, in terms of the sum of a series of Walsh functions, which is similar to the expansion of a Fourier series,

$$X(t) = W_0 \text{Wal}(0,t) + \sum_{K=0}^{\infty} W_K \text{Wal}(K, \frac{t}{T}) \quad (4.31)$$

where the coefficients are given by

$$\frac{W_0}{2} = \frac{1}{T} \int_0^T x(t) \text{Wal}(0, \frac{t}{T}) dt \quad (4.32)$$

$$W_K = \frac{1}{T} \int_0^T x(t) \text{Wal}(K, \frac{t}{T}) dt$$

$\frac{w_0}{2}$  shown in the expression of Eqn. (4.32) above is similar to  $\frac{a_0}{2}$  of Fourier series as given in Eqn. (4.12). It gives the mean value of the function.

A sequence bandlimited function, can be, however, expressed as,

$$X(t) = \sum_{K=0}^{n-1} w_K \text{Wal}(K, \frac{t}{T}) \quad (4.33)$$

The function is determined by 'n' independent signal samples. The first 8 Walsh functions are shown in Fig. 4.12.

The time consuming operations, in the Fourier analysis algorithm used by Ramamoorthy [26] can be entirely eliminated if the function  $X(t)$  is analyzed into its Walsh functions  $\text{Wal}(K, t)$ .

This is possible because,  $\text{Wal}(k, t)$  has only two values  $\pm 1$ , and so Walsh analysis can be performed by the operations of addition and subtraction routine alone. The first sixteen of these functions are shown (in terms of sign) in Fig. 4.13. These functions are undefined at the points at where they change from  $\pm 1$  to  $\mp 1$ .

From Eqn. 4.32, one can set the sample matrix with Walsh functions to find out different Walsh coefficients as follows,

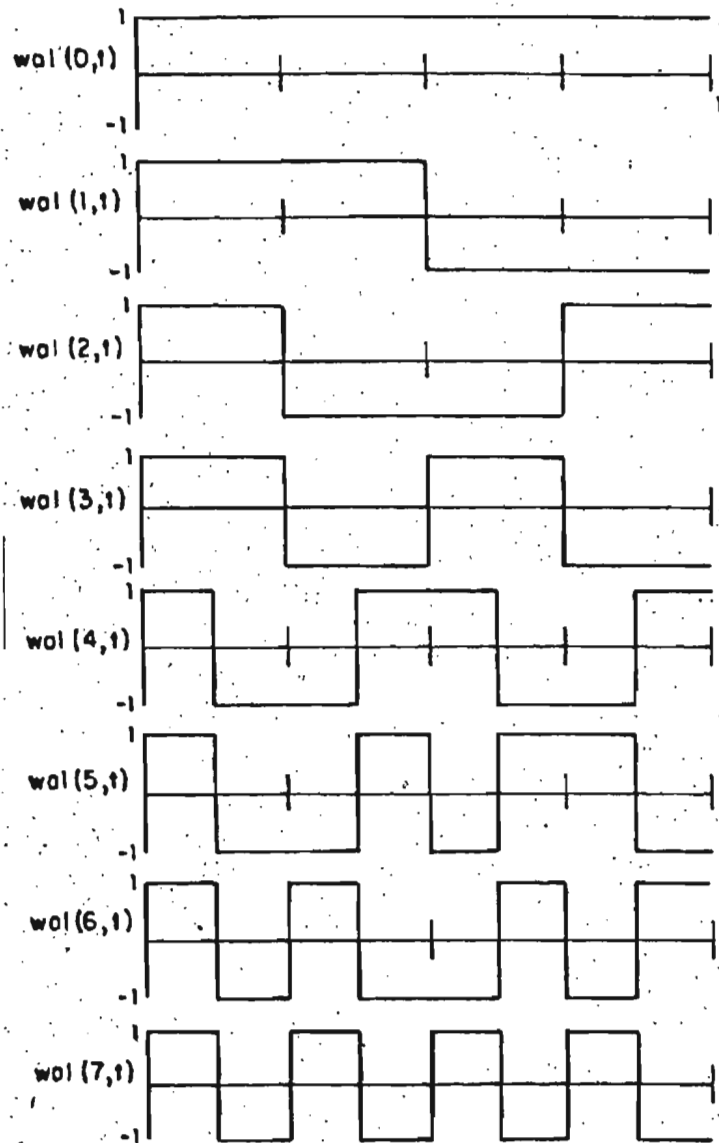


Fig. 4.12 The first eight Walsh functions of integral index  $k$  for  $0 \leq t \leq 1$

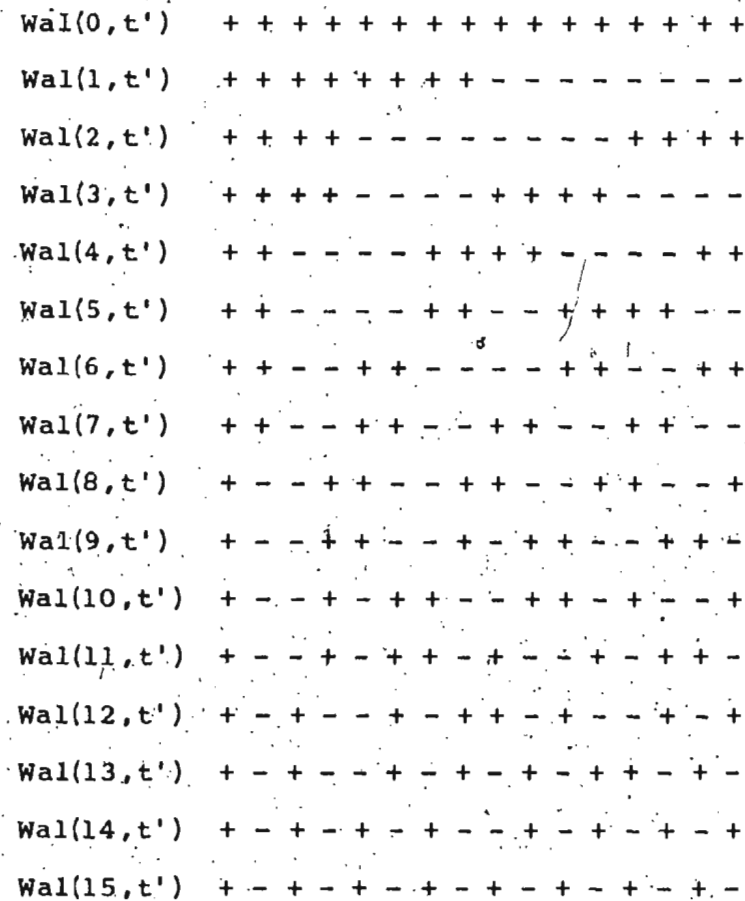


Fig. 4.13 The first sixteen Walsh Functions of integral index  $k$

$W_0$	+	+	+	+	+	+	+	+	+	+	+	+	+	+	+	$x(1)$	
$W_1$	+	+	+	+	+	+	+	-	-	-	-	-	-	-	-	$x(2)$	
$W_2$	+	+	+	+	-	-	-	-	-	-	-	-	+	+	+	$x(3)$	
$W_3$	+	+	+	+	-	-	-	-	+	+	+	+	-	-	-	$x(4)$	
$W_4$	+	+	-	-	-	-	+	+	+	+	-	-	-	-	+	$x(5)$	
$W_5$	+	+	-	-	-	-	+	+	-	-	+	+	+	+	-	$x(6)$	
$W_6$	+	+	-	-	+	+	-	-	-	-	+	+	-	-	+	$x(7)$	
$W_7$	+	+	-	-	+	+	-	-	+	+	-	-	+	+	-	$x(8)$	
$W_8 = \frac{1}{16}$	+	-	-	+	+	-	-	+	+	-	-	+	+	-	+	$x(9)$	(4.34)
$W_9$	+	-	-	+	+	-	-	+	-	+	+	-	-	+	+	$x(10)$	
$W_{10}$	+	-	-	+	-	+	+	-	-	+	+	-	+	-	+	$x(11)$	
$W_{11}$	+	-	-	+	-	+	+	-	+	-	-	+	-	+	+	$x(12)$	
$W_{12}$	+	-	+	-	-	+	-	+	+	-	+	-	-	+	-	$x(13)$	
$W_{13}$	+	-	+	-	-	+	-	+	-	+	-	+	+	-	+	$x(14)$	
$W_{14}$	+	-	+	-	+	-	+	-	-	+	-	+	-	+	+	$x(15)$	
$W_{15}$	+	-	+	-	+	-	+	-	+	-	+	-	+	-	+	$x(16)$	

Using a trapezoidal rule of integration, the individual Walsh coefficients can be determined. As a rule of trapezoidal integration, one extra term comes which is  $x(17)$ . The detail derivation is given in Appendix IV. The results for different Walsh Coefficients in a general form are given as follows,

$$16W_0(j+1) = 16W_0(j) - \frac{1}{2}x(j) - \frac{1}{2}x(j+1) + \frac{1}{2}x(j+16) + \frac{1}{2}x(j+17)$$

$$16W_1(j+1) = 16W_1(j) - \frac{1}{2}x(j) - \frac{1}{2}x(j+1) + x(j+8) + x(j+9) - \frac{1}{2}x(j+16) - \frac{1}{2}x(j+17)$$

$$16W_2(j+1) = 16W_2(j) - \frac{1}{2}x(j) - \frac{1}{2}x(j+1) + x(j+4) + x(j+5) - x(j+12) - x(j+13) + \frac{1}{2}x(j+16) + \frac{1}{2}x(j+17) \quad (4.35)$$

where  $j=0,1,2,3 \dots$

The expressions of Eqn. (4.35) are used to update the coefficients every time as a new sample comes, with minimum addition and subtraction routines. But, it is clear from the expressions that the number of terms increase as higher order coefficients are determined. And it does not very much help in such updating. Hence, the other terms which will be needed for further computations, can be written in the conventional forms as:

$$16W_3(j) = \frac{1}{2}x(j) + x(j+1) + x(j+2) + x(j+3) - x(j+5) - x(j+6) - x(j+7) + x(j+9) + x(j+10) + x(j+11) - x(j+13) - x(j+14) - x(j+15) - \frac{1}{2}x(j+16)$$

$$\begin{aligned}
 16W_4(j) = & \frac{1}{2}x(j) + x(j+1) - x(j+3) - x(j+4) - x(j+5) \\
 & + x(j+7) + x(j+8) + x(j+9) - x(j+11) - x(j+12) \\
 & - x(j+13) + x(j+15) + \frac{1}{2}x(j+16)
 \end{aligned}$$

$$\begin{aligned}
 16W_5(j) = & \frac{1}{2}x(j) + x(j+1) - x(j+3) - x(j+4) - x(j+5) \\
 & + x(j+7) - x(j+9) + x(j+11) + x(j+12) \\
 & + x(j+13) - x(j+15) - \frac{1}{2}x(j+16)
 \end{aligned}$$

$$\begin{aligned}
 16W_6(j) = & \frac{1}{2}x(j) + x(j+1) - x(j+3) + x(j+5) - x(j+7) \\
 & - x(j+8) - x(j+9) - x(j+11) - x(j+13) + x(j+15) \\
 & + \frac{1}{2}x(j+16)
 \end{aligned}$$

$$\begin{aligned}
 16W_9(j) = & \frac{1}{2}x(j) - x(j+2) + x(j+4) - x(j+6) + x(j+10) \\
 & - x(j+12) + x(j+14) - \frac{1}{2}x(j+16)
 \end{aligned}$$

$$\begin{aligned}
 16W_{10}(j) = & \frac{1}{2}x(j) - x(j+2) - x(j+6) - x(j+8) + x(j+10) \\
 & - x(j+14) + \frac{1}{2}x(j+16)
 \end{aligned}$$

$$\begin{aligned}
 16W_{11}(j) = & \frac{1}{2}x(j) - x(j+2) - x(j+10) + x(j+14) \\
 & - \frac{1}{2}x(j+16)
 \end{aligned}$$

$$\begin{aligned}
 16W_{12}(j) = & \frac{1}{2}x(j) - x(j+4) + x(j+8) - x(j+12) \\
 & + \frac{1}{2}x(j+16)
 \end{aligned}$$

$$16W_{13}(j) = \frac{1}{2}x(j) - x(j+4) + x(j+12) - \frac{1}{2}x(j+16)$$

$$16W_{14}(j) = \frac{1}{2}x(j) - x(j+8) + \frac{1}{2}x(j+16)$$

$$16W_{15}(j) = \frac{1}{2}x(j) - \frac{1}{2}x(j+16)$$

where  $j=1,2,3 \dots$

$\dots(4.36)$



The set  $W_K$  form a vector in Hilbert space like the Fourier coefficients  $F_K$ . The two vectors are related by the orthogonal matrix  $A$ ; thus

$$W = AF \quad (4.37)$$

since  $A^{-1} = A^T$  [4,15], where  $A^T$  is the transpose of  $A$ , one can also write

$$F = A^T W \quad (4.38)$$

The matrix 'A' has been found to be, in part as,

$$[A] = \begin{bmatrix} 1 & 0 & 0 & 0 & 0 & 0 & 0 & 0 & 0 & 0 & 0 & 0 & 0 \\ 0 & .900 & 0 & 0 & 0 & .300 & 0 & 0 & 0 & .180 & 0 & 0 & 0 \\ 0 & 0 & .900 & 0 & 0 & 0 & -.300 & 0 & 0 & 0 & .180 & 0 & 0 \\ 0 & 0 & 0 & .900 & 0 & 0 & 0 & 0 & 0 & 0 & 0 & .300 & 0 \\ 0 & 0 & 0 & 0 & .900 & 0 & 0 & 0 & 0 & 0 & 0 & 0 & -.300 \\ 0 & -.373 & 0 & 0 & 0 & .724 & 0 & 0 & 0 & .435 & 0 & 0 & 0 \\ 0 & 0 & .373 & 0 & 0 & 0 & .724 & 0 & 0 & 0 & .435 & 0 & 0 \\ 0 & 0 & 0 & 0 & 0 & 0 & 0 & .900 & 0 & 0 & 0 & 0 & 0 \\ 0 & 0 & 0 & 0 & 0 & 0 & 0 & 0 & .900 & 0 & 0 & 0 & 0 \\ 0 & -.074 & 0 & 0 & 0 & -.484 & 0 & 0 & 0 & .650 & 0 & 0 & 0 \\ 0 & 0 & -.074 & 0 & 0 & 0 & .484 & 0 & 0 & 0 & .650 & 0 & 0 \\ 0 & 0 & 0 & -.373 & 0 & 0 & 0 & 0 & 0 & 0 & 0 & .724 & 0 \\ 0 & 0 & 0 & 0 & .373 & 0 & 0 & 0 & 0 & 0 & 0 & 0 & .724 \end{bmatrix}$$

$$(4.39)$$

and from Eqn. 4.38, it can be written as

$$\begin{bmatrix} F_0 \\ F_1 \\ F_2 \\ F_3 \\ F_4 \\ F_5 \\ F_6 \\ F_7 \\ F_8 \\ F_9 \\ F_{10} \\ F_{11} \\ F_{12} \end{bmatrix} = \begin{bmatrix} 1 & 0 & 0 & 0 & 0 & 0 & 0 & 0 & 0 & 0 & 0 & 0 & 0 \\ 0 & .900 & 0 & 0 & 0 & -.373 & 0 & 0 & 0 & -.074 & 0 & 0 & 0 \\ 0 & 0 & .900 & 0 & 0 & 0 & .373 & 0 & 0 & 0 & -.074 & 0 & 0 \\ 0 & 0 & 0 & .900 & 0 & 0 & 0 & 0 & 0 & 0 & 0 & -.373 & 0 \\ 0 & 0 & 0 & 0 & .900 & 0 & 0 & 0 & 0 & 0 & 0 & 0 & .373 \\ 0 & .300 & 0 & 0 & 0 & .724 & 0 & 0 & 0 & -.484 & 0 & 0 & 0 \\ 0 & 0 & -.300 & 0 & 0 & 0 & .724 & 0 & 0 & 0 & .484 & 0 & 0 \\ 0 & 0 & 0 & 0 & 0 & 0 & 0 & .900 & 0 & 0 & 0 & 0 & 0 \\ 0 & 0 & 0 & 0 & 0 & 0 & 0 & 0 & .900 & 0 & 0 & 0 & 0 \\ 0 & .180 & 0 & 0 & 0 & .435 & 0 & 0 & 0 & .650 & 0 & 0 & 0 \\ 0 & 0 & .180 & 0 & 0 & 0 & -.435 & 0 & 0 & 0 & .650 & 0 & 0 \\ 0 & 0 & 0 & .300 & 0 & 0 & 0 & 0 & 0 & 0 & 0 & .724 & 0 \\ 0 & 0 & 0 & 0 & .373 & 0 & 0 & 0 & 0 & 0 & 0 & 0 & .724 \end{bmatrix} \begin{bmatrix} W_0 \\ W_1 \\ W_2 \\ W_3 \\ W_4 \\ W_5 \\ W_6 \\ W_7 \\ W_8 \\ W_9 \\ W_{10} \\ W_{11} \\ W_{12} \end{bmatrix} \quad (4.40)$$

Hence, the Fourier coefficients are derived from the matrix of Eqn. (4.40) as,

$$\begin{aligned} F_1 &= 0.900W_1 - 0.373W_5 - 0.074W_9 \\ F_2 &= 0.900W_2 + 0.373W_6 - 0.074W_{10} \\ F_3 &= 0.900W_3 - 0.373W_{11} \\ F_4 &= 0.900W_4 + 0.373W_{12} \end{aligned} \quad (4.41)$$

where  $F_1, F_2$  are the fundamental sine and cosine terms respectively and  $F_3, F_4$  are the 2nd harmonic sine and cosine terms respectively. Once, the Fourier coefficients are derived, the fundamental and the 2nd harmonic R.M.S.

quantities can be derived as,

$$\begin{aligned}\text{Fundamental} &= \sqrt{(F_1^2 + F_2^2)} \\ \text{2nd Harmonic} &= \sqrt{(F_3^2 + F_4^2)}\end{aligned}\quad (4.42)$$

In a similar manner, the algorithm, on the basis of 8-samples/cycle can be developed which is derived in Appendix D. Due to the reason that the coefficients beyond 'W<sub>7</sub>' are not available in Walsh function algorithm with 8 samples/cycle, Eqn. 4.41 is truncated as follows,

$$\begin{aligned}F_1 &= 0.900W_1 - 0.373W_5 \\ F_2 &= 0.900W_2 + 0.373W_6 \\ F_3 &= 0.900W_3 \\ F_4 &= 0.900W_4\end{aligned}\quad (4.43)$$

It is obvious from above, that the accuracy of the algorithm is hampered to some extent, while the speed of processing is increased. It is interesting to note that except for the end points of the interval (0,t), the value of the samples is zero where the jump from +1 to -1 or from -1 to +1 occurs in the respective Walsh function. This is due to reason that the Walsh function is undefined where the signal changes from +1 to -1.

An advantage of the Rectangular Transform, over Walsh Function is that no sample is missing during sign change because actual values of sine-cosines are being replaced with +1 and 0. Hence valuable information are

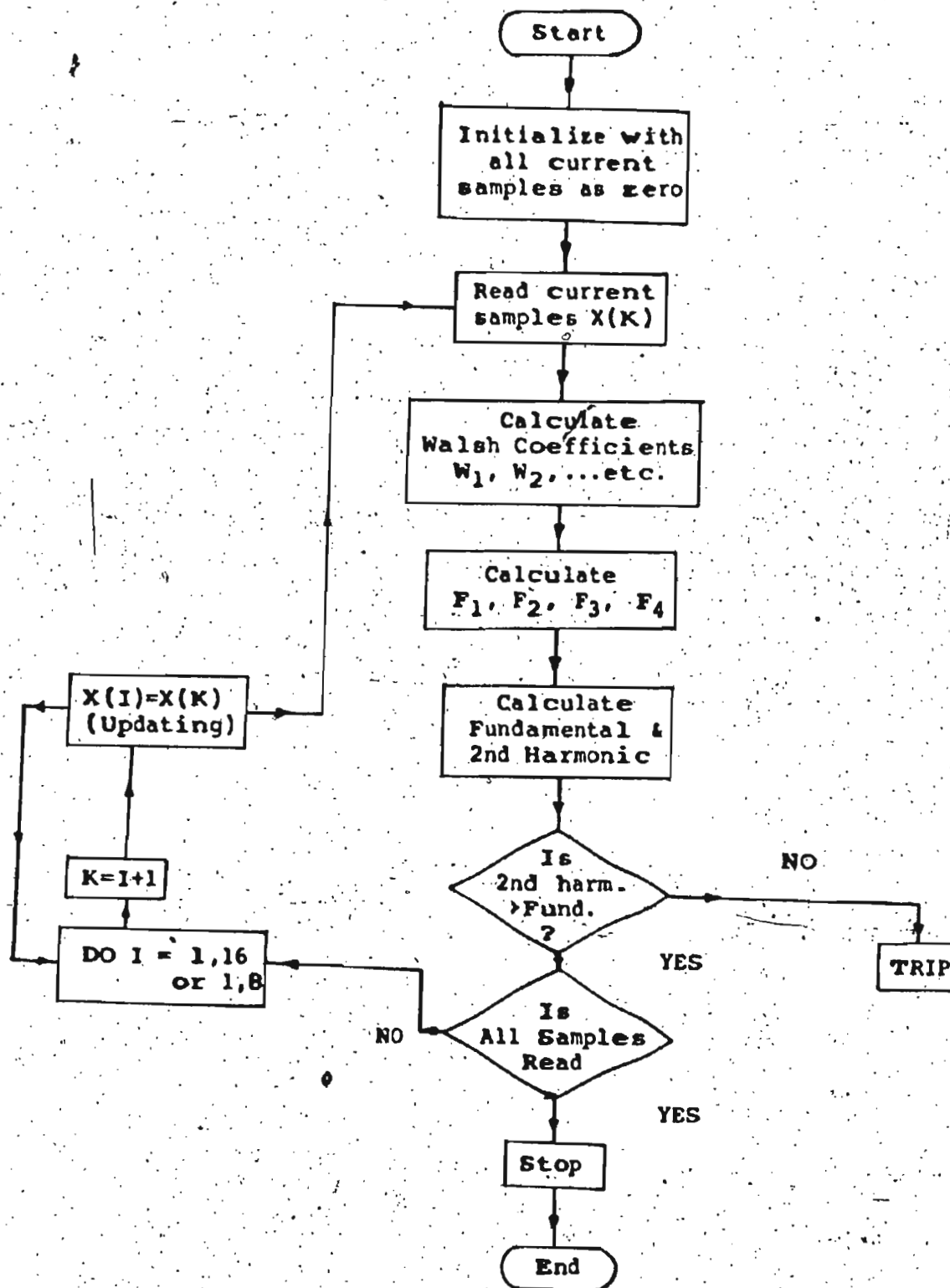


Fig. 4.14 Flowchart of programming logic of digital differential relay by Walsh function algorithm

retained in the calculation of fundamental and 2nd harmonic quantities.

### Results

A recursive programming is done to calculate the Walsh coefficients and then calculate the Fourier coefficients. Fundamental and 2nd harmonic quantities are then computed and trip or no-trip decision is initiated. The flow chart of the programming is shown in Fig. 4.14 which is very similar to those of D.F.T. and Rectangular Transform. The major difference is, unlike D.F.T. or Rectangular, various matrix elements are not required to be computed apriori and stored in the memory.

Figs. 4.15(a), (b), (c) show the performance of the algorithm on 16 samples/cycle basis, in case of a magnetizing inrush on phase A, B and C, respectively. The restraining quantity is seen to be greater than the operating quantities. The difference in restraining and operating is slightly less in comparison to those of D.F.T. and Rectangular. One of the reasons for this is, here the amplitudes are calculated in R.M.S., whereas, the amplitudes for D.F.T. or Rectangular were calculated in peak values. Figs. 4.16(a), (b), (c) show the performance of the algorithm in case of internal fault where the fault initiation angles are  $0^\circ$ ,  $90^\circ$  and  $180^\circ$  respectively. The convergence time of the algorithm corresponding to the initiation angles of  $0^\circ$ ,  $90^\circ$  and  $180^\circ$

are 13.8, 11.8 and 13.8 msec respectively. Similarly, Walsh function technique is applied to an assymetrical fault at  $\lambda=0^\circ$  and is shown in Fig. 4. 17. The convergence time is seen to be 9.8 msec.

In a similar way, the performance of this algorithm with a sampling rate of 8 samples/cycle has been tested on all the above simulated data. Figs. 4.18 (a), (b), (c) show the performance of the algorithm on inrush currents in phase A, B and C respectively. Unlike the other two cases, the value of the 2nd harmonic multiplier is to be raised to '6' from '4' to obtain adequate restraining forces in case of an inrush. Figs. 4.19(a), (b), (c) show the performance of the algorithm in case of internal fault at  $\lambda=0^\circ$ ,  $90^\circ$  and  $180^\circ$  respectively. The convergence times of the algorithms are 15.8, 13.8 and 15.8 msec respectively. The performance on the assymetrical fault is also shown in Fig. 4.20, where the convergence time is found to be 11.8 msec.

#### 4.5 Comparative Analysis of Algorithms

The three transform techniques described above have their individual characteristics. The Rectangular and Walsh Functions were compared at identical sampling rates of 16 and 8 samples/cycle, to find out their suitability for transformer protection purposes. This was done using D.F.T. with 16 samples/cycle as reference frame. The algorithms

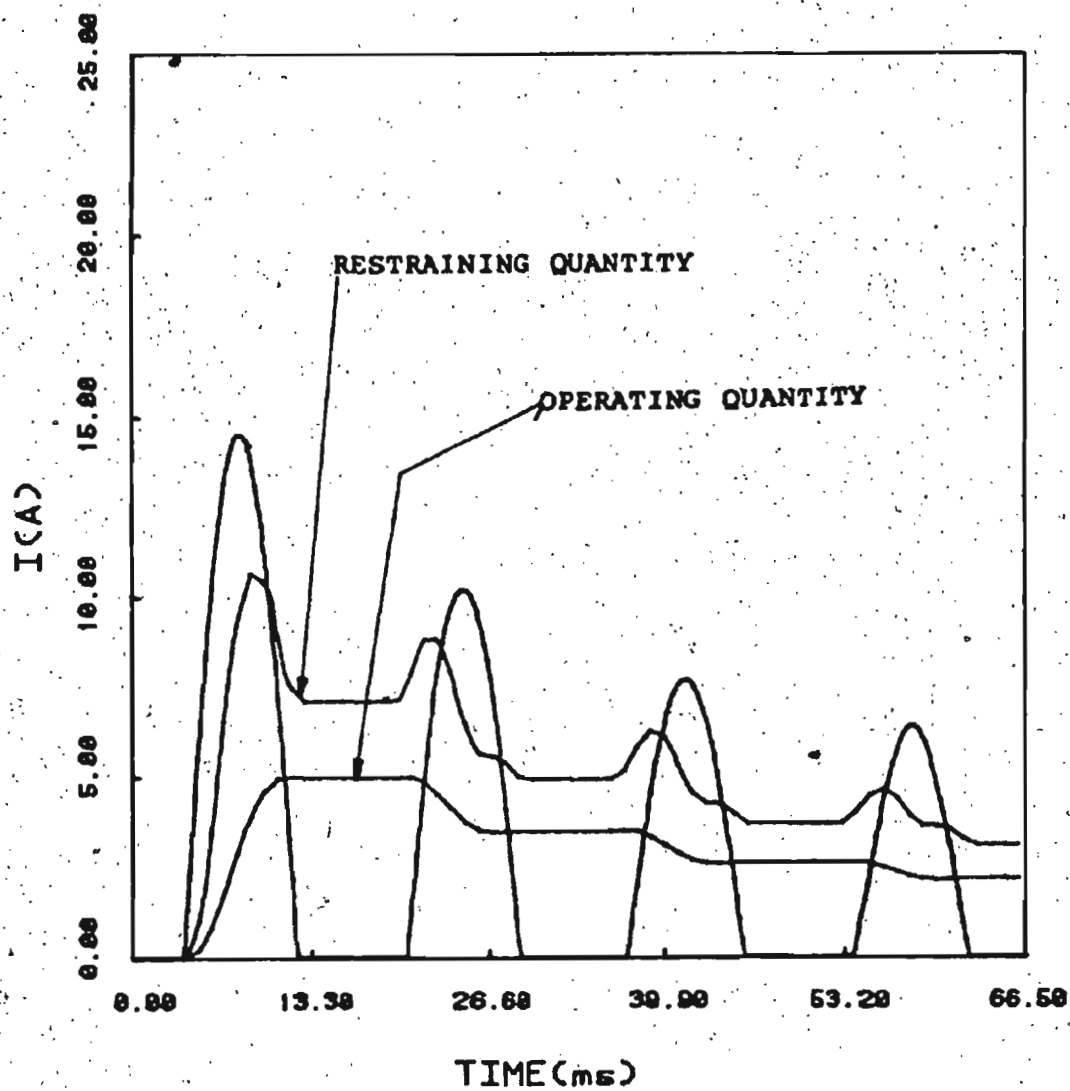


Fig. 4.15 (a) Performance of Walsh function algorithm with 16 samples/cycle during inrush in phase-a of a Y-Δ transformer.

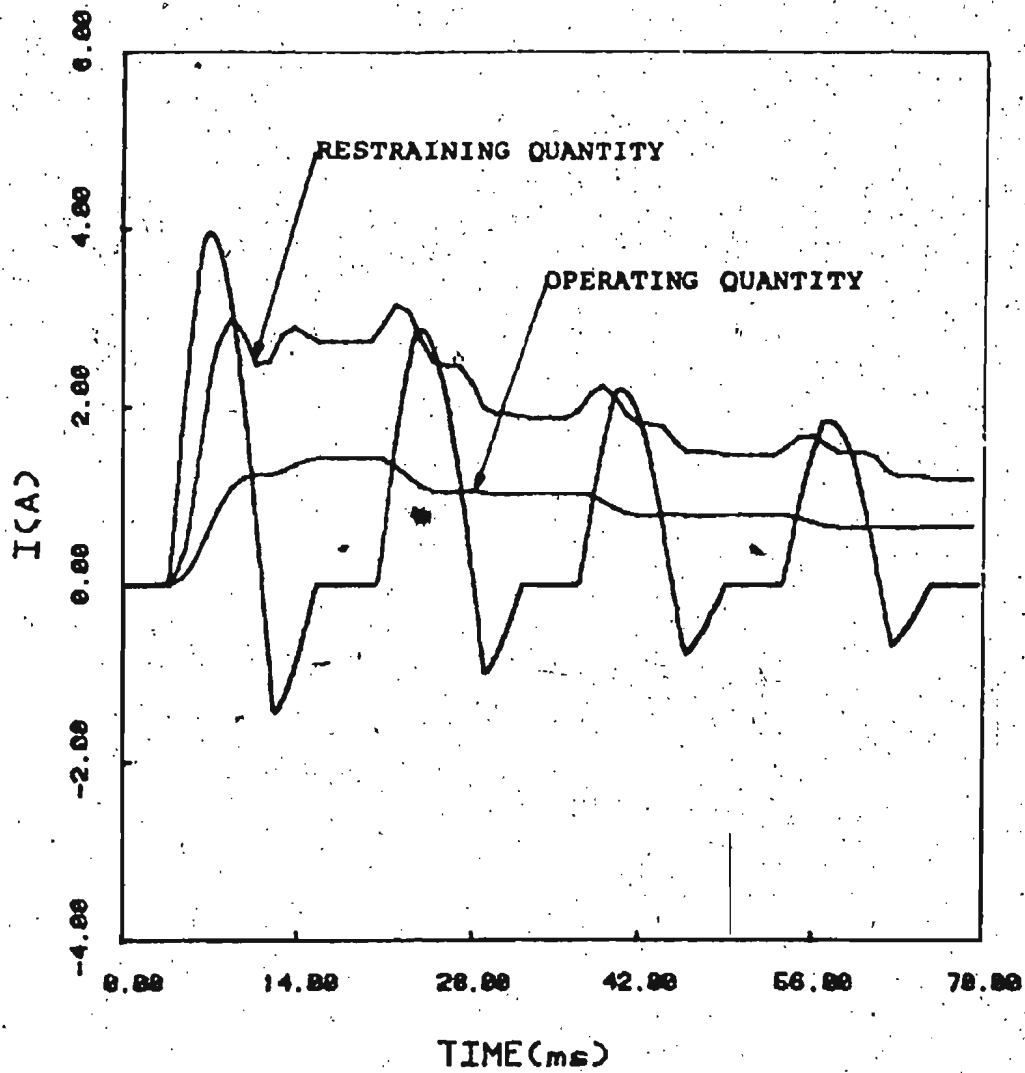


Fig. 4.15 (b). Performance of Walsh function algorithm with 16 samples/cycle during inrush in phase-b of a Y-Δ transformer



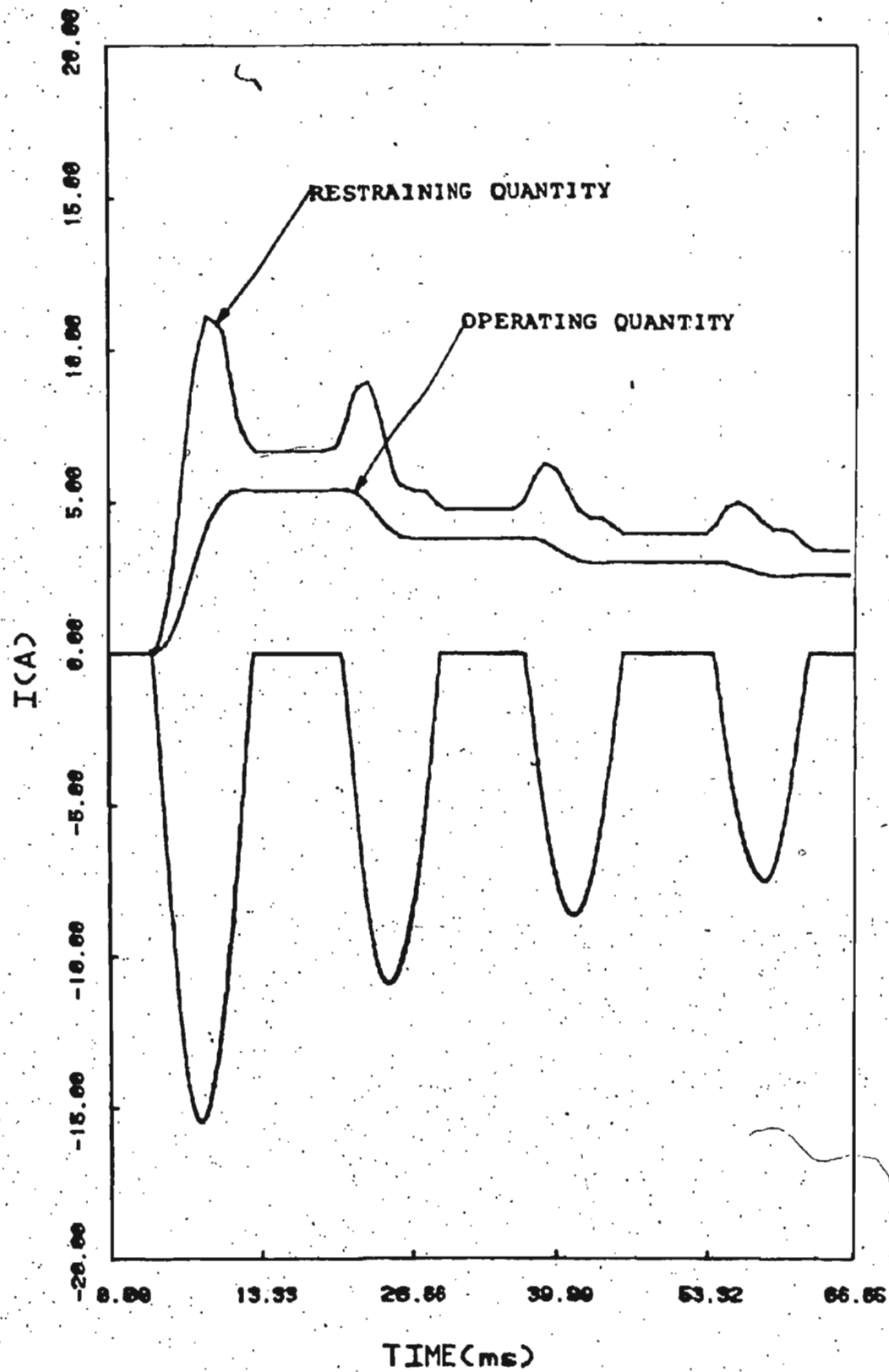


Fig. 4.15 (c) Performance of Walsh function algorithm with 16 samples/cycle during inrush in phase-c of a Y-Δ transformer.

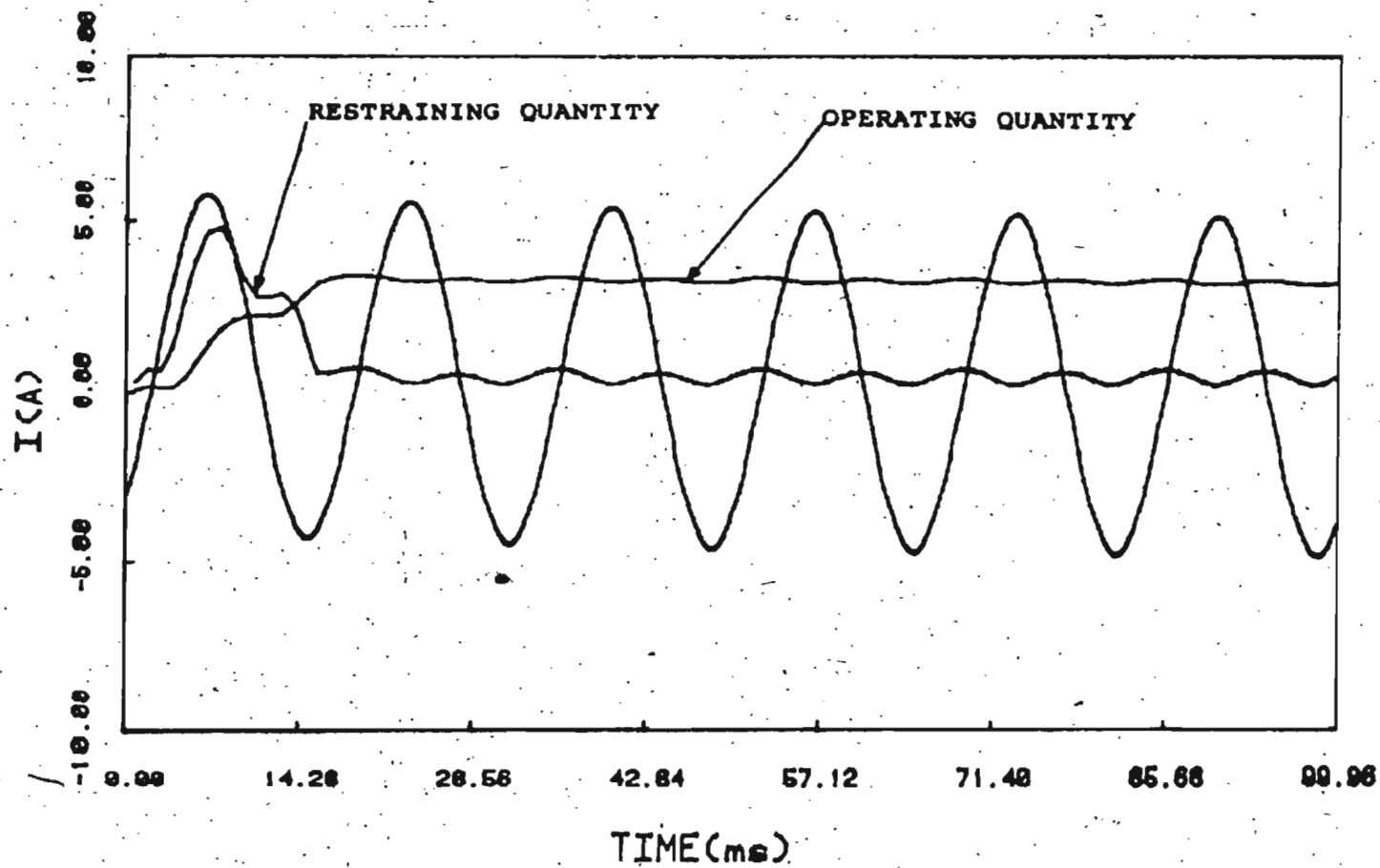


Fig. 4.16 (a) Performance of Walsh function algorithm with 16 samples/cycle during an internal fault (fault initiation angle =  $0^\circ$ )

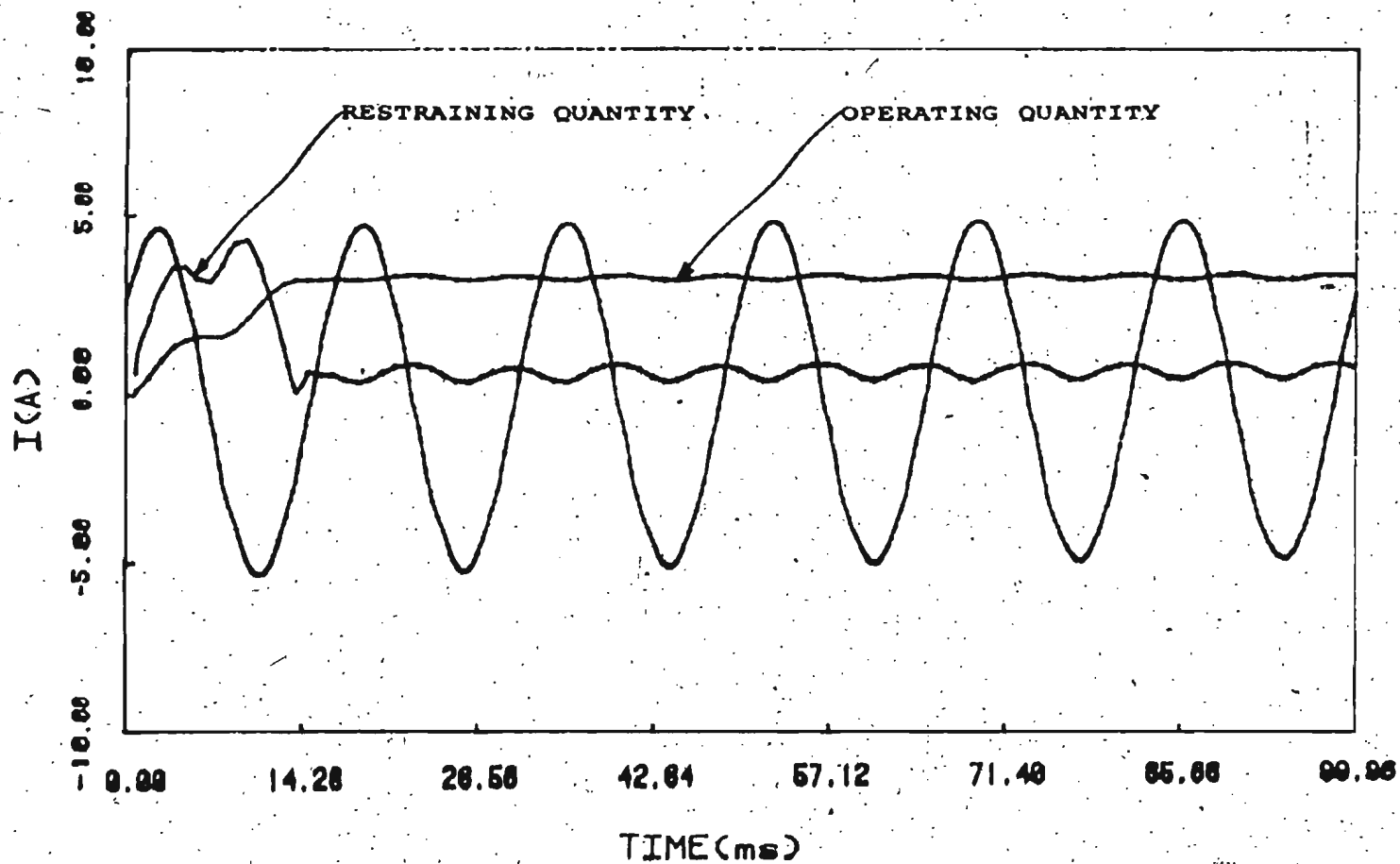


Fig. 4.16 (b) Performance of Walsh function algorithm with 16 samples/cycle during an internal fault (fault initiation angle -  $90^\circ$ )

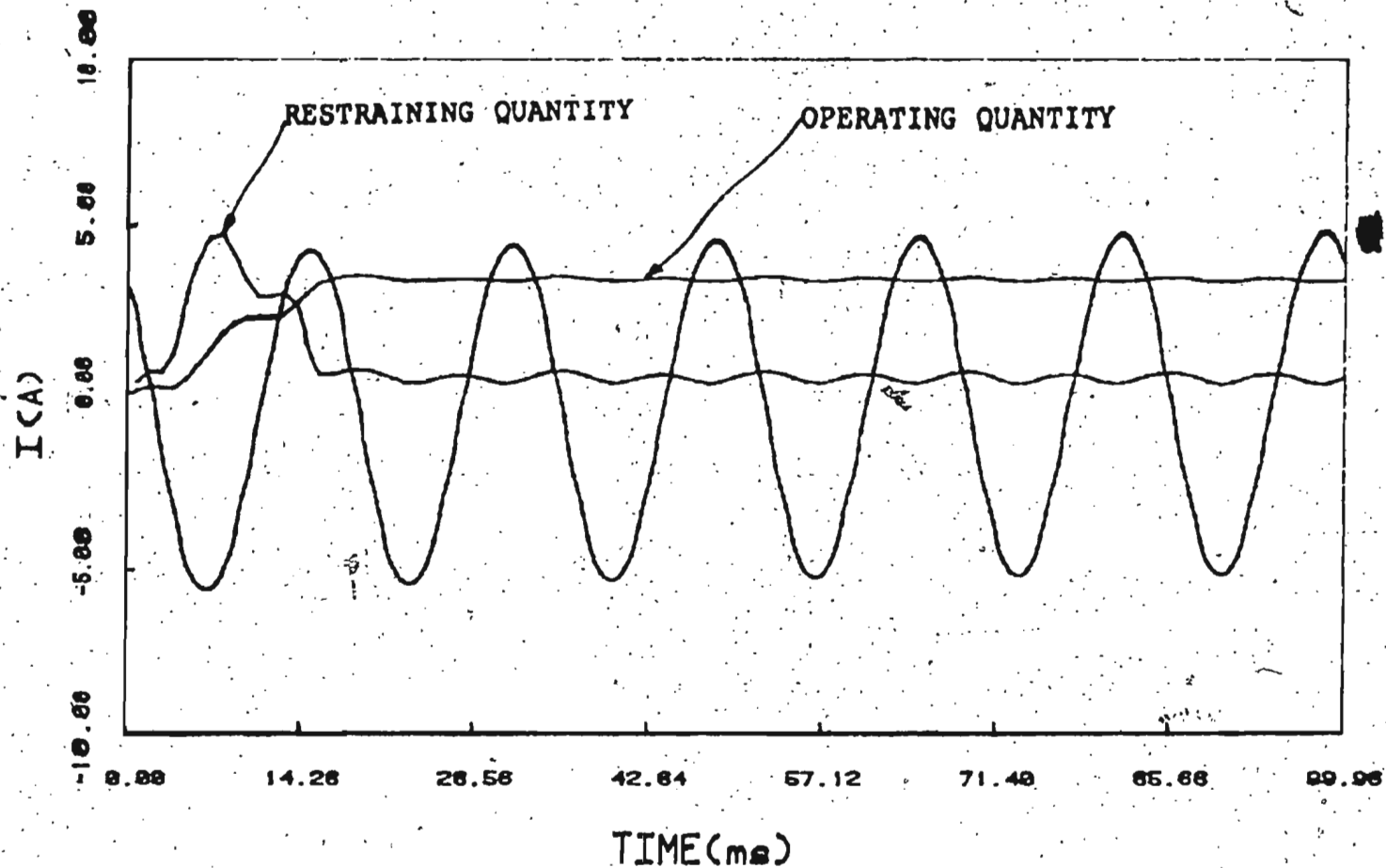


Fig. 4.16 (c) Performance of Walsh function algorithm with 16 samples/cycle during an internal fault (fault initiation angle -  $180^\circ$ )

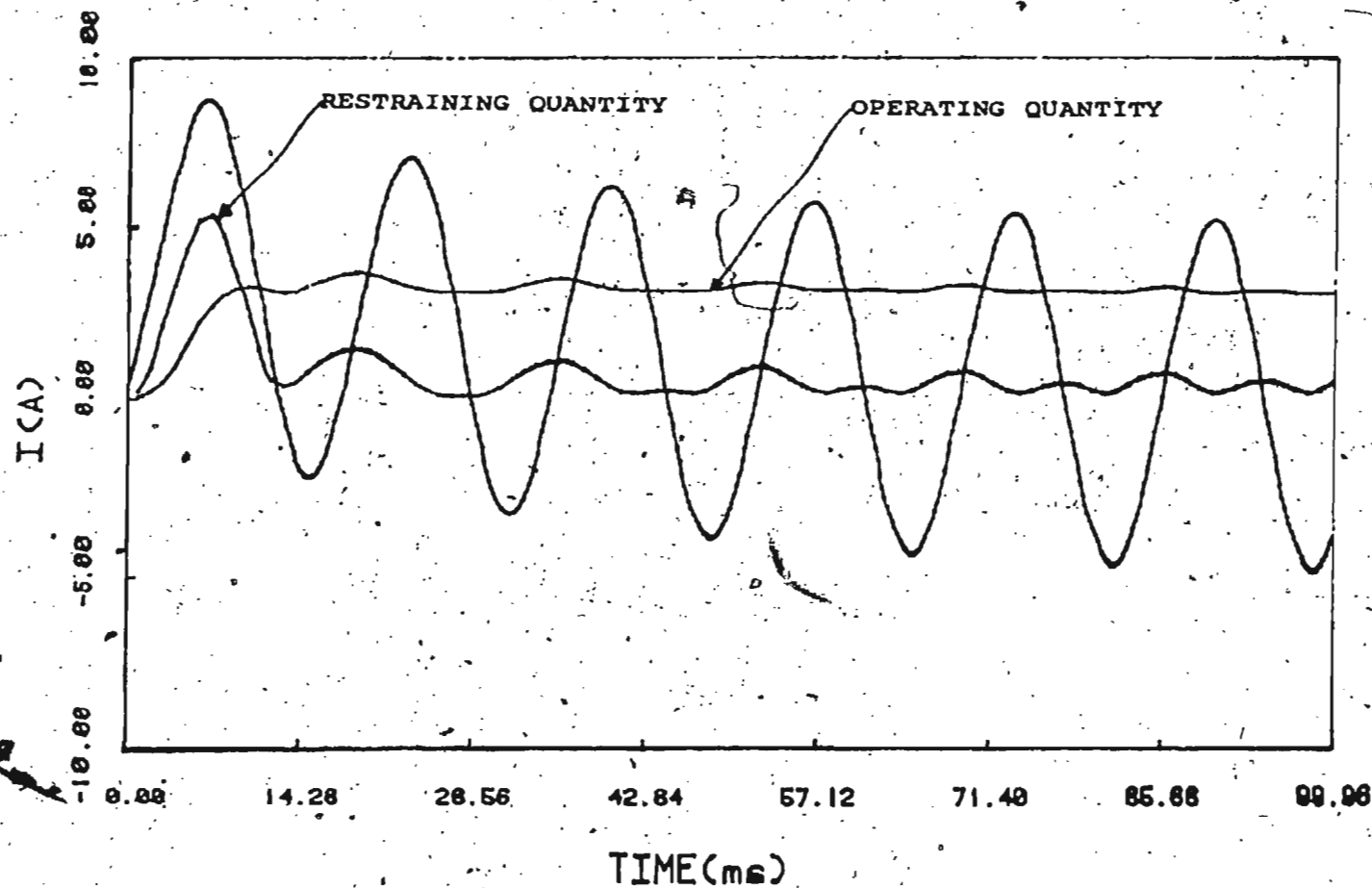


Fig. 4.17. Performance of Walsh function algorithm with 16 samples/cycle during an assymetrical internal fault (fault initiation angle -  $0^\circ$ )

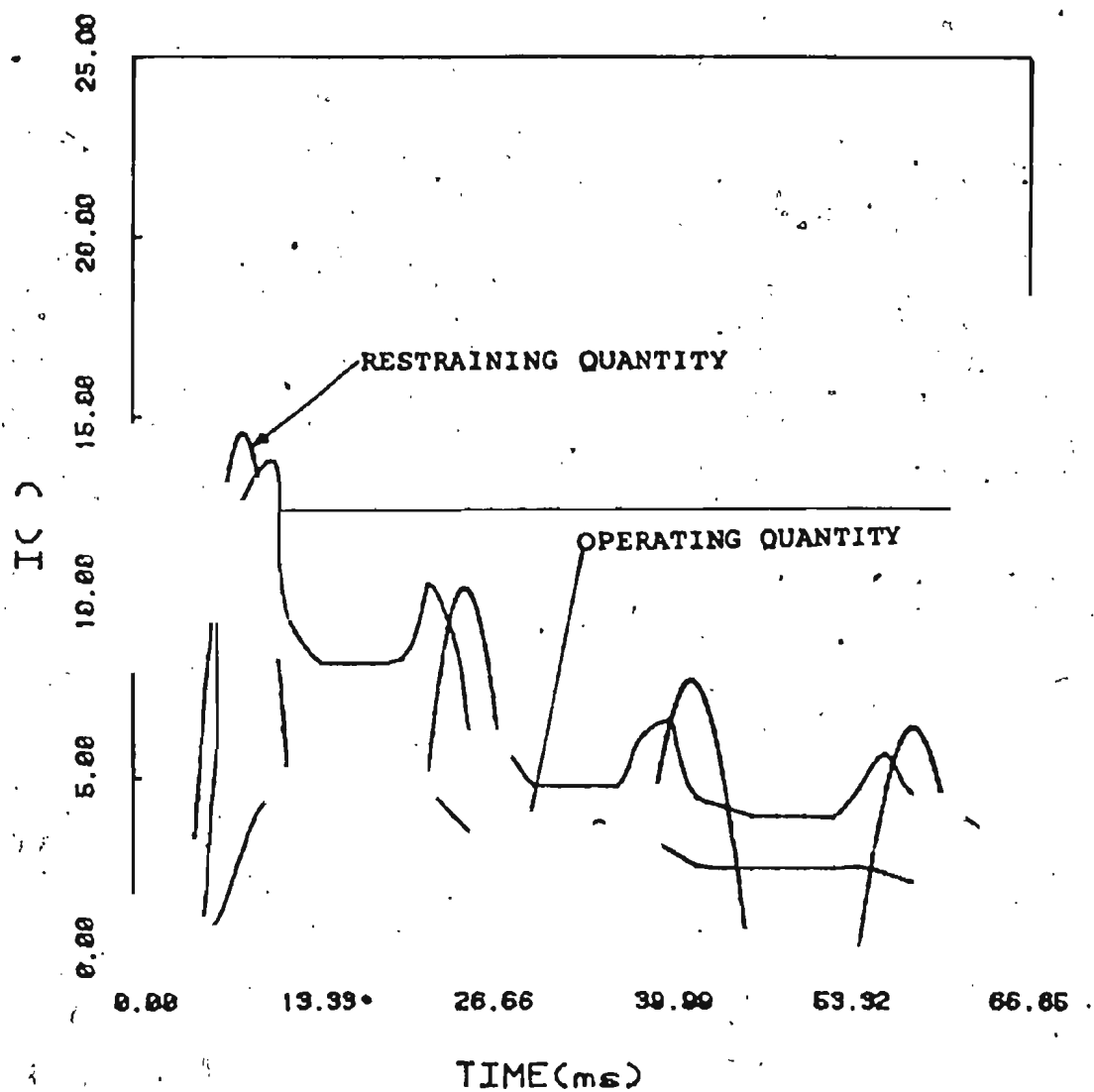


Fig. 4.18 (a) Performance of Walsh function algorithm with 8 samples/cycle during inrush in phase-a of a Y-Δ transformer

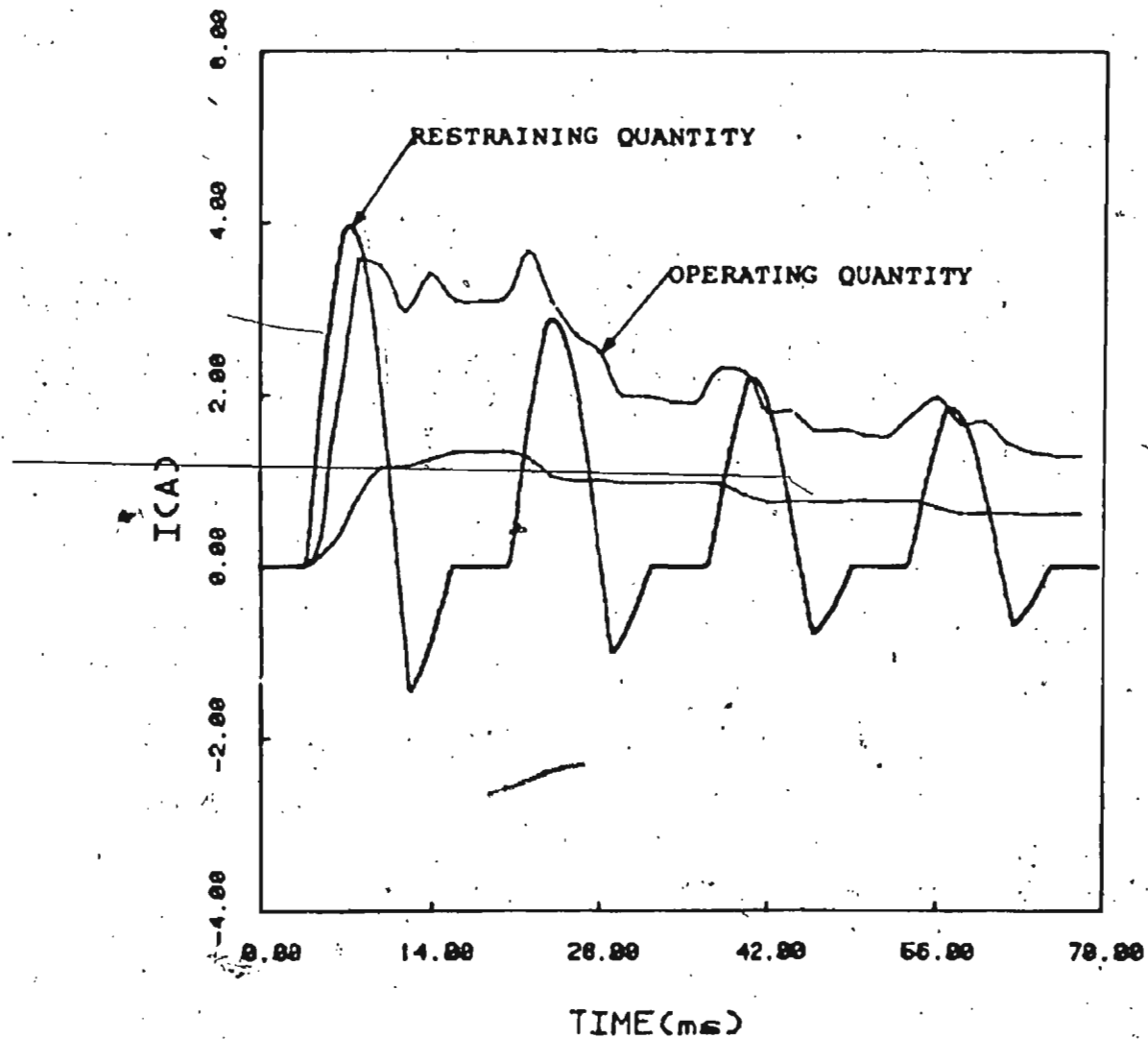


Fig. 4.18 (b) Performance of Walsh function algorithm with 8 samples/cycle during inrush in phase-b of a Y-A transformer

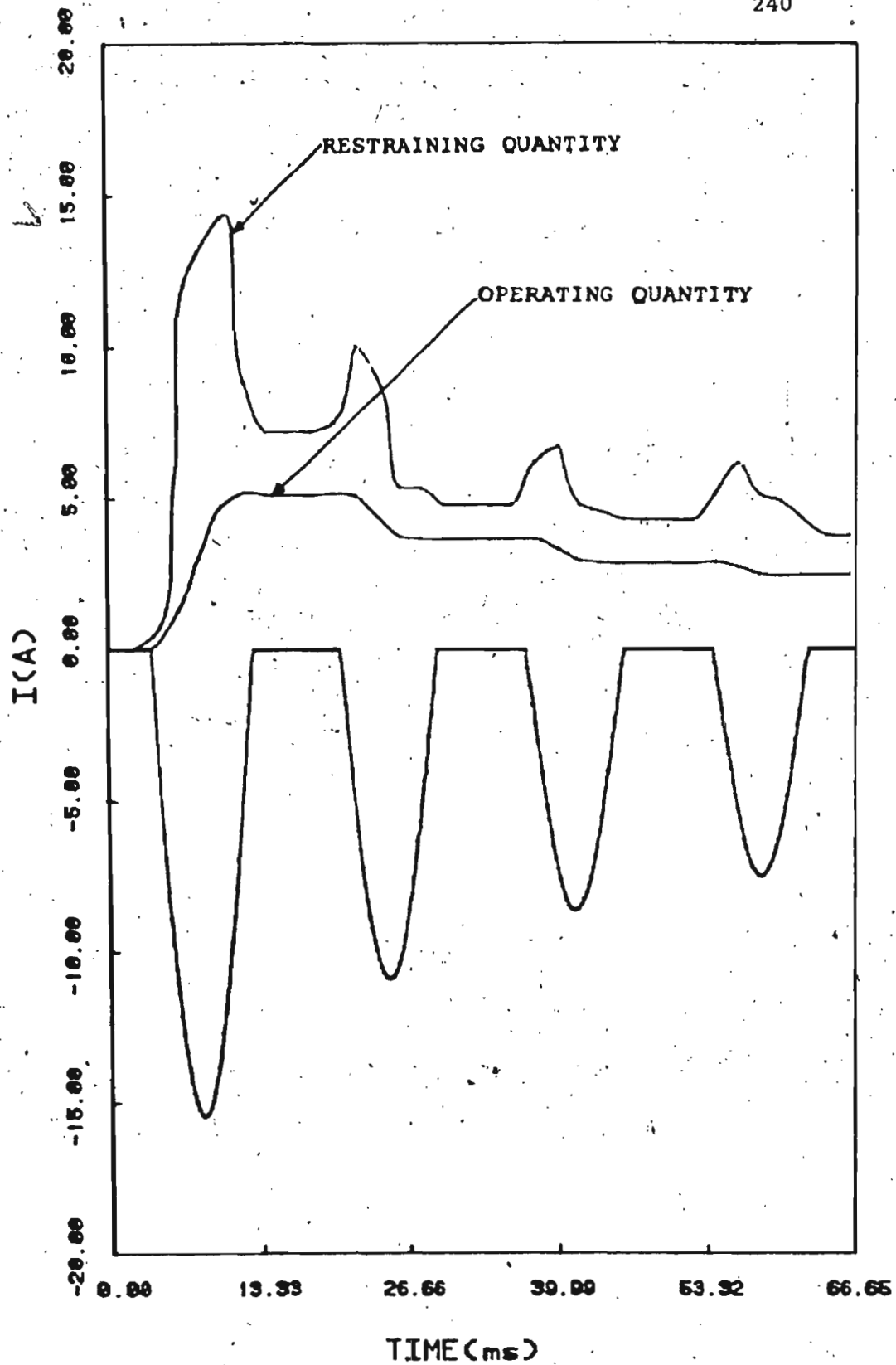


Fig. 4.18 (c) Performance of Walsh function algorithm with 8 samples/cycle during inrush in phase-c of a Y-Δ transformer



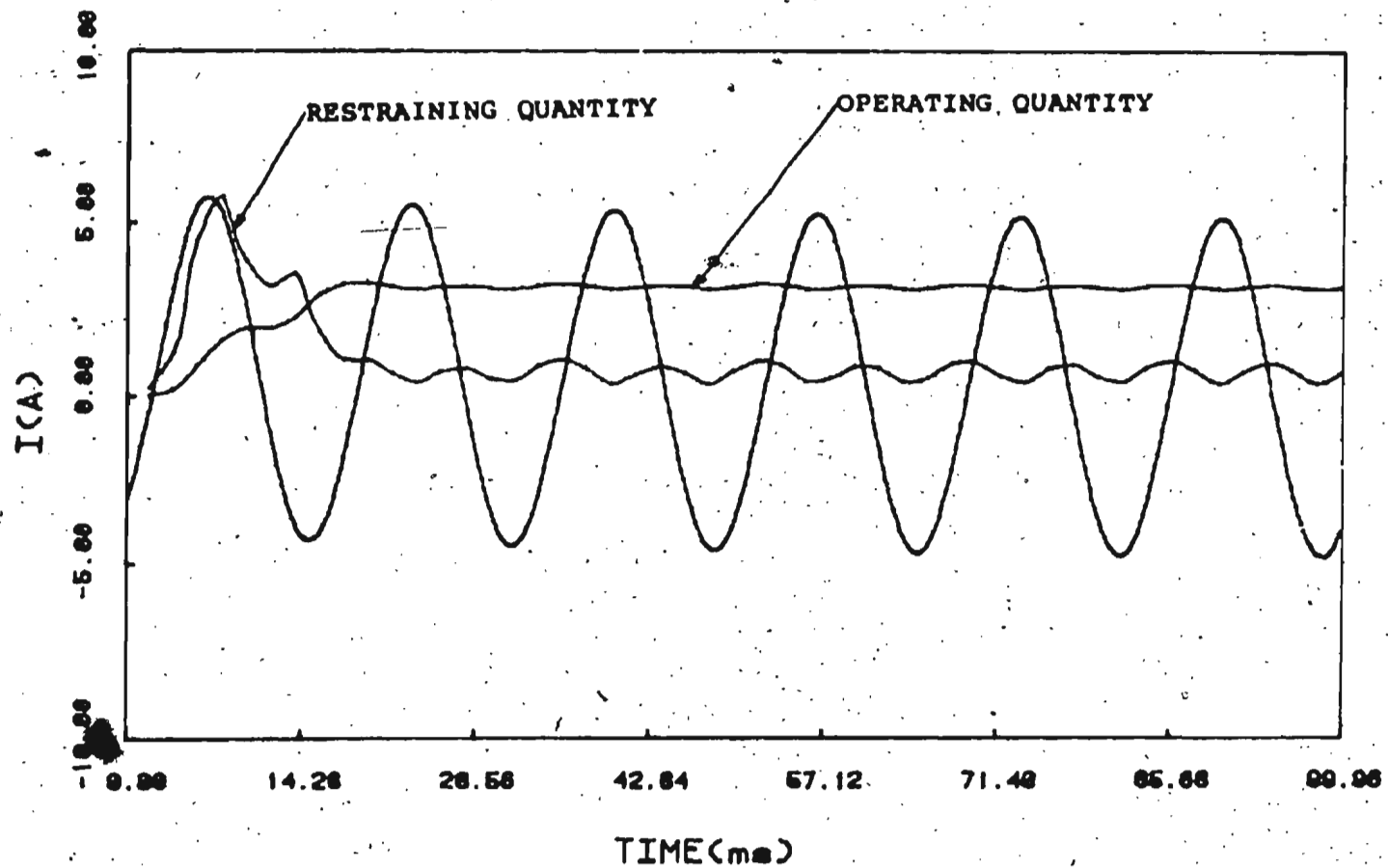


Fig. 4.19 (a) Performance of Walsh function algorithm with 8-samples/cycle during an internal fault (fault initiation angle -  $0^\circ$ )

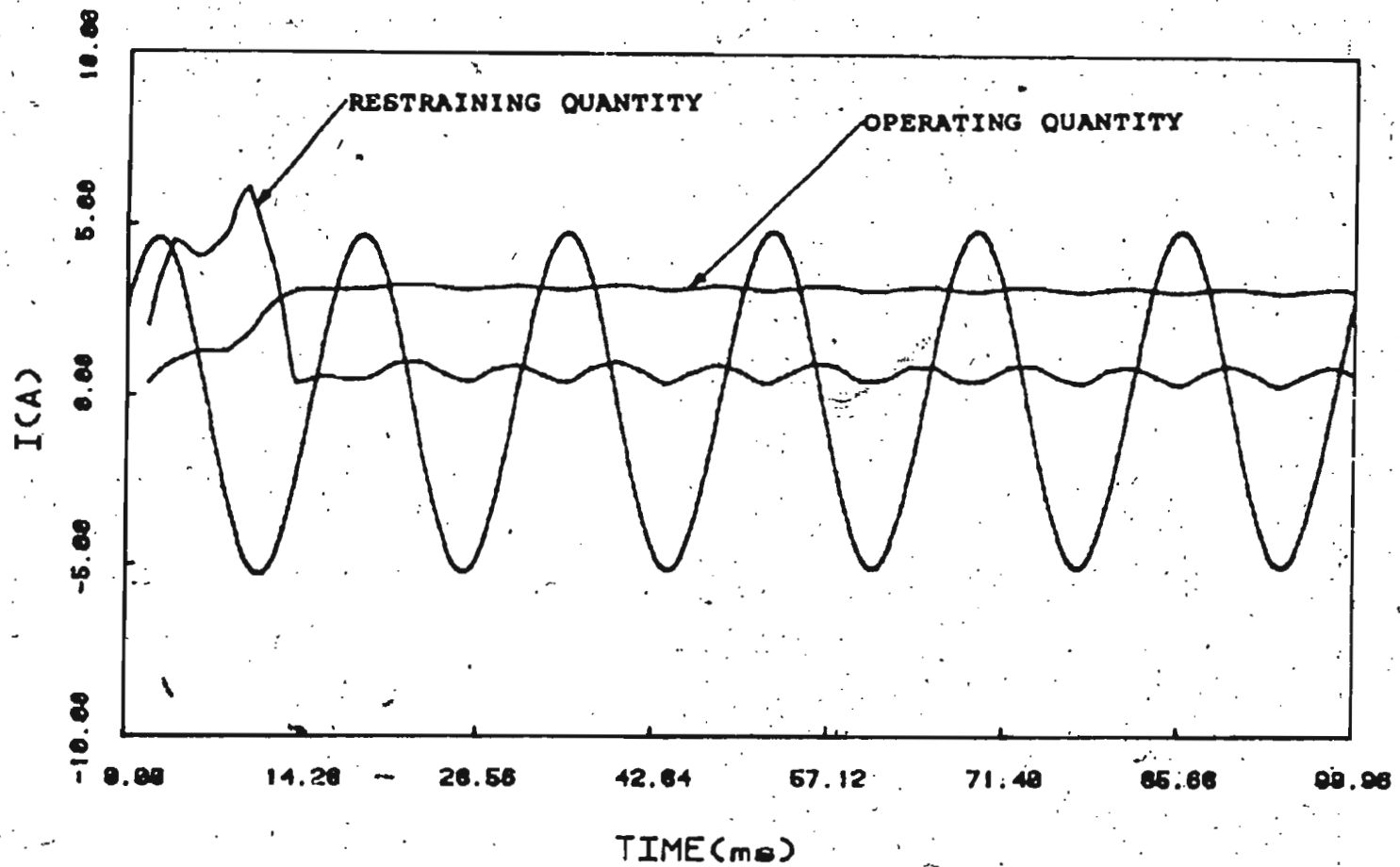


Fig. 4.19 (b) Performance of Walsh function algorithm with 8 samples/cycle during an internal fault (fault initiation angle -  $90^\circ$ )

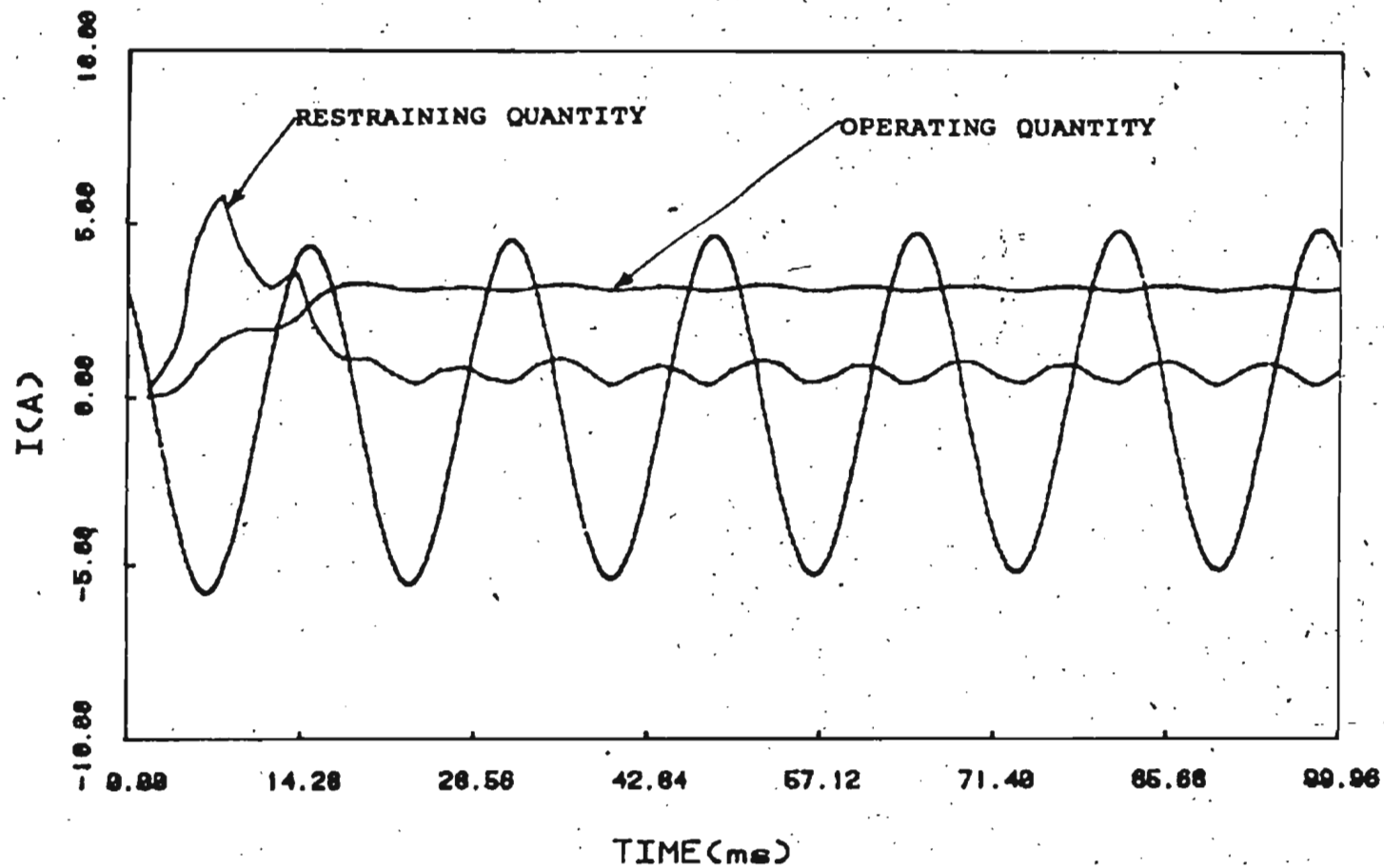


Fig. 4.19 (c) Performance of Walsh function algorithm with 8 samples/cycle during an internal fault (fault initiation angle -  $180^\circ$ )

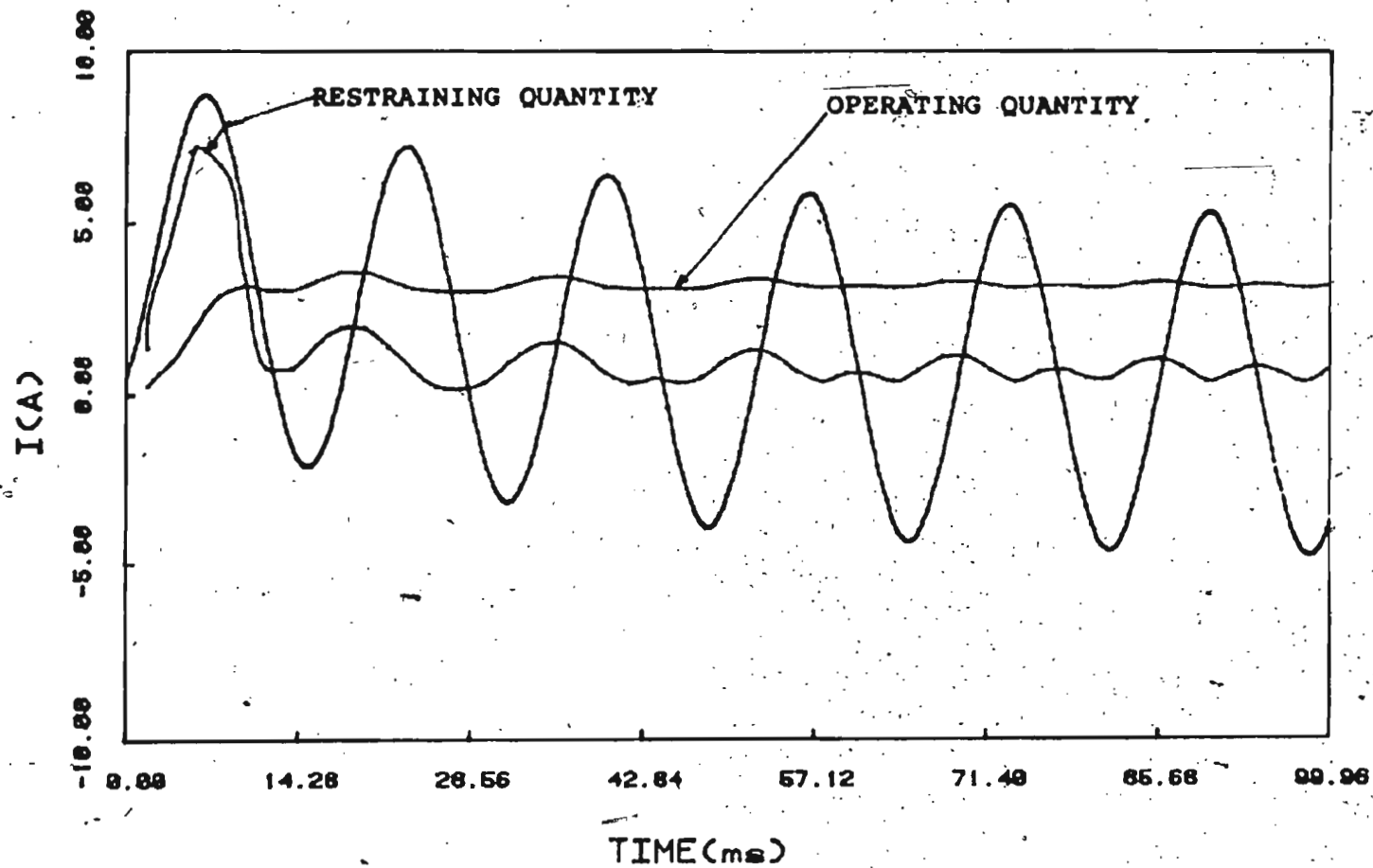


Fig. 4.20 Performance of Walsh function algorithm with 8 samples/cycle during an assymetrical fault (fault initiation angle -  $0^\circ$ )

could not be compared with an intermediate sampling rate of 12 samples/cycle. Rectangular transform can be applied with sampling rate of 12 samples/cycle. But Walsh transform is a binary function and valid for numbers of the order of  $2^x$ , where  $x$  is any positive integer. Hence, the function is not valid for 12 samples/cycle sampling rate. This is a shortcoming of the Walsh Function from the point of view of sampling rate.

For the purpose of digital relaying, these transforms can be compared from two basic points of view,

- (1) Convergence time of Algorithms,
- (2) Suitability on microprocessor applications.

(1) Convergence time

This is an inherent property of the algorithms due to which a transform converges during an internal fault of a transformer. In the time domain, the time when the 2nd harmonic quantity becomes less than the fundamental and after that remains less than the fundamental, is termed as convergence time. Initially, for all the transforms, the restraining quantity is greater than the operating quantity. This is due to the fact that, data window starts filling with substantial amount of fault data after half a cycle, restraining quantity starts coming down and approximately within  $\frac{3}{4}$ th of a cycle, it converges below the operating value.

The convergence times of the algorithms are summarized in Table 4.1, which takes into account all the types of faults described earlier. It also includes other conditions of fault inception angles which are not shown in previous sections. Table 4.2 compares the convergence time of the transforms in case of an asymmetrical fault, initiated at  $\lambda=0^\circ$ .

It is seen from Tables 4.1 and 4.2, that the transforms converge more rapidly in case of an asymmetrical fault rather than a sustained fault. Again, with a sampling rate of 16 samples/cycle, the convergence time is lower than that of 8 samples/cycle of sampling rate. This is due to the reason that the in between samples are missing in the case of lesser sampling rate and it requires more time for the data window to be filled with actual fault data.

Walsh function has one short-coming in that aspect that it loses more number of samples than other algorithms because of the undefined state of the function at the time of sign change as described earlier in the text. Hence more valuable information are missing in this aspect.

Rectangular transform gives the best convergence time than the other two algorithms under any conditions of fault initiation. However, all the transforms converge in time less than a cycle on a 60Hz waveform.

## (2) Suitability on Microprocessor Applications

Convergence time of a transform is not the operating time of a relay. Operating time depends on the computational burden involved in any algorithm. With the earlier development of digital relays, suitable algorithms were tried in 8-bit microprocessors. But now-a-days, 16-bit microprocessors are available. With any algorithm, there are some minimum computations which cannot be avoided. The rest is dependent on the software techniques used to minimize the computational burden.

In general, it is adviseable to work with lower sampling rate to provide higher sampling interval, so that, even in a slow processor, the time of computation per sample, remains well within the sampling interval. Again, it is a trade-off between accuracy and time.

In the Rectangular Transform technique the time consuming computations of the Fourier Transform have been simplified by replacing sine-cosine terms by  $\pm 1$  and 0. Most of the coefficients are computed apriori and stored in a RAM. With a sampling rate of 16 samples/cycle, apparently 14 additions or subtractions, 16 multiplications, 2 shift instructions and 2 square roots are involved per sample of calculation. With a sampling rate of 8-samples/cycle, again almost that much amount of computations are involved. With Discrete Fourier Transform technique, apparently the same

amount of computations are required as in Rectangular Transform if in the original Fortran programming is considered. But the nature of constants which appear in the Discrete Fourier technique, needs for shift instructions more than Rectangular while being translated in Assembly language for any processor.

In that aspect, in Walsh Transform technique, additions and subtractions are more. This is due to the reason that the samples are being set to zero in between the computations. Hence, no generalized technique in programming like D.F.T. or Rectangular technique is possible in such a case. With a sampling rate of 16 samples/cycle, apparently 100 additions and subtractions, 22 shift, 14 multiplications and 2 square roots are involved per sample calculations. However, this can be minimized to a certain extent by storing the similar type of additions in load accumulators but separate "move" instructions are needed to utilize those quantities. With a sampling rate of 8 samples/cycle, the computation per sample needs 31 additions or subtractions, 12 shift instructions, 11 multiplications and 2 square roots. One advantage of this method over the rectangular or D.F.T. technique is that various constants need not be stored in RAM which requires sometimes more computation time for a slow processor to move those constants. Rather, the computation is straight forward in the Walsh function technique which can



be readily applied in any processor. Now-a-days, co-processor like Intel-8087 is available to work along with Intel-8088 such as in IBM PC. This simplifies the computational difficulty to a great extent. Once again, it is a trade-off between algorithms and type of processor used to achieve a favorable result.

Table 4.1: Comparison of Convergence Times of Algorithms  
In Case of a Symmetrical Fault

Fault Angles		0°	30°	60°	90°	120°	150°	180°
Discrete Fourier (16 samples /cycle)		13.8 ms	12.8 ms	11.8 ms	11.8 ms	11.8 ms	11.8m/s	13.8 ms
Rec-tan-gular	16 Samp. /cycle	12.8 ms	12.8 ms	11.8 ms	10.8 ms	10.8 ms	10.8 ms	12.8 ms
Trans-form	8 Samp. /cycle	13.8 ms	13.8 ms	11.8 ms	11.8 ms	11.8 ms	11.8 ms	13.8 ms
Walsh Trans-form	16 Samp. /cycle	13.8 ms	13.8 ms	12.8 ms	11.8 ms	11.8 ms	11.8 ms	13.8 ms
	8 Samp. /cycle	15.8 ms	15.8 ms	13.8 ms	13.8 ms	13.8 ms	15.8 ms	15.8 ms

Table 4.2: Comparison of Convergence Times of Algorithms  
In Case of An Assymetrical Fault (Fault  
Initiation Angle =  $0^\circ$ )

Transform (Samples /Cycle)	D.F.T. (16)	Rectangular (16)	Rectangular (8)	Walsh (16)	Walsh (8)
Convergence Time (ms)	8.8	8.8	9.8	9.8	11.8

## CHAPTER 5

SUMMARY AND CONCLUSIONS5.1 Conclusions

The entire thesis may be divided into two major parts,

(1) Analysis of the magnetizing inrush current phenomena of transformers as well as their digital simulation for testing of relay algorithms.

(2) Development of algorithms for digital protection of transformer.

The analysis of magnetizing inrush currents in single phase transformers is first carried out. Detailed mathematical formulations have been given to predict single phase inrushes. Equations derived by Specht [35] have been modified taking into account the generalized reference axes.

One shortcoming of the Specht equations is that all equations were derived assuming that switching has been done at zero degree on the voltage waveform. That shortcoming has been eliminated by deriving a generalized expression of inrush current where switching may be carried out at any arbitrary angle on the voltage waveform. Determination of saturation angle for any inrush cycle is a problem. This is due to the fact that saturation angle is dependent on the residual flux associated with the core from the previous.

turnoff. A numerical technique is carried out to determine the saturation angle with the knowledge of conduction angle of any particular inrush cycle. Resistance to reactance ratio of the flux path also changes from cycle to cycle of inrush current, which is difficult to ascertain experimentally. This has also been determined by an iterative program. These methods are used for modelling a particular measured inrush for accurate testing of algorithms. Having determined the above parameters, experimental waveforms are simulated digitally, keeping the saturation angles, conduction angles and inrush peaks in different cycles identical.

Both the measured and the simulated waveforms are analyzed on a Hewlett Packard-5451B Fourier Analyzer System in order to determine the harmonic contents of the individual cycles. The respective harmonic contents of the simulated and the measured waveforms are different for two reasons. Firstly, the measured waveforms are not as smooth and uniform as the simulated waveforms which have been shown in the text. Non-uniformities are present in most of the measured waveforms which are mainly responsible for the difference in harmonics. This is due to the fact that simulated results are based on some mathematical formulation which yields the uniform waveshapes. Secondly, the signal to noise ratio of the recording magnetic tapes is one of the main sources of

discrepancy in harmonics in the measured waveforms. These are not prominent in the lower harmonics but are mainly reflected in higher harmonics.

For three phase transformers, an analysis of the magnetizing inrush is carried out using two methods. The first method is the sequence impedance method by which individual phase simulation can be carried out under different connection modes of the transformers. Rockefeller [33] derived the basic formulation of three-phase inrush in this method but he suggested a graphical way of deriving individual phase inrushes. Use of digital simulation of individual phases applying the formulation for single phase inrush has been attempted first in this section. The ultimate line inrush currents, which are the resultant effect of phase inrushes, depend upon the correct choice of sequence impedances. The line inrushes are simulated using a different routine. In this section, special behaviour in the B-phase of a Y-connected primary is dealt with in detail when the A-phase is switched on at zero degree angle. Different routines used for simulation purposes have been explained using flow-charts.

In the second method, mutual couplings between the phases are considered and mathematical formulations are carried out on the basis of nine differential and five algebraic basic equations. The solution for inrush currents

is found in a closed differential matrix form and has been solved using standard Runge-Kutta routine. This method has the advantage of simulating the three phase inrush currents using a single program, but its disadvantage lies in ascertaining the correct values of mutual couplings in different cycles of the inrushes as the mutual couplings change in various cycles. Measured waveforms and the corresponding simulated waveforms are then analyzed using a Fourier Analyzer. In both the single-phase and three-phase cases, the 2nd harmonic contents are always higher in the measured waveforms. Hence, it is ensured that when the algorithm restrains the relay during inrush on simulated test data on the 2nd harmonic restraint principle, it will definitely restrain the relay in real time performance.

Three algorithms were then considered for harmonic restraint digital relay. These are,

- (1) Discrete Fourier Transform(D.F.T.)
- (2) Rectangular Transform
- (3) Walsh Transform

Mathematical formulation of all these three algorithms were derived individually. Analysis and performance of the algorithms were done on simulated fault and magnetizing inrush data. Walsh Transform is the technique which is for the first time tried here for transformer protection purposes. The D.F.T. has been considered here as a reference

frame for comparing the performance of the other two algorithms but is not recommended for protection purpose. This is due to the fact that the D.F.T. has a comparatively high computational burden on normal processors which is difficult to carry out without special arrangements like co-processors. On the other hand, the suitability of other two algorithms are considered on microprocessor based transformer protection. That is why, D.F.T. is tested with a sampling rate of 16 samples/cycle basis, whereas Rectangular and Walsh Transforms are tried with sampling rates of both 16 and 8 samples/cycle. For all types of internal faults, the transforms converge within  $3/4$  the of a cycle on a 60 Hz waveform. This is quite a satisfactory result. The suitability of application of the algorithms is a trade off between the processor used and computational burden involved in an algorithm, as each of the algorithms has its own merits. In Rectangular Transform, the sine-cosine terms of the D.F.T. have been replaced with 1 and 0 and the recursive routine for computation is simple. The respective 1 and 0's are computed apriori and stored in the RAM. For Walsh Transform, no such apriori computations are needed. The calculations are straight-forward and mainly involves additions and subtractions. But Walsh Transform suffers from three main shortcomings while compared with Rectangular Transform:



- (1) The number of computations per sample is higher.
- (2) Valuable information are missing as the samples are set to zero where the function changes it's sign from  $\pm 1$  to  $\mp 1$ . This is because Walsh Function is undefined where it changes its state.
- (3) It is a binary function. So, Walsh function cannot be carried out with sampling rates which are not of the order of  $2^x$ . For example, it cannot be carried out with a sampling rate of 12 samples/cycle. The convergence time taken by the three algorithms for faults with different fault-initiation angles are given in a tabular form in the text. It is observed from the table that the rectangular transform yields the best result. The advantage of Walsh function technique is that it can be implemented even in a simple processor as the computations involve mainly additions and subtractions.

Finally, group-work was carried out to implement two of the algorithms on a 16-bit IBM Personal Computer on simulated data. This section is beyond the scope of this thesis and is briefly discussed here. A co-processor Intel-8087 is jointly used with Intel-8088 processor as the CPU. The advantage of using the 8087 co-processor is to ease the computational burden. Besides, programming is done in Assembly Language, with every attempt to reduce unnecessary

computations. Rectangular Transform technique is tried with 8 samples/cycle sampling rate. In such a case, the sampling interval is 2083  $\mu$ s on a 60 Hz waveform. The computations took time approximately 510  $\mu$ s. All the simulated data were stored in RAM. In real time situation, approximately 50 to 100  $\mu$ s are to be allowed for A/D conversion. Still, quite a fair amount of margin is available in the sampling interval. Walsh functions are tried with 16 samples/cycle sampling rate. The necessary additions and subtraction routines are minimized in Assembly program than those appear in the original Fortran program. Here, the sampling interval is 1042  $\mu$ s on a 60 Hz waveform. Computation time required is approximately 790  $\mu$ s. Hence, if the co-processor is available, use of either Rectangular or Walsh Transform with a sampling rate of 16 samples/cycle is recommended as it will increase reasonable accuracy within the limited sampling time interval. Also, the convergence time for 16 samples/cycle is better than 8 samples/cycle for either of these two algorithms described above.

## 5.2 Scope of Future Works

Few necessary work was not carried out to fulfil this topic as it is beyond the scope of this thesis and hence, certain suggestions are to be given for further research.

All testings of the above algorithms are carried out on simulated data and no attempt is made to interface the microcomputer with a transformer and test the relay with any of the above algorithms. It may be suggested to test first any laboratory transformer using any of the algorithms described in the thesis and with a proper interface with the microprocessor. For proper interfacing with either a single-phase or a three-phase transformer, the basic circuit requirements are described in the text. Those are the basic items but selection of the elements like A/D, sample-hold etc. should be made from a design point of view of the interface which will depend on the system that will be used. No C.T. saturation effect is being considered in testing the performance of the algorithms on simulated data. But in actual practice, C.T. saturation effects are to be considered. Sometimes, saturation of C.T. distort the actual waveform in the secondary side. Algorithms were not tested in such conditions. Prior testing is needed for such conditions on simulated data, before the relay is being tested on a fault.

A/D as well as computer output ports are to be well protected from spurious surges from analog signals by proper logic circuitry. These logic circuits will attenuate the circuitry spurious signals which can hamper the computer relay. Proper thyristor bridges are to be used to initiate

circuit-breaker. The trip signal, initiated by digital relay will be used to fire the gatings of thyristors and ultimately energize the trip coil of circuit-breakers.

Certain suggestions can be made for simulation also. Performance testing of the algorithms were carried out on simulated data of a laboratory transformer. For a large power transformer, internal fault may be more assymetrical with a slow-decay rate. In such a case fault current will be highly offset from the X-axis for more number of cycles. The performance of the algorithms are to be tested on simulated data under such conditions.

Operating time of digital relay has been considered once the fundamental became higher than the 2nd harmonic component, the latter being multiplied with the weighting factor. This is an one-sample decision. In actual practice, it will not be prudent to take trip-decision based on one sample under any circumstances. In case of a fault, a digital relay should always look for two more samples after the convergence point of any algorithm before it initiates a trip-signal.

## APPENDIX A

INTERNAL CONNECTION DIAGRAMS FOR STANDARD  
PERCENTAGE BIASED DIFFERENTIAL RELAY

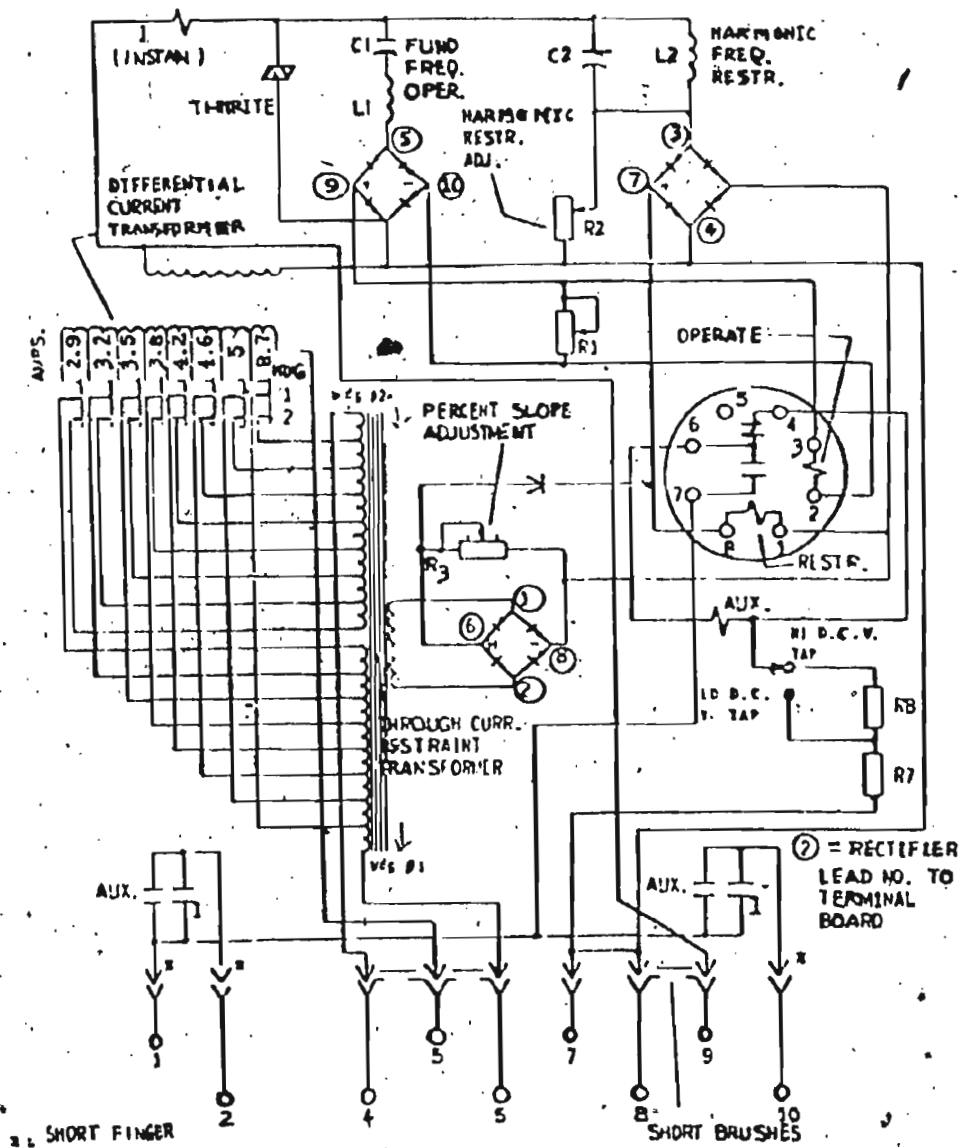


Fig. A.1: Internal connections for GE make harmonic restraint percentage biased differential relay, type BDD15B

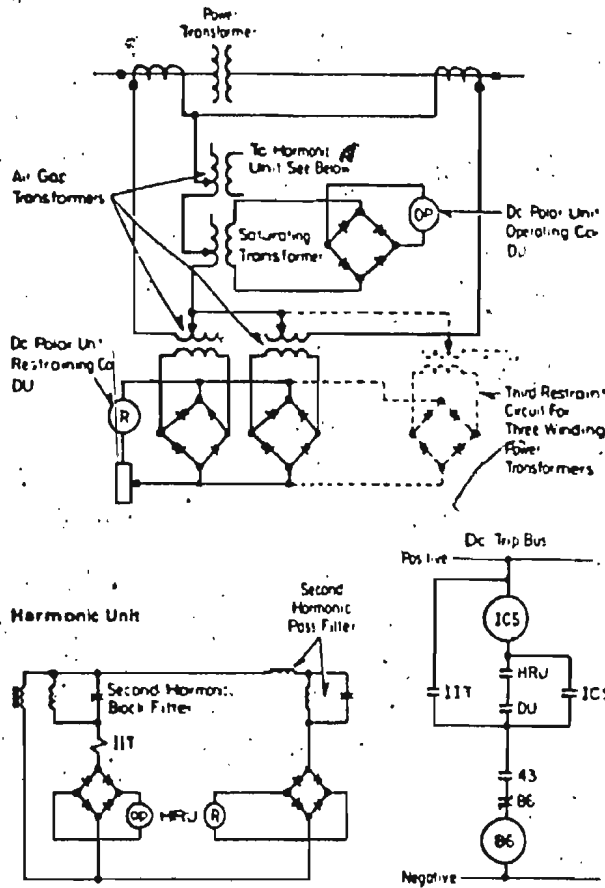


Fig. A.2: Schematic connections of the Westinghouse make harmonic restraint percentage biased differential relay type HU-1(36)

## APPENDIX B

DEVELOPMENT OF MAGNETIZING INRUSH EQUATIONS  
FOR SINGLE AND THREE-PHASE TRANSFORMERS

B.1 Development of Magnetizing Inrush Equations For a  
Single-Phase Transformer.

Case A: Switching at  $\lambda=0^\circ$

Let the applied voltage be

$$e = \sqrt{2} E \sin \omega t \quad (B.1)$$

Hence from Fig. 3.5(c), the voltage equation of the circuit can be written as,

$$e = \sqrt{2} E \sin \omega t = Ri + L \frac{di}{dt} \quad (B.2)$$

where,  $E$  = R.M.S value of applied voltage. The forced component, i.e. steady state value of the current of Eqn. (B.2) is

$$i_F = I_{\max} \sin (\omega t - \phi) \quad (B.3)$$

where,

$$I_{\max} = \frac{\sqrt{2} E}{Z} = \frac{\sqrt{2} E}{\sqrt{(R^2 + X^2)}}$$

$$\phi = \tan^{-1} \frac{X}{R}, \quad X = \omega L$$

The complementary function is obtained from Eqn. B.2 as,

$$Ri + L \frac{di}{dt} = 0$$

or

$$\frac{di}{dt} + \frac{R}{L} i = 0 \quad (B.4)$$

The solution of Eqn. B.4 is given as

$$i_N = Ae^{-\frac{R}{L}t} \quad (B.5)$$

where,

A = integration constant

$$i = i_F + i_N \quad (B.6)$$

substituting the values,

$$i = \frac{\sqrt{2}E}{Z} \sin(\omega t - \phi) + Ae^{-\frac{R}{L}t} \quad (B.7)$$

From Fig. 3.6(a), the current is zero at  $\omega t = \theta_{sl}$ , so that

$t = \frac{\theta_{sl}}{\omega}$ . Hence, from Eqn. (B.7),

$$0 = \frac{\sqrt{2}E}{Z} \sin(\theta_{sl} - \phi) + Ae^{-\frac{R\theta_{sl}}{\omega L}} \quad (B.8)$$

From Eqn. (B.8),

$$\begin{aligned} A &= \frac{-\sqrt{2}E \sin(\theta_{sl} - \phi)}{Z \cdot e^{-\frac{R\theta_{sl}}{\omega L}}} \\ &= -\frac{\sqrt{2}E}{Z} \cdot \sin(\theta_{sl} - \phi) \cdot e^{\frac{R\theta_{sl}}{\omega L}} \end{aligned} \quad (B.9)$$

Hence, substituting the value of 'A' in Eqn (B.7),

$$\begin{aligned} i &= \frac{\sqrt{2}E}{Z} \sin(\omega t - \phi) - \frac{\sqrt{2}E}{Z} \sin(\theta_{sl} - \phi) \\ &\quad \cdot e^{\frac{R\theta_{sl}}{\omega L}} \cdot e^{-\frac{Rt}{L}} \\ &= \frac{\sqrt{2}E}{Z} [\sin(\omega t - \phi) - e^{\frac{R}{X}(\theta_{sl} - \omega t)} \cdot \sin(\theta_{sl} - \phi)] \end{aligned} \quad \dots(B.10)$$



Now, expanding Eqn. (B.10),

$$i = \frac{\sqrt{2}E}{Z} [\sin \omega t \cos \phi - \cos \omega t \sin \phi - e^{\frac{R}{X}(\theta_{sl} - \omega t)} \cdot (\sin \theta_{sl} \cos \phi - \cos \theta_{sl} \sin \phi)] \dots (B.11)$$

Now  $\phi = \tan^{-1} \frac{X}{R}$ ,  $\cos \phi = \frac{R}{Z}$ ,  $\sin \phi = \frac{X}{Z}$

From Eqn. (B.11)

$$\begin{aligned} i &= \frac{\sqrt{2}E}{Z} \left[ \frac{R}{Z} \sin \omega t - \frac{X}{Z} \cos \omega t - e^{\frac{R}{X}(\theta_{sl} - \omega t)} \cdot \left( \frac{R}{Z} \sin \theta_{sl} - \frac{X}{Z} \cos \theta_{sl} \right) \right] \\ &= \frac{\sqrt{2}E}{Z} \left[ \frac{1}{Z} (R \sin \omega t - X \cos \omega t - e^{\frac{R}{X}(\theta_{sl} - \omega t)} \cdot (R \sin \theta_{sl} - X \cos \theta_{sl})) \right] \end{aligned} \quad (B.12)$$

Multiplying both numerator and denominator of Eqn. (B.12) by 'X', the following results,

$$\begin{aligned} i &= \frac{\sqrt{2}EX}{Z^2} \left[ \frac{R}{X} \sin \omega t - \cos \omega t - e^{\frac{R}{X}(\theta_{sl} - \omega t)} \cdot \left( \frac{R}{X} \sin \theta_{sl} - \cos \theta_{sl} \right) \right] \end{aligned} \quad (B.13)$$

The current goes to zero at  $\omega t = \alpha$ . Thus,

$$i = 0, \text{ at } \omega t = \alpha$$

From Eqn. (B.13),

$$\frac{R}{X} \sin \alpha - \cos \alpha - e^{\frac{R}{X}(\theta_{sl} - \alpha)} \left( \frac{R}{X} \sin \theta_{sl} - \cos \theta_{sl} \right) = 0 \quad (B.14)$$

Let  $\theta_{sl} = \alpha - \gamma$

Substituting in Eqn. (B.14),

$$\frac{R}{X} \sin \alpha - \cos \alpha - e^{\frac{R}{X} \gamma} \left[ \frac{R}{X} \sin(\alpha - \gamma) - \cos(\alpha - \gamma) \right] = 0 \quad (B.15)$$

Expanding Eqn. (B.15),

$$\begin{aligned} \frac{R}{X} \sin \alpha - \cos \alpha - e^{\frac{R}{X} \gamma} \left[ \frac{R}{X} (\sin \alpha \cos \gamma - \cos \alpha \sin \gamma) \right. \\ \left. - \cos \alpha \cos \gamma - \sin \alpha \sin \gamma \right] = 0 \end{aligned} \quad (B.16)$$

Separating  $\sin \alpha$  and  $\cos \alpha$  terms

$$\begin{aligned} \sin \alpha \left[ \frac{R}{X} - \frac{R}{X} e^{-\frac{R}{X} \gamma} \cos \gamma + e^{-\frac{R}{X} \gamma} \sin \gamma \right] \\ - \cos \alpha \left[ 1 - \frac{R}{X} e^{-\frac{R}{X} \gamma} \sin \gamma - e^{-\frac{R}{X} \gamma} \cos \gamma \right] = 0 \end{aligned}$$

From above,

$$\begin{aligned} \tan \alpha &= \frac{1 - \frac{R}{X} e^{-\frac{R}{X} \gamma} \sin \gamma - e^{-\frac{R}{X} \gamma} \cos \gamma}{\frac{R}{X} - \frac{R}{X} e^{-\frac{R}{X} \gamma} \cos \gamma + e^{-\frac{R}{X} \gamma} \sin \gamma} \\ &= \frac{e^{\frac{R}{X} \gamma} - \frac{R}{X} \sin \gamma - \cos \gamma}{\frac{R}{X} e^{\frac{R}{X} \gamma} - \frac{R}{X} \cos \gamma + \sin \gamma} \quad \dots (B.17) \end{aligned}$$

If the peak current occurs at an angle ' $\beta$ ', differentiating Eqn. (B.13), with respect to time results,

$$\begin{aligned}\frac{di}{dt} &= \frac{\sqrt{2}EX}{Z^2} \left[ \omega \frac{R}{X} \cos \omega t + \omega \sin \omega t + \frac{R}{X} e^{\frac{R}{X}(\theta_{sl} - \omega t)} \right. \\ &\quad \left. \left( \frac{R}{X} \sin \theta_{sl} - \cos \theta_{sl} \right) \right] \\ &= \frac{\sqrt{2}EX\omega}{Z^2} \left[ \frac{R}{X} \cos \omega t + \sin \omega t + \frac{R}{X} e^{\frac{R}{X}(\theta_{sl} - \omega t)} \right. \\ &\quad \left. \left( \frac{R}{X} \sin \theta_{sl} - \cos \theta_{sl} \right) \right] \\ &\dots (B.18)\end{aligned}$$

For maximum current,  $\frac{di}{dt} = 0$ ,  $\omega t = \beta$ . So, from Eqn. (B.18)

$$\frac{R}{X} \cos \beta + \sin \beta + \frac{R}{X} e^{(\theta_{sl} - \beta)} \left( \frac{R}{X} \sin \theta_{sl} - \cos \theta_{sl} \right) = 0$$

or

$$\begin{aligned}\frac{R}{X} e^{(\theta_{sl} - \beta)} \left( \frac{R}{X} \sin \theta_{sl} - \cos \theta_{sl} \right) &= - \left( \frac{R}{X} \cos \beta + \sin \beta \right) \\ &\dots (B.19)\end{aligned}$$

Substituting in Eqn. (B.13),

$$\begin{aligned}I_{pmax} &= \frac{\sqrt{2}EX}{Z^2} \left[ \frac{R}{X} \sin \beta - \cos \beta + \frac{X}{R} \left( \frac{R}{X} \cos \beta + \sin \beta \right) \right] \\ &= \frac{\sqrt{2}EX}{Z^2} \left[ \sin \beta \left( \frac{R^2 + X^2}{XR} \right) \right] \\ &= \frac{\sqrt{2}E}{X} \cdot \left( \frac{X}{R} \right) \sin \beta \\ &\dots (B.20)\end{aligned}$$

Case B: Switching at  $\lambda=180^\circ$

The applied voltage in this case is,

$$\begin{aligned}e &= \sqrt{2}E \sin (\pi + \omega t) \\ &= -\sqrt{2}E \sin \omega t. \\ &\dots (B.21)\end{aligned}$$

Hence, the voltage eqn. is

$$-\sqrt{2}E \sin \omega t = Ri + L \frac{di}{dt} \quad (B.22)$$

The forced component of current,

$$\begin{aligned} i_F &= -I_m \sin(\omega t - \phi) \\ &= -\frac{\sqrt{2}E}{Z} \sin(\omega t - \phi) \end{aligned} \quad (B.23)$$

The natural component of the current,

$$i_N = Ae^{-\frac{R}{L}t} \quad (B.24)$$

The total solution of Eqn. (B.22) is,

$$\begin{aligned} i &= i_F + i_N \\ &= -I_m \sin(\omega t - \phi) + A.e^{-\frac{R}{L}t} \end{aligned} \quad (B.25)$$

$i=0$  at  $\omega t = \theta_{sl}$ , the value of 'A' can be found as in Case A

$$A = \frac{\sqrt{2}E}{Z} \sin(\theta_{sl} - \phi) e^{\frac{R\theta_{sl}}{\omega L}} \quad (B.26)$$

Thus proceeding as in Case A,

$$i = -\frac{\sqrt{2}E}{Z} \left[ \sin(\omega t - \phi) - e^{\frac{R}{X}(\theta_{sl} - \omega t)} \sin(\theta_{sl} - \phi) \right] \quad \dots (B.27)$$

The Eqn. (B.27) can be expanded as in Case A,

$$\begin{aligned} i &= -\frac{\sqrt{2}EX}{Z^2} \left[ \frac{R}{X} \sin \omega t - \cos \omega t - e^{\frac{R}{X}(\theta_{sl} - \omega t)} \left( \frac{R}{X} \sin \theta_{sl} - \cos \theta_{sl} \right) \right] \\ &\dots (B.28) \end{aligned}$$

Again  $i=0$ , at  $\omega t=\alpha$ . From Eqn. (B.28),

$$\frac{R}{X} \sin \alpha - \cos \alpha - e^{\frac{R}{X}(\theta_{sl}-\alpha)} \left[ \frac{R}{X} \sin \theta_{sl} - \cos \theta_{sl} \right] = 0 \quad \dots (B.29)$$

Let ' $\gamma$ ' is the conduction angle. Hence, the value of ' $\alpha$ ' can be found in terms of ' $\gamma$ ' as before,

$$\tan \alpha = \frac{e^{\frac{R}{X}\gamma} - \frac{R}{X} \sin \gamma - \cos \gamma}{\frac{R}{X} e^{\frac{R}{X}\gamma} - \frac{R}{X} \cos \gamma + \sin \gamma} \quad (B.30)$$

If the current becomes maximum at an angle ' $\beta$ ', the value of maximum current can be found out by differentiating Eqn. (B.28) and setting it to zero as in Case A. So,

$$I_{pmax} = - \left( \frac{\sqrt{2}E}{X} \right) \left( \frac{X}{R} \right) \sin \beta \quad (B.31)$$

Case C: Switching at an arbitrary angle  $\lambda=\omega t$

With reference to Fig. 3.6(c), if the new axis of reference is from  $t'=0$ , so that

$$t' = t - \lambda / \omega,$$

then the transformed voltage equation is

$$e = \sqrt{2}E \sin (\omega t' + \lambda) \quad (B.32)$$

where,  $\omega t' = \omega t - \lambda$ .

The forced component of the current,

$$i_F = \frac{\sqrt{2}E}{Z} \sin (\omega t' + \lambda' - \phi) \quad (B.33)$$

And natural component,

$$i_N = Ae^{-\frac{R}{L}t'} \quad (B.34)$$

Hence, the total solution of the current is

$$i = i_F + i_N$$

$$= \frac{\sqrt{2}E}{Z} \sin(\omega t' + \lambda - \phi) + Ae^{-\frac{R}{L}t'} \quad (B.35)$$

$$i = 0, \text{ at } \omega t' = \theta_{sl}$$

or

$$t' = \frac{\theta_{sl}}{\omega},$$

' $\theta_{sl}$ ' being measured from  $t' = 0$ . From Equation (B.35)

$$0 = \frac{\sqrt{2}E}{Z} \sin(\theta_{sl} + \lambda - \phi) + Ae^{-\frac{R}{L} \cdot \frac{\theta_{sl}}{\omega}} \quad (B.36)$$

From Eqn. (B.36),

$$A = - \frac{\sqrt{2} E \sin(\theta_{sl} + \lambda - \phi)}{Z \cdot e^{-\frac{R}{L} \frac{\theta_{sl}}{\omega}}}$$

$$= - \frac{\sqrt{2} E}{Z} \sin(\theta_{sl} + \lambda - \phi) e^{\frac{R}{L} \frac{\theta_{sl}}{\omega}} \quad \dots(B.37)$$

substituting this value of 'A' in (B.35),

$$i = \frac{\sqrt{2}E}{Z} [\sin(\omega t' + \lambda - \phi) - e^{-\frac{R}{L}(\omega t' - \theta_{sl})} \sin(\theta_{sl} + \lambda - \phi)] \quad \dots(B.38)$$

substituting  $\omega t' = \omega t - \lambda$  in Eqn. (B.38),

$$i = \frac{\sqrt{2}E}{Z} [\sin(\omega t - \phi) - e^{-\frac{R}{L}(\omega t - \theta_{sl})} \sin(\theta_{sl} + \lambda - \phi)] \quad (B.39)$$

Again, expanding Eqn. (B.38)

$$i = \frac{\sqrt{2}E}{Z} (\sin(\omega t' + \lambda) \cos \phi - \cos(\omega t' + \lambda) \sin \phi) \\ - e^{\frac{R}{X}(\theta_{sl} - \omega t')} [\sin(\theta_{sl} + \lambda) \cos \phi - \cos(\theta_{sl} + \lambda) \sin \phi] \quad \dots (B.40)$$

Now,  $\tan \phi = \frac{X}{R}$ ,  $\cos \phi = \frac{R}{Z}$ ,  $\sin \phi = \frac{X}{Z}$ . Substituting in Eqn. (B.40),

$$i = \frac{\sqrt{2}E}{Z} \left[ \frac{R}{Z} \sin(\omega t' + \lambda) - \frac{X}{Z} \cos(\omega t' + \lambda) - e^{\frac{R}{X}(\theta_{sl} - \omega t')} \left\{ \frac{R}{Z} \sin(\theta_{sl} + \lambda) - \frac{X}{Z} \cos(\theta_{sl} + \lambda) \right\} \right] \\ = \frac{\sqrt{2}EX}{Z^2} \left[ \frac{R}{X} \sin(\omega t' + \lambda) - \cos(\omega t' + \lambda) - e^{\frac{R}{X}(\theta_{sl} - \omega t')} \left\{ \frac{R}{X} \sin(\theta_{sl} + \lambda) - \cos(\theta_{sl} + \lambda) \right\} \right] \quad \dots (B.41)$$

Again, substituting  $\omega t' = \omega t - \lambda$  in Eqn. (B.41),

$$i = \frac{\sqrt{2}EX}{Z^2} \left[ \frac{R}{X} \sin \omega t - \cos \omega t - e^{\frac{R}{X}(\omega t - \theta_{sl} - \lambda)} \left\{ \frac{R}{X} \sin(\theta_{sl} + \lambda) - \cos(\theta_{sl} + \lambda) \right\} \right] \quad \dots (B.42)$$

$i=0$ , at  $\omega t' = \alpha$ .

$\therefore$  From Eqn. (B.42),

$$\frac{R}{X} \sin(\alpha + \lambda) - \cos(\alpha + \lambda) - e^{\frac{R}{X}(\theta_{sl} - \alpha)} \left\{ \frac{R}{X} \sin(\theta_{sl} + \lambda) - \cos(\theta_{sl} + \lambda) \right\} = 0 \quad \dots (B.43)$$

Let  $\gamma = \alpha - \theta_{sl}$ . From Eqn. (B.43),

$$\begin{aligned} \frac{R}{X} \sin(\alpha + \lambda) - \cos(\alpha + \lambda) - e^{\frac{R}{X}(-\gamma)} \left( \frac{R}{X} \sin(\alpha - \gamma + \lambda) \right. \\ \left. - \cos(\alpha - \gamma + \lambda) \right) = 0 \end{aligned} \quad \dots (B.44)$$

Simplifying Eqn. (B.44),

$$\begin{aligned} \sin(\alpha + \lambda) \left[ \frac{R}{X} - e^{-\frac{R}{X}\gamma} \frac{R}{X} \cos \gamma + e^{-\frac{R}{X}\gamma} \sin \gamma \right] \\ - \cos(\alpha + \lambda) \left[ 1 - e^{-\frac{R}{X}\gamma} \frac{R}{X} \sin \gamma - e^{-\frac{R}{X}\gamma} \cos \gamma \right] = 0 \end{aligned} \quad \dots (B.45)$$

From Eqn. (B.45),

$$\begin{aligned} \tan(\alpha + \lambda) &= \frac{1 - e^{-\frac{R}{X}\gamma} \frac{R}{X} \sin \gamma - e^{-\frac{R}{X}\gamma} \cos \gamma}{\frac{R}{X} - e^{-\frac{R}{X}\gamma} \frac{R}{X} \cos \gamma + e^{-\frac{R}{X}\gamma} \sin \gamma} \\ &= \frac{e^{\frac{R}{X}\gamma} - \frac{R}{X} \sin \gamma - \cos \gamma}{\frac{R}{X} e^{\frac{R}{X}\gamma} + \sin \gamma - \frac{R}{X} \cos \gamma} \end{aligned} \quad \dots (B.46)$$

Differentiating Eqn. (B.46) with respect to  $t'$ ,

$$\begin{aligned} \frac{di}{dt'} &= \frac{\sqrt{2}EX}{Z^2} \left[ \omega \cdot \frac{R}{X} \cos(\omega t' + \lambda) + \omega \cdot \sin(\omega t' + \lambda) \right. \\ &\quad \left. + \frac{R}{X} \omega \cdot e^{\frac{R}{X}(\theta_{sl} - \omega t')} \left( \frac{R}{X} \sin(\theta_{sl} + \lambda) - \cos(\theta_{sl} + \lambda) \right) \right] \end{aligned} \quad (B.47)$$

If current is maximum at  $\omega t' = \beta$ ,



$$\frac{R}{X} \cos(\beta+\lambda) + \sin(\beta+\lambda) + \frac{R}{X} e^{\frac{R}{X}(\theta_{s1}-\beta)} \left( \frac{R}{X} \sin(\theta_{s1}+\lambda) - \cos(\theta_{s1}+\lambda) \right) = 0$$

From above, separating terms,

$$\begin{aligned} e^{\frac{R}{X}(\theta_{s1}-\beta)} \left( \frac{R}{X} \sin(\theta_{s1}+\lambda) - \cos(\theta_{s1}+\lambda) \right) \\ = - \left[ \frac{R}{X} \cos(\beta+\lambda) + \sin(\beta+\lambda) \right] \end{aligned} \quad (B.48)$$

Using Eqn. (B.48) and substituting in (Eqn. B.41), the peak current is,

$$\begin{aligned} I_{pmax} &= \frac{\sqrt{2}EX}{Z^2} \left[ \frac{R}{X} \sin(\beta+\lambda) - \cos(\beta+\lambda) + \frac{X}{R} \right. \\ &\quad \left. \left( \frac{R}{X} \cos(\beta+\lambda) + \sin(\beta+\lambda) \right) \right] \end{aligned}$$

Simplifying the above,

$$\begin{aligned} I_{pmax} &= \frac{\sqrt{2}EX}{Z^2} \cdot \frac{(R^2 + X^2)}{RX} \cdot \sin(\beta+\lambda) \\ &= \frac{\sqrt{2}E}{X} \left( \frac{X}{R} \right) \sin(\beta+\lambda) \quad \dots (B.49) \end{aligned}$$

## B.2 Development of Magnetizing Inrush Equations For a Y-Δ Transformer:

With reference to Fig. 3.11(a) and Fig. 3.11(b), the following equations can be written down,

$$I_a - I_{ma} = I_D \quad (B.50)$$

$$I_b - I_{mb} = I_D \quad (B.51)$$

$$I_c - I_{mc} = I_D \quad (B.52)$$

Adding equations (B.50) to (B.52) gives,

$$I_a + I_b + I_c - (I_{ma} + I_{mb} + I_{mc}) = 3I_D \quad (B.53)$$

$$I_a + I_b + I_c = 3I_O \quad (B.54)$$

Substituting in (B.53),

$$3I_O - (I_{ma} + I_{mb} + I_{mc}) = 3I_D \quad (B.55)$$

$$I_D = I_O - \frac{1}{3} (I_{ma} + I_{mb} + I_{mc}) \quad (B.56)$$

$$I_O = I_D + \frac{1}{3} (I_{ma} + I_{mb} + I_{mc}) \quad (B.57)$$

Let

$$I_{mb} = 0 \quad (B.58)$$

Then,

$$I_D = I_O - \frac{1}{3} (I_{ma} + I_{mc}) \quad (B.59)$$

$$I_O = I_D + \frac{1}{3} (I_{ma} + I_{mc}) \quad (B.60)$$

Again,

$$E_{AB} + E_{BC} + E_{CA} = 0$$

$$E_a + E_b + E_c = 0 \quad (B.61)$$

$$\begin{aligned} E_{AB} &= E_a - I_{a1}Z_s - I_{a2}Z_s - I_0Z_{0s} - I_aZ_p - I_DZ_{ss} \\ &= E_a - I_{a1}Z_s - I_{a2}Z_s - I_0Z_s + I_0Z_s - I_0Z_{0s} - I_aZ_p \\ &\quad - I_DZ_{ss} \\ &= E_a - (I_{a1} + I_{a2} + I_0)Z_s - I_0(Z_{0s} - Z_s) - I_aZ_p - I_DZ_{ss} \\ &= E_a - I_aZ_s - I_0(Z_{0s} - Z_s) - I_aZ_p - I_DZ_{ss} \end{aligned}$$

... (B.62)

Similarly,

$$E_{BC} = E_b - I_b Z_s - I_0 (Z_{0s} - Z_s) - I_b Z_p - I_D Z_{ss} \quad (B.63)$$

$$E_{CA} = E_c - I_c Z_s - I_0 (Z_{0s} - Z_s) - I_c Z_p - I_D Z_{ss} \quad (B.64)$$

Adding Eqns. (B.62) through (B.64) gives the following

$$0 = 0 - 3I_0 Z_s - 3I_0 Z_{0s} + 3I_0 Z_s - 3I_0 Z_p - 3I_D Z_{ss} \quad (B.65)$$

$$0 = -I_0 Z_{0s} - I_0 Z_p - I_D Z_{ss} \quad (B.66)$$

$$I_D = -I_0 \left( \frac{Z_p + Z_{0s}}{Z_{ss}} \right) \quad (B.67)$$

or

$$I_0 = -I_D \left( \frac{Z_{ss}}{Z_p + Z_{0s}} \right) \quad (B.68)$$

Substituting Eqn. (B.68) in Eqn. (B.59)

$$I_D = -I_D \left( \frac{Z_{ss}}{Z_p + Z_{0s}} \right) - \frac{1}{3} (I_{ma} + I_{mc}) \quad (B.69)$$

$$I_D \left[ 1 + \left( \frac{Z_{ss}}{Z_p + Z_{0s}} \right) \right] = -\frac{1}{3} (I_{ma} + I_{mc}) \quad (B.70)$$

$$I_D \left( \frac{Z_p + Z_{0s} + Z_{ss}}{Z_p + Z_{0s}} \right) = -\frac{1}{3} (I_{ma} + I_{mc}) \quad (B.71)$$

$$I_D = -\frac{1}{3} (I_{ma} + I_{mc}) \left( \frac{Z_p + Z_{0s}}{Z_p + Z_{0s} + Z_{ss}} \right) \quad (B.72)$$

Substituting Eqn. (B.72) in Eqn. (B.50),

$$I_a = I_{ma} + I_D = I_{ma} - \frac{1}{3} (I_{ma} + I_{mc}) \left( \frac{Z_p + Z_{0s}}{Z_p + Z_{0s} + Z_{ss}} \right) \quad (B.73)$$

$$\begin{aligned}
I_a &= I_{ma} \left[ 1 - \frac{1}{3} \left( \frac{Z_p + Z_{0s}}{Z_p + Z_{0s} + Z_{ss}} \right) - \frac{1}{3} I_{mc} \left( \frac{Z_p + Z_{0s}}{Z_p + Z_{0s} + Z_{ss}} \right) \right] \\
&= I_{ma} \left[ \frac{3Z_p + 3Z_{0s} + 3Z_{ss} - Z_p - Z_{0s}}{3(Z_p + Z_{0s} + Z_{ss})} \right] \\
&\quad - I_{mc} \left[ \frac{Z_p + Z_{0s}}{3(Z_p + Z_{0s} + Z_{ss})} \right] \\
&= I_{ma} \left[ \frac{2Z_p + 2Z_{0s} + 3Z_{ss}}{3(Z_p + Z_{0s} + Z_{ss})} \right] - I_{mc} \left[ \frac{Z_p + Z_{0s}}{3(Z_p + Z_{0s} + Z_{ss})} \right] \\
&\quad \dots (B.74)
\end{aligned}$$

Let

$$Z_p = Z_{ss} \quad (B.75)$$

(according to usual convention). Then,

$$I_a = I_{ma} \left( \frac{5Z_{ss} + 2Z_{0s}}{6Z_{ss} + 3Z_{0s}} \right) - I_{mc} \left( \frac{Z_{ss} + Z_{0s}}{6Z_{ss} + 3Z_{0s}} \right) \quad (B.76)$$

with the limit  $Z_{0s} \rightarrow 0$ , the following results,

$$I_a = \frac{5}{6} I_{ma} - \frac{1}{6} I_{mc} \quad (B.77)$$

Using Eqns. (B.51), (B.58), (B.72) and (B.75) gives,

$$I_b = I_D = -(I_{ma} + I_{mc}) \left( \frac{Z_{ss} + Z_{0s}}{6Z_{ss} + 3Z_{0s}} \right) \quad (B.78)$$

Using Eqns. (B.52), (B.72) and (B.75) gives,

$$I_c - I_{mc} = -\frac{1}{3} (I_{ma} + I_{mc}) \left( \frac{Z_{ss} + Z_{0s}}{2Z_{ss} + Z_{0s}} \right)$$

$$I_c = I_{mc} \left( 1 - \frac{Z_{ss} + Z_{0s}}{6Z_{ss} + 3Z_{0s}} \right) - I_{ma} \left( \frac{Z_{ss} + Z_{0s}}{6Z_{ss} + 3Z_{0s}} \right)$$

$$I_c = I_{mc} \left( \frac{5Z_{ss} + 2Z_{0s}}{6Z_{ss} + 3Z_{0s}} \right) - I_{ma} \left( \frac{Z_{ss} + Z_{0s}}{6Z_{ss} + 3Z_{0s}} \right) \quad (B.79)$$

Now assume that,

$$I_{mb} \neq 0 \quad (B.80)$$

Substituting Eqn. (B.68) in Eqn. (B.56),

$$I_D = -I_D \left( \frac{Z_{ss}}{Z_p + Z_{0s}} \right) - \frac{1}{3} (I_{ma} + I_{mb} + I_{mc}) \quad (B.81)$$

$$I_D \left( 1 + \frac{Z_{ss}}{Z_p + Z_{0s}} \right) = -\frac{1}{3} (I_{ma} + I_{mb} + I_{mc}) \quad (B.82)$$

Substituting  $Z_{ss}$  for  $Z_p$  then

$$I_D \left( \frac{2Z_{ss} + Z_{0s}}{Z_{ss} + Z_{0s}} \right) = -\frac{1}{3} (I_{ma} + I_{mb} + I_{mc})$$

$$I_D = -\frac{1}{3} \left( \frac{Z_{ss} + Z_{0s}}{2Z_{ss} + Z_{0s}} \right) (I_{ma} + I_{mb} + I_{mc}) \quad (B.83)$$

Substituting Eqn. (B.83) in Eqn. (B.50),

$$I_a = I_D + I_{ma} = I_{ma} - \frac{1}{3} \left( \frac{Z_{ss} + Z_{0s}}{2Z_{ss} + Z_{0s}} \right) (I_{ma} + I_{mb} + I_{mc}) \quad (B.84)$$

$$I_a = I_{ma} \left( 1 - \frac{Z_{ss} + Z_{0s}}{6Z_{ss} + 3Z_{0s}} \right) - \left( \frac{Z_{ss} + Z_{0s}}{6Z_{ss} + 3Z_{0s}} \right) (I_{ma} + I_{mc}) \quad (B.85)$$

Similarly,

$$I_B = I_{mb} \left( \frac{5Z_{ss} + 2Z_{0s}}{6Z_{ss} + 3Z_{0s}} \right) - \left( \frac{Z_{ss} + Z_{0s}}{6Z_{ss} + 3Z_{0s}} \right) (I_{ma} + I_{mc}) \quad (B.86)$$

$$I_C = I_{mc} \left( \frac{5Z_{ss} + 2Z_{0s}}{6Z_{ss} + 3Z_{0s}} \right) - \left( \frac{Z_{ss} + Z_{0s}}{6Z_{ss} + 3Z_{0s}} \right) (I_{ma} + I_{mb}) \quad (B.87)$$

### B.3 Development of Magnetizing Inrush Equations for 3-Phase Transformers Considering Mutual Inductive Couplings

With reference to Fig. 3.12, the following basic equations result,

$$V_A = R_A i_A + \mathcal{L}_A p i_A + M_1 p i_1 \quad (B.88)$$

$$V_B = R_B i_B + \mathcal{L}_B p i_B + M_2 p i_2 \quad (B.89)$$

$$V_C = R_C i_C + \mathcal{L}_C p i_C + M_3 p i_3 \quad (B.90)$$

$$V_a = R_a i_a + \mathcal{L}_a p i_a + M_1 p i_1 \quad (B.100)$$

$$V_b = R_b i_b + \mathcal{L}_b p i_b + M_2 p i_2 \quad (B.101)$$

$$V_c = R_c i_c + \mathcal{L}_c p i_c + M_3 p i_3 \quad (B.102)$$

By applying the magnetic circuit equation,  $\oint \phi = 0$  at any junction. Hence, from Fig. 3.12, the following equations result,

$$0 = M_1 p i_1 - M_4 p i_4 - M_7 p i_7 \quad (B.103)$$

$$0 = M_2 p i_2 - M_5 p i_5 + M_7 p i_7 + M_8 p i_8 \quad (B.104)$$

$$0 = M_3 p i_3 - M_6 p i_6 - M_8 p i_8 \quad (B.105)$$

Applying the magnetic circuit law,  $NI = \oint H dl$ ,

$$i_4 = i_A + i_a - i_1 \quad (\text{B.106})$$

$$i_5 = i_B + i_b - i_2 \quad (\text{B.107})$$

$$i_6 = i_C + i_c - i_3 \quad (\text{B.108})$$

$$i_7 = i_A + i_a - i_B - i_b - i_1 + i_2 \quad (\text{B.109})$$

$$i_8 = i_C + i_c - i_B - i_b - i_3 + i_2 \quad (\text{B.110})$$

The above 14 equations contain nine differential and five algebraic equations. For no-load condition, all these equations can be reduced to the following form

$$i_a = i_b = i_c = 0 \quad (\text{B.111})$$

$$V_A = R_A i_A + M_1 p i_1 \quad (\text{B.112})$$

$$V_B = R_B i_B + M_2 p i_2 \quad (\text{B.113})$$

$$V_C = R_C i_C + M_3 p i_3 \quad (\text{B.114})$$

Again,

$$i_4 = i_A - i_1 \quad (\text{B.115})$$

$$i_5 = i_B - i_2 \quad (\text{B.116})$$

$$i_6 = i_C - i_3 \quad (\text{B.117})$$

$$i_7 = i_4 - i_5 \quad (\text{B.118})$$

$$= i_A - i_1 - i_B + i_2 \quad (\text{B.119})$$

$$i_8 = i_6 - i_5$$

$$= i_C - i_3 - i_B + i_2 \quad (\text{B.120})$$

Now, from Eqn. (B.103),

$$M_1 p_{i_1} - M_4 p_{i_4} - M_7 p_{i_7} = 0$$

or

$$M_1 p_{i_1} - M_4 (i_A - i_1) - M_7 p (i_A - i_1 - i_B + i_2) = 0$$

or

$$M_1 p_{i_1} - M_4 p_{i_A} + M_4 p_{i_1} - M_7 p_{i_A} + M_7 p_{i_1} + M_7 p_{i_B} - M_7 p_{i_2} = 0$$

or

$$-(M_4 + M_7) p_{i_A} + M_7 p_{i_B} + (M_1 + M_4) p_{i_1} - M_7 p_{i_2} = 0$$

...(B.121)

From Eqn. (B.104),

$$M_2 p_{i_2} - M_5 p_{i_5} + M_7 p_{i_7} + M_8 p_{i_8} = 0$$

or

$$M_2 p_{i_2} - M_5 p (i_B - i_2) + M_7 p (i_A - i_1 - i_B + i_2)$$

$$+ M_8 p (i_C - i_3 - i_B + i_2) = 0$$

or

$$M_2 p_{i_2} - M_5 p_{i_B} + M_5 p_{i_2} + M_7 p_{i_A} - M_7 p_{i_1} - M_7 p_{i_B} + M_7 p_{i_2} + M_8 p_{i_C}$$

$$- M_8 p_{i_3} - M_8 p_{i_B} + M_8 p_{i_2} = 0$$

or

$$M_7 p_{i_A} - (M_5 + M_7 + M_8) p_{i_B} + M_8 p_{i_C} - M_7 p_{i_1} + (M_2 + M_5 + M_7 + M_8) p_{i_2}$$

$$- M_8 p_{i_3} = 0$$

...(B.122)



From Eqn. (B.105),

$$M_8 p_{i_3} - M_6 p_{i_6} - M_8 p_{i_8} = 0$$

or

$$M_3 p_{i_3} - M_6 p(i_C - i_3) - M_8 p(i_C - i_3 - i_B + i_2) = 0$$

or

$$M_3 p_{i_3} - M_6 p_{i_C} + M_6 p_{i_3} - M_8 p_{i_C} + M_8 p_{i_3} + M_8 p_{i_B} - M_8 p_{i_2} = 0$$

or

$$M_8 p_{i_B} - (M_6 + M_8) p_{i_C} - M_8 p_{i_2} + (M_3 + M_6 + M_8) p_{i_3} = 0$$

...(B.123)

Again from Eqn. (B.88), B.89) and (B.90),

$$L_A p_{i_A} + M_1 p_{i_1} = V_A - R_A i_A \quad (B.124)$$

$$L_B p_{i_B} + M_2 p_{i_2} = V_B - R_B i_B \quad (B.125)$$

$$L_C p_{i_C} + M_3 p_{i_3} = V_C - R_C i_C \quad (B.126)$$

Arranging the six Eqns. (B.121) to (B.126) in proper order, it can be written in matrix form as,

$$[H][pI] = [Z][V] - [Y][I] \quad (B.127)$$

where different matrices of Eqn. (B.127) are as follows,

$$[H] = \begin{bmatrix} l_A & 0 & 0 & M_1 & 0 & 0 \\ 0 & l_B & 0 & 0 & M_2 & 0 \\ 0 & 0 & l_C & 0 & 0 & M_3 \\ -(M_4+M_7) & M_7 & 0 & (M_1+M_4+M_7) & -M_7 & 0 \\ M_7 & (M_5+M_7+M_8) & M_8 & -M_7 & (M_2+M_5+M_7+M_8) & -M_8 \\ 0 & M_8 & -(M_6+M_8) & 0 & -M_8 & (M_3+M_8) \end{bmatrix}$$

$$[P] = \begin{bmatrix} p_i_A \\ p_i_B \\ p_i_C \\ p_{i_1} \\ p_{i_2} \\ p_{i_3} \end{bmatrix}$$

$$[V] = \begin{bmatrix} V_A \\ V_B \\ V_C \\ 0 \\ 0 \\ 0 \end{bmatrix}$$

$$[I] = \begin{bmatrix} i_A \\ i_B \\ i_C \\ 0 \\ 0 \\ 0 \end{bmatrix}$$

$$[Z] = \begin{bmatrix} 1 & 0 & 0 & 0 & 0 & 0 \\ 0 & 1 & 0 & 0 & 0 & 0 \\ 0 & 0 & 1 & 0 & 0 & 0 \\ 0 & 0 & 0 & 1 & 0 & 0 \\ 0 & 0 & 0 & 0 & 1 & 0 \\ 0 & 0 & 0 & 0 & 0 & -1 \end{bmatrix}$$

$$[Y] = \begin{bmatrix} R_A & 0 & 0 & 0 & 0 & 0 & 0 \\ 0 & R_B & 0 & 0 & 0 & 0 & 0 \\ 0 & 0 & R_C & 0 & 0 & 0 & 0 \\ 0 & 0 & 0 & 0 & 0 & 0 & 0 \\ 0 & 0 & 0 & 0 & 0 & 0 & 0 \\ 0 & 0 & 0 & 0 & 0 & 0 & 0 \end{bmatrix}$$

## APPENDIX C

VARIATION OF FLUX IN THREE-PHASE TRANSFORMERSC.1 Variation of Flux Phenomena

As Rockefeller [33] suggested that for calculation of three phase magnetizing current, per phase magnetizing currents are to be known, it is possible to calculate the per phase magnetizing current in the same way as single phase transformers. For this purpose, the per phase leakage reactances as well as core reactances are to be known. For three-phase transformers, O.C. and S.C. tests can be carried out in the same way as single phase transformers [36] and sequence impedances can be calculated on per phase basis like single phase transformers, [2]. But the reactance values seen by the external circuit will vary depending on the transformer connections.

Also for a core type transformer, it can be found that the rate of change of flux in the centre leg is the minimum (see derivation). The outer legs experience a maximum rate of change of  $0.625 \phi_m$  to  $-0.625 \phi_m$  while the centre leg experience a change of  $0.125 \phi_m$  to  $-0.125 \phi_m$  ideally. This is due to the flux route patterns through the core as it will be clear from derivation. At any instant, the summation of these fluxes are zero.

Hence, the induced voltage in the centre leg for the same amount of applied voltage  $e = \frac{d\psi}{dt}$  is less in

comparison to the other two legs. Here ' $\psi$ ' is the flux-linkage. So, the rate of change of current in the centre leg is small. But this induced voltage has to be equal to the applied voltage. Again, we know

$$e = -L \frac{di}{dt}, \text{ where } L = \frac{d\psi}{dt} \quad (C.1)$$

So, this voltage balance is accomplished by a higher ' $L$ ' in the right-hand side of Eqn. C.1 in comparison to the other legs. Thus ultimately higher reactance values of the centre core is seen by the external circuit. So, for all O.C. tests, the centre core has taken less current and this is reflected in the calculated core reactances shown in Table 3.5 of Chapter 3 in the text.

It is seen from the table that from A to D, the primaries are Y. The core as well as the leakage impedance values are more or less similar. The difference in the core reactance values can be attributed to the zero sequence flux-paths depending on connections of the primary, secondary and the neutral [2]. The zero sequence fluxes add to  $3\phi_0$  and finds path through oil or tank of the transformers. For an example, in Case A, zero sequence current is flowing out through the neutral. Hence, if any of the phase is considered, it is added with the normal excitation current and thus, offering lesser core reactances in calculation. While in Case B, the star connected primary being ungrounded,

no zero sequence current can flow in primary and thus it offers slightly higher core reactance. For cases E & F, the zero sequence fluxes circulate in the core and saturate the core of a transformer. Besides, for  $\Delta$ -Y or Y- $\Delta$  transformers, the current in the phase of a  $\Delta$ -circuit is  $1/\sqrt{3}$  times less than star. But it is not reflected as nearly  $1/\sqrt{3}$  times increase in reactance values, because of circulating zero sequence current is present in the  $\Delta$ -winding. Whereas, it is not present in the Y-winding without neutral grounded.

## C.2 Derivation

From Fig-A,

$$\phi_A = \phi_m \sin \omega t \quad (C.2)$$

$$\phi_B = \phi_m \sin (\omega t - 120^\circ) \quad (C.3)$$

$$\phi_C = \phi_m \sin (\omega t + 120^\circ) \quad (C.4)$$

Case 1: Phase A Has Maximum Flux

$$\phi_A = \phi_m \sin 90^\circ = \phi_m \quad (C.5)$$

$$\phi_B = \phi_m \sin (90^\circ - 120^\circ)$$

$$= -\phi_m \sin 30^\circ$$

$$= -\frac{\phi_m}{2} \quad \dots (C.6)$$

$$\begin{aligned}
 \phi_C &= \phi_m \sin(90^\circ + 120^\circ) \\
 &= \phi_m \sin 210^\circ \\
 &= -\frac{\phi_m}{2}
 \end{aligned}$$

...(C.7)

Flux in Leg A:

$$\begin{aligned}
 \phi_A + \frac{1}{2} \phi_B + 0.25 \phi_C \\
 &= \phi_m - \frac{\phi_m}{4} - 0.25 \frac{\phi_m}{2} \\
 &= \phi_m - 0.25 \phi_m - 0.125 \phi_m \\
 &= 0.625 \phi_m
 \end{aligned}$$

...(C.8)

Flux in Leg B:

$$\begin{aligned}
 0.75 \phi_A + \phi_B + 0.75 \phi_C \\
 &= 0.75 \phi_m - \frac{\phi_m}{2} - 0.75 \frac{\phi_m}{2} \\
 &= 0.75 \phi_m - 0.5 \phi_m - 0.375 \phi_m \\
 &= -0.125 \phi_m
 \end{aligned}$$

...(C.9)

Flux in Leg C:

$$\begin{aligned}
 0.25 \phi_A + 0.5 \phi_B + \phi_C \\
 &= 0.25 \phi_m - 0.5 \frac{\phi_m}{2} - \frac{\phi_m}{2} \\
 &= 0.25 \phi_m - 0.25 \phi_m - 0.5 \phi_m \\
 &= -0.5 \phi_m
 \end{aligned}$$

...(C.10)

From Eqn. (C.8), (C.9), (C.10),

$$\sum_{i=1}^3 \phi_i = (0.625 - 0.125 - 0.5) \phi_m = 0 \quad \text{... (C.11)}$$

Case 2: Phase B Has Maximum Flux

$$\begin{aligned} \phi_A &= \phi_m \sin 210^\circ \\ &= -\frac{\phi_m}{2} \quad \text{... (C.12)} \end{aligned}$$

$$\begin{aligned} \phi_B &= \phi_m \sin 90^\circ \\ &= \phi_m \quad \text{... (C.13)} \end{aligned}$$

$$\begin{aligned} \phi_C &= \phi_m \sin (210^\circ + 120^\circ) \\ &= \frac{\phi_m}{2} \quad \text{... (C.14)} \end{aligned}$$

Flux in Leg A:

$$\begin{aligned} \phi_A + \frac{\phi_B}{2} + 0.25 \phi_C \\ &= -\frac{\phi_m}{2} + \frac{\phi_m}{2} - 0.25 \frac{\phi_m}{2} \\ &= 0.125 \phi_m \quad \text{... (C.15)} \end{aligned}$$

Flux in Leg B:

$$\begin{aligned} 0.75 \phi_A + \phi_B + 0.75 \phi_C \\ &= -0.75 \frac{\phi_m}{2} + \phi_m - 0.75 \frac{\phi_m}{2} \\ &= -0.75 \phi_m + \phi_m = 0.25 \phi_m \quad \text{... (C.16)} \end{aligned}$$



Flux in Leg C:

$$\begin{aligned}
 & 0.25 \phi_A + 0.5 \phi_B + \phi_C \\
 &= -0.25 \frac{\phi_m}{2} + 0.59 \phi_m - \frac{\phi_m}{2} \\
 &= -0.125 \phi_m + 0.5 \phi_m - 0.5 \phi_m \\
 &= -0.125 \phi_m \quad \dots (C.17)
 \end{aligned}$$

From Eqns. (C.15), (C.16), (C.17),

$$\begin{aligned}
 \sum_{i=1}^3 \phi_i &= (-0.125 + 0.25 - 0.125) \phi_m \\
 &= 0 \quad \dots (C.18)
 \end{aligned}$$

Case 3: Phase C Has Maximum Flux

$$\phi_A = \phi_m \sin 330^\circ = -\frac{\phi_m}{2} \quad (C.19)$$

$$\begin{aligned}
 \phi_B &= \phi_m \sin (330^\circ - 120^\circ) \\
 &= -\frac{\phi_m}{2} \quad \dots (C.20)
 \end{aligned}$$

$$\begin{aligned}
 \phi_C &= \phi_m \sin 90^\circ \\
 &= \phi_m \quad \dots (C.21)
 \end{aligned}$$

Flux in Leg A:

$$\begin{aligned}
 & \phi_A + \frac{\phi_B}{2} + 0.25 \phi_C \\
 &= -\frac{\phi_m}{2} - \frac{\phi_m}{4} + 0.25 \phi_m \quad \dots (C.22)
 \end{aligned}$$

$$\begin{aligned}
 &= -0.5 \phi_m - 0.25 \phi_m + 0.25 \phi_m \\
 &= -0.5 \phi_m \quad \dots (C.23)
 \end{aligned}$$

Flux in Leg B:

$$\begin{aligned}
 & 0.75 \phi_A + \phi_B + 0.75 \phi_C \\
 &= -0.75 \frac{\phi_m}{2} - \frac{\phi_m}{2} + 0.75 \phi_m \\
 &= -0.375 \phi_m - 0.5 \phi_m + 0.75 \phi_m \\
 &= -0.125 \phi_m \quad \dots (C.24)
 \end{aligned}$$

Flux in Leg C:

$$\begin{aligned}
 & 0.25 \phi_A + 0.5 \phi_B + \phi_C \\
 &= -0.25 \frac{\phi_m}{2} - 0.5 \frac{\phi_m}{2} + \phi_m \\
 &= -0.125 \phi_m - 0.25 \phi_m + \phi_m \\
 &= 0.625 \phi_m \quad \dots (C.25)
 \end{aligned}$$

From Equations (C.21), (C.22) and (C.23)

$$\begin{aligned}
 \sum_{i=1}^3 \phi_i &= -0.5 \phi_m - 0.125 \phi_m + 0.625 \phi_m \\
 &= 0 \quad \dots (C.26)
 \end{aligned}$$

Similarly, for maximum fluxes of opposite polarities in each phase will result the variation of fluxes same as above but with negative signs. Hence, variations can be summarized as,

For Positive Maximum:

Leg A	Leg B	Leg C
0.625 $\phi_m$	-0.125 $\phi_m$	-0.5 $\phi_m$
-0.125 $\phi_m$	0.25 $\phi_m$	-0.125 $\phi_m$
-0.5 $\phi_m$	-0.125 $\phi_m$	0.625 $\phi_m$

For Negative Maximum

-0.625 $\phi_m$	0.125 $\phi_m$	0.5 $\phi_m$
0.125 $\phi_m$	-0.25 $\phi_m$	0.125 $\phi_m$
0.5 $\phi_m$	0.125 $\phi_m$	-0.625 $\phi_m$

## APPENDIX D

WALSH FUNCTION WITH SAMPLING RATES OF 16 & 8 SAMPLES/CYCLED.1 16 Samples/Cycle

The Walsh coefficients based on 16 samples/cycle can be derived from the matrix of Eqn 4.34 as follows:

For the first sample,

$$\begin{aligned}
 16 \ W_0(1) &= \frac{1}{2}x(1)+x(2)+x(3)+x(4)+x(5)+x(6)+x(7)+x(8)+x(9)+ \\
 &\quad x(10)+x(11)+x(12)+x(13)+x(14)+x(15)+x(16) \\
 &\quad +\frac{1}{2}x(17) \quad \dots(D.1)
 \end{aligned}$$

For the second sample, first sample goes out and the next sample comes in.

$$\begin{aligned}
 16 \ W_0(2) &= \frac{1}{2}x(2)+x(3)+x(4)+x(5)+x(6)+x(7)+x(8)+x(9)+x(10) \\
 &\quad +x(11)+x(12)+x(13)+x(14)+x(15)+x(16)+x(17) \\
 &\quad +\frac{1}{2}x(18) \quad \dots(D.2)
 \end{aligned}$$

$$\begin{aligned}
 &= \frac{1}{2}x(1)-\frac{1}{2}x(1)+x(2)-\frac{1}{2}x(2)+x(3)+x(4)+x(5)+x(6)+x(7) \\
 &\quad +x(8)+x(9)+x(10)+x(11)+x(12)+x(13)+x(14)+x(15) \\
 &\quad +x(16)+\frac{1}{2}x(17)+\frac{1}{2}x(17)+\frac{1}{2}x(18) \\
 &= 16W_0(1)-\frac{1}{2}x(1)-\frac{1}{2}x(2)+\frac{1}{2}x(17)+\frac{1}{2}x(18) \quad \dots(D.3)
 \end{aligned}$$

Similarly, for the first sample,

$$\begin{aligned}
 16 W_1(1) &= \frac{1}{2}x(1)+x(2)+x(3)+x(4)+x(5)+x(6)+x(7)+x(8)-x(10) \\
 &\quad -x(11)-x(12)-x(13)-x(14)-x(15)-x(16)-\frac{1}{2}x(17) \\
 &\quad \dots(D.4)
 \end{aligned}$$

For the second sample,

$$\begin{aligned}
 16 W_1(2) &= \frac{1}{2}x(2)+x(3)+x(4)+x(5)+x(6)+x(7)+x(8)+x(9)-x(11) \\
 &\quad -x(12)-x(13)-x(14)-x(15)-x(16)-x(17)-\frac{1}{2}x(18) \\
 &= \frac{1}{2}x(1)-\frac{1}{2}x(1)+x(2)-\frac{1}{2}x(2)+x(3)+x(4)+x(5)+x(6)+x(7) \\
 &\quad +x(8)+x(9)+x(10)-x(10)-x(11)-x(12)-x(13)-x(14) \\
 &\quad -x(15)-x(16)-\frac{1}{2}x(17)-\frac{1}{2}x(17)-\frac{1}{2}x(18) \\
 &= (\frac{1}{2}x(1)+x(2)+x(3)+x(4)+x(5)+x(6)+x(7)+x(8)-x(10) \\
 &\quad -x(11)-x(12)-x(13)-x(14)-x(15)-x(16), -\frac{1}{2}x(17) \\
 &\quad -\frac{1}{2}x(1), -\frac{1}{2}x(2)+x(9)+x(10)-\frac{1}{2}x(17)-\frac{1}{2}x(18) \\
 &= 16 W_1(1) - \frac{1}{2}x(1) - \frac{1}{2}x(2) + x(9) + x(10) - \frac{1}{2}x(17) - \frac{1}{2}x(18) \\
 &\quad \dots(D.5)
 \end{aligned}$$

For the first sample,

$$\begin{aligned}
 16 W_2(1) &= \frac{1}{2}x(1)+x(2)+x(3)+x(4)-x(6)-x(7)-x(8)-x(9)-x(10) \\
 &\quad -x(11)-x(12)+x(14)+x(15)+x(16)+\frac{1}{2}x(17)
 \end{aligned}$$

For the second sample,

$$\begin{aligned}
16W_2(2) &= \frac{1}{2}x(2)+x(3)+x(4)+x(5)-x(7)-x(8)-x(9)-x(10) \\
&\quad -x(11)-x(12)-x(13)+x(15)+x(16)+x(17)+\frac{1}{2}x(18) \\
&= \frac{1}{2}x(1)-\frac{1}{2}x(1)+x(2)-\frac{1}{2}x(2)+x(3)+x(4)+x(5)-x(6)+x(6) \\
&\quad -x(7)-x(8)-x(9)-x(10)-x(11)-x(12)-x(13)+x(14) \\
&\quad -x(14)+x(15)+x(16)+\frac{1}{2}x(17)+\frac{1}{2}x(17)+\frac{1}{2}x(18) \\
&= \frac{1}{2}x(1)+x(2)+x(3)+x(4)-x(6)-x(7)-x(8)-x(9) \\
&\quad -x(10)-x(11)-x(12)+x(14)+x(15)+x(16) \\
&\quad +\frac{1}{2}x(17)-\frac{1}{2}x(1)-\frac{1}{2}x(2)+x(5)+x(6)-x(13)-x(14) \\
&\quad +\frac{1}{2}x(17)+\frac{1}{2}x(18) \\
&= 16W_2(1)-\frac{1}{2}x(1)-\frac{1}{2}x(2)+x(5)+x(6)-x(13)-x(14) \\
&\quad +\frac{1}{2}x(17)+\frac{1}{2}x(18)
\end{aligned}$$

... (D.6)

Similarly,

$$\begin{aligned}
16W_3(1) &= \frac{1}{2}x(1)+x(2)+x(3)+x(4)-x(6)-x(7)-x(8) \\
&\quad +x(10)+x(11)+x(12)-x(14)-x(15)-x(16) \\
&\quad -\frac{1}{2}x(17) \\
16W_3(2) &= \frac{1}{2}x(2)+x(3)+x(4)+x(5)-x(7)-x(8)-x(9)+x(11)+x(12) \\
&\quad +x(13)-x(15)-x(16)-x(17)-\frac{1}{2}x(18)
\end{aligned}$$

... (D.7)

$$16W_4(1) = \frac{1}{2}x(1) + x(2) - x(4) - x(5) - x(6) + x(8) + x(9) \\ + x(10) - x(12) - x(13) - x(14) + x(16) + \frac{1}{2}x(17)$$

$$16W_4(2) = \frac{1}{2}x(2) + x(3) - x(5) - x(6) - x(7) + x(9) + x(10) + x(11) \\ - x(13) - x(14) - x(15) + x(17) + \frac{1}{2}x(18)$$

... (D.8)

$$16W_5(1) = \frac{1}{2}x(1) + x(2) - x(4) - x(5) - x(6) + x(8) - x(10) \\ + x(12) + x(13) + x(14) - x(16) - \frac{1}{2}x(17)$$

$$16W_5(2) = \frac{1}{2}x(2) + x(3) - x(5) - x(6) - x(7) + x(9) - x(11) \\ + x(13) + x(14) + x(15) - x(17) - \frac{1}{2}x(18)$$

... (D.9)

$$16W_6(1) = \frac{1}{2}x(1) + x(2) - x(4) + x(6) - x(8) - x(9) \\ - x(10) + x(12) - x(14) + x(16) + \frac{1}{2}x(17)$$

$$16W_6(2) = \frac{1}{2}x(2) + x(3) - x(5) + x(7) - x(9) - x(10) \\ - x(11) + x(13) - x(15) + x(17) + \frac{1}{2}x(18)$$

... (D.10)

$$16W_9(1) = \frac{1}{2}x(1) - x(3) + x(5) - x(7) + x(11) - x(13) + x(15) - \frac{1}{2}x(17)$$

$$16W_9(2) = \frac{1}{2}x(2) - x(4) + x(6) - x(8) + x(12) - x(14) + x(16) - \frac{1}{2}x(18)$$

... (D.11)

$$16W_{10}(1) = \frac{1}{2}x(1) - x(3) + x(7) - x(9) + x(11) - x(15) + \frac{1}{2}x(17)$$

$$16W_{10}(2) = \frac{1}{2}x(2) - x(4) + x(8) - x(10) + x(12) - x(16) + \frac{1}{2}x(18)$$

... (D.12)

$$16W_{11}(1) = \frac{1}{2}x(1) - x(3) + x(7) - x(11) + x(15) - \frac{1}{2}x(17)$$

$$16W_{11}(2) = \frac{1}{2}x(2) - x(4) + x(8) - x(12) + x(16) - \frac{1}{2}x(17)$$

... (D.13)

Hence Eqns. (D.1) to (D.13) can be written in a general form

$$16W_0(j+1) = 16W_0(j) - \frac{1}{2}x(j) - \frac{1}{2}x(j+1) + \frac{1}{2}x(j+16) + \frac{1}{2}x(j+17)$$

... (D.14)

$$16W_1(j+1) = 16W_1(j) - \frac{1}{2}x(j) - \frac{1}{2}x(j+1) + x(j+8) + x(j+9) - \frac{1}{2}x(j+16)$$

$$- \frac{1}{2}x(j+17) \quad j=1, 2, 3 \dots$$

... (D.15)

$$16W_2(j+1) = 16W_2(j) - \frac{1}{2}x(j) - \frac{1}{2}x(j+1) + x(j+4) + x(j+5) - x(j+12)$$

$$- x(j+13) + \frac{1}{2}x(j+16) + \frac{1}{2}x(j+17) \quad j=1, 2, 3, \dots$$

... (D.16)

$$16W_3(j) = \frac{1}{2}x(j) + x(j+1) + x(j+2) + x(j+3) - x(j+5) - x(j+6) - x(j+7)$$

$$+ x(j+9) + x(j+10) + x(j+11) - x(j+13) - x(j+14) - x(j+15)$$

$$- \frac{1}{2}x(j+16)$$

$$j=1, 2, 3, \dots$$

... (D.17)



$$\begin{aligned}
 16W_4(j) &= \frac{1}{2}x(j) + x(j+1) - x(j+3) - x(j+4) - x(j+5) + x(j+7) + x(j+8) \\
 &\quad + x(j+9) - x(j+11) - x(j+12) - x(j+13) + x(j+15) + \frac{1}{2}x(j+16) \\
 &\quad j=1, 2, 3, \dots, \\
 &\quad \dots (D.18)
 \end{aligned}$$

$$\begin{aligned}
 16W_5(j) &= \frac{1}{2}x(j) + x(j+1) - x(j+3) - x(j+4) - x(j+5) + x(j+7) - x(j+9) \\
 &\quad + x(j+11) + x(j+12) + x(j+13) - x(j+15) - \frac{1}{2}x(j+16) \\
 &\quad j=1, 2, 3, \dots, \\
 &\quad \dots (D.19)
 \end{aligned}$$

$$\begin{aligned}
 16W_6(j) &= \frac{1}{2}x(j) + x(j+1) - x(j+3) + x(j+5) - x(j+7) - x(j+8) - x(j+9) \\
 &\quad + x(j+11) - x(j+13) + x(j+15) + \frac{1}{2}x(j+16) \\
 &\quad j=1, 2, 3, \dots, \\
 &\quad \dots (D.20)
 \end{aligned}$$

$$\begin{aligned}
 16W_9(j) &= \frac{1}{2}x(j) - x(j+2) + x(j+4) - x(j+6) + x(j+10) - x(j+12) + x(j+14) \\
 &\quad - \frac{1}{2}x(j+16) \\
 &\quad j=1, 2, 3, \dots, \\
 &\quad \dots (D.21)
 \end{aligned}$$

$$\begin{aligned}
 16W_{10}(j) &= \frac{1}{2}x(j) - x(j+2) + x(j+6) - x(j+8) + x(j+10) - x(j+14) \\
 &\quad + \frac{1}{2}x(j+16) \\
 &\quad j=1, 2, 3, \dots, \\
 &\quad \dots (D.22)
 \end{aligned}$$

$$16W_{11}(j) = \frac{1}{2}x(j) - x(j+2) - x(j+10) + x(j+14) - \frac{1}{2}x(j+16)$$

$$j=1, 2, 3, \dots,$$

... (D. 23)

$$16W_{12}(j) = \frac{1}{2}x(j) - x(j+4) + x(j+8) - x(j+12) + \frac{1}{2}x(j+16)$$

$$j=1, 2, 3, \dots,$$

... (D. 24)

## D.2 8 Samples/Cycle:

The derivation of Walsh coefficients are based on the following matrix relationship where the respective Walsh functions correspond to double the interval shown in

Fig. 4.13

$$\begin{bmatrix} W_0 \\ W_1 \\ W_2 \\ W_3 \\ W_4 \\ W_5 \\ W_6 \\ W_7 \end{bmatrix} = \begin{bmatrix} + & + & + & + & + & + & + & + \\ + & + & + & + & - & - & - & - \\ + & + & - & - & - & - & + & + \\ + & + & - & - & + & + & - & - \\ + & - & - & + & + & - & - & + \\ + & - & - & + & - & + & + & - \\ + & - & + & - & - & + & - & + \\ + & - & + & - & + & - & + & - \end{bmatrix} \begin{bmatrix} x(1) \\ x(2) \\ x(3) \\ x(4) \\ x(5) \\ x(6) \\ x(7) \\ x(8) \end{bmatrix}$$

(D. 25)

The useful Walsh coefficients can be derived from above matrix Eqn. and are given by,

$$w_1(1) = \frac{1}{2}x(1) + x(2) + x(3) + x(4) - x(6) - x(7) - x(8) - \frac{1}{2}x(9).$$

$$w_1(2) = \frac{1}{2}x(2) + x(3) + x(4) + x(5) - x(7) - x(8) - x(9) - \frac{1}{2}x(10)$$

Hence

$$w_1(j) = \frac{1}{2}x(j) + x(j+1) + x(j+2) + x(j+3) - x(j+5) - x(j+6) - x(j+7)$$

$$- \frac{1}{2}x(j+8)$$

$$j=1, 2, 3, \dots,$$

... (D.26)

$$w_2(1) = \frac{1}{2}x(1) + x(2) - x(4) - x(5) - x(6) + x(8) + \frac{1}{2}x(9)$$

$$w_2(2) = \frac{1}{2}x(2) + x(3) - x(5) - x(6) + x(7) + x(9) + \frac{1}{2}x(10)$$

Hence

$$w_2(j) = \frac{1}{2}x(j) + x(j+1) - x(j+3) - x(j+4) + x(j+5) + x(j+7) + \frac{1}{2}x(j+8)$$

$$j=1, 2, 3, \dots$$

... (D.27)

$$w_3(1) = \frac{1}{2}x(1) + x(2) - x(4) + x(6) - x(8) - \frac{1}{2}x(9)$$

$$w_3(2) = \frac{1}{2}x(2) + x(3) - x(5) + x(7) - x(9) - \frac{1}{2}x(10)$$

Hence

$$w_3(j) = \frac{1}{2}x(j) + x(j+1) - x(j+3) + x(j+5) - x(j+7) - \frac{1}{2}x(j+8)$$

$$j=1, 2, 3, \dots$$

... (D.28)

$$w_4(1) = \frac{1}{2}x(1) - x(3) + x(5) - x(7) + \frac{1}{2}x(9)$$

$$w_4(2) = \frac{1}{2}x(2) - x(4) + x(6) - x(8) + \frac{1}{2}x(10)$$

Hence

$$w_4(j) = \frac{1}{2}x(j) - x(j+2) + x(j+4) - x(j+6) + \frac{1}{2}x(j+8)$$

$$j=1, 2, 3, \dots$$

... (D.29)

$$w_5(1) = \frac{1}{2}x(1) - x(3) + x(7) - \frac{1}{2}x(9)$$

$$w_5(2) = \frac{1}{2}x(2) - x(4) + x(8) - \frac{1}{2}x(10)$$

Hence

$$w_5(j) = \frac{1}{2}x(j) - x(j+2) + x(j+6) - \frac{1}{2}x(j+8)$$

$$j=1, 2, 3, \dots$$

... (D.30)

$$w_6(1) = \frac{1}{2}x(1) - x(5) + \frac{1}{2}x(9)$$

$$w_6(2) = \frac{1}{2}x(2) - x(6) + \frac{1}{2}x(10)$$

Hence

$$w_6(j) = \frac{1}{2}x(j) - x(j+4) + \frac{1}{2}x(j+8)$$

$$j=1, 2, 3, \dots$$

... (D.31)

BIBLIOGRAPHY

1. AIEE Committee Report, "Report on Transformer Magnetizing Current and It's Effect on Relaying and Airswitch Operation", AIEE Transactions, Vol. 70, pp. 1733-1740, 1951.
2. Anderson, Paul, "Analysis of Faulted Power Systems", Iowa State University Press, 1973.
3. Beauchamp, K. G., "Walsh Functions and Their Applications", Academic Press, 1975.
4. Blachman, W. M., "Sinusoids versus Walsh Functions", "IEEE Proceedings, Vol. 62, No. 3, pp. 346-353, March 1974.
5. Blume, L. F., Camilli, G., Farnham, S. B. and Peterson, H. A., "Transformer Magnetizing Inrush Currents and Influence on System Operation", AIEE Trans., Vol. 63, pp. 366-374, 1944.
6. Cheetham, W. J., "Computerized Protection or Not? - Primary and Local Backup Protection", IEE Conference Publication No. 125, London, pp. 291-296, March 1975.
7. Cheetham, W. J., "Computerized Protection or Not? - Remote Backup Protection", Ibid, pp. 297-303.
8. "Computer Relaying Tutorial Text", IEEE Power Engineering Society Special Publication, No. 79EH0148-7-PHR, 1979.
9. d'Assumpcao, H. A., "Rapid Estimation of Spectra From Irregularly sampled Records", Proceedings IEE, Vol. 125, No. 12, pp. 1337-1338, 1978.
10. Degens, A. J., "Microprocessor Implemented Digital Filters for Inrush Current Detection", Electrical Power and Energy Systems, pp. 196-205, Vol. 4, No. 3, July, 1982.
11. Finzi, L. A. and Mutscher, W. H., Jr., "The Inrush of Magnetizing Current in Single-phase Transformers", AIEE Transactions, Vol. 70, pp. 1436-1438, 1951.

12. Gaster, M. and Roberts, J. B., "Rapid Method of Forming Spectra From Regularly Sampled Records by Rectangular Wave Transforms", Proceedings IEE, Vol. 126, No. 7, pp. 658-663, July, 1979.
13. G.E.C. Measurements, "Protective Relays Application Guide", G.E.C. Measurements, U.K., 1975.
14. Gilchrist, G. B., Rockefeller, G. D. and Udren, E. A., "High-Speed Distance Relaying Using a Digital Computer, Part I - System Description", IEEE Transactions on Power Apparatus and Systems, Vol. 91, No. 3, pp. 1244-1258, May/June, 1972.
15. Horton, J. H., "Walsh Functions for Digital Impedance Relaying of Power Lines", IEEE PES Summer Meeting, San Francisco, pp. 530-541, July 1975.
16. Hostetter, G. H., "Recursive Discrete Fourier Transformation", IEEE Transactions on Acoustics, Speech and Signal processing, Vol. ASSP-28, No. 2, pp. 184-190, April, 1980.
17. Larson, R. R., Flechsig, A. J. and Schweitzer, E. D., "The Design and Test of a Digital Relay for Transformer Protection", Paper No. F78 688-4, IEEE PES Summer Meeting, Los Angeles, pp. 1-9, July 1978.
18. Macfadyen, W. K., Simpson, R. R. S., Slater, R. D., and Wood, W. S., "Method of Predicting Transient Current Patterns in Transformers", Proceedings, IEE, Vol. 120, No. 11, pp. 1393-1396. November 1973.
19. Malik, O. P., Dash, P. K. and Hope, G. S., "Digital Protection of a Power Transformer", IEEE Publication 76CH1075-1 PWR, Paper No. A76 191-7, IEEE PES Winter Meeting, New York, pp. 1-7, January, 1976.
20. Mann, B. J. and Morrison, I. F., "Digital Calculation of Impedance for Transmission Line Protection", IEEE Transactions, Power Apparatus and Systems, Vol. PAS-90, No. 1, pp. 270-279, January/February, 1971.
21. Mann, B. J., and Morrison, I. F., "Relaying a Three-Phase Transmission Line with a Digital Computer", IEEE Transactions, Power Apparatus and Systems, Vol. PAS-90, No. 2, pp. 742-750, March April, 1971.

22. Masson, C. R., "The Art and Science of Protective Relaying", John Wiley and Sons Inc., 1956.
23. Rabiner, L. R. and Gold, B., "Theory and Application of Digital Signal Processing", Prentice-Hall, New Jersey, 1975.
24. Rahman, M. A., Dash, P. K., and Downtown, E. R., "Digital Protection of Power Transformer on Weighted Least Square Algorithm", IEEE PES, Winter Meeting, New York, pp. 1-6, February, 1982.
25. Rahman, M. A. and Dash, P. K., "Fast Algorithm for Digital Protection of Power Transformers", Proceedings IEE, Vol. 129, Part C, No. 2, pp. 79-85, March, 1982.
26. Ramamoorthy, M., "Application of Digital Computers to Power System Protection", Journal of Institute of Engineering (India), Vol. 52, No. 10, June 1972, pp. 235-238.
27. Rao, T. S. M., "Power System Protection Static Relays", Tata-McGraw-Hill, New Delhi, 1979.
28. Roberts, J. B., Gaster, M., "Rapid Estimation of Spectra From Irregularly Sampled Records", Proceedings IEE, Vol. 125, No. 2, pp. 92-96, February, 1978.
29. Rockefeller, G. D., "Fault Protection with a Digital Computer, IEEE Transactions, on Power Apparatus and Systems, Vol. PAS-88, No. 4, pp. 438-461, April 1969.
30. Rockefeller, G. D. and Udren, E. A., "High-Speed Distance Relaying Using a Digital Computer; Part II", Ibid, pp. 1244-1258.
31. Say, M. G., "Alternating Current Machines", 4th edition, E. L. B. S and Pitman Publishing Ltd., 1976.
32. Schweitzer, E. O., Larson, R. R. and Flechsig, A. J., Jr., "An Efficient Inrush Current Detection Algorithm for Digital Computer Relay Protection of Transformer", IEEE Publication No. 77CH1193-2 PWR, Paper No. 77510-1, IEEE PES Summer Meeting, Mexico City, pp. 1-5, July 1977.
33. Sonnemann, W. K., Wagner, C. L., and Rockefeller, G. D., "Magnetizing Inrush Phenomena in Transformer Banks", AIEE Transactions on Power Apparatus and Systems, Vol. 77, pp. 884-892, October, 1958.

34. Spect, T. R., "Transformer Magnetizing Inrush Current", AIEE Trans., Vol. 70, pp. 323-328, 1951.
35. Specht, T. R., "Transformer Inrush and Rectifier Transient Currents", IEEE Transactions on Power Apparatus and Systems, Vol. PAS-88, No. 1, pp. 269-276, April, 1969.
36. Stevenson, W. D., "Elements of Power System Analysis", McGraw-Hill Book Co., 1982.
37. Sykes, J. A. and Morrison, I. F., "A proposed Method of Harmonic Restraint Differential Protection of Transformers by Digital Computer", IEEE Transactions, Power Apparatus and Systems, Vol. PAS 91, No. 3, pp. 1266-72, May/June 1972.
38. The Electricity Council, "Power System Protection", Vol. 1, Peter Peregrinus Ltd.,
39. The Electricity Council, "Power System Protection", Vol. 2, Peter Peregrinus Ltd., 1981.
40. The Electricity Council, "Power System Protection", Vol. 3, Peter Peregrinus Ltd., 1981.
41. Thorp, J. S., and Phadke, A. G., "A Microprocessor Based Three-Phase Transformer Differential Relay", IEEE, Power Apparatus and Systems, Vol. PAS-101, No. 2, pp. 426-432, February, 1982.
42. Van C. Warrington, A. R., "Protective Relays Their Theory and Practice", Vol. I, London: Chapman and Hall, 1962.
43. Van C. Warrington, A. R., "Protective Relays Their Theory and Practice", Vol. II, London: Chapman and Hall, 1969.
44. Westinghouse Electric Corporation, "Applied Protective Relaying", Westinghouse Electric Corporation, U.S.A., 1976.



